Membrane facilitated separation of NF_3 and CF_4

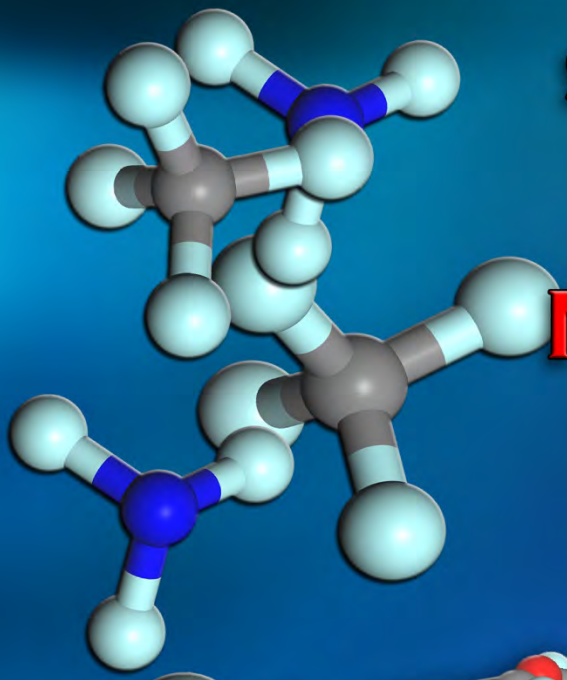

D.J. Branken

September 2013

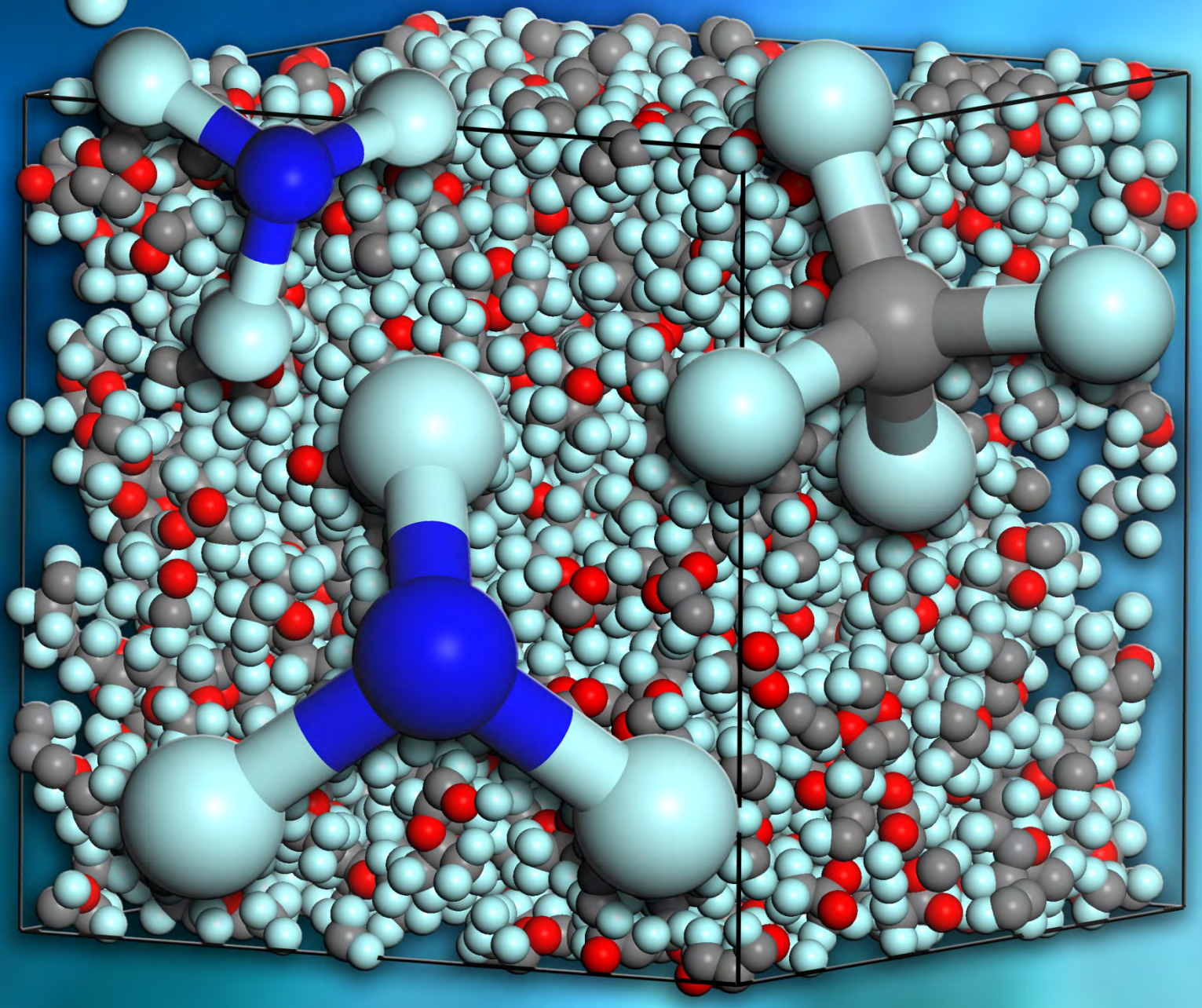

Membrane facilitated separation of NF_3 and CF_4

DJ Branken

12763764

Thesis submitted for the degree Doctor of Philosophy in Chemistry at the Potchefstroom Campus of the North-West University

Promoter: Prof HM Krieg

Co-Promoter: Dr G Lachmann

Assistant Promoter: Dr PAB Carstens

September 2013

List of Publications

The content of this thesis is based on the following publications:

1. D.J. Branken, J.P. le Roux, H.M. Krieg, G. Lachmann, A dual-channel gas chromatography method for the quantitation of low and high concentrations of NF_3 and CF_4 to study membrane separation of the two compounds. J. Chromatogr. A. 1307 (2013) 180 – 190.
2. D.J. Branken, .H.M. Krieg, J.P. le Roux, G. Lachmann, Separation of NF_3 and CF_4 using amorphous glassy perfluoropolymer Teflon AF and Hyflon AD60 membranes. J. Membr. Sci. To be submitted for review.
3. D.J. Branken, H.M. Krieg, G. Lachmann, Determining the diffusion and sorption characteristics of Teflon AF perfluoropolymer membranes towards NF_3 and CF_4 using molecular modeling and statistical thermodynamics techniques. Macromolecules, to be submitted for review.

Acknowledgements

I thank my heavenly father, God almighty, for His guidance throughout my Ph.D. study, and for bestowing me with the required cognitive abilities and perseverance to complete this thesis. Throughout my studies I have been constantly reminded of the Lord's immeasurable grace, and that we are all dependent upon Him.

I also express my sincerest gratitude towards:

- My wife, Magna Branken, for your undying love, support, and motivation during my study, as well as for your help with completing my thesis. I thank the Lord for allowing our paths to cross, for without you this journey would have been much less rewarding.
- My parents, Dawid and Hermine Branken, for giving me the opportunity to pursue my Ph.D. degree, and for your love and support to both Magna and myself, without which this thesis would not have been a reality.
- My parents-in-law, Pieter and Lousea Meintjies, for your much appreciated understanding, and loving support during my study that also played an integral role in the successful completion of this thesis. Thank you for accepting me as your son-in-law and as part of the family.
- My promotor, Prof. H.M. Krieg (Henning), for your continued and much appreciated moral support throughout the duration of my post-graduate studies. You are an outstanding friend and a true mentor. Thank you.
- My co-promoter, Dr. G. Lachmann (Gerhard), for your proficient advice, but most of all for being an outstanding role-model that many scientists can, and have looked up to.
- Mr. J.P. le Roux (John), Delta F, Necsa, for taking on the role of my "teacher" and for always looking out for me. Your advice and guidance with the technical aspects of my study were instrumental in the successful completion of my thesis, and the time spent "working" with you certainly was time well-spent.

- The South African Nuclear Energy Corporation SOC Limited (Necsa), for providing the funding related to this study, as co-ordinated by Dr. P.A.B. Carstens (Applied Chemistry), who also showed a keen interest in the many aspects of the study. I am forever thankful of the opportunity that I was granted, and for permission to spend the final year of my study on-site at Necsa.
- North-West University, Potchefstroom Campus, for providing additional financial support, as co-ordinated by Prof. H.C.M. Vosloo (Chemical Resource Beneficiation) that was used to acquire the specialised gas chromatographic (GC) analysis system that was used in this study.
- Dr. J.B. Wagener (Kobus), Delta F, Necsa, for co-ordinating my final year of study at Necsa, and for the advice you offered to me from time to time.
- Pelchem and Necsa, Pretoria, South Africa, for kindly providing the LESA-grade NF_3 used in this study.
- The Laboratory of Applied Molecular Modelling (LAMM), North-West University, for the use of their computational facilities. A special word of thanks to Dr. C.G.C.E. van Sittert for arranging the personal computer that I used for molecular modeling.
- Prof. C.A. Strydom, and Me. W. van Vuuren, for lending me the personal computer, as arranged by Dr. C.G.C.E. van Sittert, to conduct my molecular modeling simulations.
- The staff of/and the Centre for High Performance Computing (CHPC) of the Council for Scientific and Industrial Research (CSIR) in South Africa, as supported by the Department of Science and Technology (DST) for providing a unique service to South African researchers, which I relied heavily upon to conduct my molecular modeling simulations.
- Mr. R. Volsteed (Rouan), Scientific Supply Services, South Africa for his invaluable help in setting up the GC system.
- Mr. J.H. Broodryk, Instrument-making, North-West University, Potchefstroom Campus for expertly assembling the experimental setup used in this study.
- Mr. L. van Rooyen (Louis), Organic Fluorine Chemistry, Necsa, for conducting differential scanning calorimetric analysis of the perfluoropolymer films samples, and for your patience with all my “demands”.
- Mr. A. Pienaar (Andrew), Delta F, Necsa, for diligently conducting the thermal gravimetric analysis of the polymer films samples.

- Mr. J.C. Thompson (Cliff), Organic Fluorine Chemistry, Necsa, for providing the carbon tetrafluoride (CF_4) used during the preliminary stages of this study, and for your assistance whenever I needed it.
- Mr. R. van der Merwe (Ryno), Necsa, for doing the scanning electron microscopy analysis of the Hyflon AD60 perfluoropolymer film samples, and for Dr. E. Snyders who authorised the analysis.
- My brother, Henri Branken, and sister-in-law, Jacomi Benadé, for providing much appreciated laughter and for the support you both provided by just being yourselves.
- Oom Johan and Tannie Mariette du Buson, for your hospitality and kind words whenever Magna and I needed it. Thank you Tannie Mariette for designing the stunning cover for my thesis.
- Mrs. M. Venter (Marietjie), Applied Chemistry, Necsa, for your kindness and assistance with the administrative aspects of my studies at Necsa.
- Dr. H. Oosthuizen (Hester), Applied Chemistry, Necsa, for critically reviewing Chapter 2 of this thesis.
- Dr. H. Bissett (Hertzog), Derik van der Westhuizen, Andries Kruger, and Neels le Roux, for your valued friendship, and for lending a hand from time to time.

Dit is nie aan die mens self te danke dat hy kan eet en drink en onder al sy arbeid nog die goeie kan geniet nie. Ek het ingesien dat dit 'n gawe uit die hand van God is.

- Prediker 2: 24.

Abstract

Nitrogen trifluoride (NF_3) is frequently used as a source of fluorine in the electronics device manufacturing industry as a dry etchant during plasma assisted etching of silicon wafers, or during the plasma cleaning of chemical vapor deposition chambers. As a result of the electrochemical synthesis procedures in which carbon anodes are used in a fluorine-rich environment, NF_3 product streams are frequently contaminated with ppm-amounts of carbon tetrafluoride (CF_4). The electronics manufacturing industry, however, requires NF_3 of exceptional purity, i.e. so-called VLSI-grade (very large scale integration) NF_3, with CF_4 concentrations of 20 ppm and below. Due to the close chemical and physical similarities of the two compounds, the removal of CF_4 from NF_3 has proven to be rather difficult, and current NF_3 purification technologies are relatively inefficient. Although membrane gas separation has proven to be competitive in terms of operating costs and energy efficiency, its use for the purification of NF_3 seems to have remained unexplored to date.

In this study, the use of high free volume glassy perfluoropolymers of Teflon AF2400, Teflon AF1600, and Hyflon AD60 was therefore investigated. To be able to measure the pure and mixed gas permeabilities and selectivities of the solution-cast membranes towards NF_3 and CF_4, a custom built experimental setup was used, in which a newly developed gas chromatographic (GC) analysis method was implemented. Using divinylbenzene-styrene co-polymer stationary phases in the form of Super Q, a reliable quantification of mixtures of NF_3 and CF_4 were achieved without requiring additional fluorocarbon liquid stationary phases, as is commonly used in NF_3 production environments. Furthermore, by implementing a dual-channel configuration it was possible to quantify a wide range of NF_3 and CF_4 concentrations. Using the newly developed technique, NF_3 and CF_4 concentrations of ca. 1 mol% and upwards could be quantified using a Thermal Conductivity Detector (TCD) on one channel, and NF_3 and CF_4 concentrations of between ca. 40 vppm and 4000 vppm could be measured using a Pulsed Discharge Helium Ionisation Detector (PDHID) on the second channel of the GC method.

The glassy perfluoropolymer membranes of Teflon AF2400, Teflon AF1600, and Hyflon AD60 were prepared by a solution casting method, and it was found that annealing at sufficiently high temperatures (170 – 200 °C) ensured optimum permeability selectivity. In

contrast, thermal analysis of the solution-cast Hyflon AD60 membranes that were heated to only 95 °C confirmed that the polymer matrix was significantly swollen due to a residual amount of the casting solvent. Consequently, considerably reduced selectivity and increased permeability of both NF_3 and CF_4 were observed for such solvent-swollen Hyflon AD60 membranes in comparison with the non-swollen membranes that were annealed at 170 °C. Nonetheless, the measured He/N_2 permeability and permeability selectivity of all the membranes studied compared favourably with literature values, and selectively permeated NF_3 rather than CF_4 wherein the pure and mixed gas permeability selectivity displayed a clear dependence on the fractional free volume (FFV) of the polymer matrices. Thus, in accordance with the decreasing FFV of the perfluoropolymers in the order Teflon AF2400 > Teflon AF1600 > Hyflon AD60, the NF_3 permeability decreased from 227 Barrer for Teflon AF2400, to 29 Barrer for Teflon AF1600, to 1.9 Barrer for Hyflon AD60. In contrast, the NF_3/CF_4 selectivity, $\alpha(NF_3/CF_4)$, increased inversely from 4.5 for Teflon AF2400, to 6.0 for Teflon AF1600, to the highest selectivity of 12 which was obtained using Hyflon AD60.

To elucidate the mechanism of separation, the transport properties of NF_3 and CF_4 in Teflon AF2400 and Teflon AF1600 w.r.t. diffusion and solubility were studied using Molecular Dynamics (MD), Grand Canonical Monte Carlo (GCMC), and statistical thermodynamic techniques. The results indicated that NF_3/CF_4 diffusion selectivity (D_{NF_3}/D_{CF_4}) was favoured by the lower free volume of Teflon AF1600, whereas poor correlation was achieved between the GCMC calculated sorption isotherms of CF_4 and the experimentally determined isotherms as reported in the literature. Consequently, the non-equilibrium lattice fluid (NELF) model, which more accurately described the sorption isotherms of CF_4, was used to evaluate the solubility selectivity. It was found that by adjusting the NELF model interaction parameter, Ψ, favourable NF_3/CF_4 solubility selectivities (S_{NF_3}/S_{CF_4}) were predicted. Furthermore, by combining the solubility selectivity values with the diffusion selectivities calculated from the MD results, permeability selectivity predictions that correlated well with the experimentally determined values were obtained. Based on a semi-quantitative technological evaluation, it was concluded that although good NF_3/CF_4 mixed gas permeability selectivity was obtained with Hyflon AD60, further research into improving the NF_3 solubility, and hence permeability will aid in the development of an efficient membrane gas separation process for the purification of NF_3.

Keywords: NF_3 Purification; NF_3 and CF_4 Membrane Separation; NF_3/CF_4 Permeability Selectivity; Glassy perfluoropolymer membranes; Fractional free volume (FFV).

Opsomming

Stikstoftrifluoried (NF_3) word algemeen in die elektroniese vervaardigingsbedryf as ’n bron van fluoor tydens droë plasma-etsing prosesse vir die behandeling van silikoon skyfies, of gedurende die skoonmaak van chemiese damp-deponeringskamers gebruik. Omdat koolstofanodes in ’n fluoor-ryke omgewing tydens elektrochemiese sintese prosesse gebruik word, word NF_3 produkstrome gereeld met klein hoeveelhede (dpm-vlak) koolstoftetrafluoried (CF_4) gekontamineer. Die elektroniese vervaardigingsbedryf vereis egter dat NF_3 met buitengewone suiwerheid, nl. sogenaamde VLSI-graad (“very large scale integration”) NF_3, waarvan die CF_4 konsentrasie laer as 20 dpm is gebruik word. Skeiding van CF_4 vanaf NF_3 is egter uitdagend a.g.v. die noue ooreenkoms in die chemiese en fisiese eienskappe van die twee verbindings, waar huidige suiweringsprosesse relatief ondoeltreffend is. Alhoewel membraangebaseerde gas-skeiding ’n kompeterende tegnologie m.b.t. bedryfskoste en energie verbruik is, is hierdie tegnologie tot op hede nog nie vir die suiwering van NF_3 nie toegepas nie.

Vir hierdie doel is die gebruik van hoë vry-volume, glasagtige perfluoropolimeer membrane van Teflon AF2400, Teflon AF1600 en Hyflon AD60 in hierdie studie ondersoek. Om egter die suiwer- en gemengde gas permeabiliteite en selktiwiteite van die membrane teenoor NF_3 en CF_4 te meet, is ’n unieke eksperimentele opstelling in kombinasie met ’n nuut-ontwikkelde gas chromatografiese (GC) analise metode gebruik. Deur ’n divinielbenseen-stireen ko-polimeer stasionêre fase in die vorm van Super Q te gebruik, was betroubare kwantifisering van NF_3 en CF_4 mengsels moontlik sonder dat enige addisionele gefluorineerde vloeistof-stasionêre fases benodig was. Met ’n dubbele-kanaal konfigurasie kon NF_3 en CF_4 konsentrasies van ca. 1 mol% en meer gekwantifiseer word deur ’n Termiese Geledingsdetektor (TGD) op die een kanaal te gebruik, terwyl NF_3 en CF_4 konsentrasies van tussen ca. 40 vdpm en 4000 vdpm gemeet kon word deur ’n “Pulsed Discharge Helium Ionisation” Detektor (PDHID) op die tweede kanaal te gebruik.

Die glasagtige perfluoropolimeer membrane van Teflon AF2400, Teflon AF1600 en Hyflon AD60 was voorberei deur vergieting van oplossings van die polimere en daar is bevind dat uitgloeiing by hoë temperature (170 – 200 °C) nodig was om optimum permeabiliteit-selektiwiteite te verseker. Die termiese analise van die vergiete Hyflon AD60 membrane wat

slegs tot 95 °C verhit is, het bevestig dat die polimeermatriks tot ’n beduidende mate geswel was met die oorblywende oplosmiddel. As gevolg hiervan het die geswelde Hyflon AD60 membrane verlaagde selektiwiteit en verhoogde NF_3 en CF_4 permeabiliteit getoon t.o.v. die nie-geswelde Hyflon AD60 membrane wat by 170 °C uitgegloei was. Nieteenstaande, het die gemete He/N_2 permeabiliteit en permeabiliteit-selektiwiteit van al die membrane wat in hierdie studie gebruik was goed met literatuurwaardes ooreengestem en die NF_3-permeabiliteit was in alle gevalle hoër as dié van CF_4. In ooreenstemming met die afname in fraksionele vry-volume (FVV) van die perfluoropolimere in die orde Teflon AF2400 > Teflon AF1600 > Hyflon AD60, het die NF_3 permeabiliteit van 227 Barrer vir Teflon AF2400, na 29 Barrer vir Teflon AF1600 en na 1.9 Barrer vir Hyflon AD60 afgeneem. In teenstelling, het die NF_3/CF_4 selektiwiteit, $\alpha(NF_3/CF_4)$, van 4.5 vir Teflon AF2400, na 6.0 vir Teflon AF1600 en na ongeveer 12 vir Hyflon AD60 toegeneem.

Om die meganisme van skeiding verder op te klaar is die oordrageienskappe van NF_3 en CF_4 in Teflon AF2400 en Teflon AF1600 bestudeer m.b.t. diffusie en oplosbaarheid (sorpsie) deur van Molekuul Dinamika (MD), “Grand Canonical Monte Carlo” (GCMC) en statistiese termodinamika metodes gebruik te maak. Die resultate het getoon dat NF_3/CF_4 diffusieselektiwiteit (D_{NF_3}/D_{CF_4}) met die laer vry volume van Teflon AF1600 bevoordeel is, maar dat ’n swak ooreenkoms tussen die GCMC-berekende sorpsie isoterme en die eksperimenteel-bepaalde isoterme van CF_4, soos in die literatuur vermeld, verkry is. Daarom is die “non-equilibrium lattice fluid” (NELF) model, wat die sorpsie isoterme van CF_4 meer akkuraat beskryf het, gebruik om die invloed van sorpsieselektiwiteit te bepaal. Deur die NELF-model interaksie parameter, Ψ, te varieer is gunstige NF_3/CF_4 sorpsieselektiwiteite (S_{NF_3}/S_{CF_4}) voorspel en deur die sorpsieselektiwiteit waardes met die diffusieselektiwiteit soos bereken uit die MD simulasie resultate te kombineer, is permeabiliteit-selektiwiteit waardes verkry wat goed met die eksperimenteel-bepaalde waardes ooreengestem het. Deur gebruikmaking van ’n semi-kwantitatiewe tegnologiese evaluasie is dit bevind dat verdere navorsing met die doel om die NF_3 oplosbaarheid en dus permeabiliteit te verhoog, tot die ontwikkeling van ’n doeltreffende membraanskeidingsproses vir die suiwering van NF_3 sou kon bydra.

Sleutelwoorde: Suiwering van NF_3; Membraanskeiding van NF_3 en CF_4; NF_3/CF_4 Permeabiliteit-selektiwiteit; Glasagtige perfluoropolimeer membrane; Fraksionele vry-volume (FVV).

Table of Contents

Nomenclature

Latin Symbols

% RSD	Relative standard deviation	[-]
ΔH_S	Sorption enthalpy	kJ/mol
Δp	Differential pressure or trans-membrane pressure	kPa
Δp^*	Binary interaction parameter	bar
b	Langmuir affinity parameter	atm^{-1}
C	Concentration of a gaseous penetrant in the polymeric phase	$cm^3(STP).cm^{-3}$ pol
$C_H^{'}$	Langmuir capacity parameter	$cm^3(STP)/cm^3$
D	Diffusion coefficient	cm^2/s
D_{CF_4}	Infinite dilution diffusion coefficient of CF_4	cm^2/s
D_{eff}	Local effective diffusion coefficient	$cm^3.cm^2.cm^{-3}(STP).s^{-1}$
D_{loc}	Local concentration-averaged diffusion coefficient	cm^2/s
D_{NF_3}	Infinite dilution diffusion coefficient of NF_3	cm^2/s
dV/dt	Volumetric displacement rate of the soap film	cm^3/s
$E_{D.}$	Activation energy of diffusion	kJ/mol
E_p	Activation energy of permeation	kJ/mol
FFV	Fractional free volume	[-]
G	Gibbs free Energy	J or kJ
J_i	Flux of component i through the membrane	$cm^3(STP)/(cm^2.s)$
k_D	Henry sorption parameter	$cm^3(STP)/cm^3.atm$
M	Molecular Weight of a pure fluid	g/mol
n	Number of moles of a pure fluid	mol
n_i	Number of moles of component i in mixture	mol
N_α	Number of molecules of penetrant α	[-]
P	Permeability	Barrer
p	Absolute fluid pressure	bar
$\tilde{p}$	Reduced pressure of a pure fluid or gas-polyme mixture	[-]
p^*	Adjustable pure fluid or mixture characteristic pressure	bar

p_{12}^{*}	Binary parameter	bar
p_i^{*}	Adjustable characteristic pressure of component *i*	bar
P_0	Pre-exponential factor	Barrer
p_a	Atmospheric Pressure	cmHg
p_f	Membrane feed pressure	cmHg
p_p	Membrane permeate pressure	cmHg
p_r	Retentate pressure	cmHg
p_S	Standard pressure	76 cmHg
R	Universal gas constant	8.314 $J.K^{-1}.mol^{-1}$
r	Number of pure-fluid lattice sites	[-]
r_i	Number of mixture lattice sites available to species *i*	[-]
$\boldsymbol{r}_i(0)$	Initial position of the centre of mass of particle *i*	Å
$\boldsymbol{r}_i(t)$	Final position of the centre of mass of particle *i*	Å
r_i^{0}	Number of pure-fluid lattice sites	[-]
R_s	Peak resolution	[-]
S	Solubility coefficient	$cm^3(STP).cm^{-3}$ $pol.atm^{-1}$
S_0	Infinite dilution solubility coefficient	$cm^3(STP).cm^{-3}$ $pol.atm^{-1}$
S_{CF_4}	Infinite dilution solubility coefficient of CF_4	$cm^3(STP).cm^{-3}$ $pol.atm^{-1}$
S_{NF_3}	Infinite dilution solubility coefficient of NF_3	$cm^3(STP).cm^{-3}$ $pol.atm^{-1}$
T	Absolute Temperature	K
$\tilde{T}$	Reduced temperature of a pure fluid or mixture	[-]
T^{*}	Adjustable pure fluid or mixture characteristic temperature	K
T_c	Critical temperature	K
T_g	Glass transition temperature	°C
$t_R^{CF_4}$	Retention time of CF_4	min
$t_R^{NF_3}$	Retention time of NF_3	min
T_S	Standard temperature	273 K
v^{*}	Pure fluid or mixture characteristic molar volume	cm^3/mol
v_i^{*}	Characteristic molar volume of component *i*	cm^3/mol
V_c	Critical Volume	cm^3/mol
V_f	Free volume	cm^3/g
$\dot{V}_f$	Total volumetric flow rate of the feed	L/h
V_{oc}	Total volume occupied by the polymer atoms	cm^3/g

$\dot{V}_p$	Total volumetric flow rate of the feed stream	L/h
$\dot{V}_r$	Total volumetric flow rate of the retentate stream	L/h
Vsp	Specific Volume	cm^3/g
V_w	van der Waals Volume	cm^3/g
W_{CF_4}	Peak width of CF_4 Peak	min
W_{NF_3}	Peak width of NF_3 Peak	min
x_f	Mole fraction of species *i* in the feed stream	[-]
x_i	Mole fraction or volume fraction of species *i* in the feed	[-]
y_i	Mole fraction or volume fraction of penetrant *i* in the permeate	[-]
y_p	Mole fraction of penetrant *i* in the permeate stream	[-]
z_i	Mole fraction or volume fraction of penetrant *i* in the retentate	[-]
z_r	Mole fraction or volume fraction of penetrant *i* in the retentate	[-]

Greek Symbols

$\mu_1^{(E)}$	Chemical potential of a pure gaseous penetrant	J/mol
$\mu_1^{(S)}$	Non-equilibrium chemical potential of a gaseous penetrant in a polymer	J/mol
$\alpha(He/N_2)$	Ideal He/N_2 Membrane selectivity	[-]
$\alpha(NF_3/CF_4)$	NF_3/CF_4 Membrane selectivity	[-]
$\alpha(NF_3/CF_4)_{ideal}$	Ideal NF_3/CF_4 Membrane selectivity	[-]
δ	Membrane thickness	cm
θ	Stage cut	[-]
ρ	Pure fluid or mixture density	g/cm^3
$\tilde{\rho}$	Reduced density of a pure fluid or penetrant-polymer mixture	[-]
ρ^*	Adjustable pure fluid or mixture characteristic density	g/cm^3
ρ_i^*	Adjustable characteristic density of component *i* in a mixture	g/cm^3
ρ_2^0	Pure, un-penetrated polymer density	g/cm^3
$\rho_{2\infty}$	Asymptotic polymer density	g/cm^3
$\tilde{\rho}^E$	Reduced density of the pure external gaseous fluid	[-]
$\tilde{\rho}^S$	Reduced density of the solid mixture phase	[-]
φ	Pressure ratio	
ϕ_i	Volume fraction of component *i* in a penetrant-polymer mixture	[-]
Ψ	NELF Model interaction parameter	[-]

ω	Mass fraction of a gaseous penetrant in the polymeric phase	[-]
ω_i	Mass fraction of fraction of component *i* in a penetrant-polymer mixture	[-]

Abbreviations

BPR	Backward-pressure regulator
CVD	Chemical vapor deposition
DSC	Differential Scanning Calorimitery
FPR	Forward-pressure regulator
GC	Gas chromatography/ gas chromatographic
GCMC	Grand Canonical Monte Carlo
MD	Molecular Dynamics
MFCs	Mass flow controllers
MS-13X	Molecular Sieve 13X
MS-5A	Molecular Sieve 5A
MSD	Mean square displacement
NVT	Ensemble of constant number of atoms, constant volume and constant temperature
NELF	Non-equilibrium lattice fluid model
NPT	Ensemble of constant number of atoms, constant pressure and constant temperature
P&ID	Piping and Instrumentation Diagram
PDHID	Pulsed discharge helium ionisation detector
PFCs	Perfluorocarbons
ppm	Concentration in parts per million
PTFE	Poly Tetrafluoroethylene
SEM	Scanning Electron Microscopy
STP	Standard temperature and pressure at 273 K and 101.325 kPa
TCD	Thermal conductivity detector
TGA	Thermal Gravimetric Analysis
VLSI	Very large scale integration
vppm	Concentration in parts per million with respect to volume at STP

Success consists of going from failure to failure without loss of enthusiasm.

- Winston Churchill

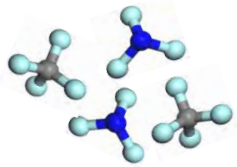

Chapter 1

Introduction

1.1 Problem Statement

Nitrogen trifluoride (NF_3) is a colorless gaseous substance at room temperature and atmospheric pressure [1, 2], which is a more convenient source of fluorine than molecular fluorine (F_2) for certain applications. This is because NF_3 is less reactive than F_2 at mild temperatures and pressures [1], it can be pressurized to higher pressures than F_2, and it can be condensed [2, 3], thus providing more convenient transport and storage options. Owing partly to these properties, NF_3 has been used in a number of applications, including [1, 2, 4, 5]:

- Preparation of fluorophosphasen by reacting NF_3 with phosphorous sulfide.
- Preparation of fluorocarbon polymer films by plasma polymerization of NF_3 and propylene.
- Preparation of carbonaceous thin films using a C_2H_4/NF_3 glow discharge plasma.
- High-energy lasers.
- As an oxidizer for liquid and solid propellants.
- For plasma etching of silicon carbide.
- For plasma cleaning of Chemical Vapour Deposition (CVD) Chambers.
- For plasma etching of silicon wafers for the manufacture of semiconductor devices.

Currently, however, NF_3 is mostly used in the electronics industry, as etchant for the cleaning of CVD chambers and the manufacture of semiconductor devices [1, 4, 6, 7], which is why it is sometimes referred to as an "electronic gas". During etching, the plasma dissociation of NF_3 is used to produce radicals such as $NF_2^{\bullet}$ and $F^{\bullet}$ [7], which act as scavengers that can react with Si, SiO_2 and SiN_x. During CVD chamber cleaning, silicon deposits are removed as volatile silicon fluorides, such as SiF_4, from the interior of such chambers that accumulate over time, thus eliminating the need for cleaning via acid bath immersion [4]. Although perfluorocarbons (PFCs) such as carbon tetrafluoride (CF_4) and perfluoroethane (C_2F_6) have also been used as etchants for CVD chamber cleaning, it has been shown that NF_3 exhibits superior etching performance [6, 7] compared to PFCs. This is attributed to the significantly

more effective plasma decomposition rates of NF_3 compared to PFCs such as CF_4, which is strongly correlated with the etching performance. Furthermore, because the plasma decomposition of PFCs is less effective than that of NF_3, recovery processes have to be used to prevent, or limit, the release of the PFCs to the atmosphere [8], which contributes to global warming. This problem may be alleviated using NF_3 as etchant as it is more completely dissociated, although NF_3 also has a high global warming potential [9]. In plasma etching of silicon wafers [4, 7, 9, 10], it has also been shown that the use of NF_3 presents advantages over the use of PFCs such as [4, 7, 10]:

- Superior etching efficiency as is the case in plasma cleaning of CVD chambers.
- The formation of silicon carbide, which plaques etching processes in which PFCs are used, is nonexistent.
- Only volatile reaction products are produced.
- Carbonaceous residue build-up is prevented.

As the semiconductor manufacturing processes are improved to afford the production of devices of ever decreasing size and increasing complexity, more stringent purity specifications are placed on NF_3 for use in the semiconductor industry. Among the current specifications, the CF_4 content is one of the major concerns, where normal electronics grade NF_3 preferably contains less than 500 ppm CF_4, whereas VLSI-grade (Very Large Scale Integration) NF_3 should contain less than 20 ppm CF_4 [10]. This stringent purity requirement with respect to the CF_4 content seems to be to eradicate the potential formation of defects on electronic devices during etching [11], which may result from the formation of unwanted residues when CF_4 is present in the NF_3 etchant. This however presents a challenge as CF_4 is often introduced into the NF_3 product stream during commercial synthesis procedures, as illustrated in Fig. 1.1, where subsequent separation of CF_4 from NF_3 is difficult as will become apparent from the discussion below.

In the electrochemical fluorination (ECF) and direct fluorination (DF) routes (Fig. 1.1), carbon anodes are commonly used for: i) the electrolysis of NH_4F-KF-HF [4] to electrochemically produce NF_3; or ii) for the electrolytic production of fluorine (F_2) with HF as reactant, where the F_2 is then used in a second gas-liquid reaction step to produce NF_3 [2, 5, 12, 13]. CF_4 is inevitably introduced into the NF_3 product streams due to breakdown of the carbon anodes. As shown in Fig. 1.1, electrochemical fluorination using nickel anodes and

$NH_4F.2HF$ as the electrolyte instead is advantageous in avoiding the CF_4 contamination problem. However, this process suffers from other drawbacks including more extensive corrosion of the anode which results in the corrosion products being deposited on the bottom of the cell, causing significant current losses [4]. In addition, dilution of the NF_3 product with N_2 has to be used to prevent explosive reactions of NF_3 with H_2 that is produced at the cathode. Another possible synthesis procedure is the gas-solid reaction of F_2 with ammonium cryolite [14], however, it would seem that this route is not used commercially.

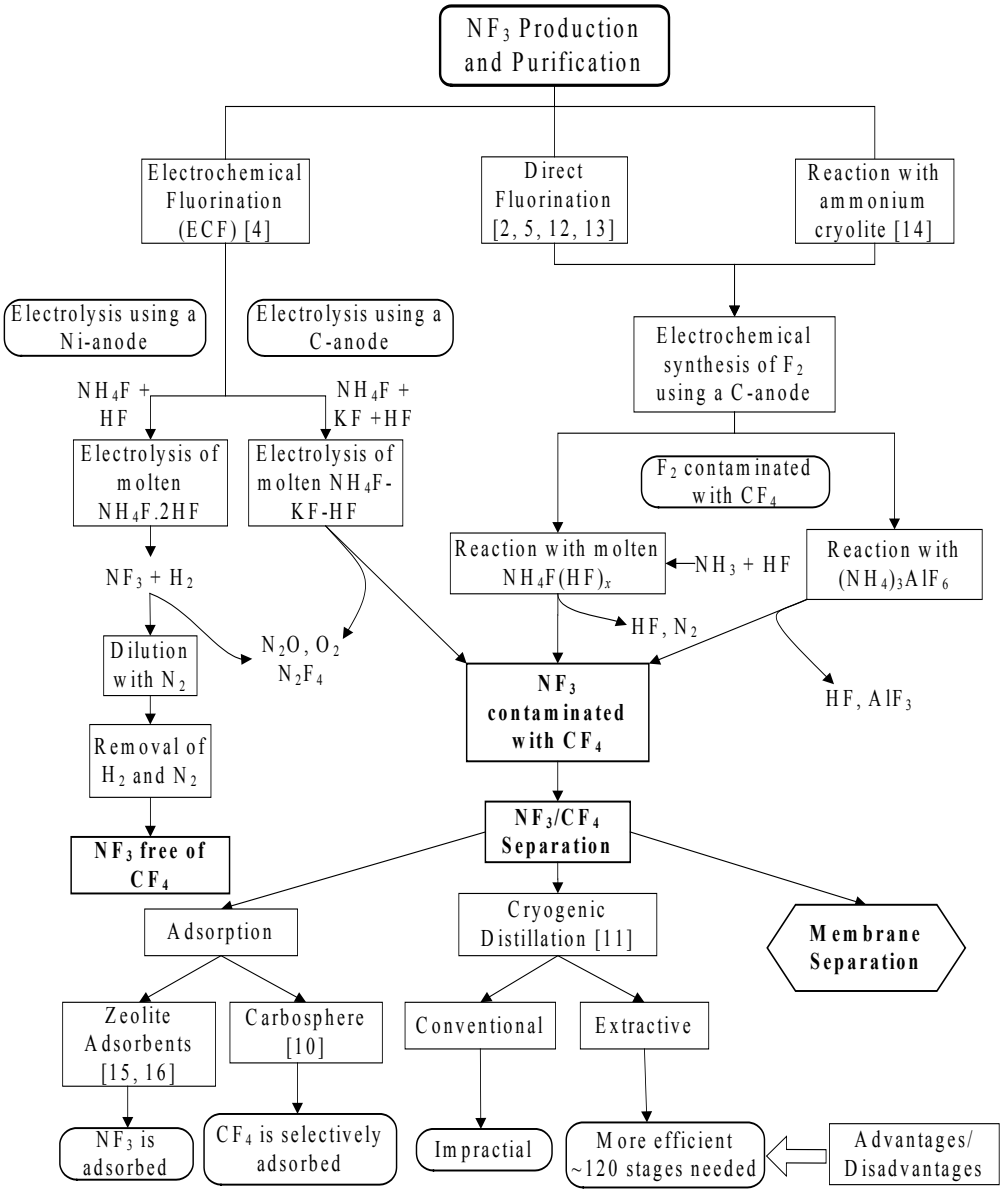

Figure 1.1: Schematic illustration summarizing the various routes of NF_3 production and purification.

The difficulty of NF_3 and CF_4 separation arises due to the similar properties of the compounds, i.e. the small difference in boiling points (-129°C and -128°C respectively), the low reactivity under normal conditions, the small difference in the molecular weights as well as the dipole moments (0.234 D) and the heats of adsorption [10]. Table 1.1 gives a summary of the physical properties of NF_3 and CF_4.

Table 1.1: Physical properties of nitrogen trifluoride (NF_3) and carbon tetrafluoride (CF_4).

Property	Value	
	NF_3	**CF_4**
Boiling point at 101.325 kPa (°C)	-129.0	-128.0
Heat of vaporization (kJ/mol)	11.59	-
Heat of formation (kJ/mol)	-131.5	-
Heat capacity at 25 °C, 101.325 kPa (J/mol.K)	53.39	61.27
Critical Temperature (°C)	-39.25	-45.60
Critical Pressure (kPa)	4530	3739
Critical Volume (cm^3/mol)	123.8	139.9
Molecular size (Å)	4.500[a]	4.800[a]
Dipole moment	0.234 D	0

Values of the physical properties of NF_3 and CF_4 were taken from references [1] and [17].
[a] Values for the molecular sizes of NF_3 and CF_4 were taken from reference [18].

Existing separation methods include the selective adsorption of NF_3 onto zeolite adsorbents [15, 16], which is however inefficient, as the matrix material (NF_3) is adsorbed rather than the minor impurity, with the consequence of large quantities of adsorbent being required. One method that has been suggested to alleviate this problem is to use a polyacrylonitrile-based carbon molecular sieve, called Carbosphere, which is claimed to selectively adsorb CF_4 instead of NF_3 [10]. Due to the close boiling points of the two compounds, the separation by conventional cryogenic distillation is impractical, which is further complicated by the formation of azeotropic compositions of NF_3 and CF_4 mixtures [11]. The efficiency of distillation as separation method could however be improved, according to Miller *et al.* [11], through the use of entraining, or extractive agents such as HCl that forms an azeotropic mixture with CF_4 under specific conditions. This azeotropic mixture has a lower boiling point at a given pressure than the two components would have had separately, thus effectively

increasing the relative volatility of NF_3 with respect to CF_4. Although an improvement in separation efficiency has been achieved through this approach, the distillation process remains relatively inefficient, requiring typically 120 stages in the distillation column, which is operated at approximately -90°C and elevated pressures.

It is therefore apparent that a need exists for the development of alternative separation techniques for the purification of NF_3 from CF_4, which up until now have been dominated by rather inefficient, energy-intensive processes. One such alternative includes the use of membrane technology, as is motivated in the following section.

1.2 Justification

A membrane can be described as a selective layer that regulates the permeation, by a certain mechanism, of components that contact the membrane to varying degrees, thereby facilitating separation of the components [19]. Rapid advances have been made in membrane science and technology since the 1960's, with the first significant industrial application being gas separation of hydrogen and other gases, as well as the separation of nitrogen from air [19], which emerged during the 1980's. Another major successful application of membranes is the dehydration of ethanol, which overcame the difficulties of azeotrope formation encountered during conventional distillation [19, 20], yielding a separation process that is more efficient in terms of energy requirements.

Following the discussion in Sec. 1.1, economical aspects are a large driving force for the development of alternative processes for the challenging NF_3/CF_4 separation, in which the development of a suitable membrane process can thus be beneficial to reduce the cost of VLSI-grade NF_3 production. This is relevant with respect to the current separation methods of i) adsorption using zeolite adsorbents where NF_3 is selectively adsorbed (undesirably so), which demand high energy requirements to release the captured NF_3 from the adsorbents [10], while ii) cryogenic distillation has obvious economical disadvantages. Thus, efficient and economically viable alternatives of separation, such as a suitable membrane process, would be beneficial. Membrane systems have been used relatively recently for the separation and recovery of PFCs from CVD chamber cleaning operations [8]. CF_4 is one such gas that could be recovered using membranes with specific properties to attain separation [21], whereas no literature evidence could be found regarding NF_3/CF_4 membrane separation.

Thus, investigating the membrane separation of NF_3 and CF_4 has potential economic as well as scientific benefits, since:

i. The potential of contributing to the development of an efficient membrane separation process as an alternative to the conventional and emerging purification processes exists;
ii. Theoretical insight into various aspects that determine membrane selectivity towards NF_3 and CF_4 can be established that can aid in further development, should this route be found to be a viable alternative.

Since the majority of membrane gas separations are done using non-porous polymeric membranes [19], this study will also focus on the use of non-porous polymeric membranes for the separation of NF_3 and CF_4.

1.3 Aim and Objectives

The aim of this thesis was to evaluate the use of solution-cast perfluoropolymer membranes for the membrane based gas separation of NF_3 and CF_4. For this purpose, the high free volume, glassy perfluoropolymers Teflon AF2400, Teflon AF1600 and Hyflon AD60 were used as membrane materials, and to attain the aim of this thesis, the main objectives were:

i. To provide experimental evidence of the permeability selectivity offered by these perfluoropolymer membranes towards NF_3 and CF_4,
ii. To provide a theoretical explanation for the observed permeability selectivity w.r.t. the solubility and diffusivity of the two gases in these perfluoropolymers, and
iii. To determine, at least semi-quantitatively, whether membrane gas separation using high free volume, glassy perfluoropolymers can, in principle, be used for the purification of NF_3 to meet the purity specifications w.r.t. CF_4.

1.4 Structure of this Thesis

In this chapter (Chapter 1) a brief overview of the importance of NF_3 and CF_4 separation was discussed and a justification for investigating the use of membrane based gas separation of NF_3 and CF_4 was given together with the aim and objectives of this thesis. To address these objectives, the different empirical components of this thesis are presented in article format in Chapters 2 – 4, which can briefly be summarized as follows:

- Chapter 2 describes the development of a robust dual-channel gas chromatographic (GC) method for the quantification of a wide range of NF_3 and CF_4 concentrations. This was a necessary component of the research, to ensure that the custom built experimental setup that was used (described in Appendix A) could be successfully implemented to measure both the pure and mixed gas permeabilities and selectivities of the different perfluoropolymer membranes that were studied.
- In Chapter 3, the separation of NF_3 and CF_4 using high free volume, glassy perfluoropolymer membranes of Teflon AF2400, Teflon AF1600 and Hyflon AD60 that were prepared by solution casting is investigated, in which the newly developed GC method described in Chapter 2 was used to measure pure and mixed gas NF_3 and CF_4 permeabilities and selectivities. In addition, helium and nitrogen pure gas permeability and ideal selectivities were used to characterize the quality of the solution cast polymer films, and it is shown that the performance of the membranes is significantly influenced by swelling induced by residual casting solvent.
- In Chapter 4, the experimentally obtained permeability selectivities was correlated with the diffusion and solubility selectivities of Teflon AF2400 and Teflon AF1600, which were calculated from molecular dynamics (MD) simulation results, and statistical thermodynamics calculations. As such, the mechanism of preferential NF_3 permeation by the perfluoropolymers, as described in Chapter 3, was evaluated according to the solution-diffusion transport model [18].

Finally, the research conducted for this thesis was evaluated in Chapter 5. Considering the experimentally determined pure and mixed gas permeability and selectivity values of the glassy perfluoropolymer membranes w.r.t. NF_3 and CF_4, two different membrane separation configurations for the enrichment of NF_3 are proposed in Chapter 5. These multi-step, multi-stage designs are semi-quantitatively evaluated, from which it becomes apparent that purification of NF_3 from CF_4 via membrane separation can be an economically viable alternative. Further research into improving the NF_3 permeability of polymer membranes is, however, recommended to further optimize the efficiency of the method.

1.4 References

1. P.B. Henderson, A.J. Woytek, Fluorine compounds, inorganic, nitrogen, in: Kirk-Othmer Encyclopedia of Chemical Technology, John Wiley & Sons, New York, 5th ed., 2010, Vol.11, pp. 852 - 858.
2. A.J. Woytek, J.T. Lileck, Preparation of nitrogen trifluoride, U.S. Pat. 4,091,081 (1987).
3. R. Herkelmann, Handling and security in the synthesis and purification of nitrogen trifluoride, J. Fluor. Chem. 54 (1991), 37.
4. A. Tasaka, Electrochemical synthesis and application of NF_3, J. Fluor. Chem. 128 (2007) 296 – 310.
5. D.P. Satchell, NF_3 production reactor, U.S. Pat. 7,128,885 B2 (2006).
6. K. Koike, T. Fukuda, S. Fujikawa, M. Saeda, Study of CF_4, C_2F_6, SF_6 and NF_3 decomposition characteristics and etching performance in plasma state, Jpn. J. Appl. Phys. 36 (1997) 5724 – 5728.
7. N.J. Ianno, K.E. Greenberg, J.T. Verdeyen, Comparison of the etching and plasma characteristics of discharges in CF_4 and NF_3, J. Electrochem. Soc. 128 (1981) 2174 – 2179.
8. J.G. Wijmans, Z. He, T.T. Su, R.W. Baker, I. Pinnau, Recovery of perfluoroethane from chemical vapor deposition operations in the semiconductor industry. Separ. Purif. Technol. 35 (2004) 203 – 213.
9. US EPA, 2009. Inventory of U.S. greenhouse gas emissions and sinks: 1990 – 2007, US EPA, Washington, DC, USA.
10. R.R. Singh, M.R. Paonessa, D.F. Orlowski, Purification of Nitrogen trifluoride, U.S. Pat. 7,384,618 B2 (2008).
11. R.N. Miller, C.-P.C. Kao, B.A. Mahler, Process for purifying perfluorinated products, U.S. Pat. 6,458,249 B2 (2002).
12. D.G. Cronell, T.H.-L. Hsiung, H.P. Whithers, A.J. Woytek, Process for nitrogen trifluoride synthesis, U.S. Pat. 5,637,285 (1997).
13. D.P. Satchell, J.P. le Roux, Method and apparatus for the production of nitrogen trifluoride, U.S. Pat. 6,986,874 B2 (2006).
14. M. Aramaki, Y. Kobayashi, T. Nakamura, H. Nakano, T. Suenaga, Process of preparing nitrogen trifluoride by Gas-solid reaction. U.S. Pat. 4,543,242 (1985).

15. T. Suenaga, T. Fujii, Y. Kobayashi, Method of refining nitrogen trifluoride gas, U.S. Pat. 5,069,887 (1991).
16. S.M. Igumnov, V.P. Kharitonov, N.V. Kharitonova, Method of purifying gaseous nitrogen trifluoride, U.S. Pat. 7,022,160 B2 (2006).
17. W. Braker, A.L. Mossman, Matheson gas data book, Matheson, 6th ed., 1980.
18. P.B. Henderson, C.G. Coe, D.E. Fowler, M.S. Benson, Process for kinetic gas-solid chromatographic separations, U.S. Pat. 5,069,690 (1991).
19. R.W. Baker, Membrane technology, in: Kirk-Othmer Encyclopedia of Chemical Technology, John Wiley & Sons, New York, 5th ed., 2010; Vol.15, pp 796 - 852.
20. R.W. Baker, Membrane technology and applications, John Wiley & Sons, Chichester, 2nd ed., 2004.
21. T.C. Merkel, V.I. Bondar, K. Nagai, B.D. Freeman, I. Pinnau, Gas sorption, diffusion and permeation in poly(dimethylsiloxane), J. Polym. Sci. Pol. Phys. 38 (2000) 415 – 434.

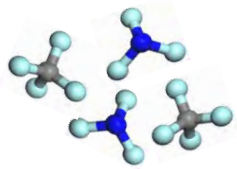

Chapter 2

A Compact dual-channel GC method for multi-level quantification of mixtures of NF_3 and CF_4

Abstract

A dual-channel gas chromatographic method is described in this paper that can be conveniently used for multi-level quantification of mainly NF_3/CF_4 mixtures with a Thermal Conductivity Detector (TCD) on one channel and a Pulsed Discharge Helium Ionisation Detector (PDHID) on a second channel for low-level quantification. It is shown that adequate separation is achieved on both channels with this dual single-column setup in which column switching as used for NF_3/CF_4 analysis in industrial chromatographic methods are not required, thus yielding an effective analysis method for laboratory-scale investigations. In addition, the use of packed columns with purified divinylbenzene-styrene co-polymers as the sole stationary phase yields satisfactory resolution between NF_3 and CF_4 at isothermal conditions of 30 °C, with elution times of less than 8 min on the TCD channel and less than 4 min on the PDHID channel. Consequently, this method allows for reliable, straight-forward quantification of NF_3/CF_4 mixtures, which is necessary when studying the commercially important problem of NF_3 and CF_4 separation by different methods. Therefore, the applicability of the method to studying membrane separation of NF_3 and CF_4 is briefly discussed and illustrated, for which the dual-channel setup is especially beneficial.

Keywords: NF_3 quantification, CF_4 quantification, Separation of NF_3 and CF_4, Pulsed discharge helium ionization, Super Q.

2.1 Introduction

Nitrogen trifluoride (NF_3) is a highly oxidising gas and serves as a convenient fluorine source, having many safety advantages over the use of elemental fluorine (F_2) as it is less reactive at normal temperatures and pressures [1], can be pressurized to pressures higher than F_2, and can be condensed [2, 3], facilitating transport and storage. NF_3 can be dissociated to form reactive fluorine radicals and various gas-phase species via thermal or plasma dissociation [1, 4],

which can then be used in various applications that require a fluorinating agent such as etching and patterning of sapphire [5] and high temperature fluorination reactions [6, 7]. NF_3 has also been used in hydrogen and deuterium fluoride (HF/DF) high energy chemical lasers wherein NF_3 acts as the fluorine source, reacting with H_2 and D_2 to form HF and DF whereby a high fraction of the energy being released upon reaction can be converted to laser radiation [1]. In addition, NF_3 has recently been shown to be a viable substitute to the much more hazardous and aggressive fluorinating agents HF and F_2 for the production of UF_6 from UO_2, wherein UF_6 is required for uranium enrichment [8]. NF_3 has its principal use, however, in the electronic and semiconductor manufacturing industry as dry etchant for plasma etching of silicon wafers and plasma assisted cleaning of chemical vapour deposition chambers used in electronic device manufacturing [1, 4, 9, 10].

While perfluorocarbon gases (PFCs) such as carbon tetrafluoride (CF_4), and perfluoroethane (C_2F_6) have also been used as electronic etching gases, it has been shown that NF_3 exhibits superior etching performance compared to PFCs (especially CF_4), mainly because NF_3 dissociates much more efficiently, yielding higher etching rates, while also excluding the formation of carbonaceous residues [10, 11]. Thus, to enhance productivity and to avoid defect formation during high density integrated circuit manufacture processes it is necessary to use NF_3 of exceptionally high purity, i.e. VLSI-grade NF_3 (very large scale integration), where the CF_4 content must be lower than at least 20 ppm [12] to avoid the formation of carbon-containing particulates. During NF_3 production however, CF_4 is introduced into the product stream as a result of using carbon anodes in a fluorine-rich environment during the electrochemical conversion of the NH_4F –species [9, 13]. Electrochemical synthesis routes in which nickel anodes are used to eliminate the CF_4 contamination problem has also been investigated, although the method suffers from some serious drawbacks [9, 14]. With the high demand placed on VLSI-grade NF_3 by the electronic industry, and the almost unavoidable CF_4 contamination problem, separation of the two gases has become mandatory. However, separation of the two gases has proven to be a challenging affair, with only a few processes being patented [12, 15, 16], albeit with some economical and technical disadvantages.

Studying the separation of NF_3 from CF_4 by different methods therefore has much to offer both from an academic and technical point of view. However, for this a reliable and robust method of NF_3/CF_4 quantification to determine the efficiency of separation is required, regardless of the separation method being investigated. Gas chromatography (GC) can be

conveniently applied for this purpose, where de Coning and Swinley [17] have developed a dual-channel column sequence reversal method to quantify trace amounts of CF_4 and other impurities present in NF_3 matrices to determine NF_3 purity within a production environment. This method however, does not allow simultaneous quantification of NF_3 and CF_4 as the NF_3 matrix is separated from the impurities during the column sequence reversal method. Yang *et al.* [18] have also reported a GC method to determine the abatement and removal efficiency of NF_3 and other PFCs from the exhaust streams of semiconductor manufacturing plants using a multi-column analysis system, although upon closer inspection some of their chromatographic results seem to differ from that of de Coning and Swinley (see Sec. 2.3.1). This multi-column method of Yang *et al.* did not yield good separation of CF_4 from air, and produced rather broad NF_3 peaks, which is not desirable.

Therefore, the need for a robust GC method for direct quantification of NF_3/CF_4 mixtures needs to be addressed, and given that the methods mentioned above are not exactly suited for this purpose, this paper describes a simplified dual channel GC method for multi-level quantification of NF_3/CF_4 mixtures. The possibility exists to extend the method relatively easily to accommodate other analytes as well, for example SF_6, NO_2, C_2F_6, and C_3F_8. Chromatographic results of various analytical columns that were screened for NF_3/CF_4 resolution are also presented, thereby elucidating the behaviour of NF_3 and CF_4 on various stationary phases reported previously.

2.2 Materials and Methods

2.2.1 Materials

Nitrogen trifluoride (NF_3), certified to be 99.99 vol% pure was purchased from Linde Electronics South Africa (Pty) Ltd. (LESA Grade) was used for screening, calibration and method optimization purposes. Tetrafluoromethane (CF_4) with a purity of ca. 99 vol% (kindly provided by Applied Chemistry, Necsa) was used for screening of the different packed columns investigated in this study, while CF_4 with a certified purity of 99.99 vol%, purchased from Air Liquide, Germany GmbH, was used for method optimization and calibration. The following gases were also used for column screening purposes: Nitrogen (N_2) with a purity of 99.999 vol%, oxygen (O_2) with a purity of 99.999 vol%, and carbon dioxide (CO_2), technical grade, with a purity of 99.995 vol%, all purchased from Afrox, South Africa, and methane

(CH_4), with a purity of 99.95 vol%, purchased from Air Liquide, South Africa. Helium with a purity of 99.999 vol% was purchased from Afrox South Africa, and was used as carrier gas on both channels of the current GC system, and also for flushing of the system.

A static gas mixture containing ca. 350 vppm NF_3 and CF_4 each, in a matrix of helium, was prepared in-house as such a mixture was not readily available commercially and was used for the calibration of the Pulsed Discharge Helium Ionisation Detector (PDHID). Blending was achieved through expansion of a calibrated volume, filled with a mixture of NF_3 and CF_4 (with equal partial pressures), to an evacuated, helium-purged, cylinder of known volume, and subsequent filling with helium to the desired pressure. The exact concentrations of NF_3 and CF_4 were then determined using the Thermal Conductivity Detector (TCD) with a 5mL sample loop as described in more detail in Sec. 2.3.2.

The following stationary phases were screened for NF_3/CF_4 resolution, all of which were packed in stainless steel columns of 3.2 mm O.D. by the suppliers and all obtained through Scientific Supplies Services, South Africa: A 1.5 m molecular sieve 5A (80/100 mesh) and a 1 m Molecular Sieve 13X (80/100 mesh) both from Supelco; a 2 m ShinCarbon ST (80/100 mesh) from Restek; a 4 m Hayesep N (100/120 mesh), a 4 m Super Q (80/100 mesh) and a 2 m Super Q (100/120 mesh) all from Alltech. The two 4 m columns consisted of two 2m columns of each that were coupled in series, effectively yielding 4 m-long columns. All columns were conditioned overnight at a few degrees Celsius below the maximum allowable temperature of each column under a constant flow of 99.999 vol% helium. In the case of analyses on the PDHID channel (Channel A, Fig. 2.2), the 2 m Super Q (100/120 mesh) column that was used was flushed with purified helium from the gettering system for a few minutes before any samples were injected, in addition to the conditioning as described above.

2.2.2 Instrumentation

A partial piping & instrumentation diagram (P&ID) of the custom-built plumbing system used in this study is shown schematically in Fig. 2.1. It should be noted that the code of practice for nitrogen trifluoride [19] should always be adhered to when working with NF_3. Thus, for this system, stainless steel tubing and fittings were used throughout, while the construction materials of all valves, regulators and controllers were chosen specifically to be compatible with NF_3. Brooks thermal mass flow controllers (from Brooks Instrument, Holland) were used

to control the flow rate of the gases. The pressure applied across both sample loops (Sec. 2.3.2) was measured using an electronic pressure transducer from Wika, Germany, with a span of 0 – 2.5 bar.

An Agilent 7890A GC system (firmware Rev. A.01.10.2) from Agilent Technologies, USA, equipped with a Thermal Conductivity Detector (TCD) and a custom-installed Valco D-3 PDHID from VICI, Houston, TX, USA, was used. The Agilent ChemStation software (Rev. B.04.02 [96]) was used for all GC data acquisition and analysis. A section of the plumbing diagram of the dynamic sampling system used for calibration is shown in Fig. 2.2.

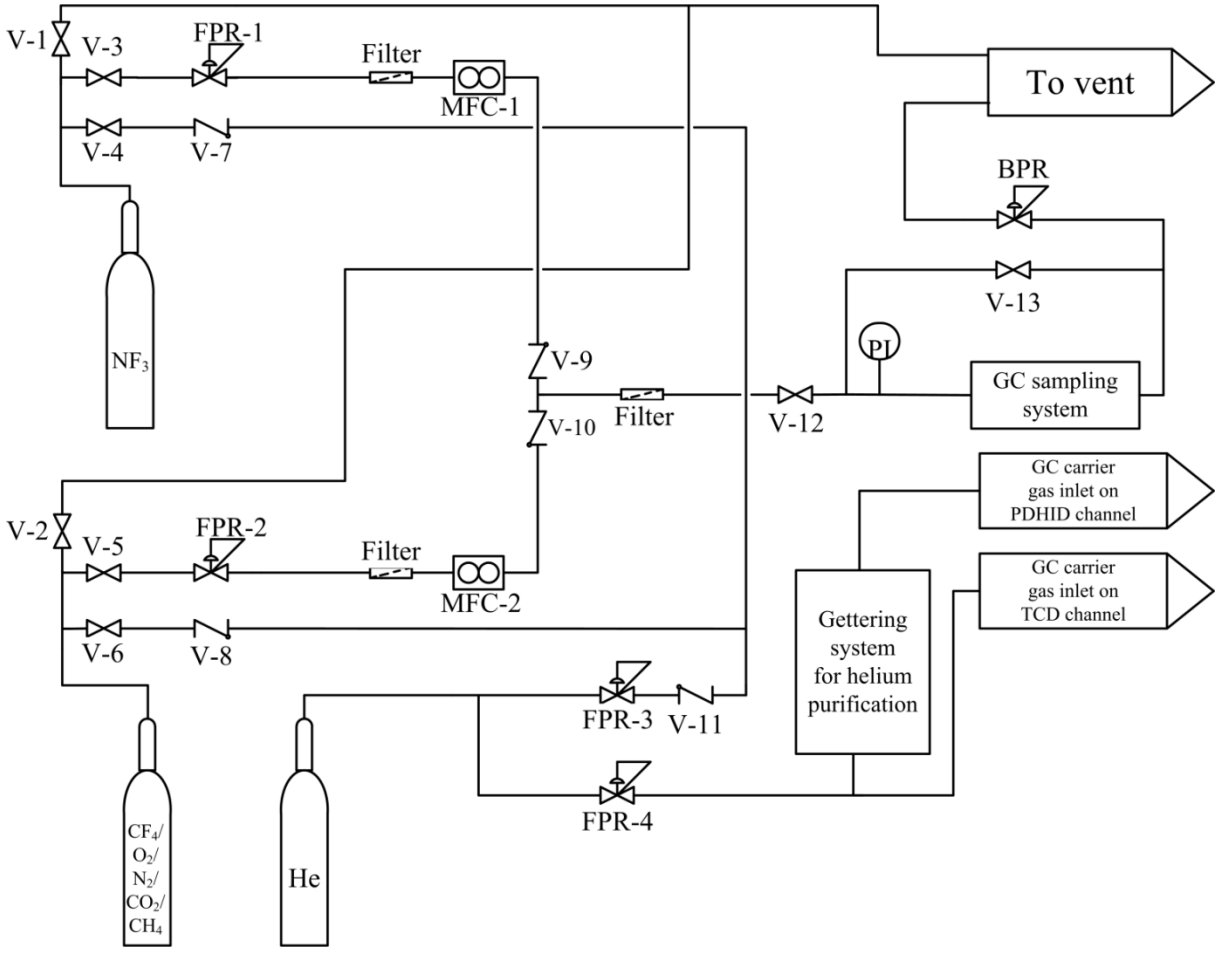

Figure 2.1: Piping and instrumentation diagram of the system used to develop the current GC method. FPR designates a forward-pressure regulator, and BPR a back-pressure regulator, valves V-7, V-8, V-9, V-10, and V-11 represent one-way valves, MFC-1 and MFC-2 indicates the mass flow controllers while PI represents an electronic pressure indicator.

For analysis pneumatically actuated 10-port Valco sampling valves from VICI, were used on both channels that were connected in series, where the sampling valve on the PDHID channel was equipped with a helium purged-housing, also from VICI, that was used to prevent the ingress of air. Helium that was purified with an in-line mini gettering system (also from VICI), as shown in Fig. 1 was used for the PDHID ionisation gas, the feed to the. helium-purged–housing and as the carrier gas on the PDHID channel. The gettering system consists of a zirconium alloy that is heated to a constant temperature which removes oxygen and other impurities from the 99.999 vol% helium fed to the purifier thereby producing helium with a purity in the order of 99.9999 vol%.

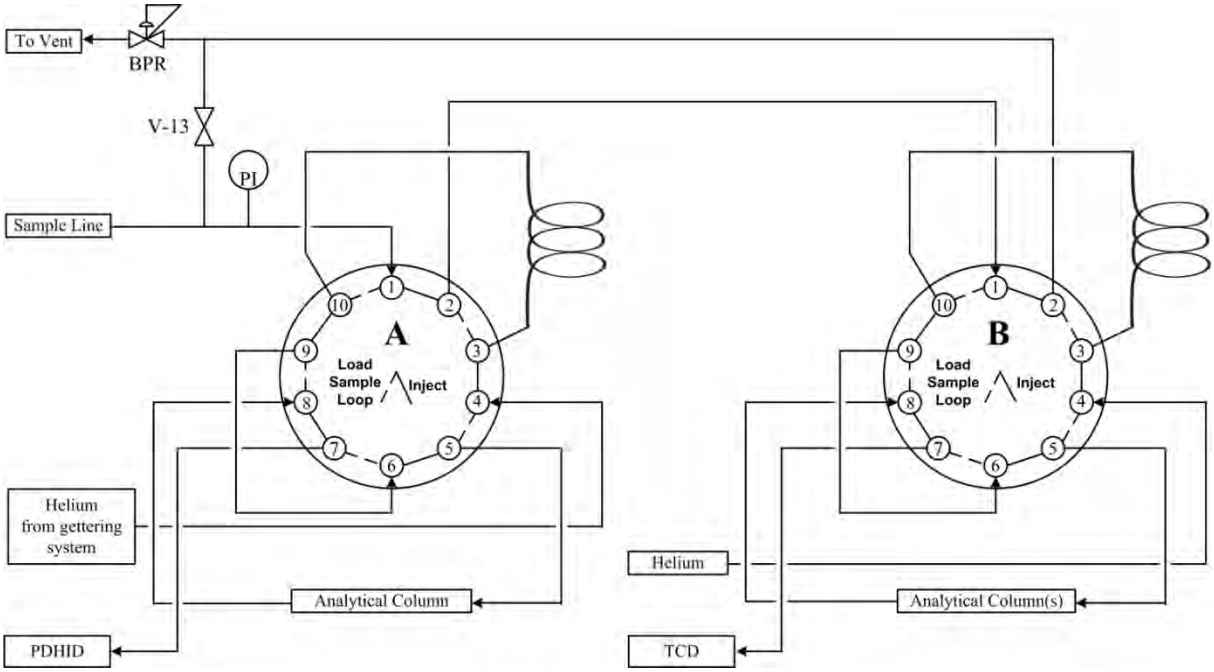

Figure 2.2: Dual-channel GC dynamic sampling system used in this study. Sampling valve A was equipped with a helium purged-housing. Note that although 10-port sampling valves were used in this study, these can be replaced with 6-port sampling valves. Both sampling valves (and sample loops) were temperature controlled.

The flow rate of the purified helium from the gettering system to the PDHID and the purged-housing was controlled using in-line restrictors, where the helium carrier flow rate and pressure on both channels were controlled using the built-in inlet system on each channel that allows for the optimization of column pressure and carrier flow in addition to other GC parameters. The use of an in-line restrictor to control the flow of purified helium to the PDHID facilitates a stable base-line, as the PDHID response is flow-sensitive [17]. The

implementation of a dual-channel system as described here allows for versatile, multi-level quantification while also permitting individual optimization of GC parameters on each channel.

2.2.3 Analysis

For all analyses, both detector temperatures were kept constant at 200 °C, where the TCD reference flow was set at 20 mL/min helium and, the flow of purified helium to the PDHID was controlled using an in-line restrictor. In all cases, the sampling valves were switched at the start of a run to inject test and calibration samples, and were only switched back near the end of the run. In all cases, samples were injected using the splitless mode, where both sampling valves were kept in a temperature-controlled environment. Because packed columns were investigated, the carrier gas pressure was used as the control variable, although the carrier gas flow rate could also be adjusted.

For column screening, qualitative analyses were performed on the TCD channel (Channel B, Fig. 2.2) using a sample loop of 10 μL, where gas samples of the respective pure gases were injected at a gauge pressure of 50 kPa. In the case of NF_3 and CF_4, mixtures of the two pure species were injected, where these mixtures were produced by mixing the gases dynamically in a 50:50 molar ratio, in terms of the volumetric flow rate, controlled by the respective mass-flow controllers (MFCs) as shown in Fig. 2.1. Three consecutive runs were performed at the reported conditions (Table 2.1) for each of the tested columns for each gas species (O_2, N_2, CH_4, and CO_2) and the NF_3/CF_4 mixture to ensure that repeatable results could be obtained. The position of both the NF_3 and CF_4 peaks on each chromatogram were determined by injecting pure samples of each gas, which was also repeated three consecutive times.

2.2.4 Calibration

Pure NF_3 and CF_4 were dynamically mixed to obtain a constant 50:50 molar ratio using the MFCs and setup shown in Fig. 2.1 for both qualitative and quantitative analysis. However, no further blending or dilution of the mixture was performed for the determination of column resolution, repeatability and linearity. Instead, both detectors' simultaneous response to NF_3 and CF_4 in the present dual-channel method were tested for linearity in terms of the total number of moles injected using specific sample loop volumes while varying the pressure

applied across these sample loops. The same procedure was also used for varying the number of moles of both NF_3 and CF_4 in the static gas mixture containing ca. 350 vppm of each in a helium matrix (Sec. 2.2.1) for calibration and testing the repeatability of the PDHID channel. The discussion in Sec. 2.3.2 can be consulted for a motivation for the use of the number of moles as quantification parameter.

In all cases the pressure applied across the sample loops was controlled by careful manipulation of the back-pressure regulator and valve V-13 (Fig. 2.1 and Fig. 2.2) using the following basic procedure. First, valve V-13 and the back-pressure regulator was fully opened, resulting in the flow thus mostly bypassing the constricted sampling system. Hereafter, the back-pressure regulator was used to set the pressure of the sampling system to the desired value as measured with the electronic pressure transducer. Sufficient time was hereafter allowed (more than 10 minutes) to reach both steady state flow and adsorption equilibrium between the tubing walls and the process fluid. Subsequently valve V-13 was either closed or only throttled; resulting in an increase in pressure as was measured using the pressure indicator. The increased pressure thus forced flow through the sampling system, flushing the sample loops and connecting tubing. After flushing the sample loops, V-13 was again opened, resulting in the pressure in the sample loops returning to their original value. Hereafter, V-13 was slowly closed until a rise in pressure of only approximately 0.5 kPa was measured on the pressure indicator, thus ensuring that only a small portion of the flow is throttled through the sample loops at the desired pressure setting, while simultaneously minimizing the pressure drop across the sampling system. After allowing for steady state flow and adsorption equilibrium to be achieved at the specific sampling pressure (after at least 10 minutes), the appropriate sampling valve was actuated, resulting in the calibration sample (of constant composition) with a specific total number of moles being injected.

For all calibrations, the sampling valves and sampling loops on both channels were temperature controlled to 80 °C to minimise possible adsorption effects. The temperature of the sample loops was measured directly with a thermocouple. The temperature of the helium carrier gas on the inlet of both channels was also controlled at 80 °C to prevent/limit any possible adsorption of the injected sample on the walls of the inlet tubing before the sample has reached the analytical columns. A 5 µL sample loop was used on the TCD channel to calibrate the TCD with the dynamically blended NF_3/CF_4 sample stream of constant composition. A 50 µL sample loop was used on the PDHID channel to calibrate the PDHID

with the ca. 350 vppm NF_3/CF_4 mixture in a helium matrix (Sec. 2.2.1) after determining the exact concentrations of NF_3 and CF_4 in this mixture using the calibrated TCD channel with a sample loop with a volume of 5 mL. The sample loop volumes were varied to account for the much smaller concentration of the analytes in the case of the 350 vppm mixture compared to the sample stream when calibrating the TCD channel.

2.3 Results and Discussion

2.3.1 Column Screening

The main objective in this study was to develop a robust method for the resolution and analysis of NF_3 and CF_4. However, common impurities (or co-analytes) that can be present in both of these gases include O_2, N_2, CO, CH_4, CO_2, NO_2, and SF_6 [17, 18]. Therefore, the columns tested in this study were also screened for O_2 and N_2 (representing the lighter impurities), CH_4 and CO_2 (representing the heavier, condensable impurities) to determine whether any of these impurities would interfere with the quantification of NF_3 and CF_4, especially when analysis is to be performed on the PDHID channel. A summary of the GC parameters used for screening of each column is given in Table 2.1. These parameters were obtained by varying column pressure, carrier flow and column temperature and selecting those that gave a reasonable trade-off between peak widths, NF_3/CF_4 resolution and retention times.

Table 2.1: Summary of GC parameters used for screening of the different stationary phases.

Stationary Phase	Column Temperature (°C) *	Column Pressure (kPa)	Carrier Flow Rate (mL/min)	Sample loop Temperature (°C)
MS-13X	30	150	45	30
MS-5A	100	200	45	100
ShinCarbon ST	65	150	30	65
Hayesep N	30	85	30	30
Super Q	30	85	30	30

* Isothermal

Since zeolite molecular sieves are used industrially to purify NF_3 from CF_4 via adsorption [15], molecular sieves MS-5A and MS-13X were chosen because they have been used previously in GC methods for resolving analyte mixtures containing NF_3 and CF_4 [17, 18]. The chromatographic separation performance of these molecular sieves towards NF_3 and CF_4 specifically, however, remains unclear and therefore needed to be elucidated. It has been shown that carbon molecular sieves, particularly the polyacrylonitrile-based adsorbent known as Carbosphere with a high surface area of 500 to 1500 m^2/g [16], show good selectivities toward NF_3 and CF_4, where CF_4 is reportedly adsorbed more selectively than NF_3 in contrast to zeolite molecular sieves (such as MS-5A and MS-13X). ShinCarbon ST, also a carbon molecular sieve, is known to yield good resolution for a range of condensable and non-condensable gases [20], and for this reason, it was also included in this study. Hayesep N and Super Q both consist of a porous divinylbenzene-styrene co-polymer adsorbent, with Super Q having been marketed in the past as a purified form of the well-known Porapak Q stationary phase which is equivalent to the purified Hayesep porous polymer packings offered by Valco Instruments Co. Inc. In addition, Super Q, along with Hayesep Q and Hayesep D, are much less polar than the Hayesep N formulation, according to the manufacturer (Valco Instruments Co. Inc.), and comparison of the performance of Super Q and Hayesep N towards resolution of NF_3 and CF_4 therefore needed to be investigated. Also, it was evident from the results of de Coning and Swinley [17], that Hayesep Q coated with krytox, configured in a column sequence reversal method, was successful at resolving the trace impurities CF_4, CO_2, SF_6, and NO_2 in an NF_3 matrix [17]. The krytox liquid phase (a fluorocarbon oil) was used to increase the retention of NF_3 and CF_4 so that these compounds eluted last in their column sequence reversal method whereby the NF_3 matrix was vented before reaching the detector. In the present study, the divinylbenzene-styrene co-polymer stationary phase, in the form of Super Q and Hayesep N, was thus investigated for NF_3/CF_4 resolution without the use of the fluorocarbon liquid phase.

The use of silica gel as a stationary phase for chromatographic separation of NF_3 and CF_4 has been reported in the past by Richmond [21], where the packing was coated with 10% halocarbon oil. Yang *et al.* [18] however, obtained inadequate resolution between NF_3 and CF_4 with this stationary phase, in the form of a shorter column free of the halocarbon oil liquid phase and with a smaller particle size packing than the one used by Richmond [21]. Silica gel as stationary phase was therefore not included in this study. It would appear, however, that the use of a halocarbon liquid phase [17, 21] improves the retention of NF_3 on

the silica gel stationary phase, which also seemed to be the case with the Haysep Q stationary phase used by de Coning and Swinley [17] as discussed above. In the present study, however, no additional fluorocarbon liquid stationary phase was used in an attempt to simplify the analytic method as much as possible.

The results of the MS-13X column presented in Fig. 2.3(a) is consistent with that of de Coning and Swinley [17] who analysed for trace amounts of O_2, N_2, CO, and CH_4 in an NF_3 matrix on one channel of their dual-channel method [17], and back-flushed NF_3 and CF_4 from the column before these compounds eluted. If CO was present, it would have eluted just after CH_4 in the chromatogram of Fig. 2.3 (a), whereas it is clear that no separation is obtained between NF_3 and CF_4 on the MS-13X column. The results of Yang *et al.* [18], however, are contradictory to these collective results where they found that CF_4 eluted very early, before O_2 and N_2, with NF_3 eluting as a broad peak at approximately 6 – 8 min. The inability of MS-13X to separate NF_3 and CF_4 was confirmed by pure-gas chromatograms of NF_3 and CF_4, the results of which are not shown. It is however clear that excellent resolution is achieved between the light compounds O_2, N_2 and CH_4, as is typical for the MS-13X and MS-5A stationary phases [17]. The heavier CO_2 adsorbs semi-irreversibly on these two stationary phases, and therefore this compound could not be analyzed with the MS-13X and MS-5A columns.

Apart from satisfactory resolution between the light compounds O_2, N_2, and CH_4 also being obtained on the MS-5A column (Fig. 2.3 (b)), only partial resolution between CF_4 and NF_3 was obtained. Also, CF_4 eluted as a very broad peak that overlapped with the light "impurities" O_2, N_2, and CH_4 with significant tailing that caused poor resolution between NF_3 and CF_4. This result was confirmed (results not shown) even when using different MS-5A columns with different lengths (1 and 2 m) and particle sizes (80/100 and 100/120 mesh), and by adjusting the column temperature (from 30 to 200 °C), column pressure (from 85 to 350 kPa) and carrier flow (from 30 to 150 mL/min). These results seem similar to those obtained by Yang *et al.* [18], who used a 2 m column with a mesh size of 60/80 (larger particle size), which apparently resolved the issue of the CF_4/NF_3 pair eluting with O_2 and N_2, although tailing remained a problem. The tailing of the CF_4-peak shown in Fig. 2.3(b) suggests that CF_4 desorbs slowly from the MS-5A stationary phase although adsorption of CF_4 is slightly less favored than that of NF_3 and therefore elutes first. Desorption of the adsorbed CF_4 fraction in turn seems to be strongly concentration dependent, resulting in the CF_4

concentration in the mobile phase to slowly return to zero. These chromatographic results therefore also illustrate that the MS-5A adsorbent does not discriminate very well between NF_3 and CF_4, and is therefore also not particularly efficient at purifying NF_3 from CF_4 [15, 16].

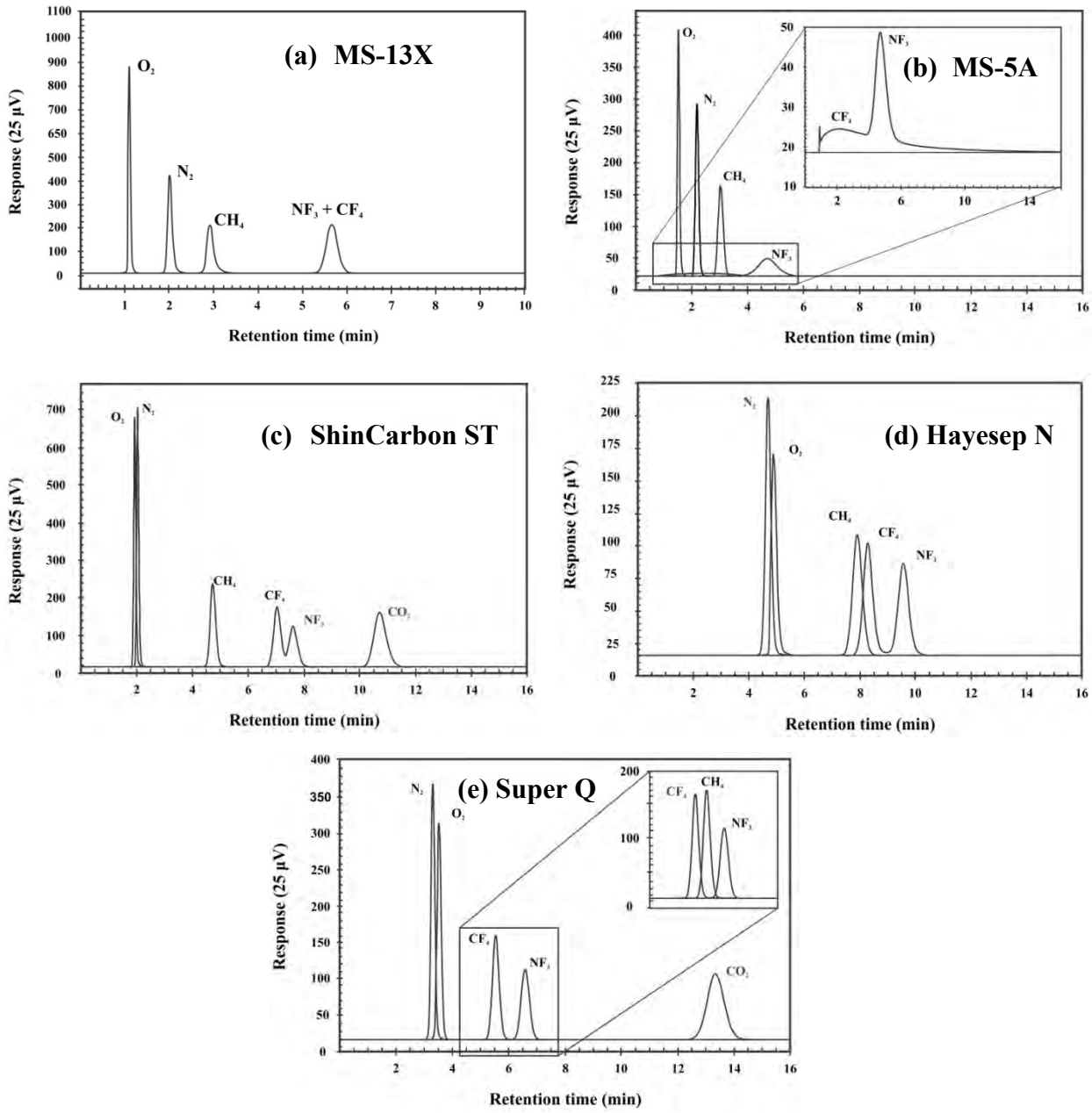

Figure 2.3: Chromatograms of N_2, O_2, NF_3, CF_4 and CO_2 for packed columns with (a) MS-13X, (b) MS-5A, (c) ShinCarbon ST, (d) Hayesep N and (e) Super Q stationary phases. N_2, O_2 and CO_2 were analysed as pure gases, NF_3 and CF_4 were mixed dynamically in a 50:50 ratio. The chromatograms from the NF_3/CF_4 mixtures and the other pure gases were superimposed to produce these chromatograms. Analysis was performed on the TCD channel, with 540 nmol injected for N_2, O_2, CH_4 and CO_2 and 270 nmol injected for NF_3 and CF_4.

Compared to the MS-13X and MS-5A columns, the ShinCarbon ST column (Fig. 2.3 (c)) performed better in terms of NF_3/CF_4 separation, but still, only partial resolution was obtained, although NF_3 and CF_4 were well separated from CH_4 and other possible impurities. Also, as confirmed by pure-gas chromatograms (results not shown), CF_4 still elutes before NF_3 on the ShinCarbon ST stationary phase as was observed for the zeolite molecular sieves, and not inversed as had been anticipated on the basis of the stronger adsorption affinity of Carbosphere towards CF_4 [15, 16]. However, unlike the zeolite molecular sieves, which adsorbs CO_2 semi-irreversibly, this component eluted after approximately 10 min, in which other condensable compounds such as SF_6 and NO_2 will probably have similar elution times.

A representative chromatogram obtained with the Hayesep N column (Fig. 2.3 (d)) shows that the NF_3/CF_4 resolution improved compared to that achieved with ShinCarbon ST, although complete separation between the peaks was not possible, which could probably be achieved using a smaller particle size packing and by either shortening the column length or increasing the column pressure. These variations were, however, not tested in this study. It is apparent from Fig. 2.3 (d) that CH_4 and CF_4 overlapped on this column, implying that this configuration will not be suitable for low-level analysis, with for example a PDHID, in which an appreciable number of CH_4 is present in a diluted matrix of NF_3 and CF_4. In addition, CO_2 and other heavier compounds such as SF_6 and NO_2 elute much later through this stationary phase, as a broad, flat peak which does not lends itself to quantify such impurities, if present in an NF_3/CF_4 mixture.

Comparison of the representative chromatogram of Super Q (Fig. 2.3 (e)) it is clear that the best (and fastest) separation between NF_3 and CF_4 was achieved on this stationary phase, with the only disadvantage that CH_4 (when present) eluted between CF_4 and NF_3, overlapping partially with both peaks as shown in the insert in Fig. 2.3 (e). An advantage however of this stationary phase is that CO_2 elutes relatively early without any exceptional peak broadening, which allowed de Coning and Swinley [17] to use Hayesep Q (assumed here to be analogous to Super Q) in a column sequence reversal method whereby CO_2, SF_6 and NO_2 reached the detector first, as these compounds were only passed through one analytical column. In contrast, CF_4 and CH_4 contained within the NF_3 matrix passed through a second analytical column and through the first analytical column again through careful valve switching so that the NF_3 matrix eluted last before being vented by heart-cutting. Consequently, CF_4 and CH_4 eluted just before the NF_3 matrix, in accordance with the results presented in Fig. 2.3 (e). The

use of two 4 m 150/180 mesh Hayesep Q columns in the column sequence reversal configuration by de Coning and Swinley presumably yielded the necessary column capacity for separation of the analytes in the presence of the NF_3 matrix, while the additional 10% krytox coating possibly improved the retention of NF_3 to ensure adequate resolution between CF_4, CH_4, and the NF_3 matrix. Although the authors did not stipulate the carrier gas parameters, a high carrier flow was probably used to prevent peak broadening, thus ensuring low detection limits on the PDHID. It is therefore shown here (Fig. 2.3 (e)) that for the present application of isolation from other possible components and resolution of NF_3 and CF_4, a simple, single-column setup is sufficient which does not require any additional fluorocarbon liquid phase as used by de Coning and Swinley [17]. These features therefore contribute to creating a reliable and robust method that can be conveniently applied to studying the separation of NF_3 and CF_4 on laboratory scale as is discussed in Sec. 2.3.3.

Although the results of the tests are not shown, it should be noted that Porapak Q, which, as previously mentioned, is not subjected to the various purification steps of the Super Q packing used in this study, is inadequate at resolving NF_3 and CF_4 as the two analytes elutes together, nearly overlapping with air; a result that has been confirmed by Yang *et al.* [18]. From this fact and the discussion above one can conclude that divinylbenzene-styrene co-polymer based porous polymers are adequate for chromatographic NF_3/CF_4 separation, but highly purified formulations must be used to obtain satisfactory resolution. One can only speculate that this difference in results obtained with the purified and unpurified packing materials could be due to modification of adsorption sites that has a marked influence on the affinity of the stationary phase towards NF_3 and CF_4. Nevertheless, as de Coning and Swinley [17] already were able to separate CF_4, CH_4 and NF_3 in an NF_3 matrix with Hayesep Q + Krytox in the column sequence reversal configuration, it was decided to further investigate the applicability of Super Q (which seems to be closely related to Hayesep Q) to the resolution and quantification of NF_3/CF_4 mixtures of varying composition as discussed in the following sections.

2.3.2 Multi-level Quantification

Since the Super Q stationary phase (4 m packed column) yielded the best resolution of NF_3 and CF_4, this stationary phase was also tested for reproducibility with the TCD of Channel B as shown in Fig. 2.2. The results indicate that high reproducibility was obtained (Table 2.2),

where a good linear relationship between the peak areas and the number of moles, which was determined by the sampling pressure (Sec. 2.2.4), was obtained for both NF_3 and CF_4 (Fig. B.1 in Appendix B). The values presented in Table 2.2 were calculated from a dataset resulting from three independent injections for each data point.

Table 2.2: Statistical data for the NF_3 and CF_4 calibration curves obtained on the TCD channel. The corresponding calibration curves are shown in Fig. B.1 (Appendix B).

Nominal Sampling Pressure (kPa)	Average number of moles (nmol)	%RSD* number of moles	%RSD NF_3 Peak Area	%RSD CF_4 Peak Area
100	85.1	0.145	1.77	0.37
125	106.4	0.210	2.05	0.49
150	127.7	0.186	1.12	0.16
175	148.9	0.130	0.75	0.62

NF_3 calibration curve: $A = 3.874x - 5.438$, $R^2 = 0.9999$.

CF_4 calibration curve: $A = 4.601x + 0.164$, $R^2 = 0.9997$.

A = peak area, x = number of mol (nmol).

* Variation in the number of moles caused by slight variation in the measured pressure of each injected sample.

Although a high degree of repeatability in terms of peak area was achieved for each data point as shown in Table 2.2, the detector response for CF_4 was slightly more reproducible than for NF_3. Furthermore, the relative standard deviation (%RSD) with respect to the slopes of the calibration curves for NF_3 and CF_3 was 1.68 and 1.85% respectively. Consequently, a variation of 2% in the peak area corresponding to an arbitrary amount of 130 nmol NF_3, equates to an uncertainty of ±2.6 nmol NF_3 according to the obtained calibration curve, which is an acceptable level of accuracy. It should be mentioned that the number of moles were chosen as the quantification parameter, since a clear and direct definition of the order of magnitude of the number of moles, irrespective of the concentrations, of each NF_3 and CF_4 that can be measured without adversely affecting resolution on each channel in the present method, was thus obtained. In the following discussions, it is shown how this definition is useful to aid in calibration with and quantification of NF_3/CF_4 mixtures of varying concentrations on both channels of the present method. Furthermore, by keeping the composition constant while varying only sample loop pressure to obtain a linear variation in

the number of moles injected, possible uncertainties that could arise during dynamic mixing were eliminated. Thus, the linearity and repeatability reported hereafter give a clear representation of the reliability of the GC setup that was used in this study.

Since adequate resolution between NF_3 and CF_4 was obtained with Super Q as the stationary phase, and good repeatability and accuracy was obtained (Table 2.2), it can be concluded that the sample introduction system and technique (Sec. 2.2.4) that was used was also reliable. From the overlaid chromatograms of both NF_3 and CF_4 in Fig. 2.4 (a), which represents the different calibration levels used to obtain the data given in Table 2.2 for the TCD, it is clear that reasonable resolution between the peaks was achieved within the range of the number of moles injected. Quantitatively, the resolution between the NF_3 and CF_4 peaks of the chromatogram of Fig. 2.4 (a), as calculated according to Eq. (2.1) [22]:

$$R_s = 2\frac{\left[t_R^{NF_3} - t_R^{CF_4}\right]}{W_{CF_4} + W_{NF_3}} \tag{2.1}$$

was 1.9, where R_s is the resolution, t_R^i is the retention time of component i (in minutes, taken at the middle of the peak), and W_i is the peak width (min) at the base of peak i. Since a resolution value of 1.5 is normally accepted to represent complete baseline separation [22], sufficient resolution was therefore obtained, which contributed to the good reproducibility that was obtained with this method as reported above. In other words, the peak widths and degree of separation between the peaks were such that the integration of the peak areas was not hampered at the level of quantification as reported in Table 2.2. If improved resolution is desired, capillary columns with corresponding stationary phases can be implemented which would possibly also lead to improved detection limits on the TCD channel although this would place some restriction on sample volumes that can be analyzed.

Thus, it is shown that reliable and accurate quantification of mixtures of NF_3 and CF_4 was obtained using the method and parameters developed for the TCD channel with the setup shown in Fig. 2.2. Considering the resolution of R_s = 1.9 obtained with the number of moles used during calibration on the TCD channel (Table 2.2), it is estimated that reliable and accurate quantification of NF_3 and CF_4 mixtures containing between 10 and at least 500 nmol of each species can be obtained using this method. By varying the sample loop volume and pressure (such that the number of moles of both NF_3 and CF_4 lies roughly within the range

specified above), this method can thus be used to accommodate a wide range of sample streams with different compositions and NF_3/CF_4 concentrations, as illustrated in Sec 2.3.3.

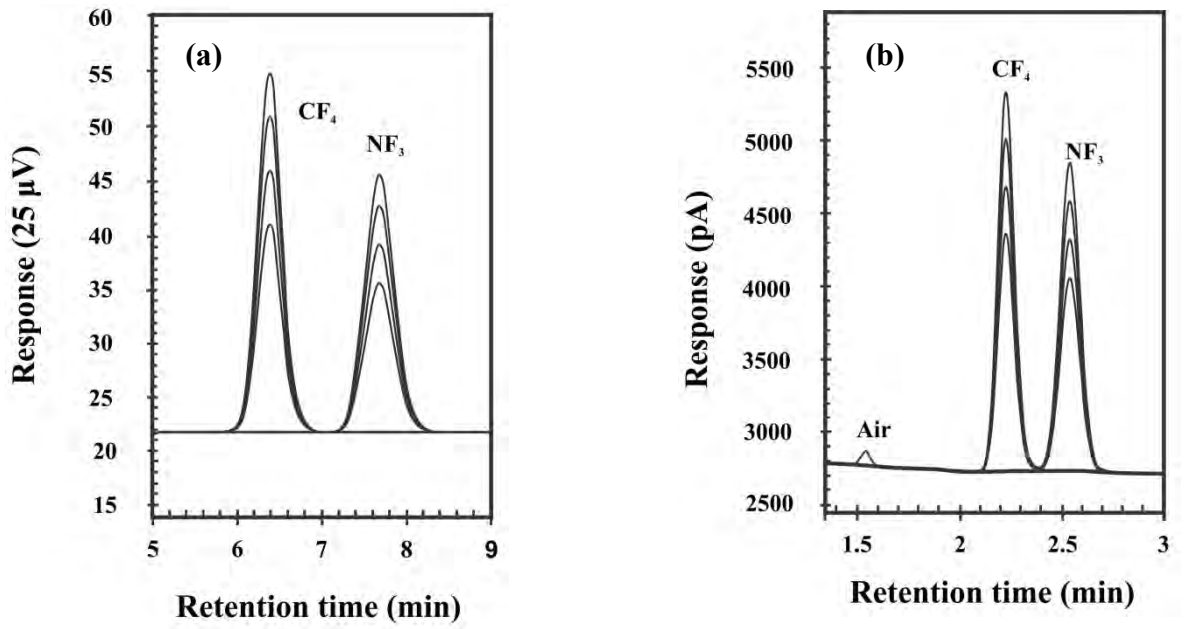

Figure 2.4: Overlaid chromatograms of both NF_3 and CF_4 representing different calibration levels on (a) the TCD channel (Table 2), and (b) the PDHID channel (Table 4).

To determine the concentrations of NF_3 and CF_4 in the ca. 350 vppm mixture contained in a helium matrix for calibration and testing the linearity of the PDHID, the calibration obtained for the TCD channel (Table 2.2) was used while the 5 µL sample loop was substituted with a 5 mL sample loop. With the total theoretical number of moles of the injected sample known from the sample loop volume, temperature and pressure, the number of moles of NF_3 and CF_4 in the mixture was determined at five different sampling pressures with two repeats for each (Tables B.1 and B.2 in Appendix B). The average fraction of NF_3 and CF_4 was then calculated at each of the five different pressures (Table 2.3) from which the overall average was determined that was taken as the final concentration of NF_3 and CF_4 in the mixture. Although the number of moles of NF_3 and CF_4 detected increased with increasing sampling pressure (Table 2.3), the average concentrations remained more or less constant, as was expected. The maximum %RSD for the calculated average concentrations of both NF_3 and CF_4 at each sampling pressure did not exceed 0.9%. Also, the relative standard deviations of the average concentrations of both NF_3 and CF_4, calculated as 343 and 326 vppm respectively, from the

averages of the five different measurements given in Table 2.3 was 1 and 1.3% respectively. This indicates a reliable quantification of the calibration mixture using this method.

Table 2.3: Data used to determine the average NF_3 and CF_4 concentrations of the prepared calibration-mixture on the TCD channel. Refer to Tables B.1 and B.2 in Appendix B for raw data.

Absolute Sampling Pressure (kPa)	Average number of moles (nmol)		Average concentration (vppm) *	
	NF_3	CF_4	NF_3	CF_4
160.1	105.8	100.1	337.8	319.5
170.2	114.8	108.9	344.7	326.9
179.9	121.4	115.3	344.9	327.7
190.0	129.0	122.9	347.1	330.6
200.1	133.9	127.3	341.9	325.2

* Concentrations in vppm calculated from the number of moles detected and the theoretical total number of moles, calculated from the sample loop volume, temperature and pressure.

Using the 350 vppm calibration mixture, with the calculated concentrations, the PDHID channel (Channel A in Fig. 2.2) was calibrated and tested for linearity. Since the Super Q stationary phase provided adequate resolution between NF_3 and CF_4 on the TCD channel (Fig. 2.4 (a)), it was also used for the PDHID channel. However, since the PDHID channel was intended for low-level quantification, only a single 2 m column with a smaller packing size (100/120 mesh) compared to the 4 m (80/100 mesh) column used on the TCD channel was used. This resulted in adequate resolution still being obtained between NF_3 and CF_4 (Fig. 2.4 (b)) at shorter elution times with the added benefit of sharper peaks, resulting in even lower quantification limits. For Fig. 2.4(b), the calibration was performed using a 50 µL sample loop with the same GC parameters used for the TCD channel as shown for Super Q in Table 2.1, except that for the quantification on both channels, the sample loop temperatures were kept at 80 °C using external temperature controlling devices. Using the static gas mixture with the calculated concentrations of NF_3 and CF_4, a varying number of moles of both NF_3 and CF_4 were injected by varying the sampling pressure using the method described in Sec. 2.2.4. The PDHID was therefore also calibrated in terms of the number of moles, with the repeatability results presented in Table 2.4, which was obtained from three consecutive injections at each sampling pressure.

From the data presented in Table 2.4 (also see Fig. B.2 in Appendix B) it is apparent that a satisfactory linear relationship was obtained for both NF_3 and CF_4. The data also shows that good repeatability was achieved for the three sets of calibrations performed on the PDHID channel, and that a similar and satisfactory relative standard deviation was obtained for both the NF_3 and CF_4 peak areas. Also, the relative standard deviation with respect to the slopes of the calibration curves for NF_3 and CF_3 was respectively 2.63 and 2.65%. The maximum relative error with regard to the peak area for the data shown in Table 2.4, i.e. 1.9% for CF_4, corresponds to an uncertainty of ± 18.9 pmol, relative to 1000 pmol CF_4 according to the corresponding calibration curve, which is an acceptable level of accuracy, as it is estimated that the PDHID channel can be used for quantification of NF_3 and CF_4 mixtures containing between 0.01 to 2 nmol (10 to 2000 pmol) of each in the present method.

Table 2.4: Statistical data for the NF_3 and CF_4 calibration curves obtained on the PDHID channel. The corresponding calibration curves are shown in Fig. B.2 (Appendix B).

Average number of moles (pmol)		**%RSD number of moles**		**%RSD Peak Area**	
NF_3	**CF_4**	**NF_3**	**CF_4**	**NF_3**	**CF_4**
725.8	689.8	0.18	0.01	1.48	1.90
871.3	828.1	0.00	0.00	0.73	1.13
1016.3	965.9	0.07	0.01	1.47	0.73
1161.0	1103.5	0.09	0.01	0.70	0.80

NF_3 calibration curve: $A = 13.181x - 299.77$, $R^2 = 0.9996$.

CF_4 calibration curve: $A = 13.887x - 102.6$, $R^2 = 0.9992$.

A = peak area, x = number of mol (pmol).

The variation in peak height with increasing sampling pressure is illustrated in Fig. 2.4(b). Also shown is a minute amount of air that was detected on the chromatograms, indicating that the 350 vppm calibration mixture could possibly have been contaminated with air. Another feature shown in the chromatogram is a slightly downward sloping baseline after the samples have been injected. This is an almost inevitable result of using a sample loop and connecting tubing with a small inside diameter. As the sampling valve switches, the sample loop is placed in-line with the analytical column. As a result, the helium carrier from the gettering system must follow a slightly more constricted path through the sample loop and the

connecting tubing, causing a specific pressure drop. This pressure drop is slightly larger compared to the pressure drop achieved with the valve in the load position. Consequently, a smaller pressure drop exists across the analytical column causing a slightly lower flow rate through the analytical column and ultimately through the detector. Since the response of the PDHID is flow sensitive [17], the detector response takes a few minutes to stabilize following the slight change in flow rate. However for any practical applications, this effect would not influence accurate quantification as long as the calibration and sampling is performed under identical conditions.

Although the resolution obtained on the shortened column is lower (R_s = 1.3) than that obtained for the longer column on the TCD channel (R_s = 1.9), it is apparent from the data presented that reproducible and reliable low-level quantification with acceptable accuracy is still obtained on the PDHID channel with the present method. With the setup as shown in Fig. 2.2, this method can thus conveniently be applied to quantify NF_3/CF_4 mixtures of various compositions and absolute amounts, where a possible application is discussed in the next section.

2.3.3 Application to Membrane Separation of NF_3 and CF_4

As shown above (Fig. 2.3 (e)), the use of a divinylbenzene-styrene co-polymer stationary phase (Super Q) resulted in a reliable and accurate quantification of NF_3 and CF_4 mixtures at amounts of ca. 100 nmol on the TCD channel, and with increased sensitivity at amounts of ca. 10 – 1000 pmol on the PDHID channel. An additional liquid phase as was used by de Coning and Swinley [17] for the quantification of CF_4 and other trace impurities in an NF_3 matrix was also not necessary. However, as mentioned in Sec. 2.3.1, contamination of NF_3/CF_4 mixtures with appreciable amounts (in the order of 1 – 10 mol%) of methane would restrict the applicability of this method of quantification. Nonetheless, for one indented application of this method, shown schematically in Fig. 2.5, this factor would not present any difficulties when using NF_3 and CF_4 of high purity.

Purification of NF_3 from CF_4 is a challenging problem (Sec. 1.1), for which membrane separation is a possible process that may be suitable, which has not been investigated until now since no literature evidence thereof could be found. The present GC method combined with a basic experimental membrane process as illustrated in Fig. 2.5 can be used to

determine the permeability and selectivity of different membranes towards NF_3 and CF_4. For such membrane separation studies, high purity NF_3 and CF_4 could be mixed in a 50:50 molar ratio to serve as the feed stream to the membrane module where this feed stream and resulting retentate (or residue) stream could be sampled and analyzed on the TCD channel of the current GC method. Depending on the membrane permeability (intrinsic membrane property) and total flow rate, which depends on the permeability, membrane area and membrane thickness, the permeate stream can either be sampled and analyzed through the TCD channel, or through the PDHID channel.

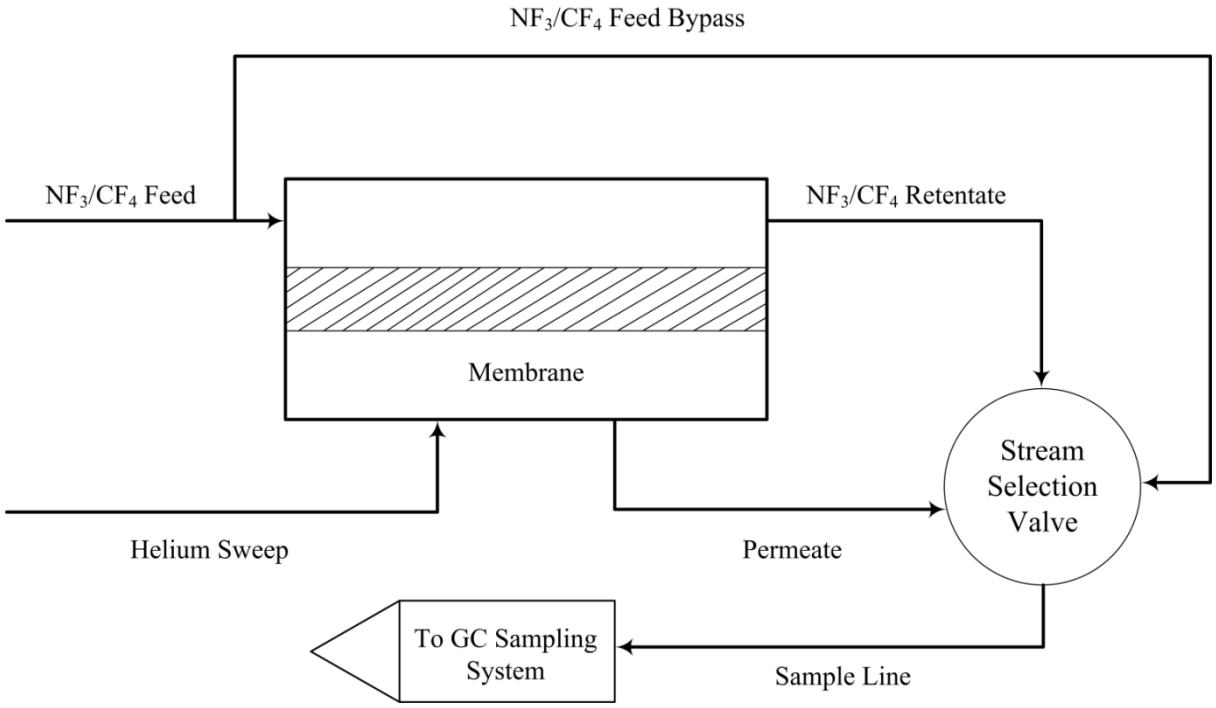

Figure 2.5: Schematic representation of a simple membrane separation setup, to which the current GC method can be applied to study membrane selectivity towards NF_3 and CF_4 permeability.

For membranes with low permeability, where a very low permeate flow rate would be observed, helium could be used to sweep analytes from the permeate side of the membrane to the GC sampling system. The PDHID channel would then be used for the quantification of small amounts, i.e. between c.a. 10 to 2000 pmol, for which the chromatogram presented in Fig. 2.6 (a) serves as an example of this scenario. When testing membranes with a high permeability for which a helium sweep is either not required, or where membrane permeate flow rate is comparable with the helium sweep flow rate, quantification can be performed on the TCD channel, for which Fig. 2.6(b) serves as an example. By using a helium sweep gas it

is possible to control the partial pressures of NF_3 and CF_4 on the permeate side of the membrane, thereby ensuring a constant composition of the permeate stream once steady state conditions have been reached, irrespective of membrane permeability [23].

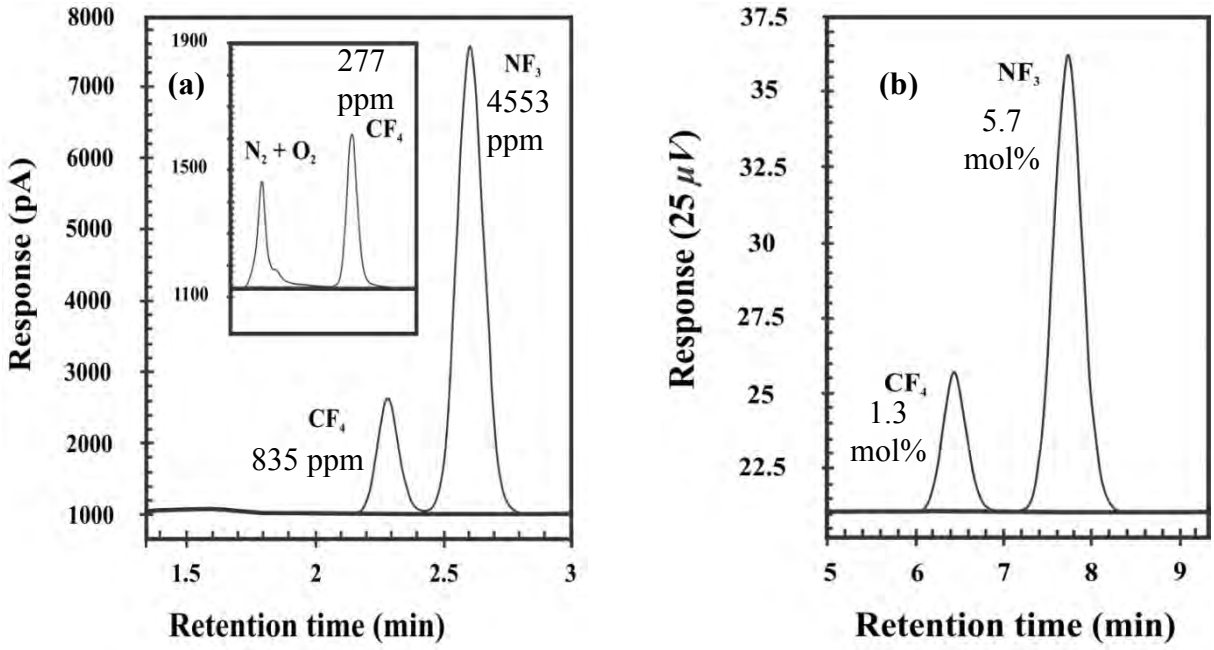

Figure 2.6: Examples of chromatograms obtained with the permeate stream from the membrane setup shown in Fig. 2.5, when testing two polymer membranes with (a) low permeability, and (b) a polymer membrane with intermediate permeability towards NF_3 and CF_4. The insert in figure (a) serves as an example of CF_4 detector response at a concentration more than three times lower than that shown in the main figure.

In the example shown in Fig. 2.6(a), a representative chromatogram obtained for the permeate stream while testing a polymer membrane using the basic setup illustrated in Fig. 2.5 with a helium sweep of constant flow rate (controlled using a Brooks thermal mass flow controller) is shown. For the quantification of the analytes calibration was performed while keeping the sample loop pressure constant and varying the concentrations of both NF_3 and CF_4. The concentrations were varied by dynamic dilution with helium of a static gas mixture (prepared as described in Sec. 2.2.1) containing ca. 1 mol% NF_3 and CF_4 each in a helium matrix, using the thermal mass flow controllers and setup shown in Fig. 2.1. Consequently, the final calibration curves of NF_3 and CF_4 (Fig. B.3 in Appendix B) for quantification on the PDHID had concentrations between a minimum of 270 vppm and a maximum of 5000 vppm with

correlation coefficients better than 0.999. In all instances, a 10 μL sample loop was used for calibration and quantification resulting in the number of moles of each analyte ranging between a minimum of 108 pmol and a maximum of 1745 pmol, which is within the range specified in Sec. 2.3.2 for the PDHID channel. The average concentrations of NF_3 and CF_4 shown in Fig. 2.6(a) both had relative standard deviations of 0.31%, as determined from three consecutive injections, spaced at least 15 minutes apart. In this case, it is therefore concluded that accurate and reliable quantification can be obtained on the PDHID channel when the concentrations of NF_3 and CF_4 differ by a factor of 5.5 while using an appropriate sample loop volume to favorably adjust the number of moles (and therefore detector response) of the analytes to facilitate reliable integration of the peak areas.

The insert in Fig. 2.6(a) illustrates a representative chromatogram for the determination of the CF_4 concentration in the permeate stream that originated from the membrane cell with a polymer film with an even lower permeability as that shown in the main figure. The same basic method of calibration with the same 10 μL sample loop was used as described for the previous case, except that the concentrations of both NF_3 and CF_4 were varied by dynamic dilution of the 350 vppm gas mixture mentioned in Sec. 2.3.2. The resulting calibration curve for CF_4, varying in concentrations of between 47 and 326 vppm, corresponding to 18 to 128 pmol, had a correlation coefficient of better than 0.99. Furthermore, the relative standard deviation of the average concentration of 277 vppm as shown in the insert of Fig. 2.6(a) was 0.17%, as determined from three consecutive samples. It is therefore concluded that reliable quantification is possible at such a low detector response (corresponding to 10 pmol of the analyte), where concentrations in the order of 1 – 10 vppm and lower may be accommodated by using larger sample loops. Following the previous example with the clear decrease in CF_4 permeability that resulted in the concentration decreasing from 835 to 277 vppm, it can be anticipated that the NF_3 permeability for the particular membrane should also be lower than in the previous example. However, if the NF_3 concentration in the permeate stream for this particular membrane would to be larger than that of CF_4 by a factor of 10, i.e. ca. 2700 vppm, the total number of moles of both analytes would still fall favorably within the estimated 10 to 2000 pmol range that is required to prevent significant overlap of the CF_4 and NF_3 peaks. Therefore, it is evident that reliable quantification on the PDHID channel should be possible when the CF_4 and NF_3 concentrations differ by as much as a factor of 10, although slightly larger differences (within multiples of 10) can also be analyzed, as is evident from membrane selectivity results obtained with a low-permeability polymer membrane (Chapter 3). In this

example (Sec. 3.3.3), the membrane module was fitted with a Hyflon AD60 polymer membrane that was fed with a mixture of NF_3 and CF_4 containing 15 mol% CF_4 and 85 mol% NF_3. This produced a permeate stream, which, when analyzed on the PDHID channel using a helium sweep as in Fig (2.5), had an average CF_4 concentration of 40 vppm (%RSD = 0.52 %) and an average NF_3 concentration of 2645 vppm (%RSD = 0.23 %). In this case the sample loop volume was, however, adjusted slightly to ensure that a reliable detector response is obtained for the minor component (CF_4), while also preventing the detector response of the major component (NF_3) from overshadowing that of CF_4.

In the case of quantifying mixtures wherein the concentration of the major component is larger than the minor component by a factor in the order of 100, the longer 4 m, 80/100 mesh analytical column of the TCD channel (Fig. 2.4 (a)), which showed better resolution (R_s = 1.9) compared to the 2 m, 100/120 mesh column (R_s = 1.3) of the PDHID channel (Fig. 2.4 (b)) may be used instead to avoid integration errors. Nevertheless, the physical setup of the present dual-channel GC method allows the use of the stationary phases and column sequence reversal configuration of de Coning and Swinley [17] on the PDHID channel to enable the measurement of even lower CF_4 concentrations in mixtures containing a predominant amount of NF_3. Consequently, the method of de Coning and Swinley can then be used to measure the permeability and efficiency of membranes being fed with an NF_3 feed that contains CF_4 as contaminant when pilot scale studies are undertaken to further investigate the efficiency of membrane separation. However, for laboratory scale membrane screening studies, where pure NF_3 and CF_4 are fed in relative equal amounts, the simplified method presented in this paper may be more conveniently applied.

In Fig. 2.6(b), a representative chromatogram obtained while analyzing the permeate stream from the membrane cell with a polymer membrane of intermediate permeability towards NF_3 and CF_4, using a sample loop volume of 50 µL is shown. In this case, calibration was also performed by keeping the sample loop pressure constant while varying the individual NF_3 and CF_4 concentrations by dynamic blending of the pure gases with helium, which was done with the current experimental setup as shown in Fig. 2.1. The resulting linear calibration curves (Fig. B.4 in Appendix B) for NF_3 and CF_4 had correlation coefficients of better than 0.999, with the concentrations that was varied between 1 and 7 mol% (16 – 115 nmol) for NF_3 and 0.5 and 3 mol% (9 – 65 nmol) for CF_4. The relative standard deviations of the average concentrations as shown in Fig. 2.6(b) was 1.2% for NF_3 and 5.7% for CF_4, resulting from

two sample injections. Once again, it is clear that reliable quantification was obtained, where the CF_4 concentration in the analyte stream was in this case a factor of 4.4 times smaller than that of NF_3, and the use of an appropriate sample loop volume facilitated a reliable detector response and integration of peak areas for both analytes. Although the results are not shown here, it is also possible on the TCD channel, just as in the case of the PDHID channel shown above, to obtain reliable quantification when the concentrations of NF_3 and CF_4 differ by at least a factor of 10.

It should be kept in mind that interference of CH_4 is a potential issue with the current method as noted in Sec. 2.3.1. However, no CH_4 with NF_3/CF_4 was detected on either the TCD or PDHID channel as illustrated in the above examples, due to the fact that high purity NF_3 and CF_4 were blended to form the feed stream to the membrane module. Consequently, any traces of CH_4 present in either of the individual NF_3 or CF_4 feed streams was not detectable on the TCD of Channel B during analysis of the feed, retentate or permeate streams, in accordance with Fig. 2.6(b). Additionally, CH_4 was also not detected on the PDHID of Channel A, as helium was used to sweep the permeate stream to the sampling system resulting in dilution of the NF_3/CF_4 permeate mixture as well as any possible traces of CH_4, so that this species was diluted to well below its detection limit on the PDHID channel, as is clear from Fig. 2.6(a). Therefore, the accuracy of membrane separation efficiency measurements using the present analysis method and experimental technique as shown in Fig. 2.5 would not be hampered when using high-purity NF_3 and CF_4 as the feed to the membrane module, since CH_4 would be present in quantities that are below the limits of detection. Possible interference from CH_4 may be completely alleviated by using capillary PLOT Q columns, for which improved resolution between CF_4, CH_4 and NF_3 can be expected. However, it is apparent from the examples given in Fig. 2.6 that membranes with increasingly low permeability will produce permeate streams with low concentrations of NF_3 and CF_4 since a sweep of helium is used to enable sample analysis. Therefore, it might be required to inject large sample volumes to be able to measure NF_3 and CF_4 concentrations when studying low permeability polymer membranes, for which packed columns are necessary.

Nonetheless, the chromatographic method developed here allows flexibility for NF_3/CF_4 quantification not only when studying the membrane separation of these two gases, but also any separation process in which quantification at either high concentrations and/or low concentrations are required. In addition, this method has the advantage over that of Yang *et*

al. [18] that both NF_3 and CF_4 can be detected at both high and low concentrations by employing a single-column system without the need for additional valve switches. Also, many of the analytes they focused on, such as CO_2, SF_6, and C_3F_8 should also be quantifiable using the present method presented here, or minor modifications thereof. This is because CO_2 elutes after NF_3 and CF_4 as shown in Fig. 2.3 (e), and the heavier components such as SF_6 and C_3F_8 typically elutes after CO_2 on the divinylbenzene-styrene co-polymer stationary phase as shown by the Hayesep Q column sequence reversal results of de Coning and Swinley [17]. The present method can therefore be altered by, for example, using a temperature program to achieve faster resolution of said heavier components that may yield a robust analytical method that could therefore also be of some use in the electronics fabrication industry, where such species must either be recovered or destroyed to prevent atmospheric pollution [18].

2.4 Conclusions

It was shown that accurate and reliable quantification of mixtures of NF_3 and CF_4 can be achieved using a divinylbenzene-styrene co-polymer stationary phase (in this case Super Q) for the resolution of mixtures of NF_3 and CF_4 that can be conveniently applied to any separation study involving these two compounds. Using a dual-channel setup with a TCD on one and a PDHID on another channel, results in a versatile analytical system for the quantification of mixtures of NF_3 and CF_4 at both low levels, where a high sensitivity is required (PDHID), and at normal to high levels, where a less sensitive detector (TCD) is required. It was estimated that with this dual-channel setup, absolute analyte amounts of between 10 – 500 nmol on the TCD channel, and between 0.01 to 2 nmol on the PDHID channel could be quantified with high accuracy, which implies that NF_3/CF_4 mixtures of different compositions with concentrations varying over a broad range can be quantified using the basic method described here, with consideration of course, of the sample loop volume used for calibrations and analyses. As an example, it was shown how this dual-channel setup could be usefully applied in membrane separation studies related to NF_3 and CF_4 where multi-level quantification is a necessity. Consequently, it was shown that good reliability should still be achieved at low concentrations of both NF_3 and CF_4 when these concentrations differ by a factor of at least 10. It is therefore clear that this method or variations thereof could most probably also be suitable for other applications in which quantification, at different levels of sensitivity of both NF_3 and CF_4 in mixtures of the two gases is required.

2.5 References

1. P.B. Henderson, A.J. Woytek, Fluorine compounds, inorganic, nitrogen, in: Kirk-Othmer Encyclopedia of Chemical Technology, John Wiley & Sons, New York, 5th ed., 2010, Vol.11, pp. 852 - 858.
2. A.J. Woytek, J.T. Lileck, Preparation of nitrogen trifluoride, U.S. Pat. 4,091,081 (1987).
3. R. Herkelmann, Handling and security in the synthesis and purification of nitrogen trifluoride, J. Fluor. Chem. 54 (1991), 37.
4. N.J. Ianno, K.E. Greenberg, J.T. Verdeyen, Comparison of the etching and plasma characteristics of discharges in CF_4 and NF_3, J. Electrochem. Soc. 128 (1981) 2174 – 2179.
5. D.-J. Kang, I.-S. Kim, J.-H. Moon, B.-T. Lee, Inductively coupled plasma reactive ion etching of sapphire using C_2F_6- and NF_3-based gas mixtures, Mat. Sci. Semicon. Proc. 11 (2008) 16 – 19.
6. R.K. Belter, M.S. Sweval, Y. Iikubo, Nitrogen trifluoride as an oxidative co-reagent in high temperature vapor phase hydrofluorinations, J. Fluor. Chem. 127 (2006) 816 – 820.
7. R.K. Belter, High temperature vapor phase reactions of nitrogen trifluoride with benzylic substrates, J. Fluor. Chem. 132 (2011) 318 – 322.
8. R.D. Scheele, B.K. McNamara, Nitrogen trifluoride, a new fluorinating agent for the nuclear fuel cycle, Trans. Am. Nucl. Soc. 99 (2008) 225 – 226.
9. A. Tasaka, Electrochemical synthesis and application of NF_3, J. Fluor. Chem. 128 (2007) 296 – 310.
10 K. Koike, T. Fukuda, S. Fujikawa, M. Saeda, Study of CF_4, C_2F_6, SF_6 and NF_3 decomposition characteristics and etching performance in plasma state, Jpn. J. Appl. Phys. 36 (1997) 5724 – 5728.
11. M. Konuma, F. Banhart, F. Phillipp, E. Bauser, Damage-free reactive ion etching of silicon in NF_3 at low temperature, Mat. Sci. Eng. B-Solid. 4 (1989) 265 – 268.
12. R.N. Miller, C.-P.C. Kao, B.A. Mahler, Process for purifying perfluorinated products, U.S. Pat. 6,458,249 B2 (2002).
13. D.P. Satchell, J.P. le Roux, Method and apparatus for the production of nitrogen trifluoride, U.S. Pat. 6,986,874 B2 (2006).

14. A. Mimoto, T. Maeda, T. Ueno, T. Nakajima, T. Maekawa, T. Tsukayoshi, M. Kamiyoshi, A. Oda, H. Takemura, O. Yamaguchi, A. Tasaka, Effect of oxide in nickel-based composite anodes on current efficiency for NF_3 formation and current loss caused by nickel dissolution in molten $NH_4F.2HF$, Electrochim. Acta. 50 (2005) 2563 – 2571.
15. S.M. Igumnov, V.P. Kharitonov, N.V. Kharitonova, Method of purifying gaseous nitrogen trifluoride, U.S. Pat. 7,022,160 B2 (2006).
16. R.R. Singh, M.R. Paonessa, D.F. Orlowski, Purification of Nitrogen trifluoride, U.S. Pat. 7,384,618 B2 (2008).
17. J.P. de Coning, J.M. Swinley, Optimisation of a gas chromatographic method for trace gaseous impurities in nitrogen trifluoride by column sequence reversal, J. Chromatogr. A 1180 (2008) 151 – 158.
18. C.-F.O. Yang, S.-H. Kam, C.-H. Lui, J. Tzou, J.-L. Wang, Assessment of removal efficiency of perfluorocompounds (PFCs) in a semiconductor fabrication plant by gas chromatography, Chemosphere 76 (2009) 1273 – 1277.
19. J.-P. Barbier, G. Bissolotti, K. Cleaver, J.-C. Goffinet, B. Hussler, P. Wolf, 2009, Code of practice nitrogen trifluoride, IGC Doc. 92/10/E. European Industrial Gases Association, EIGA. Available: http://www.eiga.org/fileadmin/docs_pubs/Doc_92_10_E.pdf. Date of access: 05 November 2011.
20. J. Matěcha, J. Berka, F.Sus, M. Černý, J. Lengyel, V. Tekáč, Testing of analytical and purification methods for HTR helium coolant, Nucl. Eng. Des. 251 (2011) 208 – 215.
21. A.B. Richmond, Separation of nitrogen trifluoride from carbon tetrafluoride by gas chromatography, Anal. Chem. 33 (1961) 1806.
22. R.L. Grob, E.F. Barry (eds.), Modern Practice of Gas Chromatography, John Wiley & Sons, New Jersey, 4th ed., 2004.
23. R.W. Baker, Membrane technology and applications, John Wiley & Sons, Chichester, 2nd ed., 2004.

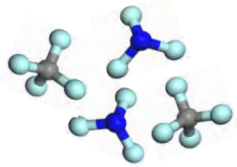

Chapter 3

Separation of NF_3 and CF_4 using amorphous glassy perfluoropolymer Teflon AF and Hyflon AD60 membranes

Abstract

In this study, the pure and mixed gas permeabilities of Teflon AF2400, Teflon AF1600 and Hyflon AD60 membranes towards NF_3 and CF_4 were measured to determine whether membrane gas separation can be applied to purify NF_3 of CF_4. In addition, the pure gas He and N_2 permeabilities of the membranes were also measured showing good correlation with the available literature data. Also, in accordance with literature results, it was shown that thermal annealing of the solution cast films was necessary to reach optimum performance, wherein all membranes studied had a preferential permeation of NF_3 rather than CF_4. The Teflon AF and Hyflon AD60 membranes displayed rather high pure and mixed gas selectivities ($\alpha(NF_3/CF_4)$) considering the high free volume of the polymers. Furthermore, the $\alpha(NF_3/CF_4)$ increased with increasing diffusion selectivity of the glassy perfluoropolymers, of which the He/N_2 ideal selectivities gave an indication, and which is related to the fractional free volume (FFV). As a result, Hyflon AD60 displayed the highest NF_3/CF_4 pure and mixed gas selectivity just above 12, albeit with a rather low NF_3 permeability of ca. 1.9 Barrer. Although the membranes were sufficiently inert towards penetrant induced swelling, a Hyflon AD60 membrane swollen by residual casting solvent displayed an increase in the pure and mixed gas NF_3 and CF_4 permeabilites and reduced selectivity compared to that of an annealed, fully relaxed Hyflon AD60 membrane. Considering a mixed gas selectivity of 12, it could therefore be concluded that membrane separation could be a competitive technology for the purification of NF_3 from CF_4.

Keywords: Perfluoropolymer membranes; Teflon AF, Hyflon AD60; NF_3/CF_4 Membrane separation; NF_3/CF_4 Permeability selectivity.

3.1 Introduction

Nitrogen trifluoride (NF_3), serves as a convenient fluorine source that is used mainly in the electronic and semiconductor manufacturing industry in plasma assisted etching of silicon wafers and cleaning of chemical vapour deposition chambers [1 – 4]. The use of NF_3 as etchant rather than perfluorocarbon gases (PFCs) such as carbon tetrafluoride (CF_4), perfluoroethane (C_2F_6) is motivated by the fact that NF_3 displays superior etching performance and does not lead to the build-up of carbonaceous residues [4, 5]. Fearing defect formation during high density integrated circuit manufacture as a result of potential carbonaceous build-up, the electronic manufacturing industry demands high purity NF_3 (VLSI-grade NF_3) in which the CF_4 content must be below 20 ppm [6]. This is a challenging specification to reach, as NF_3 is usually contaminated with the physically and chemically similar CF_4 when obtained from the so-called two-step synthesis procedures [7, 8] that uses electrochemically produced fluorine (F_2) as a reactant. CF_4 contamination originates during the electrochemical production of F_2 due to the use of carbon anodes in a fluorine-rich environment [3], whereas alternative electrochemical synthesis methods, in which nickel anodes are used, are often not used due to various other disadvantages [3, 9].

Purification of NF_3 from CF_4 is therefore crucial to meet the high standards set by the electronic industry, but this has proven to be a daunting task. Although adsorption processes using porous zeolite adsorbents has been the most popular [10 – 12], distillation processes have also been developed [13, 14] for the separation of CF_4 from NF_3. Cryogenic distillation of NF_3 and CF_4, would be impractical due to the small difference of 1 °C in the normal boiling points of NF_3 and CF_4 [15]. As a result, extractive distillation processes have been developed wherein entraining agents such as hydrochloric acid [13] and ionic liquids [14] have been used to enhance the efficiency of separation. A major drawback with zeolite adsorbents is that NF_3, the major component, is preferentially adsorbed [10 – 12], thus requiring high adsorbent volumes that need to be periodically regenerated. In this regard, a polyacrylonitrile-based carbon molecular sieve, Carbosphere®, has been claimed to preferentially adsorb the minor component, CF_4 [6], which represents the most efficient separation to date.

Gas separation using polymeric membranes has enjoyed major developments since they were first used on industrial scale in the 1980's for hydrogen separation [16, 17]. Industrially,

membrane based separations offer the advantage of being more energy efficient when compared to conventional gas separation methods such as adsorption and cryogenic distillation. In addition, advances in polymer chemistry have led to the development of membrane materials that offer a good trade-off between permeability and selectivity [18 – 20], which, however, remains a major obstacle preventing the widespread implementation of the technology. However, membrane gas separation has been used for the recovery of PFCs, such as perfluoroethane (C_2F_6), from semiconductor manufacturing plants in which the unreacted gases are separated from diluents such as N_2 using glassy polymers [21 – 23]. These membrane recovery methods have been mentioned to be suitable for the recovery of NF_3 and CF_4 as well; however, no literature evidence regarding a membrane based separation method for the purification of NF_3 from CF_4 could be found.

In this study, the polymer membrane based separation of NF_3 and CF_4 was therefore investigated to establish the applicability of the technology to this seemingly formidable separation challenge. High performance glassy perfluoropolymers of Teflon AF and Hyflon AD60, which display permeability-selectivity relationships that lie close to the current Robeson upper bound [18] were used. Considering the oxidising character of NF_3 [1], these polymers also offer satisfactory stability due to their fluorinated character. In addition, it is known that PFCs such as CF_4 are significantly more soluble in perfluorocarbon polymers compared to conventional hydrocarbon based polymers [24, 25], which would therefore also lead to optimum permeabilities. Consequently, pure and mixed gas permeability and selectivity was determined, wherein the GC method described in the previous chapter was used for quantitative analysis during the mixed gas permeability experiments. It is shown that surprisingly good permeability selectivity towards NF_3 was obtained, which showed a clear dependence on the FFV of the polymer membranes.

3.2 Materials and Methods

3.2.1 Materials

The random copolymers of tetrafluoroethylene (TFE) and 2,2-bis(trifluoromethyl)-4,5-difluoro-1,3-dioxole (BDD) containing 87 and 65 mol% BDD (Fig. 3.1 (a)), which is commercially available as Teflon AF2400 and Teflon AF1600 respectively (Du Pont, Wilmington, DE) were used as received. In addition, the random co-polymer of

tetrafluoroethylene (TFE) and 2,2,4-trifluoro-5-trifluorometoxy-1,3-dioxole (TTD) containing 60 mol% TTD that is commercially available as Hyflon AD60 (Solvay Solexis, Italy), with the chemical structure shown in Fig. 3.1 (b), was used as received. From this point onward, Teflon AF2400 and Teflon AF1600 will be referred to in the text as AF2400 and AF1600 respectively, for the sake of brevity. Fluorinert^{TM} FC-770, a perfluoro N-alkylmorpholine with a normal boiling point of 95 °C (3M, Belgium), was used as the solvent to prepare solutions of the abovementioned polymers.

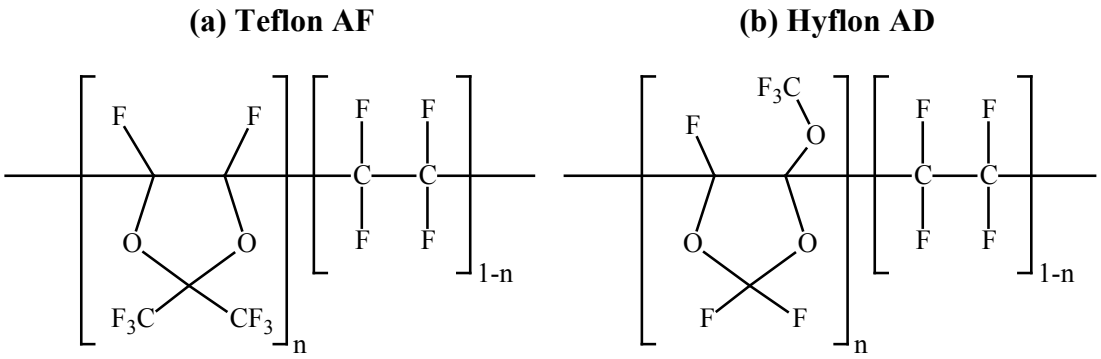

Figure 3.1: Molecular structure of (a) Teflon AF and (b) Hyflon AD60 amorphous, glassy perfluoropolymers.

Linde electronic-grade nitrogen trifluoride (NF_3), certified to be 99.99 vol% pure (LESA Grade) and tetrafluoromethane (CF_4) with a certified purity of 99.99 vol%, purchased from Air Liquide, Germany GmbH, were used for pure and mixed gas membrane permeability and selectivity measurements. In addition, nitrogen (N_2) with a purity of 99.999 vol% and helium (He) with a purity of 99.999 vol%, both purchased from Air Products, South Africa, were used for pure gas membrane permeability measurements. He of the same purity was also used as carrier gas in the on-line gas chromatographic (GC) system that was used for sample analysis.

3.2.2 Membrane Preparation

Isotropic, dense films of all three of the amorphous, glassy fluoropolymers shown in Fig. 3.1 were prepared by the solution casting method with Fluorinert^{TM} FC-770 as the solvent. 2wt% Solutions of AF2400 and 4wt% solutions of both AF1600 and Hyflon AD60 were prepared,

which were agitated at room temperature using a magnetic stirrer and left for at least 16 h (while stirring) to obtain homogenous solutions. Glass templates consisting of flat, smooth glass discs and flanged glass cylinders that fitted together to form small containers were used for the polymer film preparation. For this, 5 mL of the AF2400 solutions and 2 – 2.5 mL of the AF1600 and Hyflon AD60 solutions, as measured with a B-grade glass pipette, were withdrawn and transferred to the glass templates that were placed on a level surface resulting in the polymer solutions spreading out evenly across the exposed area. Subsequently, solvent evaporation was allowed to proceed at room temperature for at least two days (48 h), wherein the cylindrical sections of the templates (approximately 4 cm in depth) were covered with watch glasses in the case of AF2400, and overturned funnels in the case of AF1600 and Hyflon AD60 to slow the rate of evaporation from the cast films.

After solvent evaporation, the films were cut out of the templates using a scalpel and were lifted from the glass surfaces by the addition of deionised water and were then dried on a paper towel. The clear, transparent circular films were then heat treated in two separate stages to ensure complete solvent removal. During the first stage the films were heated in a convection oven, without controlling the heating rate, to 125 °C for AF2400, 65 °C for AF1600 and 50 °C for Hyflon AD60 respectively, and were kept at these temperatures for at least 16 h. These temperatures were chosen such that the films were only heated to approximately 100 °C below the respective glass transition temperatures of the different polymers, i.e. T_g = 240 °C (AF2400), T_g = 160 °C (AF1600), T_g = 130 °C (Hyflon AD60), to avoid deformation of the films during this stage. The films were cooled down to room temperature, without controlling the cooling rate, and were subsequently stored. During the second heat treatment, the films were annealed by heating in a GC oven from 30 °C to 200 °C for AF2400 and AF1600, and to 170 °C for Hyflon AD60 at a rate of 0.2 °C/min. The temperature was then kept constant at the maximum value for 30 min followed by cooling to 30 °C at a rate of 0.4 °C/min after which the temperature was kept constant for at least 30 min to ensure that thermal equilibrium was reached. For the annealing stage, the membranes were placed on porous, hydrophobic PTFE films (manufactured by PALL Corporation, USA) that were stretched over petri dishes onto which the films adhered after the annealing cycle. The AF2400 and AF1600 films could be easily removed from the PTFE support layers, whereas the Hyflon AD60 membranes were used in the resulting composite form.

Membrane thicknesses were measured after removal of the AF2400 and AF1600 films from the PTFE support layers, while the Hyflon AD60 membrane thickness was measured after the first heat treatment stage and again after permeability and selectivity measurements were conducted with the composite membranes, when the films could be stripped from the PTFE support layers. In all cases, the average film thickness was determined from 15 random measurements across the surface of the individual films using a Mitutoyo dial gauge that was accurate to 1 μm.

In addition, Hyflon AD60 polymer membranes that were not annealed, but that were subjected to a second heat treatment that consisted of only heating the membranes to 95 °C after being secured inside the permeation cell (Sec. 3.2.5) were also studied. The temperature was kept constant at 95 °C for approximately 8 h where after the cell was slowly cooled to 35 °C while He was allowed to permeate through the membranes at a trans-membrane pressure of 600 kPa during both stages. Hereby, the effect of different heat treatment conditions on the Hyflon AD60 polymer membrane thermal characteristics and gas permeability performance was evaluated. The thickness of these membranes had already been determined after completion of the first heat treatment stage as described above, where no PTFE support layer was used with these membranes at any stage.

3.2.3 Thermal Analysis

The glass transition temperatures, T_g, of the pure AF2400, AF1600 and Hyflon AD60 polymers, and of the solution cast membranes obtained from various stages in the membrane preparation process were determined from Differential Scanning Calorimetry (DSC) analysis. For all of the annealed films, samples of the pure polymers after being stripped from the PTFE support layers were used for analysis, after permeability and selectivity measurements were conducted. A Perkin-Elmer Pyris 1 instrument that was calibrated using an indium reference sample was used for all DSC analysis. Polymer samples of between 15 – 22 mg were loaded into aluminium sample pans, which were then sealed with accompanying lids. The samples were then analysed in a nitrogen atmosphere using a thermal cycle that consisted of a heating run, a subsequent cooling run, and a final heating run at rates of 15 °C/min in the ranges of 80 – 300 °C for AF2400, 60 – 200 °C for AF1600, and 40 – 160 °C for Hyflon AD60. Both the first and second heating runs were used to compare the T_g values of all analysed samples. The T_g values were determined in most cases as the temperature

corresponding to the *half-c_P extrapolated* value, which is the temperature corresponding to half of the c_p increase for the complete transition as determined from extrapolation of the baseline before and after the transition. In some cases, however, the onset of the glass transitions was determined by analysing the peak areas for samples that registered the transitions in the form of peaks.

The residual solvent content of the membranes, after being subjected to the various heat treatment stages as described in Sec. 3.2.2, was characterized using Thermal Gravimetric Analysis (TGA) on a TA Instruments SDT Q6000 simultaneous TG/DSC system. Film samples of between 1 – 10 mg were loaded into the alumina sample crucible and runs were performed under either a nitrogen or argon purge while heating from 30 °C to 300 °C. Samples of the same films used for DSC analysis were also used for these analyses, after permeability and selectivity measurements had been completed.

3.2.4 Scanning Electron Microscopy (SEM) Analysis

The annealed Hyflon AD60-PTFE composite membranes were qualitatively analysed using SEM. Images were generated under vacuum using a FEI Quanta 200 ESEM electron microscope with the voltage set to 20 kV. Film samples were cut using a scalpel, and cross sectional images were obtained by securing the samples onto the sampling buttons using copper adhesive tape, where the films were held in place in an L-shape with specialised sample holders.

3.2.5 Gas Permeation Measurements

The pure and mixed gas permeability was measured by applying the basic principle of the constant-pressure variable-volume method [26]. A stainless steel permeation cell that could be used in both a flow-through or dead-end configuration, depending on the individual experimental requirements, was used. After being secured inside the permeation cell, the exposed area of the circular membranes equated to 19.64 cm^2. A partial piping and instrumentation diagram (P&ID) of the custom-built experimental setup that was used is shown in Fig. 3.2, which provided the versatility for both pure and mixed gas permeation measurements. It should be noted that the code of practice for nitrogen trifluoride [27] should always be obeyed when working with NF_3. Thus, the construction materials of all the system

components were chosen specifically to be compatible with NF_3, and engineering controls were used to protect against undesirably high pressures and temperatures that could possibly arise accidentally.

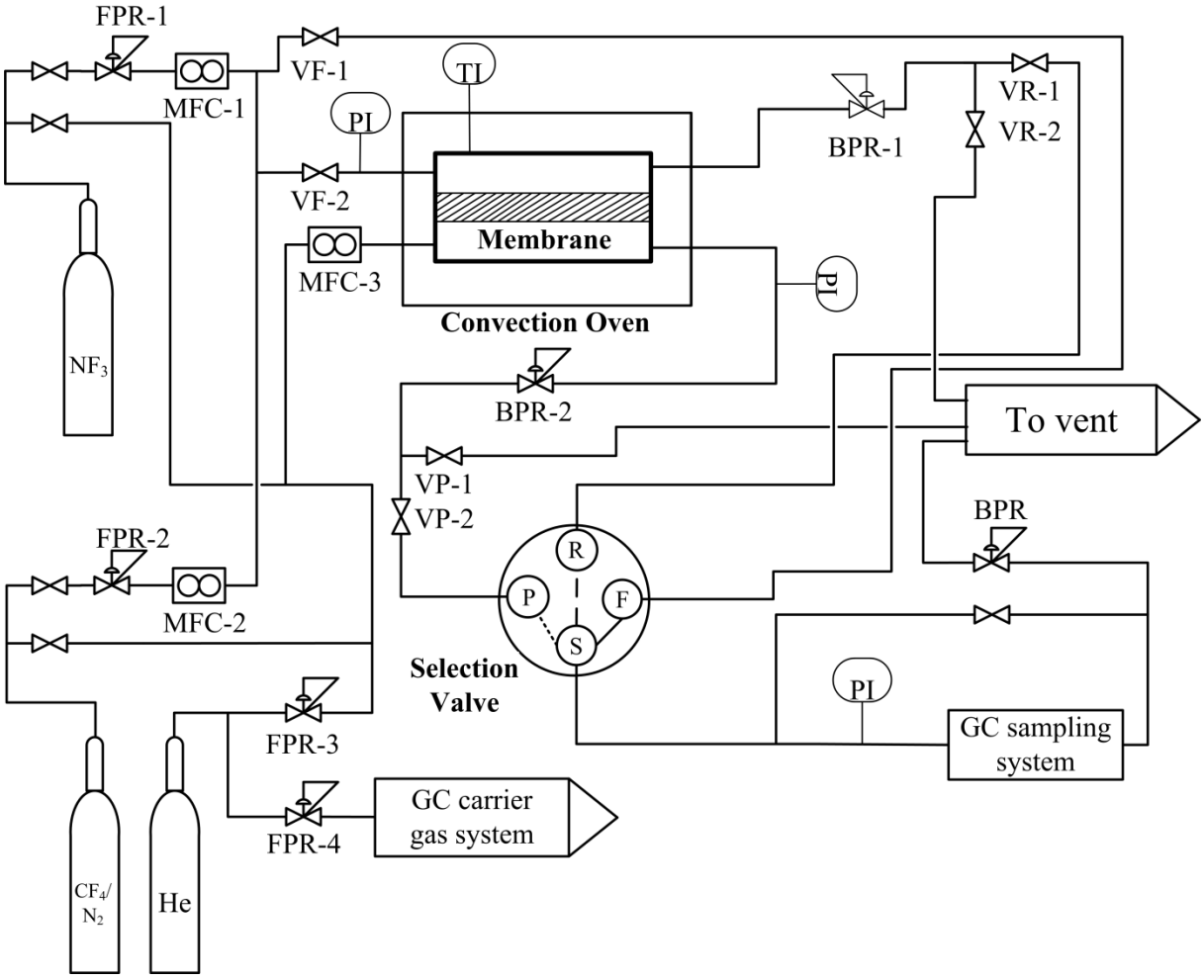

Figure 3.2: Partial plumbing and instrumentation diagram (PID) of the experimental setup used for pure and mixed gas permeation measurements. The text may be consulted for a brief description.

The permeation cell was placed inside a convection oven where the temperature of the surroundings as well as that of the fluid at the feed side of the membrane was measured using Type K thermocouples (Wika, Germany). Effective temperature control was thus achieved, where the temperature inside the permeation cell was stable to within ± 0.5 °C of the desired setting. The absolute pressure was measured at both the feed and permeate side of the membrane using UT-10 electronic pressure transmitters (Wika, Germany), which were set to a span of 0 – 2000 kPa (abs) and had an accuracy of 0.2 kPa. The feed flow rate of NF_3 and CF_4 to the permeation cell was controlled using Brooks thermal mass flow controllers

(Brooks Instrument, Holland) that were accurate to within 2.5% according to the manufacturer. In many cases, He was used as a sweep gas on the permeate side of the membrane for quantitative analysis of NF_3 and/or CF_4 in the permeate stream using the on-line, dual channel GC system described in the previous chapter. Therefore, an additional Brooks thermal mass flow controller was used to control the flow rate of the He sweep gas to the permeate side of the membrane.

The feed pressure to the permeation cell was regulated using the respective forward-pressure regulators (FPR-1 and FPR-2) on each feed line, in combination with the back-pressure regulator on the retentate line (BPR-1) in the case of continuous flow (Fig. 3.2). Alternatively, closing of both valves on the retentate line (V-R1 and VR-2), resulted in a dead-end flow configuration that was used for pure gas permeation measurements (Sec. 3.2.5.1). Consequently, the feed pressure was regulated using only the respective forward-pressure regulators (FPR-1 and FPR-2), with the back-pressure regulator (BPR-1) being fully opened. Similarly, the permeate pressure could be controlled using the corresponding back-pressure regulator (BPR-2), if required. In all instances, a manual selection valve (Fig. 3.2) was used to select the desired stream for measuring the corresponding flow rate using a soap film bubble flow meter (not shown) and/or for sampling and quantitative analysis with the on-line GC system. As such, the feed flow rate and composition could also be determined by bypassing the permeation cell using the appropriate valves. The pressure applied across the GC sampling system, wherein the appropriate sample loops were installed, was controlled using the additional back-pressure regulator and accompanying needle valve as discussed in detail in the previous chapter (Sec. 2.2.4).

3.2.5.1 Pure Gas Permeation Measurements

Pure gas permeabilities for He, N_2, NF_3 and CF_4 were determined at trans-membrane pressures (Δp) between ca. 100 and 800 kPa by varying the feed pressure while keeping the permeate pressure constant at atmospheric pressure. The permeate pressure did, however, rise by ca. 2 kPa above atmospheric pressure during He permeation, due to the large flux displayed by the membranes used in this study towards this penetrant. This was, however, factored into the calculations for determining the permeability coefficients. In addition to the pressure variations, the temperature of the permeation cell was also varied, where the pure gas

permeability of all membranes towards NF_3 and CF_4 were determined at a fixed trans-membrane pressure of ca. Δp = 500 kPa at temperatures from 35 to 95 °C in 20 °C intervals.

Prior to the permeation measurements, the feed side of the permeation cell was thoroughly flushed with each of the penetrant gases using a continuous flow at an arbitrary pressure. Simultaneously, the permeate side was repeatedly bled off by keeping valve VP-1 closed and opening and closing valve VP-2 while the penetrant permeated through the membrane. Afterward, the feed side of the permeation cell was pressurised, with the pressure being regulated with the forward pressure regulator of the appropriate feed stream. After steady state conditions were reached, i.e. after at least 30 min when permeability measurements stabilised, the permeability coefficients of each of the penetrants were determined according to the following expression as has been used in previous studies [24, 28, 29]:

$$P = \frac{T_S . p_a . \delta}{p_S \left(p_f - p_p \right) T . A} \left(\frac{dV}{dt} \right) \tag{3.1}$$

In Eq. (3.1), T_S is the standard temperature (273 K), p_S is the standard pressure (76 cmHg), p_f and p_p is the feed and permeate pressure (cmHg) respectively, p_a is the atmospheric pressure (cmHg), δ is the membrane thickness (cm), T is the temperature (K), A is the membrane area (cm^2), (dV/dt) is the volumetric displacement rate (cm^3/s) of the soap film in the bubble flow meter, and P is the permeability coefficient (cm^3(STP).cm/(cm^2.cmHg.s)). It is important to note that p_a and T represent the atmospheric pressure and temperature, respectively, at which the soap film bubble flow rate was measured. Although non-SI units are used for calculation of the permeability, these units will be used throughout to assist the reader in comparing the results obtained in this study with appropriate literature data.

During the measurement of AF1600 permeability towards CF_4, and of Hyflon AD60 permeability towards NF_3 and CF_4, the flux obtained was too low to enable flow rate measurements using the soap film bubble flow meter. In these instances, He was used as sweep gas on the permeate side of the membrane whereby the permeate stream composition could be determined. After flushing the feed side of the permeation cell with the penetrant gas as described above, the back-pressure regulator (BPR-1) and appropriate forward-pressure regulator (FPR-1 or FPR-2) was used to control the feed pressure while the feed flow rate was controlled using the appropriate mass flow controller. The pressure of the He sweep gas at the

permeate side was kept constant at ca. 130 kPa (abs) throughout using back-pressure regulator BPR-2. The feed flow rate was chosen to be at least 50-fold higher than the maximum He flow rate that could be achieved through the membrane in the opposite direction, due to the He pressure applied on the permeate side. Also, the maximum stage-cut achieved, i.e. the ratio of the permeate flow rate to the feed flow rate, was 0.0003. Therefore, the feed composition could be assumed to remain constant throughout. Consequently, the feed pressure was varied between ca. 100 and 800 kPa (abs), and the permeability coefficients, P were determined using Eq. (3.2):

$$P = \frac{T_S . p_a . \delta . y_p}{p_S \left(p_f - y_p . p_p \right) T . A} \left(\frac{dV}{dt} \right) \tag{3.2}$$

In Eq. (3.2), y_p is the mole fraction of the penetrant in the permeate stream as determined from the on-line GC analysis, p_p is the total pressure at the permeate side of the membrane (cmHg), and, in this case, (dV/dt) is the volumetric displacement rate (cm^3/s) of the soap film in the bubble flow meter pertaining to the flow rate of the He sweep gas. From the pure gas permeability data the ideal selectivity, $\alpha(He/N_2)$ or $\alpha(NF_3/CF_4)$, was calculated as the ratio of the corresponding pure gas permeability values for each membrane.

3.2.5.2 Mixed Gas Permeation Measurements

Mixed gas permeability coefficients of NF_3 and CF_4 were determined for all the membranes studied, at a constant 50:50 molar feed composition controlled using the respective mass flow controllers. In the case of Hyflon AD60 however, mixed gas permeability was also determined at CF_4 feed compositions of 15, 30, 50 and 61 mol%. All experiments were done using the same basic procedure outlined above for the pure gas permeation using He as the sweep gas, with the main difference being that the feed comprised of mixtures of NF_3 and CF_4. In all instances, the total feed pressure was regulated to a constant value of ca. 750 kPa (abs), with the combined flow rate kept fixed at 224 cm^3/min, resulting in a maximum stage-cut of 0.012 having been reached for the most permeable membrane (AF2400). The ratio of the feed flow rate to the maximum attainable He flow rate due to back-diffusion from the permeate side was lower than in the special case of pure gas permeability measurements described above. Therefore, both the compositions of the feed and retentate streams were

quantitatively analysed, whereby the mixed gas permeability was determined according to Eq. (3.3) [28, 30]:

$$P = \frac{T_S.p_a.\delta.y_p}{p_S\left(z_r p_f - y_p.p_p\right)T.A}\left(\frac{dV}{dt}\right) \tag{3.3}$$

The only difference between Eq. (3.3) and Eq. (3.2) is that the mole fraction of each gas species in the retentate stream, z_r, needs to be accounted for as the feed gas comprises of a mixture of NF_3 and CF_4. Normally, one would use the mole fraction of each gas species in the feed mixture, x_f, together with the total feed pressure, p_f, to calculate the individual permeabilities. However, because He was used as a sweep gas for analysis of the permeate stream, back-diffusion of He occurred from the permeate side to the feed side of the membrane which slightly altered the composition of the gas mixture on the feed side of the membrane. Therefore, to obtain a more accurate representation of the composition of the fluid on the feed side of the membrane, the mole fractions of the gas species in the retentate stream needed to be used instead. Although this effect would have been negligible if a higher total feed flow rate was used instead, the permeability and selectivity results would have been unaffected. Furthermore, no distinction had to be made in Eq. (3.3) between the feed pressure, p_f, and the retentate pressure, p_r, as these two quantities are the same, as was measured using the pressure transducer on the feed side of the permeation cell (Fig. 3.2). Having determined the individual permeabilities of NF_3 and CF_4 according to Eq. (3.3), the permeability selectivity, $\alpha(NF_3/CF_4)$, could be evaluated using Eq. (3.4) [30, 31]:

$$\alpha\left(\mathrm{NF_3}/\mathrm{CF_4}\right) = \frac{P_{\mathrm{NF_3}}}{P_{\mathrm{CF_4}}} = \frac{y_{\mathrm{NF_3}} \big/ y_{\mathrm{CF_4}}}{z_{\mathrm{NF_3}} \big/ z_{\mathrm{CF_4}}} \tag{3.4}$$

where y_i is the mole fraction of component i in the permeate stream, and z_i is the mole fraction of component i in the retentate stream. Normally, x_i, the mole fraction of component i in the feed stream [30, 31] would have been used instead of z_i, but as explained above the mole fraction of each component in the retentate stream was used in this study instead for a more accurate representation of the composition of the fluid at the feed side of the membrane. As such, the mass balance conditions were tested for all mixed gas permeability experiments, and

the percentage error between the total NF_3 and CF_4 flow rate of the feed and the sum of the total NF_3 and CF_4 flow rate in the retentate and permeate did not exceed ± 1.6 %. Table 3.1 gives a summary of the various permeability measurement methods and equations that were used to determine the permeability of the membranes studied in this thesis towards the various pure gases and NF_3/CF_4 mixtures.

Table 3.1: Summary of the various methods and equations used to measure the pure and mixed gas permeability of the three different membranes studied in this thesis towards He, N_2, NF_3 and CF_4.

Measurement Method	**Equation used**	**Membrane**		
		Teflon AF2400	**Teflon AF1600**	**Hyflon AD60**
Soap film bubble flow meter	3.1	He, N_2, NF_3, CF_4	He, N_2, NF_3	He, N_2
Soap film bubble flow meter with GC	3.2	-	CF_4	NF_3, CF_4
Soap film bubble flow meter with GC	3.3	NF_3/CF_4 Mixture	NF_3/CF_4 Mixture	NF_3/CF_4 Mixtures

3.3 Results and Discussion

3.3.1 Membrane Characterization

The rate of solvent evaporation from the AF2400 cast films was critical to ensure smooth films of homogenous thickness [32], and therefore, it was necessary to cover the glass cylinders with watch glasses to sufficiently slow the rate of evaporation. Since the solvent evaporation rate for the AF1600 and Hyflon AD60 films was however less critical, overturned funnels were sufficient to aid in the formation of flat, smooth films of these polymers, thus ensuring good integrity of the resulting polymer membranes.

It is generally known, however, that residual solvent as well as factors such as the film treatment history and physical aging can have detrimental effects on membrane performance [33, 34]. Jansen *et al.* [35] and Macchione *et al.* [36] found that the thermal and gas transport properties of solution cast Hyflon AD60 membranes are significantly influenced by the residual solvent content, showing that the films had to be annealed at a temperature well

above the polymer's glass transition temperature, T_g, of 130 °C to obtain films that were not swollen due to residual solvent. Therefore, the Hyflon AD60 films prepared in this study were annealed by heating to 170 °C, in contrast to the 200 °C used by Jansen *et al.* [35] and Macchione *et al.* [36], followed by subsequent cooling (Sec. 3.2.2). AF2400 and AF1600, however, which have higher glass transition temperatures, were annealed by heating to a maximum of 200 °C.

During the annealing of the individual polymer membranes, the use of porous PTFE support layers (Sec. 3.2.2) prevented the membranes from being damaged due to softening when heated to above or close to their respective glass transition temperatures. The adhesion obtained between the Hyflon AD60 films and the PTFE support layers was such that the two layers could not be separated without damaging the films. These membranes were thus used in this composite form, as shown in Fig. 3.3 for permeability and selectivity measurements. In the case of both AF2400 and AF1600, the degree of adhesion was such that the films could be easily stripped from the PTFE support layers before further use.

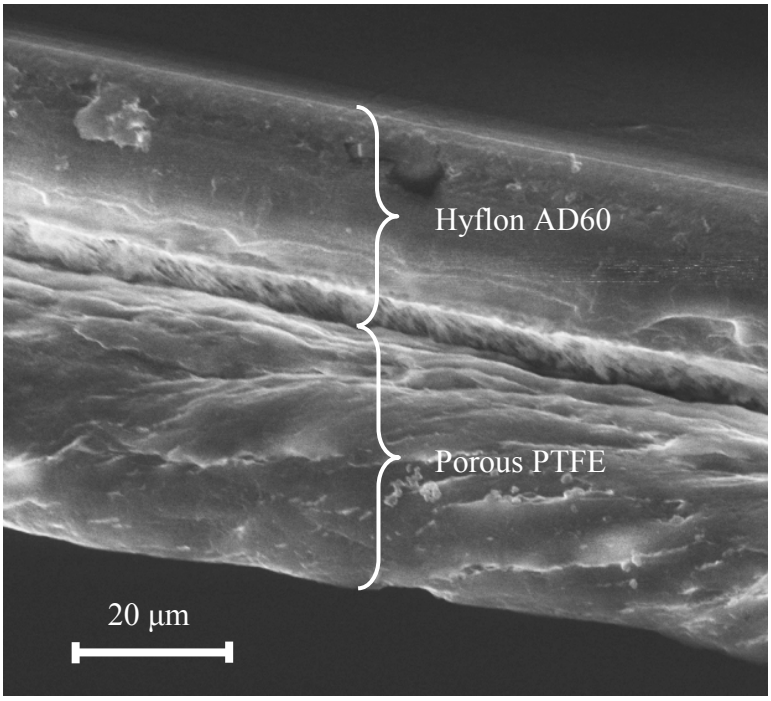

Figure 3.3: Cross sectional SEM micrograph of a composite Hyflon AD60 membrane as used in this study. The dense Hyflon AD60 films are located on top, and the porous PTFE support layer used for the annealing stage is located at the bottom.

The cross sectional image of an annealed Hyflon AD60 composite membrane (Fig. 3.3), as used in this study, clearly illustrates the strong adhesion between the two layers. Although a degree of separation between the two layers can also be seen in the image of Fig. 3.3, this was not expected to have a significant influence on the permeability and selectivity results. The approximate Hyflon AD60 film thickness of ~20 μm, as shown in Fig. 3.3, was typical of all the Hyflon AD60 membranes (Table 3.2) used in this study as determined from the dial gauge measurements. In this study, two films of each membrane were used to determine the repeatability of all subsequent results obtained, where a summary of the membranes studied, together with their corresponding thickness is given in Table 3.2.

Table 3.2: Different membranes with the corresponding average thickness of each of the individual films used for membrane characterization and permeation studies.

Membrane	Heat treatment	Average Film Thickness (μm)	
		Film 1	Film 2
Teflon AF2400	Annealed at 200 °C	25 ± 1	24 ± 3
Teflon AF1600	Annealed at 200 °C	32 ± 5	33 ± 4
Hyflon AD60[a]	Annealed at 170 °C	19 ± 2	18 ± 2
Hyflon AD60[b]	Heat treated at 95 °C	19 ± 3	24 ± 3

[a] Thickness measured after first heat treatment at 50 °C and after annealing at 170 °C (Sec. 3.2.2). [b] Thickness measured after first heat treatment at 50 °C (Sec. 3.2.2).

DSC analysis of the AF2400 powder (Fig. 3.4, Curves A), as received from the manufacturer, showed that during the first heating run, a T_g value of 254 °C was obtained, while a value of 239 °C was obtained during the second heating run. This seems to correspond with the results of Dlubek *et al.* [37] who noted that after heating AF2400 film samples under vacuum the T_g values were appreciably higher (267 °C) than the reported literature value of 240 °C, but that these returned to more or less the expected value (237 ± 2 °C) during a second heating run. The authors attributed this result to so-called "overaging" of AF2400 during the prolonged heat treatment. As the treatment history of the AF2400 powder received from Du Pont is unknown, it is difficult to draw the same conclusion here. However, from the two DSC curves of an annealed AF2400 film (Fig. 3.4, Curves B) it is clear that the same trend is observed, where the T_g determined from the first heating curve (252 °C) is noticeably higher than that determined from the second heating curve (241 °C). The downward slope of the first heating

curve after the transition event was present during DSC analysis of all the AF2400 film samples, but returned to normal during the second heating run.

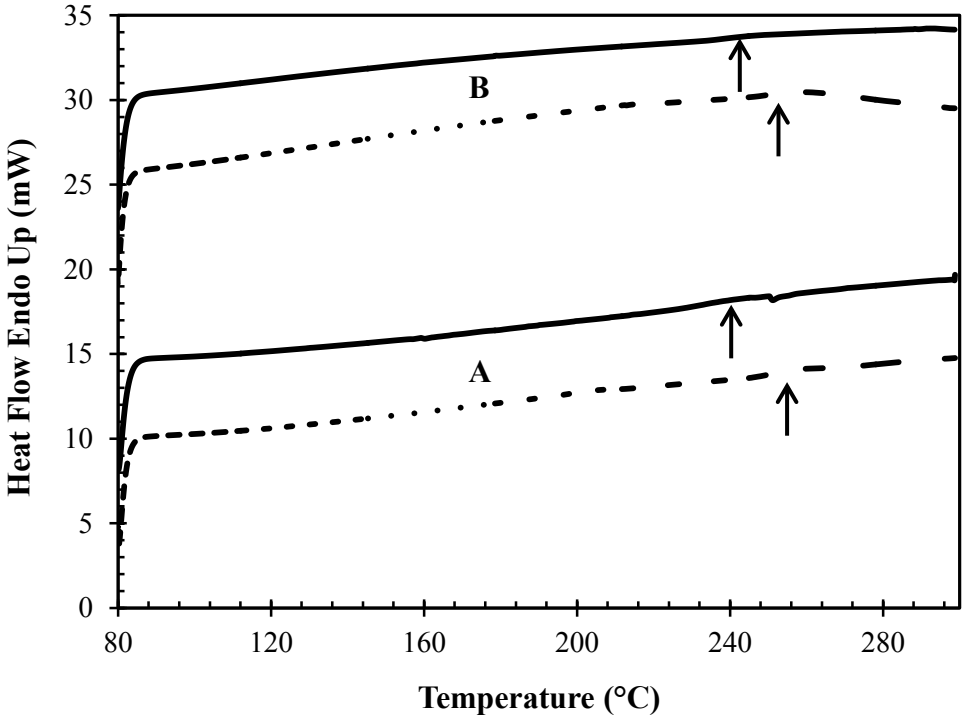

Figure 3.4: DSC Curves of the pure AF2400 powder (curves A), and an annealed solution cast AF2400 film (curves B). In both cases the dashed lines represent the first heating runs. The arrows mark the glass transition temperatures determined from each curve. The curves were shifted vertically to allow convenient comparison.

Regardless, it therefore seems plausible that prolonged thermal treatment of AF2400, in this case the AF2400 films that were annealed at 200 °C, caused some overaging of the polymer matrix, as reported by Dlubek *et al.* [37]. The T_g-values returned to normal, however, during subsequent cooling and a second heating run with the DSC. As all the films used in this study were subjected to DSC and TG analysis after the permeation experiments were completed, one can conclude that the membranes were used in a slightly "overaged" form. However, it is not expected that the overaging effect adversely affected the permeability and selectivity results, but rather that it could have further enhanced membrane performance as suggested by Alentiev at al. [34].

Contrary to the case of AF2400, the DSC results of the AF1600 powder (Fig. 3.5, curves A) show that more or less the same T_g values are obtained from both heating curves (166 ± 1.4

°C), although this is slightly higher than the accepted literature value of 160 °C, as was also reported by Dlubek *et al.* [37].

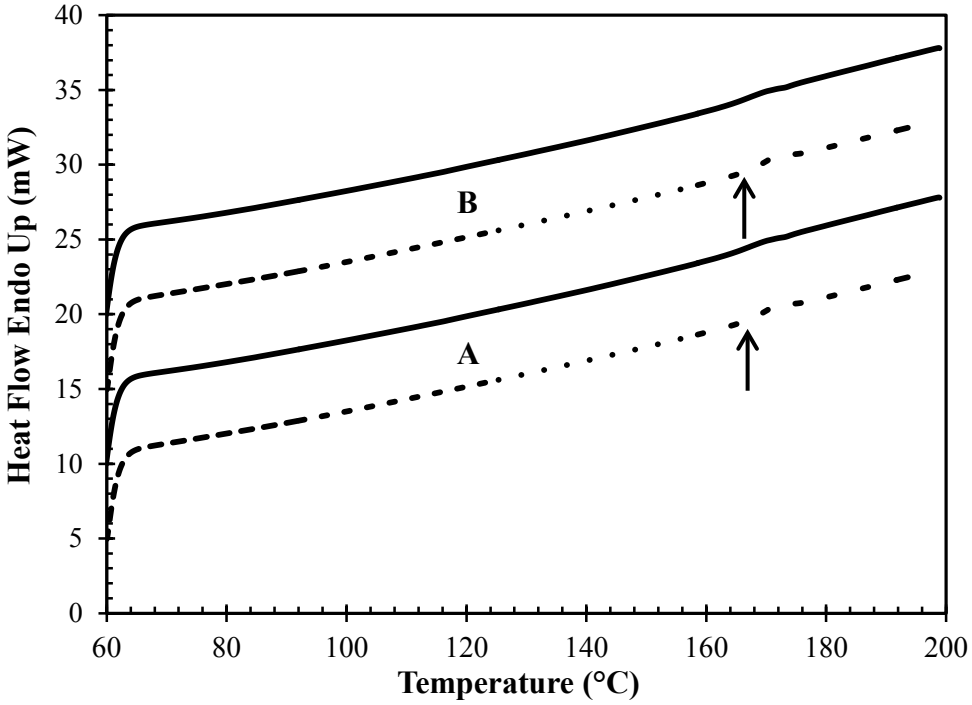

Figure 3.5: DSC Curves of the pure AF1600 powder (curves A), and an annealed solution cast AF1600 film (curves B). In both cases the dashed lines represent the first heating runs. The arrows mark the glass transition temperatures determined from each curve. The curves were shifted vertically to allow convenient comparison.

The same is also true of the AF1600 membrane sample (Fig. 3.5, curves B), wherein an average T_g of 168 ± 1.4 °C was obtained. During the first heating run, however, both the powder and the film samples registered a well-defined peak instead of the normal baseline transition. Therefore, the temperature corresponding to the onset of the glass transition event was used as the T_g value in these and any subsequent cases. Nevertheless, it is therefore clear that well equilibrated, if not slightly "overaged" polymer membranes of AF1600 were obtained after being subjected to the annealing process.

The DSC analysis of the Hyflon AD60 powder sample (Fig. 3.6, curves A) confirm the T_g of Hyflon AD60 of approximately 130 °C [35, 36], wherein a value of 128 °C was obtained from the second heating curve. The first heating curve showed some hysteresis around 130 °C, which is not uncommon for DSC analysis [36]. Correspondingly, the DSC curves of an

annealed Hyflon AD60 film sample (Fig. 3.6, curves B) indicate a similar average T_g of 127 ± 0.7 °C, which agrees with the results of Macchione *et al.* [36] who obtained a T_g of approximately 130 °C for their solution cast films that were annealed at 200 °C.

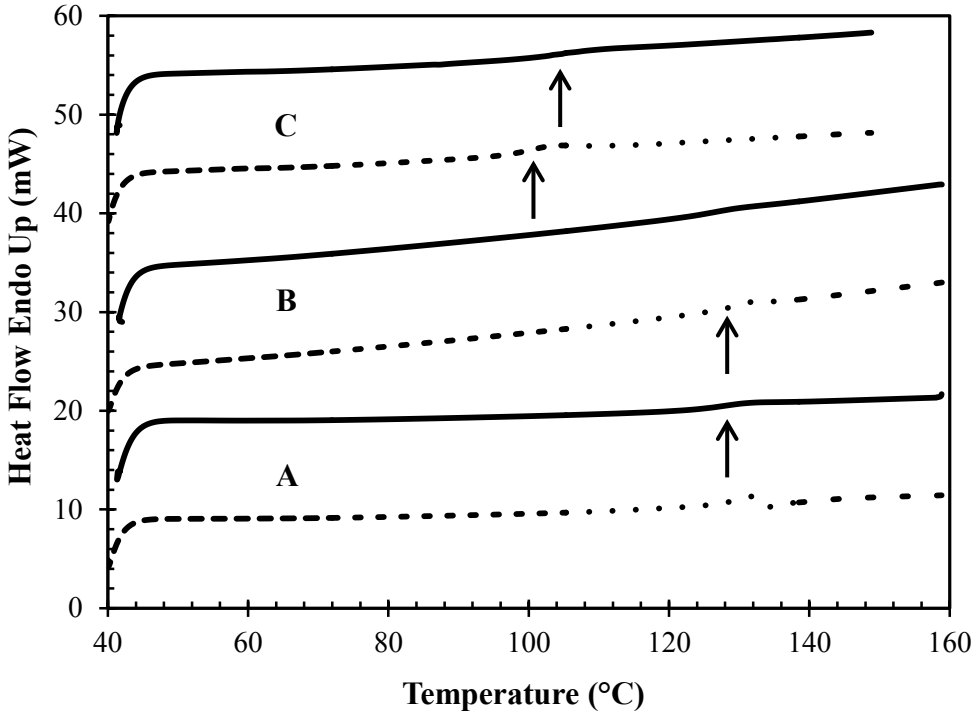

Figure 3.6: DSC Curves of the pure Hyflon AD60 powder (curves A), an annealed solution cast Hyflon AD60 film (curves B), and a Hyflon AD60 film that was heat treated at only 95 °C. In instances the dashed lines represent the first heating runs. The arrows mark the glass transition temperatures determined from each curve. The curves were shifted vertically to allow convenient comparison.

A significantly lowered T_g of 103 ± 3 °C (Fig. 3.6 curves C) was however obtained for the Hyflon AD60 film samples that were heat treated at 95 °C (inside the permeation cell – Sec. 3.2.2), compared to the value of 90 °C reported by Jansen *et al.* [35] for a solution cast Hyflon AD60 film heated in vacuum to 90 °C. Macchione *et al.* [36] on the other hand reported a value of approximately 80 °C for a solution cast Hyflon AD60 film that was heated slowly under vacuum to 98 °C when using the same solvent as Jansen *et al.* [35].These differences therefore seem to be influenced by the temperature program used, although the casting solvent has also been shown to have a significant influence on the resulting T_g values of solution cast Hyflon AD60 films that were annealed under identical conditions [36]. Regardless of the solvent used however, the T_g values of solution cast Hyflon AD60 films converged as the

annealing temperature was increased to 200 °C according to the results of Macchione *et al.* [36].

The TGA results (Fig. C.1 – Fig. C.3) gave further evidence that solvent-free, non-swollen membranes were obtained after the annealing process, where a negligible amount of weight loss (in the order of 1 %) occurred upon in situ heating of all the annealed membrane samples up to 300 °C. However, the Hyflon AD60 membranes that were heated up to 95 °C while secured inside the permeation cell (Sec. 3.2.2) underwent a significant weight loss of approximately 8 % (Fig. C.4). In accordance with the results presented by both Jansen *et al.* [35] and Macchione *et al.* [36], the lowered T_g (103 °C) obtained from the corresponding DSC analysis of this film (Fig. 3.6, curves C) can therefore be ascribed to the residual solvent that caused significant swelling and plasticisation of the polymer matrix. Furthermore, TG analysis of a Hyflon AD60 film that was only subjected to the initial heating to only 50 °C (Sec. 3.2.2) yielded an even larger weight loss of almost 16% (Fig. C.5), which related to an even higher degree of swelling, corresponding to an even lower T_g (86 ± 2 °C) for this film sample. One can therefore conclude, based on the DSC and TGA results, that the annealed membranes of Hyflon AD60 (in composite form) and Teflon AF used were mostly void of any solvent-induced plasticisation effects. To further elucidate the possible solvent effect, the swollen Hyflon AD60 membranes that were only heated to 95 °C in the permeation cell were used to compare the membrane performance with the annealed, non-swollen Hyflon AD60 membranes (Sec. 3.3.4).

3.3.2 Pure Gas Permeability and Selectivity

In this section, only the results obtained with the annealed, fully relaxed polymer membranes (first three listed in Table 3.2) will be discussed. In addition to NF_3 and CF_4, He and N_2 permeability and He/N_2 ideal selectivity were determined to characterise the performance of the membranes for comparison with literature results. Therefore, membrane performance as characterised by the He/N_2 permeability selectivity will first be evaluated, where after NF_3/CF_4 permeability and permeability selectivity will be discussed in detail.

From the summary presented in Table 3.3 it is evident that a satisfactory agreement between the average pure gas permeability and selectivity results of the three different membranes studied and the available literature data was obtained. This is despite the fact that the pure gas

permeability values taken from literature were in most instances determined under slight variations of temperature and pressure using, in some cases, different measurements techniques.

Table 3.3: Comparison between the available literature data and the average pure gas permeability and He/N_2 ideal selectivity of Teflon AF2400, Teflon AF1600 and Hyflon AD60 determined at 35 °C and Δp = 200 kPa in this study.

Membrane	Permeability (Barrer[a])				Ideal Selectivity	Reference
	He	N_2	NF_3	CF_4	$\alpha(He/N_2)$	
AF2400	2501 ± 9	479 ± 7	227 ± 9	53 ± 2	5.2	This study
	2700	490	-	-	5.5	[38]
	-	480	-	66	-	[39]
	2910	584	-	-	5.0	[32]
AF1600	1207 ± 43	94 ± 0.7	29 ± 0.7	4.8 ± 0.2	12.9	This study
	861	75.6	-	-	11.4	[32]
	-	~ 102	-	~ 35	-	[40]
Hyflon AD60	396 ± 24	9.6 ± 0.5	1.9 ± 0.08	0.19 ± 0.04	41.3	This study
	405	8.3	-	-	49.0	[35]
	455	11.1	-	-	41.0	[36][b]
	476	9.46	-	-	50.3	[36][c]

[a] 1 Barrer = 10^{-10} $cm^3(STP).cm/(cm^2.cmHg.s)$. [b] Hyflon AD60 membrane cast from a HFE 7100 solution and annealed at 200 °C. [c] Hyflon AD60 membrane cast from a Galden HT 55 solution and annealed at 200 °C.

It is interesting to note that the He/N_2 performance data of Jansen *et al.* for AF2400 and AF1600 membranes [32] was obtained using solution cast membranes that were subsequently heat treated at only 70 °C under vacuum. From the data presented in Table 3.3 it is evident that their AF1600 membranes had a slightly lower selectivity compared to the annealed membranes of AF1600 used in this study. Furthermore, the He/N_2 membrane performance data obtained in this study compared favourably with the respective melt-pressed AF2400 films used by Nemser and Roman [38], the melt-pressed Hyflon AD60 films used by Jansen

et al. [35], and the annealed solution cast Hyflon AD60 films used by Macchione *et al.* [36]. Jansen *et al.* [35] and Macchione *et al.* [36] have shown that the Hyflon AD60 membrane performance and selectivity was significantly reduced by plasticisation induced by residual casting solvent as was evident from the lowered T_g-values. Consequently, the plasticisation effect could only be corrected by annealing the polymer films well above their glass transition temperatures as discussed in Sec. 3.3.1. Therefore, the satisfactory He/N_2 separation performance (Table 3.3) obtained with the annealed membranes in this work also confirmed the non-swollen character of the polymer films as verified by the thermal analysis results discussed in Sec. 3.3.1.

It is also clear from the results presented in Table 3.3 that satisfactory repeatability was obtained with respect to the measured permeability coefficients of all gases, thus indicating that the membranes were also free of micro-defects that would have had detrimental effects on membrane performance. Based on all the presented evidence, it could therefore be concluded that high quality membranes of AF2400, AF1600 and Hyflon AD60 were obtained. The CF_4 permeability coefficient as shown in Table 3.3 was lower than that obtained by Merkel *et al.* [39] for AF2400, and significantly lower than that obtained by Alentiev *et al.* [40] for AF1600. Both Merkel *et al.* [39] and Alentiev *et al.* [40] however only dried their solution cast Teflon AF films in ambient conditions and did not report that the films were subjected to any further heat treatment. It is therefore possible that the Teflon AF membranes they used were swollen with residual solvent, which would result in higher permeability values for CF_4 in both cases due to solvent induced plasticisation effects (discussed further in Sec. 3.3.4).

It is apparent from the data presented in Table 3.3 that both the He and N_2 permeability for the membranes used in this study decreased in the order AF2400 > AF1600 > Hyflon AD60, with a resulting increase in He/N_2 selectivity. The decreasing He and N_2 permeability was also accompanied with a decrease in the permeability of both NF_3 and CF_4. As it was shown (Table 3.3) that reliable and repeatable permeability and selectivity results were obtained using the annealed AF2400, AF1600 and Hyflon AD60 membranes, single films were subsequently used to study the permeability and selectivity as a function of trans-membrane pressure. Accordingly, the results shown for AF2400 in Fig. 3.7 (a), for AF1600 in Fig. 3.7 (b), and for Hyflon AD60 in Fig. 3.7 (c) indicate that the permeability coefficients of He, N_2, NF_3, and CF_4 remained practically constant as the trans-membrane pressure, Δp, was varied

between ca. 100 and 800 kPa. This is a significant result with respect to NF_3 and CF_4 as the solubilities of the two gases are therefore such that they did not cause penetrant induced swelling and plasticisation of the amorphous glassy perfluoropolymer matrices.

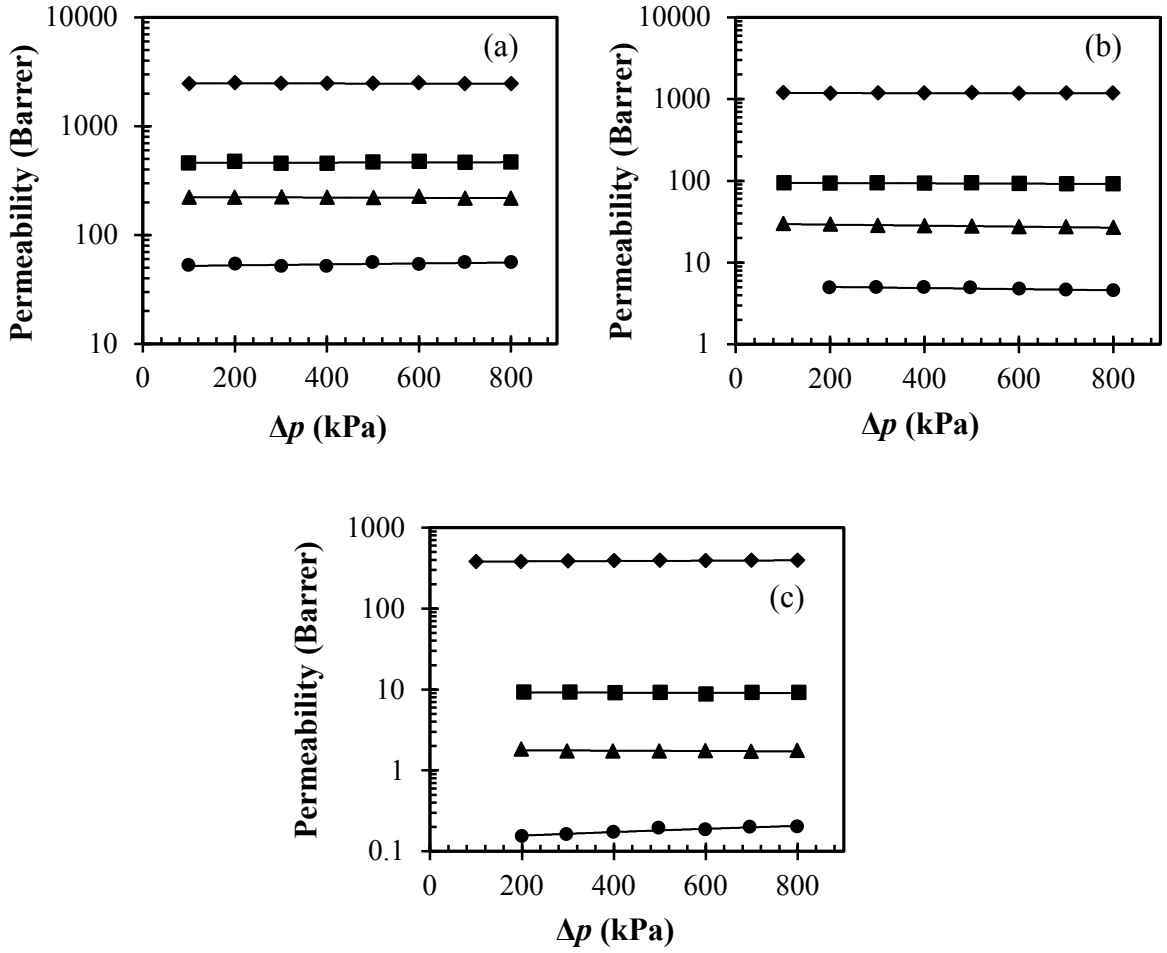

Figure 3.7: Representative pure gas permeability coefficients of He (♦), N_2 (■), NF_3 (▲), and CF_4 (●) for AF2400 (a), AF1600 (b), and Hyflon AD60 (c) as a function of trans-membrane pressure, Δp, at a constant temperature of 35 °C. Lines are drawn to serve as a visual guide only.

In fact, in some cases, although the effect is practically negligible, there was an apparent decrease in permeability coefficients with increasing trans-membrane pressure. This could be related to the fact that transport of gas penetrants through dense polymeric membranes is described by the well-established solution-diffusion model as expressed by Eq. (3.5) [16, 24, 28, 29, 31]:

$$P = S.D \tag{3.5}$$

where P is the permeability (cm^3(STP).cm/(cm^2.cmHg.s)), S is the solubility coefficient (cm^3(STP)/cm^3.cmHg), and D is the diffusion coefficient (cm^2/s). For weakly soluble penetrants such as He, or penetrants with relatively low solubility coefficients that do not cause plasticisation or swelling of the polymer matrix with increasing pressure, the solubility coefficient either stays constant with increasing feed pressure (linear sorption isotherm) or decreases slightly (non-linear sorption isotherm). Furthermore, the polymer matrix is slightly compressed as a result of the increasing hydrostatic feed pressure, causing a slight decrease in penetrant diffusion coefficients [24]. Because of these two effects, it is thus possible for the permeability coefficient expressed by Eq. (3.5) to exhibit a slight decrease with increasing feed pressure (and also trans-membrane pressure, Δp) for relatively weakly soluble penetrants.

Regardless, it is apparent from the permeability results presented in Fig. 3.7 that the NF_3 permeability is consistently higher than the CF_4 permeability, implicating that all the membranes studied were selective towards the permeation of NF_3 rather than CF_4. Furthermore, in accordance with the results shown in Table 3.3, it is apparent from Fig. 3.7 that both the NF_3 and CF_4 permeability coefficients of the membranes decreased in the order AF2400 > AF1600 > Hyflon AD60 resulting in an increase in the ideal NF_3/CF_4 permeability selectivity. The consistent decrease in permeability of the three membranes towards all four different gases is a natural consequence of the decreasing fractional free volume (FFV) of these polymers, defined as [28, 41 – 44]:

$$FFV = \frac{V_f}{V_{sp}} = \frac{V_{sp} - 1.3V_w}{V_{sp}} \tag{3.6}$$

In Eq. (3.6), V_{sp} is the specific volume of the polymer (cm^3/g), V_f is the free volume (cm^3/g), which can be estimated from the van der Waals volume (V_w), i.e. the volume occupied by the polymer chains, which can in turn be calculated from the Bondi group contribution method [42, 45]. Accordingly, the FFV of AF2400 is 32 % [39, 46, 47], that of AF1600 is 28 % [46], and that of Hyflon AD60 is 23 % [43]. The high permeability coefficients displayed by these perfluoropolymers towards permanent gases such as He, N_2, NF_3, and CF_4 is therefore attributed, as is widely known, to the high fractional free volumes of these polymers as noted in Sec. 3.1. The dioxole rings present in chemical structures of these perfluoropolymers (Fig. 3.1) disrupts the chain packing density, resulting in fully amourphous glassy matrices.

Consequently, large occluded excess free volume elements are present in the glassy polymer matrices of the Teflon AF and Hyflon AD perfluoropolymers [43, 44, 47]. Therefore, the solubility coefficients (S in Eq. (3.5)) of permanent gases in these high free volume perfluoropolymer matrices, although lower than highly condensable gases such as CO_2, increase with the amount of fractional free volume that is accessible to the penetrants [40, 48]. Also, the diffusivity of penetrants, i.e. D in Eq. (3.5), is normally restricted in classical glassy polymers due to the poor chain flexibility. However, higher diffusion coefficients are reached in these perfluoropolymers because of the higher free volume, which forms a semi-porous network within the glassy polymer matrix [28, 44, 49, 50]. As a result, penetrant diffusivity therefore also increases with increasing fractional free volume (FFV) [49], thus explaining the relatively high permeability coefficients shown in Fig. 3.7 (a) and (b). However, as the FFV decreases, both the diffusivity and solubility (Eq. 3.5) of the penetrants in the amorphous perfluoropolymer matrices decrease [32, 40, 48, 49]. Consequently, Hyflon AD60, which has the smallest FFV, therefore exhibited the lowest gas permeability coefficients of the three membranes studied, but also the highest ideal selectivity values. Since the permeability coefficients of NF_3 and CF_4 remained more or less constant over the differential pressure range used, the ideal permeability selectivity, $\alpha(NF_3/CF_4)_{ideal}$, remained constant for all the membranes with increasing Δp.

The increase in the ideal selectivity of NF_3 relative to CF_4 in the order AF2400 < AF1600 < Hyflon AD60 was accompanied by the decrease of both the NF_3 and CF_4 permeability over three orders of magnitude (Table 3.4), confirming the general challenge associated with membrane gas separation, in which high permeability selectivity is associated with low gas flux through a membrane [18 – 20]. Although relatively low selectivity was obtained with AF2400, it displayed the highest NF_3 permeability due to its high FFV (Table 3.4) as discussed above.

Furthermore, in terms of performance, the NF_3/CF_4 ideal selectivity of 4.5 is comparable to the O_2/N_2 selectivity of 4.5 obtained with a PIM-7 membrane [18], wherein the O_2 permeability equalled 190 Barrer. This lies close to the current Robson upper bound for O_2/N_2 separation [18], which represents the limit of current polymer membrane performance, based on the collection of a large number of literature data. Based on this analogous case of O_2/N_2 separation, it is therefore clear that although AF2400 yielded the lowest NF_3/CF_4 selectivity, its performance, i.e. high NF_3 permeability, is rather remarkable. Because of the lower FFV of

both AF1600 and Hyflon AD60, both the solubility and diffusivity of both NF_3 and CF_4 decreased, resulting in lower permeabilities in these two cases. It is, however, difficult at this stage to identify whether diffusion selectivity or solubility selectivity is responsible for the observed separation efficiency.

Table 3.4: Optimum pure gas permeability and ideal selectivity of NF_3 and CF_4 obtained for the different membranes studied at 35 °C and Δp = 200 kPa.

Membrane	Fractional Free Volume (FFV %)	Permeability (Barrer)*		Ideal Selectivity $\alpha(NF_3/CF_4)$
		NF_3	CF_4	
AF2400	32	233.5	52	4.5
AF1600	28	28.4	4.7	6.0
Hyflon AD60	23	1.83	0.15	12.2

* Permeability values differ slightly from those presented in Table 3.3, which represented the averages obtained from two individual films of each membrane, whereas the values given here represent the best results obtained in each case.

It is well known that the permeability can be expressed as a function of temperature according to the Arrhenius-type relation [39]:

$$P = P_0 . exp\left[-\frac{E_p}{RT} \right] \tag{3.7}$$

where P_0 is a pre-exponential factor with units of permeability, E_p is the activation energy of permeation (kJ/mol), R is the universal gas constant (J/K.mol) and T is the temperature (K). By writing Eq. (3.7) in linear form it is therefore possible to determine the activation energy of permeation by measuring the permeability as a function of membrane temperature. The results of permeability as a function of temperature are shown in Fig. 3.8 (a) – (c), with the activation energy results summarised in Table 3.5, which show that in all cases relatively low activation energies were obtained, with that of NF_3 and CF_4 for AF2400 being the lowest. In addition, the ideal selectivity, $\alpha(NF_3/CF_4)_{ideal}$ decreased in all cases as a result of the increase in permeability of both NF_3 and CF_4 with increasing temperature.

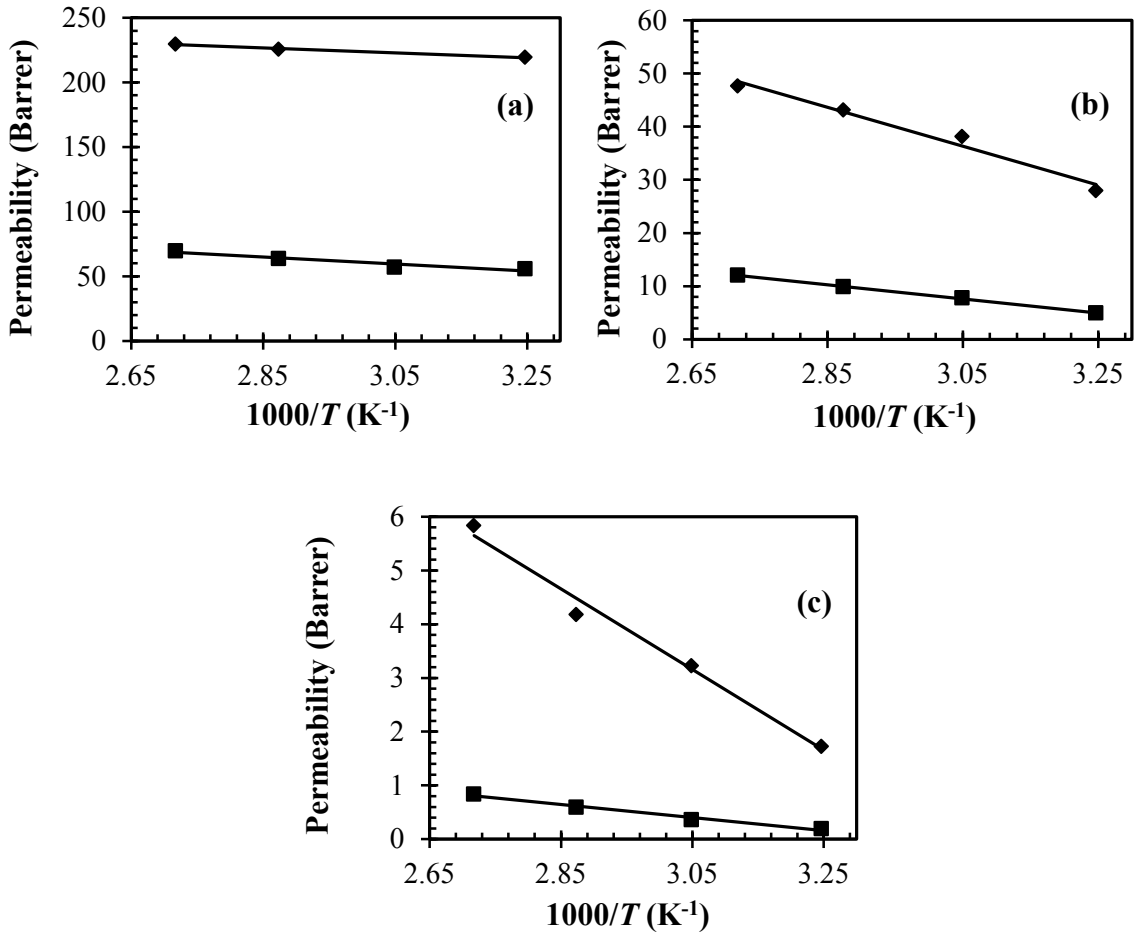

Figure 3.8: Representative pure gas permeability coefficients of NF_3 (♦) and CF_4 (■) for AF2400 (a), AF1600 (b), and Hyflon AD60 (c) as a function of temperature. Lines are drawn to serve as a visual guide.

Table 3.5: Activation energies of permeation, E_p, of NF_3 and CF_4 for the various membranes studied.

Membrane	E_p (kJ/mol)	
	NF_3	CF_4
AF2400	0.7	3.6
AF1600	8.2	13.9
Hyflon AD60	18.5	23.1

The low activation energies, especially in the case of AF2400, were obviously due to the small variation in the permeability coefficients of both gases with increasing temperature. Furthermore, because the activation energy of permeation is the sum of the activation energy

of diffusion, E_D (kJ/mol) and the enthalpy change associated with sorption, ΔH_s (kJ/mol) [28, 40]:

$$E_p = E_D + \Delta H_s \tag{3.8}$$

a positive E_p implies that $E_D > |\Delta H_s|$. Therefore, the small increase in permeability of AF2400 towards NF_3 and CF_4, and therefore the small E_p-values, was caused by the activation energy of diffusion, E_D, only being slightly larger than the enthalpy of sorption, $|\Delta H_s|$. The small E_p-value of NF_3 could, however, also be caused by a large enthalpy of sorption, $|\Delta H_s|$, relative to the activation energy of diffusion, E_D. However, the variation of solubility with temperature, and therefore ΔH_s, could not be determined with the current experimental setup. Nonetheless, low activation energies of diffusion, E_D, are common in high free volume polymers [40], where $E_D < |\Delta H_s|$ for small, fast diffusing penetrant gases such as He and N_2, which results in negative E_p-values [28]. Also, due to the large FFV of AF2400, and the fact that the free volume elements start forming interconnected pore structures at high FFVs [28, 44, 49, 50], the diffusivity of NF_3 and CF_4 could not have increased significantly with increasing temperature. Thus, the evidence seems to indicate that small activation energies of diffusion, E_D, could have been responsible for the small E_p-values, especially in the case of NF_3. Further, E_D should increase as the FFV becomes smaller, because diffusion becomes more strongly dependent on temperature. If it is assumed that the variation in $|\Delta H_s|$ with decreasing FFV is negligible, because the chemical nature of the three perfluoropolymers are quite similar, E_p should increase as the FFV decreases because the diffusivity, and thus permeability, is then more strongly affected by an increase in temperature. This therefore explains the increasing E_p-values of both NF_3 and CF_4 for AF1600 and Hyflon AD60 compared to AF2400 (Table 3.5).

From Eq. (3.5) it follows directly that permeability selectivity is the product of diffusion selectivity and solubility selectivity. As CF_4 had consistently higher E_p-values throughout (Table 3.5), it follows from the above discussion that its diffusion coefficients were more strongly influenced by a rise in temperature (higher E_D-values). Thus, one may argue that the permeability selectivity observed with respect to NF_3 and CF_4 can be attributed to diffusion selectivity, which increased from AF2400 to AF1600 to Hyflon AD60 due to the decreasing FFV in the same order. This increase in selectivity is characteristic of glassy polymers,

wherein the selectivity of permanent gases are determined largely by the sieving ability, or diffusion selectivity offered by the glassy matrix [29, 39, 40]. Therefore, it is possible that the increase in $\alpha(NF_3/CF_4)_{ideal}$ in the order AF2400 < AF1600 < Hyflon AD60 may be due to an increase in the diffusion selectivity of the membranes, caused by the decreasing FFV, keeping in mind that an effect of solubility selectivity could not be excluded at this point.

3.3.3 Mixed Gas Permeability and Selectivity

The pure gas permeability and selectivity results (Sec. 3.3.2) showed that the permeability of NF_3 and CF_4 and the selectivity towards NF_3 remained constant as a function of trans-membrane pressure, and therefore feed pressure for all three membranes. This was encouraging results as it suggested that membrane selectivity would not be influenced by the composition of the feed stream fed to any of the membranes that were used. Indeed, the results shown in Table 3.6 indicate that the mixed gas permeability of NF_3 and CF_4 and selectivity compared favourably with the pure gas results. In Table 3.6, the pure gas permeability and selectivity results according to Table 3.4 are also included for convenient comparison.

Table 3.6: Comparison between the pure and mixed gas permeability and selectivity of NF_3 and CF_4.

Membrane	Pure Gas Permeability (Barrer)		Mixed Gas Permeability (Barrer)		Selectivity, $\alpha(NF_3/CF_4)$	
	NF_3	CF_4	NF_3	CF_4	Pure	Mixed
AF2400	233.5	52	200.4	62.9	4.5	3.2
AF1600	28.4	4.7	31.2	5.1	6.0	6.1
Hyflon AD60	1.83	0.15	1.78	0.14	12.2	12.7

Note: Pure gas permeability and selectivity values were determined at 35 °C and Δp = 200 kPa (as reported in Table 3.4), and mixed gas permeability and selectivity were determined at 35 °C and total feed pressure of 750 kPa with a 50:50 molar composition (Sec. 3.2.5.2).

Reduced mixed gas selectivity was only obtained for AF2400 when compared to the ideal selectivity determined from the pure gas permeability measurements. This reduction in $\alpha(NF_3/CF_4)$ was the result of a lower NF_3 permeability and higher CF_4 permeability for the mixed gas experiments compared to the pure gas experiments, which could possibly have

been caused by competing solubility and diffusivity of NF_3 and CF_4 in the high free volume perfluoropolymer. Because of the high free volume of AF2400, not only the diffusion coefficients, but also the solubilities of both penetrants would have been at a maximum in this polymer compared to that in AF1600 and Hyflon AD60.

Furthermore, it is suspected that the consistently higher permeabilities of NF_3 relative to CF_4 were not only because of favourable diffusion selectivity as noted above (Sec. 3.3.2), but also because of favourable solubility selectivity, which is investigated in Chapter 4. This hypothesis is based on literature evidence that indicates that NF_3 is more favourably adsorbed onto porous adsorbents [10 – 12] compared to CF_4 and is more soluble than CF_4 in perfluorocarbon and halogenated fluids [51]. As also shown in the previous chapter, NF_3 is also more strongly adsorbed onto porous polymer packing materials used in analytical GC columns, causing it to frequently elute after CF_4 [52, 53]. It is therefore possible that the solubility selectivity of the high free volume AF2400 towards NF_3 deteriorated with the mixed gas feed, owing to the high sorption capacity of the matrix that contributed to the poor mixed gas selectivity when compared to the pure gas selectivity. It is also possible however, that this discrepancy was simply caused by experimental error.

The relative standard deviation (% RSD) in the mixed gas selectivity, $\alpha(NF_3/CF_4)$, for two Hyflon AD60 membranes were 7.2 %, which is reasonable. Based on this indication of repeatability, the deviation of the mixed gas permeability results for AF1600 and Hyflon AD60 from the pure gas permeability results was therefore insignificant. Essentially, similar performance was therefore achieved for these two membranes during both the pure gas and mixed gas permeability and selectivity measurements. Using the same Hyflon AD60 membrane, the results of the mixed gas permeability and selectivity measurements as a function of the CF_4 feed concentration (x_{CF4}) showed a slight decline in the selectivity, $\alpha(NF_3/CF_4)$, with decreasing CF_4 concentration (Fig. 3.9). Since any method of purifying NF_3 from CF_4 needs to be effective at ppm levels of CF_4 as noted in Sec. 1.1 and Sec. 3.1, this result therefore has important consequences. As such it is therefore clear that reduced selectivity is predicted at x_{CF4} values close to 0 (ppm levels) compared to the selectivity obtained at 50 and 61 mol % CF_4.

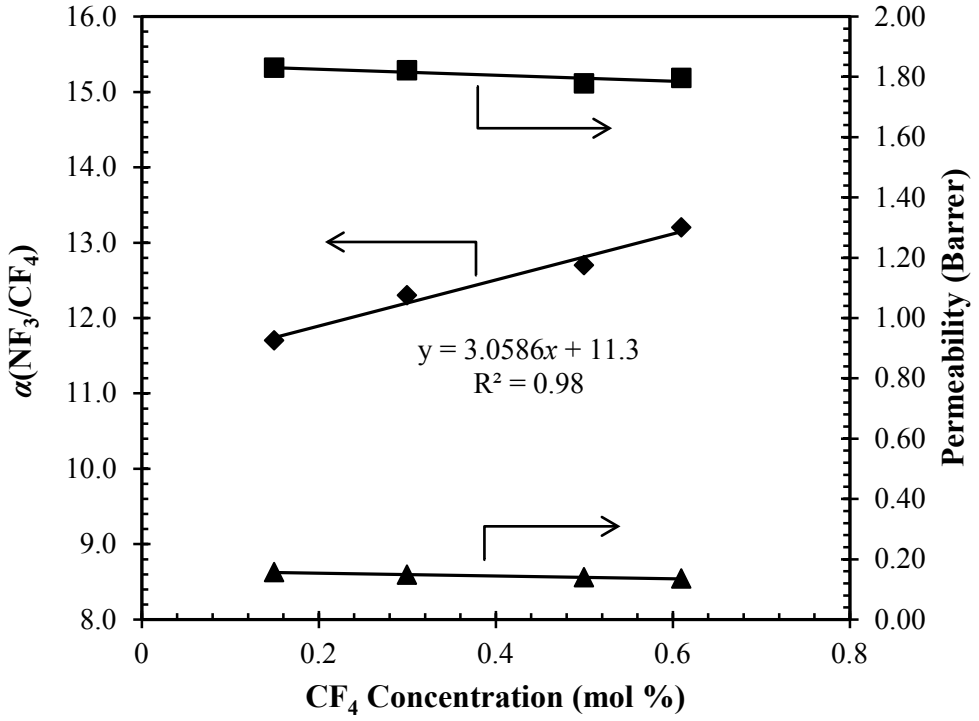

Figure 3.9: Mixed gas NF_3 (■) and CF_4 (▲) permeability (right axis) as a function of CF_4 feed concentration for an annealed Hyflon AD60 membrane. Also shown in the NF_3/CF_4 permeability selectivity, $\alpha(NF_3/CF_4)$ (♦) as a function of the CF_4 feed concentration (left axis) at a constant temperature of 35 °C.

The reason for this decline in selectivity is a result of a small but quantifiable increase in the permeabilities of both NF_3 and CF_4 with decreasing x_{CF4} as shown in Fig. 3.9. This observation may be explained based on the hypothesis that the observed NF_3 permeability selectivity was caused by both diffusion selectivity and solubility selectivity towards NF_3 as described in the preceding paragraphs. As the CF_4 concentration in the feed declined, the NF_3 concentration therefore increased which implies that the partial NF_3 pressure of the feed stream also increased. As the partial pressure of NF_3 in the feed stream increased, so did the concentration of NF_3 adsorbed in the polymer matrix, leading to a slight increase in the NF_3 permeability. Such an increase in permeability with increasing feed pressure, however slight, is indicative of a marginal amount of penetrant induced swelling [25] by NF_3 on the Hyflon AD60 matrix.

As a result of the minimal dilation of the polymer matrix a small yet significant increase in both the solubility and diffusivity [25] of CF_4 in the Hyflon AD60 membrane probably occurred, which lead to a deteriorating selectivity. Although this is a somewhat negative result

with regard to the applicability of membrane separation to the purification of NF_3 from CF_4, the extrapolated line fitted to the data points predicts that a selectivity of at least 11.3 should still be obtained with the current membrane at low CF_4 concentrations. Consequently, the applicability of membrane based purification of NF_3 from CF_4 using the amorphous glassy perfluoropolymers discussed in this chapter should, in principle, be attainable and will be further evaluated in Chapter 5.

3.3.4 The Effect of Solvent Induced Swelling on Hyflon AD60 Performance

The thermal analysis results (Sec. 3.3.1) indicated that a significant difference in the character of the Hyflon AD60 films annealed at 170 °C and those that were heat treated at 95 °C inside the permeation cell (Sec. 3.2.2) existed. As explained in Sec. 3.3.1, as well as in previous studies [35, 36], the observed effect on the glass transition temperature, T_g, of the films could be attributed to residual amounts of the casting solvent that had a plasticisation effect on the polymer matrix. Only after annealing at temperatures well above the T_g of Hyflon AD60 were non-swollen films free of any residual solvent obtained, as verified by the DSC (Fig. 3.6) and TGA results. Therefore, the permeability and selectivity of the swollen Hyflon AD60 membranes was also determined for comparison with the non-swollen Hyflon AD60 membranes, which yielded the best He/N_2 and NF_3/CF_4 selectivity (Sec. 3.3.2 and Sec. 3.3.3).

The data shown in Table 3.7 clearly illustrates, in accordance with the work of Jansen *et al.* [35] and Macchione *et al.* [36] that the swollen Hyflon AD60 membrane performance was significantly inferior to that of the non-swollen membranes shown in Table 3.3. The data from the different sources shown in Table 3.7 were obtained with solution cast Hyflon AD60 films, using different solvents, that were subjected to different heat treatment regimes [32, 35], or with no heat treatment at all [36]. Therefore, the different films were swollen to varying degrees, as was illustrated by the comparison of the T_g-values of the swollen Hyflon AD60 films obtained in this study (Fig. 3.6) with that of Jansen *et al.* [35] and Macchione *et al.* [36] (Sec. 3.3.1). This explains the rather poor correlation between the different data sets of Table 3.7, and the varying He/N_2 ideal selectivities that were obtained in each case.

Regardless, it is clear that the swollen membranes used in this study gave the best He/N_2 ideal selectivity compared to the various literature values, but the selectivity was almost half of that obtained with the non-swollen membranes (Table 3.3). Further comparison of the results

presented in Table 3.7 and Table 3.3 also shows that the reduction in membrane performance towards He and N_2 from the annealed to the freshly cast membranes of Macchione *et al.* [36], was even more pronounced. The distinct influence of swelling induced on the Hyflon AD60 polymer matrix by residual solvent as noted previously [35, 36] was therefore confirmed in this study.

Table 3.7: Comparison of the average pure gas permeabilities and He/N_2 ideal selectivity of swollen Hyflon AD60 membranes at 35 °C and Δp = 200 kPa (this study) with available literature data of swollen or partially swollen Hyflon AD60 membranes.

Permeability (Barrer)				Ideal Selectivity α(He/N_2)	Reference
He	N_2	NF_3	CF_4		
318 ± 67.4	13.7 ± 2	4.0 ± 0.6	0.6 ± 0.06	23.2	This study
369	20.5	-	-	18.0	[35]
357	38.1	-	-	9.4	[36][a]
339	26.2	-	-	12.9	[36][b]
330	18.9	-	-	17.5	[32]

[a] Hyflon AD60 membrane freshly cast from a Galden HT 55 solution. [b] Hyflon AD60 membrane freshly cast from a HFE 7100 solution.

Also in accordance with the literature data presented in Table 3.3 and Table 3.7, the reduction in He/N_2 selectivity of the swollen Hyflon AD60 membranes compared to the non-swollen ones were caused by a decrease in He permeability, coupled with an increase in N_2 permeability. Similarly, both the NF_3 and CF_4 permeabilities of the swollen Hyflon AD60 membranes were approximately double that of the non-swollen membranes, which again resulted in a reduced NF_3/CF_4 ideal selectivity of $\alpha(NF_3/CF_4)_{ideal}$ = 6.7. It is also apparent from the data obtained in this study (Table 3.7) that the repeatability of the permeability values also suffered somewhat compared to the non-swollen results (Table 3.3), which is attributed to the slight instability of the swollen polymer matrix.

The pure gas permeability coefficients of He and N_2 showed a negligible variation with increasing trans-membrane pressure, Δp, as shown in Fig. 3.10, while the permeability coefficients of NF_3, and especially CF_4, displayed a steady increase with increasing Δp. It would therefore seem that the residual solvent trapped inside the polymer matrix (concluded

from TGA results) induced a significant degree of plasticisation of the polymer chains such that the diffusion coefficients and thus permeability of the larger penetrants were increased.

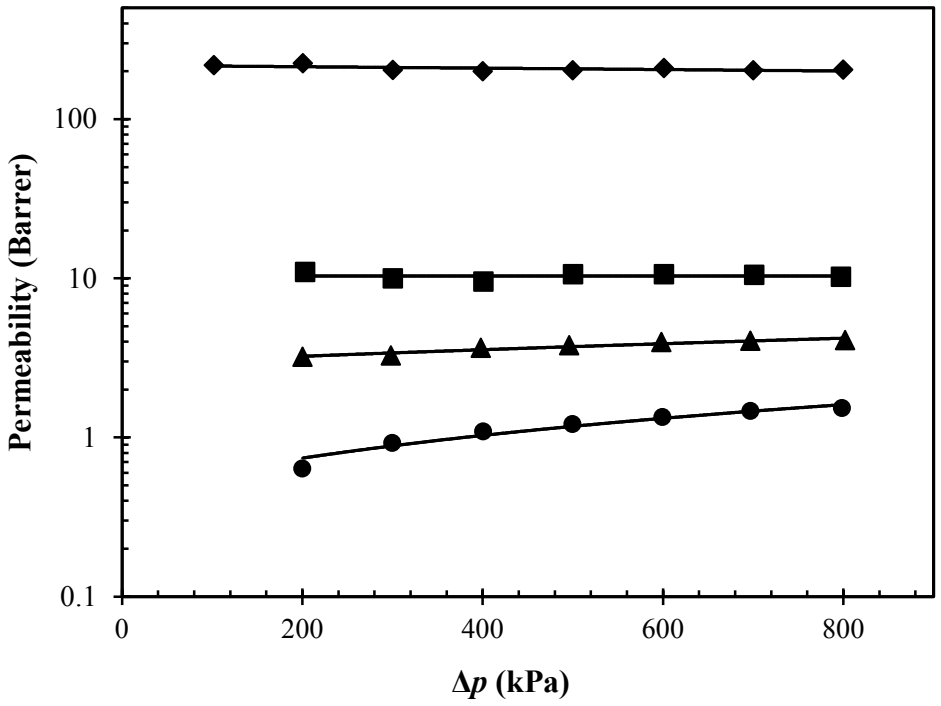

Figure 3.10: Representativie pure gas permeability coefficients of He (♦), N_2 (■), NF_3 (▲), and CF_4 (●) for a swollen Hyflon AD60 membrane as a function of trans-membrane pressure, Δp, at a constant temperature of 35 °C. Lines are drawn to serve as a visual guide only.

This effect is frequently observed with penetrant induced plasticisation in glassy polymers [25]. However, with increasing Δp, and therefore increasing feed pressure, the concentration of penetrants in the polymer also would have increased. It is therefore hypothesised that the diffusivity of NF_3 and CF_4 increased with increasing Δp as a result of the solvent induced plasticisation. This hypothesis is based on the fact that the effective diffusion coefficient, D, is a concentration averaged diffusivity [29, 39]:

$$D = \int_{C_1}^{C_2} \frac{D_{loc}}{1-\omega} dC = \int_{C_1}^{C_2} D_{eff} dC \qquad (3.9)$$

where D_{loc} is the local concentration-averaged diffusion coefficient, ω is the mass fraction of the gas in the polymer at concentration C, D_{eff} is the local effective diffusion coefficient, and

C_1 and C_2 are the gas concentrations at the feed and permeate side of the membrane. Merkel *et al.* [39] showed that the concentration averaged diffusion coefficient, D, of penetrants that do not induce swelling and plasticisation in AF2400, such as CF_4, increases linearly with penetrant concentration in the polymer. They further showed that this behaviour can be well described by the dual-mode transport model. However, for the larger more soluble gas C_2F_6, they found that D increased nearly by an order of magnitude over the range of concentrations investigated, which could not be described by the dual-mode transport model. They concluded that this behaviour was caused by plasticisation induced by C_2F_6, and that the vast increase in permeability with increasing Δp observed for AF2400 towards this gas was because of increased penetrant mobility. By analogy, it is therefore possible in the present case of solvent induced plasticisation, that the NF_3 and CF_4 diffusivity displayed a substantial increase with increasing Δp. This, in turn is a direct result of uncharacteristically higher D_{eff} values (Eq. (3.9)) due to the increased polymer chain mobility caused by the presence of the solvent molecules.

Consequently, this probable increase in the diffusivity with increasing Δp was more prominent for CF_4 (the larger molecule), leading to a larger increase in the permeability coefficient with increasing Δp compared to NF_3. As a result, the ideal selectivity, $\alpha(NF_3/CF_4)$, of the specific membrane for which the permeability data is shown in Fig. 3.10, decreased significantly from 5.0 at Δp = 200 kPa to 2.7 at Δp = 800 kPa. Although this trend was also observed with two other swollen Hyflon AD60 membranes, tested at Δp = 200 and 600 kPa, the results of the particular membrane presented in Fig. 3.10 was the most pronounced. Thus, it is also evident that varying results can be expected with such partially swollen membranes due to the unstable character of the swollen polymer matrix, which is therefore difficult to reproduce. Furthermore, because the swollen character of the membranes was unstable with increasing temperature, the permeabilities could not be reliably measured as a function of temperature. Nonetheless, greatly reduced NF_3/CF_4 selectivity was obtained with the swollen Hyflon AD60 membranes (Table 3.7) compared to the non-swollen membranes (Table 3.3), which was comparable to that of AF1600 (Table 3.4). Also, the average pure gas permeability and selectivity of three swollen Hyflon AD60 membranes as shown in Table 3.7 ($\alpha(NF_3/CF_4)_{ideal}$ = 6.7) compared well with the mixed gas permeability and selectivity of the most selective swollen membrane, for which P_{NF3} = 4.5 Barrer, P_{CF4} = 0.79 Barrer, and $\alpha(NF_3/CF_4)$ = 5.7.

The reduced selectivity for the swollen Hyflon AD60 membranes compared to the non-swollen membranes was therefore most probably caused by an increase in the diffusivity of the heavier penetrants due to the plasticisation effect, which is also evident from the results of Macchione *et al.* [36]. However, close inspection of the pure gas permeability, diffusivity and solubility results obtained by Macchione *et al.* [36] with two different annealed membranes and two different freshly cast membranes indicates that a loss in both diffusion selectivity and solubility selectivity might be to blame for the generally reduced permeability selectivity. For example, they obtained an O_2/N_2 permeability selectivity with annealed membranes that was typically 33 to 65 % higher than that of freshly cast membranes. This was as a result of the O_2 diffusion selectivity, D_{O2}/D_{N2}, of the annealed membranes being 20 to 50 % higher than that of the freshly cast membranes. However, with O_2 being the more easily condensable molecule of the two, the solubility selectivity, S_{O2}/S_{N2}, was also approximately 10 % higher with the annealed membranes compared to the freshly cast membranes. Similarly, the CO_2/N_2 solubility selectivity, S_{CO2}/S_{N2}, was 26 to 46 % higher with their annealed membranes, while the diffusion selectivity, $D_{CO2}/D_{N2,}$ was increased with annealing in one instance, but was decreased in another. The apparent decrease in solubility selectivity is understandable, considering that the swollen polymer matrix, although partially occupied by residual solvent molecules, would have had an increased sorption capacity. Such an increased sorption capacity would relate to decreased solubility selectivity, which is also observed with increasing FFV of the polymer matrix [32].

As noted previously, literature evidence of preferential adsorption of NF_3 onto adsorbent surfaces [10 – 12] and a generally higher solubility of NF_3 in perfluorcarbon and halogenated fluids [51] compared to CF_4 exist. This suggests that sorption selectivity with respect to NF_3, i.e. S_{NF3}/S_{CF4}, must have played an important part in the observed permeability selectivity (Sec. 3.3.3) displayed by AF2400, AF1600 and Hyflon AD60 towards NF_3. However, based on the sorption selectivity data of Macchione *et al.* [36], it is therefore also possible that not only deteriorated diffusion selectivity, D_{NF3}/D_{CF4}, but also weaker solubility selectivity, S_{NF3}/S_{CF4}, prevailed with the swollen Hyflon AD60 membranes compared to the non-swollen membranes. It is therefore evident that favourable solubility selectivity, S_{NF3}/S_{CF4}, as well as favourable diffusion selectivity, i.e. D_{NF3}/D_{CF4}, could have been jointly responsible for the observed NF_3 permeability selectivity obtained with the membranes used in this study. Both these aspects will, however, be further investigated in the next chapter.

3.4 Conclusions

It was shown that annealing of AF2400, AF1600 and Hyflon AD60 solution cast films above or near the glass transition temperatures of the respective polymers was crucial to yield high quality membranes that displayed optimum selectivity. Consequently, the pure gas permeability coefficients of NF_3 and CF_4 showed that all membranes were selective towards NF_3, and that the ideal selectivity increased in the order AF2400 < AF1600 < Hyflon AD60. Simultaneously, a decrease in the permeability coefficients over three orders of magnitude were observed, which was associated with the decreasing FFV of the perfluoropolymers. As NF_3 is a smaller, lighter molecule compared to CF_4, conventional wisdom would therefore suggest that the increase in permeability selectivity with decreasing FFV of the glassy perfluoropolymer membranes used was due to an increase in the diffusion selectivity towards NF_3. This indeed seemed to be the case, based on the analysis presented with respect to the dependence of the activation energies of permeation, E_p, of NF_3 and CF_4 on the FFV of the polymers. In addition, the pure gas permeabilities displayed no significant variation with increasing trans-membrane pressure, Δp, which suggested that the polymers were relatively inert towards both gases in terms of swelling and plasticisation. As a result, satisfactory ideal selectivity was obtained at relatively high trans-membrane pressures, and the pure and mixed gas permeabilities and selectivities compared well with each other.

When using the most NF_3 selective membrane, Hyflon AD60, a slight decrease in the mixed gas selectivity, $\alpha(NF_3/CF_4)$, with decreasing CF_4 feed concentration was observed. This was due to a small, but quantifiable increase in the permeability coefficients of both NF_3 and CF_4 with decreasing CF_4 concentration, which suggested that the polymer matrix was marginally plasticised with increasing NF_3 concentration. It was further shown that the selectivity of partially swollen Hyflon AD60 membranes, i.e. still containing appreciable amounts of the casting solvent, was significantly less selective towards NF_3 than fully relaxed, non-swollen membranes. This could be explained in terms of a loss in diffusion selectivity, which deteriorated with increasing Δp, that was caused by plasticisation induced by the residual solvent. However, the available literature evidence suggests that solvent induced swelling also leads to deterioration in the solubility selectivity of pairs such as O_2/N_2 and CO_2/N_2. This therefore also supports the notion that not only diffusion selectivity, but also solubility selectivity towards NF_3 was responsible for the observed permeability selectivity.

Further, a mixed gas selectivity, $\alpha(NF_3/CF_4)$, of ca. 12 was achieved with Hyflon AD60, albeit at a relatively low NF_3 permeability of ca. 1.9 Barrer. Although the total NF_3 throughput and required membrane area will be detrimental factors in the ultimate implementation of a Hyflon AD60 membrane separation system for purifying NF_3 of CF_4, these results are encouraging. Further studies will therefore need to focus on the optimisation of NF_3 permeability without sacrificing selectivity, in which an investigation into the diffusivity and solubility of NF_3 and CF_4 in polymer matrices will be helpful.

3.5 References

1. P.B. Henderson, A.J. Woytek, Fluorine compounds, inorganic, nitrogen, in: Kirk-Othmer Encyclopedia of Chemical Technology, John Wiley & Sons, New York, 5th ed., 2010, Vol.11, pp. 852 - 858.
2. N.J. Ianno, K.E. Greenberg, J.T. Verdeyen, Comparison of the etching and plasma characteristics of discharges in CF_4 and NF_3, J. Electrochem. Soc. 128 (1981) 2174 – 2179.
3. A. Tasaka, Electrochemical synthesis and application of NF_3, J. Fluor. Chem. 128 (2007) 296 – 310.
4. K. Koike, T. Fukuda, S. Fujikawa, M. Saeda, Study of CF_4, C_2F_6, SF_6 and NF_3 decomposition characteristics and etching performance in plasma state, Jpn. J. Appl. Phys. 36 (1997) 5724 – 5728.
5. M. Konuma, F. Banhart, F. Phillipp, E. Bauser, Damage-free reactive ion etching of silicon in NF_3 at low temperature, Mat. Sci. Eng. B-Solid. 4 (1989) 265 – 268.
6. R.R. Singh, M.R. Paonessa, D.F. Orlowski, Purification of Nitrogen trifluoride, U.S. Pat. 7,384,618 B2 (2008).
7. D.P. Satchell, J.P. le Roux, Method and apparatus for the production of nitrogen trifluoride, U.S. Pat. 6,986,874 B2 (2006).
8. D.P. Satchell, NF_3 production reactor, U.S. Pat. 7,128,885 B2 (2006).
9. A. Mimoto, T. Maeda, T. Ueno, T. Nakajima, T. Maekawa, T. Tsukayoshi, M. Kamiyoshi, A. Oda, H. Takemura, O. Yamaguchi, A. Tasaka, Effect of oxide in nickel-based composite anodes on current efficiency for NF_3 formation and current loss caused by nickel dissolution in molten $NH_4F.2HF$, Electrochim. Acta. 50 (2005) 2563 – 2571.

10. Y.-C. Park, W.-S. Jeong, K.-C. Hyun, J.-W. Lee, I.-H. Kwon, Process for refining nitrogen trifluoride gas using alkali earth metal exchanged and impregnated zeolite, U.S. Pat. 7,637,986 B2 (2009).
11. S.M. Igumnov, V.P. Kharitonov, N.V. Kharitonova, Method of purifying gaseous nitrogen trifluoride, U.S. Pat. 7,022,160 B2 (2006).
12. T. Suenaga, T. Fujii, Y. Kobayashi, Method of refining nitrogen trifluoride gas, U.S. Pat. 5,069,887 (1991).
13. R.N. Miller, C.-P.C. Kao, B.A. Mahler, Process for purifying perfluorinated products, U.S. Pat. 6,458,249 B2 (2002).
14. M.B. Shiflett, A. Yokozeki, Process for purifying perfluorinated products, U.S. Pat. 2007/0297965 A1 (2007).
15. W. Braker, A.L. Mossman, Matheson gas data book, Matheson, 6th ed., 1980.
16. R.W. Baker, Membrane technology and applications, John Wiley & Sons, Chichester, 2nd ed., 2004.
17. R.W. Baker, Membrane technology, in: Kirk-Othmer Encyclopedia of Chemical Technology, John Wiley & Sons, New York, 5th ed., 2010; Vol.15, pp 796 - 852.
18. L.M. Robeson, The upper bound revisited, J. Membr. Sci. 320 (2008) 390 – 400
19. L.M. Robeson, Correlation of separation factor versus permeability for polymeric membranes, J. Membr. Sci. 62 (1991) 165 – 185.
20. N.A. Belov, A.A. Zharov, A.V. Shashkin, M.Q. Shaikh, K. Raetzke, Y.P. Yampolskii, Gas transport and free volume in hexafluoropropylene polymers, J. Membr. Sci. 383 (2011) 70 – 77.
21. J.G. Wijmans, Z. He, T.T. Su, R.W. Baker, I. Pinnau, Recovery of perfluoroethane from chemical vapor deposition operations in the semiconductor industry. Separ. Purif. Technol. 35 (2004) 203 – 213.
22. I. Pinnau, J.G. Wijmans, Z. He, S. Goakey, R.W. Baker, Process for recovering semiconductor industry cleaning compounds, U.S. Pat. 5,779,763 (1998).
23. I. Chernyakov, T.H.-L. Hsiung, A. Schwarz, J.H.-K. Yang, Fluorochemical recovery and recycle using membranes, U.S. Pat, 5,730,779 (1998).
24. T.C. Merkel, V.I. Bondar, K. Nagai, B.D. Freeman, I. Pinnau, Gas sorption, diffusion and permeation in poly(dimethylsiloxane), J. Polym. Sci. Pol. Phys. 38 (2000) 415 – 434.
25. T.C. Merkel, V. Bondar, K. Nagai, B.D. Freeman, Hydrocarbon and perfluorocarbon gas sorption in poly(dimethylsiloxane), poly(1-trimethylsilyl-1-propyne), and

copolymers of tetrafluoroethylene and 2,2-bis(trifluoromethyl)-4,5-difluoro-1,3-dioxole, Macromolecules, 32 (1999) 370 – 374.

26. S.A. Stern, P.A. Gareis, T.F. Sinclair, P.H. Mohr, Performance of a versatile variable-volume permeability cell. Comparison of gas permeability measurements by the variable-volume and variable-pressure methods, J. Appl. Polym. Sci. 7 (1963) 2035 – 2051.
27. J.-P. Barbier, G. Bissolotti, K. Cleaver, J.-C. Goffinet, B. Hussler, P. Wolf, 2009, Code of practice nitrogen trifluoride, IGC Doc. 92/10/E. European Industrial Gases Association, EIGA. Available: http://www.eiga.org/fileadmin/docs_pubs/Doc_92_10_E.pdf. Date of access: 05 November 2011.
28. I. Pinnau, L.G. Toy, Gas and vapor transport properties of amorphous perfluorinated copolymer membranes based on 2,2-bistrifluoromethyl-4,5-difluoro-l,3-dioxole/tetrafluoroethylene, J. Membr. Sci. 109 (1996) 125 – 133.
29. R.S. Prabhakar, B.D. Freeman, I. Roman, Gas and vapor sorption and permeation in poly(2,2,4-trifluoro-5-trifluoromethoxy-1,3-dioxole-co-tetrafluoroehtylene), Macromolecules 37, (2004) 7688 – 7697.
30. K.C. O'Brien, W.J. Koros, T.A. Barbari, A new technique for the measurements of multicomponent gas transport through polymeric films, J. Membr. Sci. 29 (1986) 229 – 238.
31. M. Mulder, Basic principles of membrane technology, Kluwer Academic Publishers, Dordrecht, 2nd ed., 2003.
32. J.C. Jansen, K. Friess, E. Drioli, Organic vapour transport in glassy perfluoropolymer membranes: A simple semi-quantitative approach to analyze clustering phenomena by time lag measurements, J. Membr. Sci. 367 (2011) 141 – 151.
33. B.W. Rowe, B.D. Freeman, D.R. Paul, Physical aging of ultrathin glassy polymer films tracked by gas permeability, Polymer 50 (2009) 5565 – 5575
34. A. Alentiev, Y. Yampolski, J. Kostina, G. Bondarenko, New possibilities for increasing the selectivity of polymer gas separation membranes, Desalination 199 (2006) 121 – 123.
35. J.C. Jansen, M. Macchione, E. Drioli, On the unusual solvent retention and the effect on the gas transport in perfluorinated Hyflon AD® membranes, J. Membr. Sci. 287 (2007) 132 – 137.

36. M. Macchione, J.C. Jansen, G. de Luca, E. Tocci, M. Longeri, E. Drioli, Experimental analysis and simulation of the gas transport in dense Hyflon® AD60X membranes: Influence of residual solvent, Polymer 48 (2007) 2619 – 2635.
37. G. Dlubek, J. Pionteck, K. Rätzke, J. Kruse, F. Faupel, Temperature Dependence of the Free Volume in Amorphous Teflon AF1600 and AF2400: A Pressure-Volume-Temperature and Positron Lifetime Study, Macromolecules 41 (2008) 6125 – 6133.
38. S.M. Nemser, I.C. Roman, Perfluorodioxole membranes, U.S. Pat. 5,051,114 (1991).
39. T. C. Merkel, V. Bondar, K. Nagai, B. D. Freeman, Y.P. Yampolskii, Gas sorption, diffusion, and permeation in poly(2,2-bis(trifluoromethyl)-4,5-difluoro-1,3-dioxole-*co*-tetrafluoroethylene), Macromolecules 32 (1999) 8427 – 8440.
40. A.Y. Alentiev, V. P. Shantarovich, T. C. Merkel, V. I. Bondar, B. D. Freeman, Y.P. Yampolskii, Gas and vapor sorption, permeation, and diffusion in glassy amorphous Teflon AF1600, Macromolecules 35 (2002) 9513 – 9522.
41. A.Y. Alentiev, Y.P. Yampolskii, V.P. Shantarovich, S.M. Nemser, N.A. Platé, High transport parameters and free volume of perfluorodioxole copolymers, J. Membr. Sci. 126 (1997) 123 – 132.
42. J.Y. Park, D.R. Paul, Correlation and prediction of gas permeability in glassy polymer membrane materials via a modified free volume based group contribution method, J. Membr. Sci. 125 (1997) 23 – 39.
43. J.C. Jansen, M. Macchione, E. Tocci, L. De Lorenzo, Y.P. Yampolskii, O. Sanfirova, V.P. Shantarovich, M. Heuchel, D. Hofmann, E. Drioli, Comparative study of different probing techniques for the analysis of the free volume distribution in amorphous glassy perfluoropolymers, Macromolecules, 42 (2009) 7589 – 7604.
44. D. Hofmann, M. Entrialgo-Castano, A. Lerbret, M. Heuchel, Y.P. Yampolskii, Molecular modeling investigation of free volume distributions in stiff chain polymers with conventional and ultrahigh free volume: Comparison between molecular modeling and positron lifetime studies, Macromolecules 36 (2003) 8528 – 8538.
45. A. Bondi, van der Waals Volumes and Radii, J. Phys. Chem. 68 (1964) 441 – 451.
46. V.P. Shantarovich, I.B. Kevdina, Y.P. Yampolskii, A.Y. Alentiev, Positron annihilation lifetime study of high and low free volume glassy polymers: Effects of free volume sizes on the permeability and permselectivity, Macromolecules, 33 (2000) 7453 – 7466.

47. X.-Y. Wang, K.M. Lee, Y. Lu, M.T. Stone, I.C. Sanchez, B.D. Freeman, Cavity size distributions in high free volume glassy polymers by molecular simulation, Polymer 45 (2004) 3907 – 3912.

48. M.G. De Angelis, T.C. Merkel, V.I. Bondar, B.D. Freeman, F. Doghieri, G.C. Sarti, Gas sorption and dilation in poly(2,2-bistrifluoromethyl-4,5-difluoro-1,3-dioxole-*co*-tetrafluoroethylene): Comparison of experimental data with predictions of the Nonequilibrium Lattice Fluid Model, Macromolecules 35 (2002) 1276 – 1288.

49. A.W. Thornton, K.M. Nairn, A.J. Hill, J.M. Hill, New relation between diffusion and free volume: I. Predicting gas diffusion, J. Membr. Sci. 338 (2009) 29 – 37.

50. Y.P. Yampolskii, Amorhpous perfluorinated membrane materials: Structure, properties and application, Russ. J. Gen. Chem. 79 (2009) 657 – 665.

51. D.A. Mukhortov, I.A. Blinov, E.S. Kurapova, P.S. Kambur, Solubility of nitrogen trifluoried and tetrafluoromethane in perfluorinated and highly halogenated fluids, Russ. J. Appl. Chem. 83 (2010) 31 – 35.

52. J.P. de Coning, J.M. Swinley, Optimisation of a gas chromatographic method for trace gaseous impurities in nitrogen trifluoride by column sequence reversal, J. Chromatogr. A 1180 (2008) 151 – 158.

53. C.-F.O. Yang, S.-H. Kam, C.-H. Lui, J. Tzou, J.-L. Wang, Assessment of removal efficiency of perfluorocompounds (PFCs) in a semiconductor fabrication plant by gas chromatography, Chemosphere 76 (2009) 1273 – 1277.

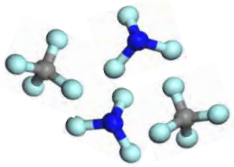

Chapter 4

Determining the diffusion and sorption characteristics of Teflon AF perfluoropolymer membranes towards NF_3 and CF_4 using molecular modeling and statistical thermodynamics techniques

Abstract

The permeability selectivity previously obtained with perfluoropolymer membranes towards NF_3 and CF_4 was further investigated using molecular dynamics (MD) and Grand Canonical Monte Carlo (GCMC) simulations with Teflon AF2400 and Teflon AF1600 to evaluate the diffusion and solubility selectivity of these polymers w.r.t. NF_3 and CF_4. Various atomistic packing models of Teflon AF2400 and Teflon AF1600 were generated using an extensive equilibration method and was shown to accurately represent the FFV of the two polymers, which could effectively be used to determine the diffusion and solubility characteristics of He and N_2 that offered a second validation criterion. Consequently, the MD simulation results of NF_3 and CF_4 predicted that NF_3 had a higher diffusivity than CF_4 in the glassy perfluoropolymer matrices. Also, the NF_3/CF_4 diffusion selectivity was predicted to be 67 % higher with Teflon AF1600 compared to Teflon AF200, which is supportive of the previously reported experimental results that showed the permeability selectivity to increase with decreasing FFV of these glassy perfluoropolymers. However, GCMC simulations failed to offer a conclusive answer as to the role of solubility selectivity, and as a result the non-equilibrium lattice fluid (NELF) model was used to further evaluate this aspect. It was shown that by using a value of 1.2 for the NELF model adjustable interaction parameter, Ψ, favourable solubility selectivity w.r.t. NF_3 was also predicted. Furthermore, the combined NF_3/CF_4 diffusion and solubility selectivity values predicted permeability selectivities that corresponded well with the previously reported experimental data, and that a lower FFV yielded optimum NF_3/CF_4 solubility and diffusion selectivity.

Keywords: Molecular dynamics; Grand Canonical Monte Carlo simulations; NELF model; NF_3/CF_4 Membrane separation; Teflon AF.

4.1 Introduction

With regard to the purification of nitrogen trifluoride (NF_3) from carbon tetrafluoride (CF_4) as contaminant as required by the electronic device manufacturing industry, it was shown in the previous chapter that the membrane based separation using glassy perfluoropolymer membranes yielded appreciable NF_3 permeability selectivity. For the glassy perfluoropolymer membranes studied (Teflon AF2400, Teflon AF1600 and Hyflon AD60), it was shown that the NF_3/CF_4 permeability selectivity increased with decreasing fractional free volume (FFV), and it was hypothesised that NF_3/CF_4 diffusion selectivity increased because of the decreasing FFV.

However, literature evidence suggests that NF_3 is more favourably adsorbed onto porous inorganic adsorbents [1-3] compared to CF_4, and is more soluble than CF_4 in perfluorocarbon and halogenated fluids [4]. It was also shown in Chapter 2 that NF_3 is more strongly adsorbed onto porous polymer packing materials used in analytical GC columns, causing it to frequently elute after CF_4 [5, 6]. Furthermore, NF_3 has been shown to undergo dissociative chemisorption on silicon surfaces [7], but can also be adsorbed by gold (Au) and platinum (Pt) surfaces by physisorption in which the nitrogen lone-pair electrons are involved [8, 9]. Additionally, NF_3 can form various weakly-bonded gas-phase complexes with cations of H, Li, Na, and K (acting as electrophiles) [10, 11], and has been shown to exhibit a bifunctional Lewis base character [12] such that it can behave as both a nitrogen and fluorine base. NF_3 can also interact with ambidentate electron donor/acceptor systems such as HF and HCN to form semi-stable dimer and trimer complexes [13]. It is therefore apparent that NF_3 can interact with a wide range of chemical species in a way that distinguishes it from CF_4, and the "chemical reactivity" as mentioned above may well be the reason for the higher activity observed for NF_3 in solid and liquid adsorbents compared to CF_4, which has been utilized for separation, for example via adsorption [1-3].

It is therefore conceivable that the observed permeability selectivity of perfluorpolymer membranes towards NF_3 (Chapter 3) might not only have been due to favourable NF_3/CF_4 diffusion selectivity, but might also have been supplemented by favourable NF_3/CF_4 solubility selectivity. Complementary to experimental methods that have traditionally been used to elucidate the transport phenomena of penetrant gases and vapours in polymeric membranes, molecular simulation tools have received much attention in recent years and have been shown

to be useful to describe transport processes occurring in polymeric matrices. In this regard, molecular dynamics (MD) simulations in which macromolecular systems can be theoretically described by the implementation of forcefields have proven useful to evaluate the free volume properties of glassy polymers [14-17] that further enhance our understanding of polymeric membrane materials. In addition, MD simulations can also be used to model the diffusive behaviour of small gaseous penetrants in polymeric matrices that offers a predictive tool to calculate penetrant diffusion coefficients [18-26]. Also, Grand Canonical Monte Carlo (GCMC) simulation methods have been used to model the solubility and sorption isotherms of gaseous penetrants in polymeric matrices [22, 26-29], and by combination with simulated diffusion coefficients the permeability ($P = D.S$) and permeability selectivity ($\alpha = (D_i/D_j).(S_i/S_j)$) of polymeric membranes towards various gases can be theoretically evaluated. With respect to solubility predictions of gases in polymers, the non-equilibrium lattice fluid (NELF) model has also been useful [30-37]. For example, De Angelis *et al.* [35] have shown that sorption isotherms of CF_4 in Teflon AF2400 and Teflon AF1600 could be predicted with sufficient accuracy using the NELF model.

Although a minimal amount of literature data w.r.t. the transport coefficients of CF_4 in Teflon AF2400 and Teflon AF1600 are available, no such information is available at present for NF_3. Therefore, to evaluate the previous hypotheses that both diffusion and solubility selectivity w.r.t. NF_3 was responsible for the observed permeability selectivity, MD and GCMC simulations were used in this study to calculate diffusion and solubility coefficients of NF_3 and CF_4 in Teflon AF2400 and Teflon AF1600. To validate the equilibrated three-dimensional atomistic packing models of Teflon AF2400 and Teflon AF1600 used in this study, the FFV predicted by each individual packing model was determined and compared to literature data. Further validation of the packing models was also obtained by calculating the diffusion and solubility coefficients and sorption isotherms of He and N_2, which compared favourably with literature data. Subsequently, the sorption behaviour of NF_3 and CF_4 in Teflon AF2400 and Teflon AF1600 predicted by GCMC simulations was also compared with the NELF model predictions.

4.2 Basic Theoretical Background of the NELF Model

In this section, the basic theoretical principles of the non-equilibrium lattice fluid (NELF) model will be briefly discussed for the sake of convenience and continuity. Further details

regarding the theory can be found in the original works of Sanchez and Lacombe [30, 31] and the subsequent development thereof by Doghieri and Sarti [32-34] for the specific case of predicting the solubility of gases in glassy polymers. In addition, reference will also be made here to the work of De Angelis *et al.* [35, 36] and Baschetti *et al.* [37].

Pure Fluids

For the purpose of applying the NELF model to binary mixtures of glassy polymers and gaseous penetrants, it is useful to recall the results obtained by Sanchez and Lacombe for pure lattice fluids. In their original lattice fluid theory, Sanchez and Lacombe [30, 31] showed that the following expression for the Gibbs free energy of a pure fluid containing n moles which each occupies r lattice sites is valid:

$$G = rnRT^* \left\{ \tilde{\rho} + \frac{\tilde{p}}{\tilde{\rho}} + \frac{\tilde{T}}{\tilde{\rho}} \left[\left(1-\tilde{\rho}\right) ln\left(1-\tilde{\rho}\right) + \frac{\tilde{\rho}}{r} ln\left(\tilde{\rho}\right) \right] \right\} \tag{4.1}$$

where R is the universal gas constant, while the reduced density ($\tilde{\rho}$), pressure ($\tilde{p}$), and temperature ($\tilde{T}$) are defined as:

$$\tilde{\rho} = \rho / \rho^* \qquad \tilde{p} = p / p^* \qquad \tilde{T} = T / T^* \tag{4.2}$$

The quantities ρ^*, p^*, and T^* are the characteristic density, pressure and temperature respectively and represent the adjustable model parameters, which are related to the molar volume, v^*, of the lattice sites through:

$$r = \frac{M}{\rho^* v^*} \tag{4.3}$$

$$v^* = \frac{RT^*}{p^*} \tag{4.4}$$

where M is the molecular weight of the pure fluid. The density of the fluid that minimizes the Gibbs free energy, Eq. (4.1) at specific values of temperature, T and pressure, p, can thus be found by applying the equilibrium condition:

$$\left(\frac{\partial G}{\partial \rho}\right)_{T,p,n} = 0 \tag{4.5}$$

which yields the Sanchez-Lacombe equation of state:

$$\tilde{\rho}^2 + \tilde{p} + \tilde{T}\left[ln\left(1-\tilde{\rho}\right) + \left(1-\frac{1}{r}\right)\tilde{\rho}\right] = 0 \tag{4.6}$$

In Eq. (4.6) the dimensionless density, $\tilde{\rho}$, and therefore the fluid density, ρ, is the dependent variable, while $\tilde{p}$ and $\tilde{T}$, and therefore the absolute temperature, T, and pressure, p, are the independent variables. Any fluid can therefore in principle be described by Eq. (4.6), whereby the characteristic model parameters ρ^*, p^*, and T^* can be found by fitting Eq. (4.6) to saturated vapour pressure and liquid density data [30, 31], whereas *PVT* data may be used in the case of polymers.

Binary Mixtures

Using the abovementioned basic principles, the Sanchez-Lacombe lattice fluid theory may be extended to the case of gas-polymer binary mixtures containing n_1 moles of the penetrant and n_2 moles of the polymer, such that the Gibbs free energy of the mixture is given by [31-35]:

$$G = RT^*\left(r_1 n_1 + r_2 n_2\right)\left\{-\tilde{\rho} + \frac{\tilde{p}}{\tilde{\rho}} + \frac{\tilde{T}}{\tilde{\rho}}\left[\left(1-\tilde{\rho}\right)ln\left(1-\tilde{\rho}\right) + \frac{\phi_1}{r_1}\tilde{\rho}ln\left(\phi_1\tilde{\rho}\right) + \frac{\phi_2}{r_2}\tilde{\rho}ln\left(\phi_2\tilde{\rho}\right)\right]\right\} \tag{4.7}$$

wherein ϕ_i is the volume fraction of component i, which is related to the mass fractions and the characteristic densities of the pure components by:

$$\phi_i = \frac{\omega_i / \rho_i^*}{\omega_1/\rho_1^* + \omega_2/\rho_2^*} \tag{4.8}$$

Accordingly, the mixture characteristic parameters may be obtained by application of appropriate mixing rules. For the mixture characteristic density and molar volume the mixing rules are:

$$\frac{1}{\rho^*} = \frac{\omega_1}{\rho_1^*} + \frac{\omega_2}{\rho_2^*} \tag{4.9}$$

$$\frac{1}{v^*} = \frac{\phi_1}{v_1^*} + \frac{\phi_2}{v_2^*} \tag{4.10}$$

For the mixture characteristic pressure, the following mixing rule applies:

$$p^* = \phi_1 p_1^* + \phi_2 p_2^* - \phi_1 \phi_2 \Delta p^* \tag{4.11}$$

where Δp^* is the binary interaction parameter written as:

$$\Delta p^* = \left(\sqrt{p_1^*} - \sqrt{p_2^*}\right)^2 = p_1^* + p_2^* - 2p_{12}^* \tag{4.12}$$

in which it has become customary to write the binary parameter p_{12}^* as [35, 36]:

$$p_{12}^* = \Psi\sqrt{p_1^* p_2^*} \tag{4.13}$$

The quantity Ψ is used as a single adjustable interaction parameter for binary mixtures, and Eq. (4.11) can therefore be written as:

$$p^* = \phi_1^2 p_1^* + \phi_2^2 p_2^* + 2\phi_1\phi_2 p_{12}^* \tag{4.14}$$

When $\Psi = 1$ (the usual case) the binary parameter, p_{12}^*, is therefore the geometric mean of the pure component characteristic pressures as given by Eq. (4.14), which gives an indication of the interaction energy between the penetrant molecules and the polymer matrix [36]. Therefore, the specific value of Ψ is an indication of the relative strength of the interactions between the gaseous penetrant and the polymer matrix and can be adjusted to more accurately describe the behaviour of specific gas-polymer mixtures [35, 36].

The pure component characteristic volumes and densities are related through Eq. (4.3), which with the appropriate notation applied for the case of binary mixtures becomes:

$$r_i^0 = \frac{M_i}{\rho_i^* v_i^*} \tag{4.15}$$

where r_i^0 is the number of lattice sites occupied by a mole of component i in the pure component lattice, as explained above for pure fluids. The designation r_i^0 is only used here to distinguish the parameter from the number of lattice sites, r_i, occupied by a mole of species i in the mixture, whereby the two are related to one another according to:

$$\frac{r_i}{r_i^0} = \frac{v_i^*}{v^*} \tag{4.16}$$

with v^* the characteristic mixture molar volume. Finally, the mixture characteristic temperature, T^*, is given by Eq. (4.4), but in terms of the mixture characteristic parameters given by Eq. (4.10) and Eq. (4.14).

In principle, the mixture density, ρ, at equilibrium can be obtained by applying the equilibrium criterion of Eq. (4.5), which would yield an equation of state for the binary mixture, analogous to Eq. (4.6) that was obtained for pure fluids. However, during the sorption of gases by glassy polymers, this condition no longer holds true since the glassy polymer can be described as a non-equilibrium solid phase of which the density, ρ_2, undergoes asymptotic relaxation towards a pseudo-equilibrium value, $\rho_{2\infty}$, under specific conditions of temperature (T) and external gas pressure (p). As the polymer density reaches its pseudo-equilibrium value, $\rho_{2\infty}$, so does the composition, ω_1, of the mixture phase. This density response of the polymer matrix towards sorption of a penetrant gas species can be described by a bulk rheology model, or alternatively, can be obtained from experimental volumetric dilation data. For such pseudo-equilibrium systems, it was however shown [34] that Eq. (4.7) gives an appropriate expression for the non-equilibrium Gibbs free energy of a binary mixture, which is unique to the NELF model. Therefore, the Gibbs free energy expression of Eq. (4.7), combined with the appropriate mixing rules described above, accurately describes a glassy polymer-gaseous mixture.

Consequently, the pseudo-equilibrium mass fraction of the gaseous penetrant, ω_1, in the glassy polymer phase can be obtained by considering the non-equilibrium chemical potential of the penetrant in the glassy phase that can be defined as:

$$\mu_1^{(s)} = \left(\frac{\partial G}{\partial n_1} \right)_{T,p,\rho_2,n_2} \tag{4.17}$$

Although the solid phase essentially represents a non-equilibrium system, phase equilibrium is still established at the interface between a pure external gaseous phase and the solid glassy polymer phase, such that the following pseudo-equilibrium condition must be satisfied:

$$\mu_1^{(s)}(T, p, \omega_1, \rho_{2\infty}) = \mu_1^{(E)}(T, p) \tag{4.18}$$

The asymptotic value of the pseudo-equilibrium polymer density, $\rho_{2\infty}$, as used in Eq. (4.18) can be determined from volumetric dilation measurements, or from a reliable rheology model as mentioned above. However, to be able to use the predictive capabilities of the NELF model, it can be readily assumed that the asymptotic polymer density, $\rho_{2\infty}$, can be approximated by the pure, un-penetrated polymer density, ρ_2^0 [33, 35]:

$$\rho_{2\infty} \approx \rho_2^0 \tag{4.19}$$

This approximation is especially effective in the low pressure regime where negligible polymer dilation occurs during sorption of a gaseous species. However, for penetrants that do not induce a significant amount of swelling of the polymer under consideration, and particularly for high-free volume glassy polymers, the approximation of Eq. (4.19) can be used to effectively predict sorption isotherms over larger pressure ranges [33, 35]. As a result, one obtains the following expression for the chemical potential of the penetrant in the glassy polymeric phase by applying Eq. (4.17) [35]:

$$\begin{aligned} \frac{\mu_1^{(s)}}{RT} = ln\left(\tilde{\rho}^s \phi_1\right) - \left[r_1^0 + \frac{\left(r_1 - r_1^0\right)}{\tilde{\rho}^s} \right] ln\left(1 - \tilde{\rho}^s\right) - r_1 \\ - \tilde{\rho}^s \left[\frac{2 r_1^0 v_1^* \left(\phi_1 p_1^* + \phi_2 \Psi \sqrt{p_1^* p_2^*} \right)}{RT} \right] \end{aligned} \tag{4.20}$$

where the designation $\tilde{\rho}^s$ is used to distinguish between the dimensionless density of the solid mixture phase and that of the external gaseous phase, where it follows from mass balance conditions and Eq. (4.9) that:

$$\tilde{\rho}^s = \frac{\rho_2^0}{1-\omega_1}\left(\frac{\omega_1}{\rho_1^*}+\frac{1-\omega_1}{\rho_2^*}\right) \tag{4.21}$$

Accordingly, the chemical potential of the external gaseous phase can be shown to be [33]:

$$\frac{\mu_1^{(E)}}{RT} = ln\left(\tilde{\rho}^E\right) - r_1^0 \ln\left(1-\tilde{\rho}^E\right) - r_1^0 - \frac{\tilde{\rho}^E r_1^0 v_1^* p_1^*}{RT} \tag{4.22}$$

where the notation $\tilde{\rho}^E$ is used to indicate the dimensionless density of the pure external gaseous fluid, which can be calculated at a predefined temperature, T, and pressure, p, according to the Sanchez-Lacombe equation of state, i.e. Eq. (4.6). By equating Eq. (4.20) and Eq. (4.22), as dictated by Eq. (4.18), one can therefore predict the sorption isotherms of non-swelling gaseous penetrants in glassy polymers with the assumption of Eq. (4.19), by calculating the penetrant mass fraction, ω_1, in an iterative manner.

It was shown in the previous chapter that both CF_4 and NF_3 do not induce an appreciable amount of penetrant swelling in Teflon AF2400 and Teflon AF1600, as was evident from the practically constant permeabilities as a function of trans-membrane pressure. Also, De Angelis *et al.* [35] have shown that good sorption isotherm predictions for CF_4 in Teflon AF2400 and Teflon AF1600 were obtained over a wide pressure range with the assumption of a constant polymer density. Therefore, this approach was also followed in this work to compare the NELF model predictions with the GCMC simulations of sorption of NF_3 and CF_4 in Teflon AF2400 and Teflon AF1600.

4.3 Atomistic Simulation Methods

All molecular simulations were conducted using the Materials Studio 6.0 software package of Accelrys, Inc. (San Diego, CA) [38]. Atomistic packing models were generated using the Amorphous Cell module and were subsequently equilibrated using molecular dynamics (MD) simulations with the Forcite module, which was also used for diffusion simulations. Penetrant

sorption isotherms were calculated through Grand Canonical Monte Carlo (GCMC simulations, as implemented in the Sorption module of Materials Studio 6.0. The COMPASS forcefield [39, 40] was used during each stage of the simulations. In all cases, the non-bond interactions were calculated up to a cut-off distance of 18.5 Å, which was truncated using a cubic spline function with a width of 1 Å. For this, a group based representation for summation of the electrostatic interactions, and an atom based representation for summation of the van der Waals interactions was used during packing model generation, equilibration and subsequent production runs. In the case of GCMC simulations, however, the Ewald [41] summation method was used to calculate the electrostatic interactions, and a group based representation was used to calculate the van der Waals interactions. The respective Andersen [42] temperature, and Berendsen [43] pressure control algorithms were used throughout, and the Smart minimization algorithm as implemented in the Amorphous Cell and Forcite modules of Materials Studio 6.0 [38] was used for all geometry optimizations. A collision ratio of 1.0 was used for the external Andersen thermostat; while a decay constant of 5 ps was applied for the Berendsen barostat.

4.3.1 Polymer Packing Model Generation and Equilibration

The method used for generating and equilibrating Teflon AF2400 and Teflon AF1600 polymer packing models, were based on previously described methods [14, 15, 17, 24, 44], with a few minor changes, and will thus be briefly described here. For the sake of brevity, Teflon A2400 and Teflon AF1600 will hereafter be abbreviated as AF2400 and AF1600. Single random co-polymer chains containing 400 (AF2400) and 500 (AF1600) co-monomer repeat units with the appropriate molar compositions as shown in Fig. 4.1 were generated using the Polymer Builder tool of the Materials Studio Modeling Environment [38]. The respective polymer chains of AF2400 (5588 atoms) and AF1600 (5954 atoms) were subsequently relaxed using geometry optimizations with a maximum of 5000 iterations. Afterwards, the polymer chains were packed into cubic cells under periodic boundary conditions at a temperature of 303 K using the Theodorou-Suter method [45, 46] as implemented in the Amorphous Cell module. To prevent ring spearing and catenations, 200 CF_4 molecules were packed into the cubic cells together with the polymer chains at low packing densities of 0.3 – 0.4 g/cm^3.

Teflon AF

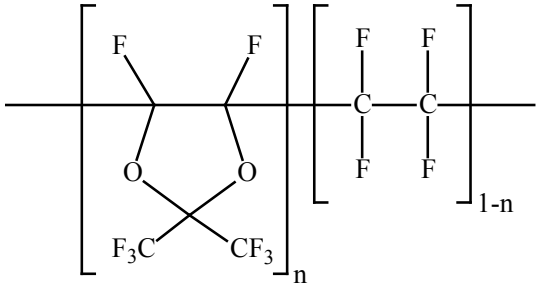

n = 0.87: AF2400; n = 0.65: AF1600

Figure 4.1: Molecular structure of Teflon AF, where n = 0.87 for Teflon AF2400, and n = 0.65 for Teflon AF1600.

The use of single long chains rather than a collection of shorter oligomer chains have been shown to effectively reproduce polymer bulk properties, while limiting possible chain-end effects [14, 15, 17]. For this reason, this computationally more intensive, but physically more accurate approach was used for the construction of polymer packing models of AF2400 and AF1600. Numerous independent amorphous packing models of AF2400 and AF1600 were realised in this manner, where after each was geometrically optimized using 5000 iterations. Subsequently, only three of the resulting packing models of both AF2400 and AF1600 (a total of six packing models) that had the lowest total energy in each case were further equilibrated. The three optimum packing models of AF2400 and AF1600 were then each subjected to an extensive equilibration using several stages of NVT (N: constant particle number, V: constant volume, T: constant temperature) and NPT (P: constant pressure) Molecular Dynamics (MD) as well as static geometry optimizations as described hereafter.

Although Hofmann *et al.* [14, 15] reported the use of forcefield parameter scaling during the initial stages of equilibration of their low density starting models, it is shown here that reliable packing models can still be obtained without using any forcefield parameter scaling. A summary of the various stages of the equilibration procedure used in this study is given in the scheme of Fig. 4.2, which will be referred to hereafter. The positions of the CF_4 obstacle molecules were first constrained and the first equilibration stage (Stage 1) consisted of three NVT-MD runs, each followed by a static geometry optimization of 5000 iterations, which was then followed by a final NVT-MD as summarised in Table 4.1. In these NVT-MD runs the temperature was kept constant at 303 K.

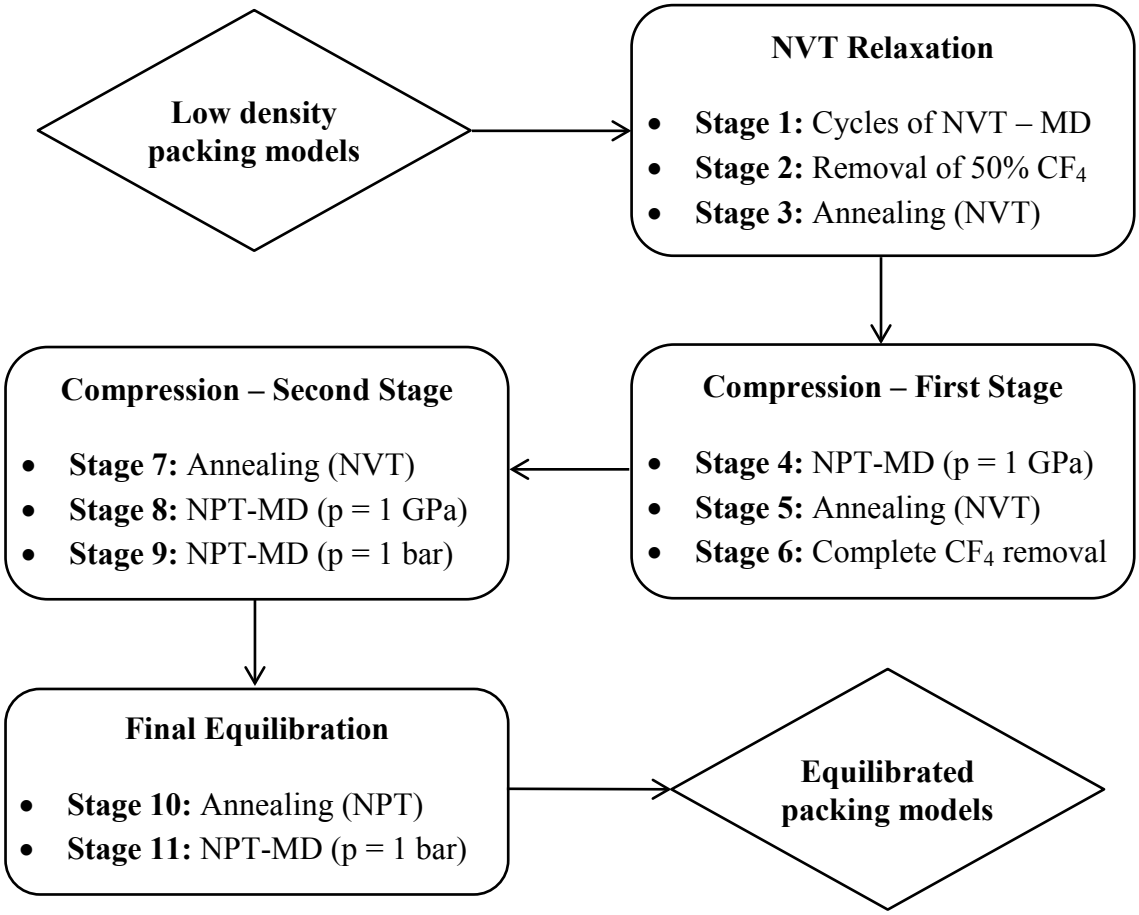

Figure 4.2: Summary of the equilibration scheme used in this study to prepare well equilibrated amorphous packing models of AF2400 and AF1600.

Table 4.1: Simulation parameters used during Stage 1 of the relaxation procedure used to equilibrate the initial low-density packing models of AF2400 and AF1600. The first three NVT runs were followed by a geometry optimization as explained in the text.

NVT-MD Run	Simulation Parameters	
	Simulation time (ps)	Time step (fs)
1	200	0.5
2	400	0.5
3	600	0.25
4	50	0.25

Approximately 50 % of the CF_4 obstacle molecules were then removed (Stage 2), which was then followed by a simulated NVT annealing stage (Stage 3) that consisted of three annealing

cycles wherein the temperature was ramped from 300 K to 750 K and back to 300 K in 90 K intervals during each cycle, with NVT-MD at each interval that lasted for 5 ps with a time step of 0.5 fs. This simulated annealing process was then followed by another geometry optimization of 5000 iterations to minimize the energies of the respective packing models. After completion of the simulated annealing, the remaining CF_4 molecules were unconstrained and NPT-MD of 30 ps with a time step of 0.25 fs at a constant pressure of 1 GPa, and constant temperature of 303 K (Stage 4), was used to compress the packing models slightly. The positions of the remaining CF_4 molecules were then fixed yet again and the compressed packing models were subjected to another simulated annealing stage (Stage 5) in the same manner as in Stage 3, however, here the NVT-MD simulations at each temperature interval was lengthened to 10 ps.

The annealing cycle of Stage 5 was also followed by another geometry optimisation, where after the remaining CF_4 molecules were completely removed from the respective packing models (Stage 6). Another simulated annealing stage (Stage 7) was subsequently performed in the same manner as in Stage 5, which preceded the final geometry optimization of 5000 iterations. The resulting packing models were then compressed (Stage 8) to slightly above their respective experimental densities of 1.77 g/cm^3 for AF2400 [35, 47] and 1.84 g/cm^3 for AF1600 [35, 47] using NPT-MD of 10 ps with a time step of 0.25 fs, at a constant pressure of 1 GPa and constant temperature of 303 K. This was followed by an NPT relaxation stage (Stage 9) that was performed at a constant pressure of 1 bar and constant temperature of 303 K, while using a time step of 0.5 fs and a total simulation time of 500 ps.

After the relaxation stage of Stage 9 the packing models exhibited densities that were slightly (~ 5 %) above the reported experimental densities. Therefore, additional relaxation was necessary to obtain packing models that gave the most accurate representation possible. Thus, the models were allowed to expand and contract under annealing using an NPT ensemble (Stage 10) rather than an NVT ensemble as was done with the previous annealing stages. This so-called NPT-annealing stage was performed by setting the pressure constant at 1 bar throughout while applying a single temperature cycle wherein the temperature was ramped from 300 K to 750 K and back to 300 K in 45 K intervals, with NPT-MD performed at each temperature interval that lasted for 10 ps with a time step of 0.5 fs. This physically accurate simulated annealing process led to densities of the packing models that were slightly below the experimental densities. However, a final NPT-MD run (Stage 11) at a constant

temperature of 303 K and constant pressure of 1 bar that lasted for 500 ps while applying a time step of 0.5 fs was sufficient to bring the densities of the packing models closer to their respective experimental values. Finally, these extensively equilibrated packing models of AF2400 and AF1600 that were free of any ring spearing or catenations were utilized for the preparation of packing models containing penetrant molecules for diffusion simulations as described in Sec. 4.3.3, as well as for the simulation of sorption isotherms via the GCMC method described in Sec. 4.3.4.

4.3.2 Free Volume Calculation Method

In addition to the correlation of the packing model densities with experimentally determined densities from the literature, the fractional free volume (FFV) predicted by the AF2400 and AF1600 packing models were also determined and compared to literature values to validate the applicability of the relaxed models. Experimentally, the FFV is calculated using Eq. (4.23) [14, 15, 17, 27, 48, 49, 50]:

$$FFV = \frac{V_f}{V_{sp}} = \frac{V_{sp} - 1.3V_w}{V_{sp}} \tag{4.23}$$

wherein V_f (cm^3/g) is the free volume, or void volume, of the polymer, and V_{sp} (cm^3/g) is the specific volume (reciprocal of polymer density). The free volume is frequently calculated by subtracting the volume occupied by the polymer chains per unit mass from the polymer specific volume, or total volume. The occupied volume is then calculated from the total van der Waals volume, V_w (cm^3/g), of the participating functional groups in the polymer repeat units that is in turn calculated with the Bondi group contribution method [50, 51], which uses a rather arbitrary so-called “universal packing constant” of 1.3. Thus, the total occupied volume, $V_{oc} = 1.3V_w$.

However, in this study, as was done in the literature, the total occupied volume (V_{oc}), or total volume occupied by the single polymer chains of the respective AF2400 and AF1600 relaxed packing models were determined by geometric calculations. In this regard, the atoms of each polymer chain was represented as hard spheres with radii derived from the van der Waals radii of the respective atoms as used by Hofmann *et al.* [14, 15] and Hölck *et al.* [27] (C: 1.55 Å; O: 1.35 Å, F: 1.30 Å). Subsequently, the Atom Volumes and Surfaces tool of the Materials

Studio 6.0 Modeling Environment [38] was used to calculate the total volume occupied (V_{oc}) by the atoms of the respective polymer chains, and as a result the total free volume (V_f) predicted by each of the relaxed packing models. This was achieved by superimposing a three-dimensional grid with a grid spacing of 0.4 Å onto the cubic simulations cells and then determining the amount of grid points where a test particle, also represented by a hard sphere with a specific radius, can be inserted without any overlap with the hard spheres of the polymer atoms [14, 15, 17, 27]. Such grid points are thus marked as "free", while grid points in which overlap is observed is marked "occupied". The sum of the "free" volume elements thus gives the total free volume (V_f) predicted by each packing model, whereas the sum of the "occupied" volume elements gives the predicted total occupied volume (V_{oc}). Finally, the FFV was calculated using the first part of Eq. (4.23).

Considering the calculation method described above, it is clear that the values of the free volume and occupied volume for each packing model are dependent on the radius of the test particle that is used. As such, Hofmann *et al.* [14, 15] found that the use of a test particle with a radius of r_{test} = 0.43 Å gave satisfactory agreement between their geometrically calculated FFV values and the FFV values calculated using the Bondi group contribution method for a range of different polymers. On the other hand, Hölck *et al.* [27], showed that the use of a test particle radius of r_{test} = 0.473 Å yielded better agreement between the Bondi-FFV and geometrically calculated FFV values of their polymer packing models. In addition, Jansen *et al.* [17] also obtained good correlations between the Bondi-FFV values and the FFV values calculated for their Hyflon AD60 and Hyflon AD80 polymer packing models when using r_{test} = 0.473 Å. The test particle insertion method therefore displays a certain "empirical character" as noted by Hölck *et al.* [27], in which the radius of the test particle (r_{test}) is frequently varied in the literature to obtain good correlations between the FFV calculated from geometric analyses of three-dimensional polymer packing models and the FFV calculated using the Bondi group contribution method.

In this study, it was therefore decided to use a more direct approach for calculating the FFV represented by the relaxed packing models of AF2400 and AF1600 that is more consistent with the Bondi group contribution method (Eq. 4.23). Consequently, the polymer chain atoms were represented as hard spheres with the radii as mentioned above, but which was scaled by applying a universal scaling factor of 1.3, while using r_{test} = 0 Å. As a result, the grid elements that are occupied by the polymer atoms contribute to the total occupied volume (V_{oc}), while

grid elements that are free of polymer atoms contribute to the total free volume of the packing model. The use of $r_{test} = 0$ is not uncommon; for example, Hofmann *et al.* [14, 15] showed that even the most minute free volume elements, or spaces between neighbouring polymer atoms, are taken into account when $r_{test} = 0$ Å, while using the original atom radii as mentioned above. However, by scaling the atom radii by a factor of 1.3, as suggested by the Bondi group contribution method [50, 51] given by Eq. (4.23), such interstitial voids therefore disappear leaving only the realistically accessible free volume elements. Therefore, the method of Hofmann *et al.* [14, 15], Hölck *et al.* [27] and Jansen *et al.* [17], in which $r_{test} = 0.473$ Å, without using any scaling factor, is equivalent in its results to the method proposed here in which $r_{test} = 0$ Å and the scaling factor 1.3 is applied to the atom radii, because, only the realistically accessible free volume elements are taken into account in both cases. Although the free volume distribution is another important quantity that could be calculated from the results of a geometric analysis as described here, the computational algorithms necessary to do so [14, 15, 21, 27] were not available to us, and was therefore not determined in this study. In addition to the density and FFV data, the results of He and N_2 diffusion and solubility simulations (described below) was also used and compared with literature data to validate the quality of the packing models thus obtained.

4.3.3 Diffusion Simulations

In this study the diffusion simulations were conducted with He, N_2, NF_3 and CF_4 as penetrants. Atomistic models of these penetrants were constructed using the Materials Studio 6.0 Modeling Environment [38], which was then geometrically optimized (except for He) using the Forcite module with the COMPASS forcefield and the same parameters as given in Sec. 4.3. Typically, 10 – 16 atoms (He) or molecules (N_2, NF_3 and CF_4) of each of the individual penetrants were then randomly inserted into the relaxed packing models of AF2400 and AF1600 (Sec. 4.3.1) at a temperature of 303 K using the packing task of the Amorphous Cell module [38]. Random insertion of this amount (10 – 16) of penetrant atoms (He) or molecules (N_2, NF_3 and CF_4) resulted in a maximum increase in the density of the packing models of 1.5 %. After insertion of the penetrants, each of the packing models were subjected to another brief geometry optimization, after which a NVT-MD run at 303 K that lasted for 200 ps with a time step of 0.5 fs was used for final equilibration so that all the atomic motions approached an elastic state.

Following the random insertion of penetrant atoms (He) and molecules (N_2, NF_3 and CF_4) and subsequent NVT-MD equilibration, the diffusivity of each species was studied using the Molecular Dynamics (MD) method, via the Einstein diffusion equation [20, 22, 24-26, 44, 52]:

$$D = \frac{1}{6N_\alpha} \lim_{t\to\infty} \frac{d}{dt} \sum_{i=1}^{N_\alpha} \left\langle \left[\boldsymbol{r}_i(t) - \boldsymbol{r}_i(0) \right]^2 \right\rangle \tag{4.24}$$

where N_α is the number of molecules of penetrant α, $\boldsymbol{r}_i(0)$ and $\boldsymbol{r}_i(t)$ are the initial and final positions of the centre of mass of particle i over the simulation time t that was used, and the term in angular brackets is the mean square displacement (MSD) averaged over the total number of molecules of penetrant α. The trajectory of the inserted atoms (He) and molecules (N_2, NF_3 and CF_4) were therefore tracked over the simulation time t that was chosen, and the MSD was computed from the results of this MD method. It is inherently assumed that the movements of the diffusing particles follow a random walk mechanism through the amorphous matrices in which penetrants jump from one free volume element to adjacent free volume elements when an opening presents itself as a results of the elastic motion of the polymer chains. Until such an opening becomes available to the inserted particles, they tend to oscillate around their respective equilibrium positions [20, 24, 25], and therefore are characterised by rather long residence times inside each free volume element. Therefore, to obtain a meaningful estimation of the diffusion coefficients via Eq. (4.24), a minimum of 10 jumps are required [44, 52] during the MD simulation to overcome the anomalous diffusion regime, which is characterised by a log(MSD) vs. log(t) graph having a slope of less than unity [20, 24, 25, 44, 52, 53]. Only when the log(MSD) vs. log(t) curve approaches unity at sufficiently long simulation times, the so-called Fickian diffusion regime, has sufficient jump events taken place to accurately estimate the diffusion coefficient from the MSD, as the oscillatory movement of particles in individual cavities become statistically insignificant.

Therefore, to enhance the statistical sampling of the MSD of each penetrant through the polymer packing models, a relatively large number of particles (10 – 16) were used. In addition, the MD production runs for all penetrants were done using the NVT ensemble (T = 303 K) whereby the density of the packing models was therefore kept constant. In all cases a time step of 1 fs was used, where the rest of the simulation parameters that were used for AF2400 and AF1600 for each penetrant are summarised in Table 4.2. For both AF2400 and

AF1600 the final MSD curves for each penetrant were determined as the average from at least two of the three individual packing models of each polymer. In each case, the log(MSD) vs. log(t) was used to evaluate whether the Fickian diffusion regime was reached (Appendix D), which will be further discussed in the results section.

Table 4.2: Summary of the computational parameters used for the NVT-MD production runs for simulating diffusion of He, N_2, NF_3, and CF_4 in AF2400 and AF1600.

Polymer Packing Model	Penetrant	Simulation time (ns)	Trajectory saved every # Steps
AF2400	He	10	2500
	N_2	10	2500
	NF_3	25	8000
	CF_4	25	8000
AF1600	He	10	2500
	N_2	20	5000
	NF_3	22.6	8000
	CF_4	25	8000

4.3.4 Grand Canonical Monte Carlo Simulations

The solubility of He, N_2, NF_3 and CF_4 in AF2400 and AF1600 was studied by calculating the sorption isotherms of each using the equilibrated packing models of AF2400 and AF1600 (Sec. 4.3.1) via the Grand Canonical Monte Carlo (GCMC) method. The Metropolis [54] algorithm was used for the GCMC simulations whereby the temperature (T), volume (V) and chemical potential (μ) of the polymer-gas system was kept constant at each fugacity (f) data point while the total number of molecules (N) was allowed to vary to satisfy the equilibrium condition $\mu_s(T, f) = \mu_g(T, f)$ (s= solid phase, g = gas phase). At each pure-component fugacity point (varied between 10 and 2500 kPa) 1,000,000 equilibration steps followed by 10,000,000 production steps that consisted of a combination of insertion, deletion, translation, and rotation steps were used.

The penetrant fugacities were converted to pressure with the help of the Peng-Robinson equation of state [55], and the Myers and Monson [56, 57] method was followed to calculate

the excess amount of each penetrant adsorbed in the AF2400 and AF1600 packing models for direct comparison to the available experimental isotherm data. Accordingly, the "pore volume" or total accessible free volume of each of the three packing models for AF2400 and AF1600 was determined from the simulated He adsorption isotherms. Thereby, the simulated isotherm values of N_2, NF_3 and CF_4 were corrected to represent the excess amount adsorbed, as is measured experimentally, opposed to the absolute amount adsorbed as given by the raw simulation results [56, 57]. The predicted average concentration of each penetrant adsorbed in AF2400 and AF1600 was then fitted to the dual sorption model given by [26, 27, 58]:

$$C = k_D p + \frac{C_H' b p}{1 + b p} \tag{4.25}$$

where C is the equilibrium concentration (cm^3(STP)/cm^3 polymer), k_D is the Henry sorption parameter (cm^3(STP)/cm^3.atm), C_H' is the Langmuir capacity parameter (cm^3(STP)/cm^3), b is the Langmuir affinity parameter (atm^{-1}), and p is the absolute pressure (atm). Each of these parameters was determined by non-linear least square fits to the average adsorption isotherm data of each penetrant. Accordingly, the infinite dilution solubility coefficients, i.e. S_0 (cm^3(STP)/cm^3.atm), were determined from the simulated average adsorption isotherms of each penetrant for AF2400 and AF1600 as the slope of the adsorption isotherm curve in the zero pressure limit:

$$S_0 \equiv \lim_{p \to 0} \frac{C}{p} = k_D + C_H' b \tag{4.26}$$

4.4 Results and Discussion

4.4.1 Packing Model Validation

The characteristic properties of the relaxed packing models of AF2400 and AF1600, of which an illustrative example is shown in Fig. 4.3, are summarised in Table 4.3, from which it is clear that good correlations were obtained with the experimental evidence. In general, the physical properties of the AF1600 packing models were more accurately reproduced. The noticeably smaller FFV predicted by the AF2400 packing models compared to the literature values can be attributed to the positive deviations of the predicted densities from the literature

values. The packing models of AF1600, which exhibits smaller deviations from the literature values, represented FFVs that correlated excellently with that obtained from the literature. The geometric analysis method as described in Sec. 4.3.2 was therefore effective in evaluating the correlation between the predicted total FFV and the FFV obtained through the Bondi group contribution method.

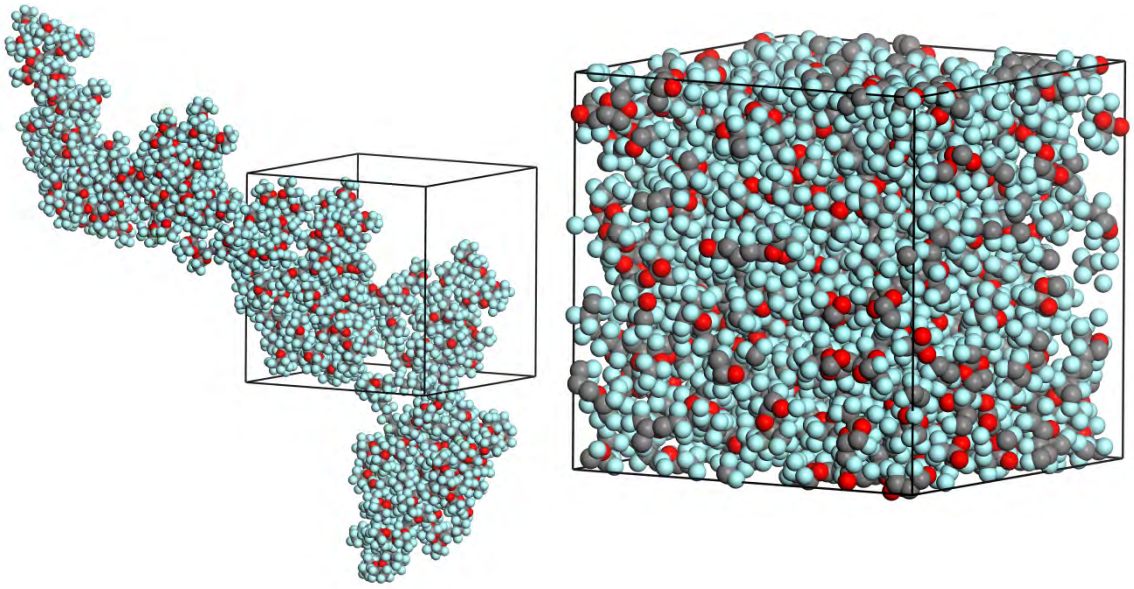

Figure 4.3: Illustrative example of a relaxed AF1600 packing model showing the single polymer chain entering and exiting the cubic simulation cell (left), which under periodic boundary conditions "folds in on itself" yielding an amorphous polymer model (right). Polymer atoms are represented as spheres, with carbon atoms colored grey, oxygen atoms colored red, and fluorine atoms colored light blue.

Although analysis of the fractional free volume distribution predicted by the relaxed packing models would give a better indication of the correlation between the predicted FFV properties and that obtained by experimental methods [14, 15, 17, 21], simulation of the transport properties of penetrants may also be used to gauge the quality of the atomistic packing models [14, 15]. For this reason, the diffusivities and solubilities of He and N_2 was also simulated using the respective packing models of AF2400 and AF1600 according to the methods described in Sec. 4.3.3 and Sec. 4.3.4.

Table 4.3: Characteristic properties of the relaxed packing models of AF2400 and AF1600 used for the diffusivity and solubility simulations conducted in this study.

Packing Model	Density (g/cm^3)	Deviation[a] (%)	Cell Side Length (Å)	FFV (%)	Literature FFV[b] (%)
AF2400-1	1.786	0.9	43.91	30.7	
AF2400-2	1.818	2.71	43.66	29.5	32
AF2400-3	1.802	1.81	43.78	30.0	
Average	**1.802**			**30.1**	
AF1600-1	1.846	0.33	44.40	28.0	
AF1600-2	1.845	0.27	44.41	28.1	28
AF1600-3	1.843	0.16	44.42	28.2	
Average	**1.845**			**28.1**	

[a] Deviation in terms of the experimental densities reported by De Angelis [35], i.e. 1.77 g/cm^3 for AF2400 and 1.84 g/cm^3 for AF1600. [b] FFV values as reported by Shantarovich *et al.* [59].

The average mean square displacement (MSD) plots of He and N_2 for AF2400 and AF1600 (Fig. 4.4 (a) and (b)), which was taken as the average MSD of the individual MSDs of each penetrant for each individual packing model, clearly indicate that the N_2 MSDs exhibited a lower slope for both polymers. In accordance with Eq. (4.24) the diffusion coefficients were calculated in each case from the slope (m/6) of a straight line fitted to the portion of each MSD curve that exhibited Fickian diffusion behaviour, as determined using log(MSD) vs. log(t) plots (refer to Figs. D.1 and D.2 in Appendix D). As a result, the calculated He diffusion coefficient was at least an order of magnitude larger than that of N_2 for both AF2400 and AF1600, as is also experimentally observed [60]. The log(MSD) vs. log(t) curves showed that Fickian diffusion behaviour was reached after approximately 3 – 4 ns for N_2 for both polymers (Fig. D.2 in Appendix D), while He displayed faster convergence to Fickian behaviour as a result of its higher diffusivity (Fig. D.1 in Appendix D). Furthermore, the average slope of the N_2 log(MSD) vs. log(t) curve for AF1600 was somewhat lower than unity (m = 0.90). Therefore, the diffusive movement of the inserted N_2 molecules only approximated Fickian diffusion behaviour in this case. Nevertheless, the calculated diffusion coefficient of N_2 through AF1600 still correlated satisfactorily with literature data, which will be discussed in detail in the subsequent paragraphs.

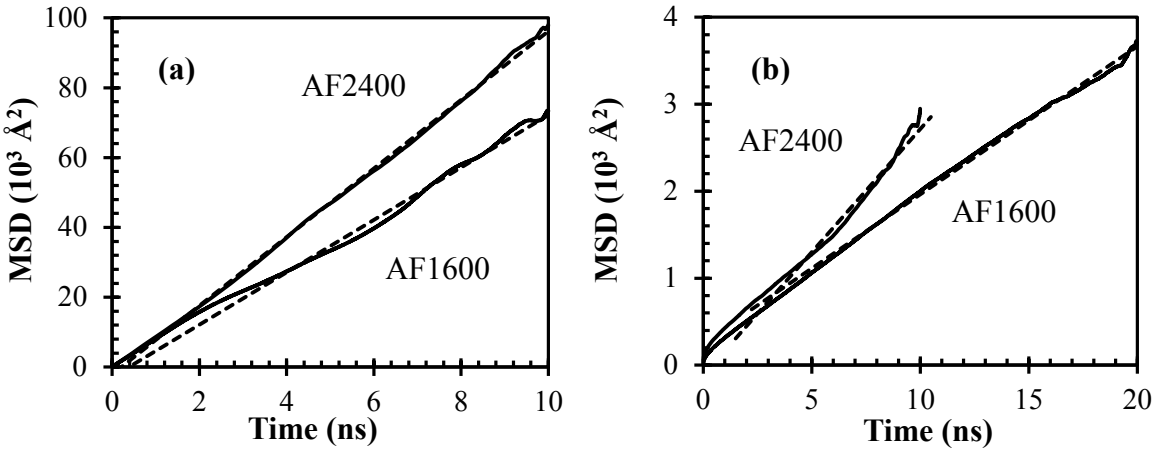

Figure 4.4: Mean square displacement (MSD) curves of He (a) and N_2 (b) for AF2400 and AF1600 resulting from atomistic molecular dynamics (MD) simulations. Each of the curves represents the average MSD, calculated from at least two independent packing models of each polymer. The dashed lines are linear least square fits to the portions of the MSD curves that represent Fickian, or at least near-Fickian behavior.

The simulated sorption isotherms of He and N_2 for AF2400 and AF1600 displayed the expected behaviour in terms of the shapes of the isotherms, where He exhibited linear sorption isotherms that correlated well with literature data as shown in Fig. 4.5 (a). Weakly soluble permanent gases such as He and H_2 typically exhibit such linear sorption isotherms [58, 61], whereas gases and vapours that are more soluble in glassy polymers (such as N_2 as shown in Fig. 4.5 (b)) normally exhibit concave isotherms relative to the pressure axis [58, 61], due to stronger interactions with the polymer matrix, which is also concentration dependent. Consequently, the sorption behaviour of light, sparingly soluble gases (such as He) is described according to Eq. (4.25) as $C = k_D p$, with k_D giving the slope of the linear sorption isotherms, as well as the infinite dilution solubility coefficients in accordance with Eq. (4.26), such that $S_0 = k_D$. For this reason, the infinite dilution solubility coefficients of He in AF2400 and AF1600 as reported by Merkel *et al.* [61] were used to construct the linear sorption isotherms shown in Fig. 4.5 (a). It is clear from the results presented in Fig. 4.5 (a) and (b) that the simulated He sorption isotherm values were consistently lower than that reported in the literature for both AF2400 and AF1600, although only slightly. In contrast, the simulated sorption isotherm values of N_2 were somewhat higher than that reported in the literature for both AF2400 and AF1600, but generally a good correlation was observed. In all cases, the individual simulated data points were calculated as the average of the results obtained from at least two individual packing models. Consequently, the maximum % error of

the GCMC data reported in Fig. 4.5 was 11.8% (for N_2 sorption in AF1600). Further comparison between the simulated GCMC sorption isotherms and that reported in the literature can be obtained by comparing the dual sorption model parameters. Accordingly, the parameters as determined by a non-linear least square fitting of Eq. (4.25) to the data points in each case are shown in Table 4.4 along with the corresponding literature values.

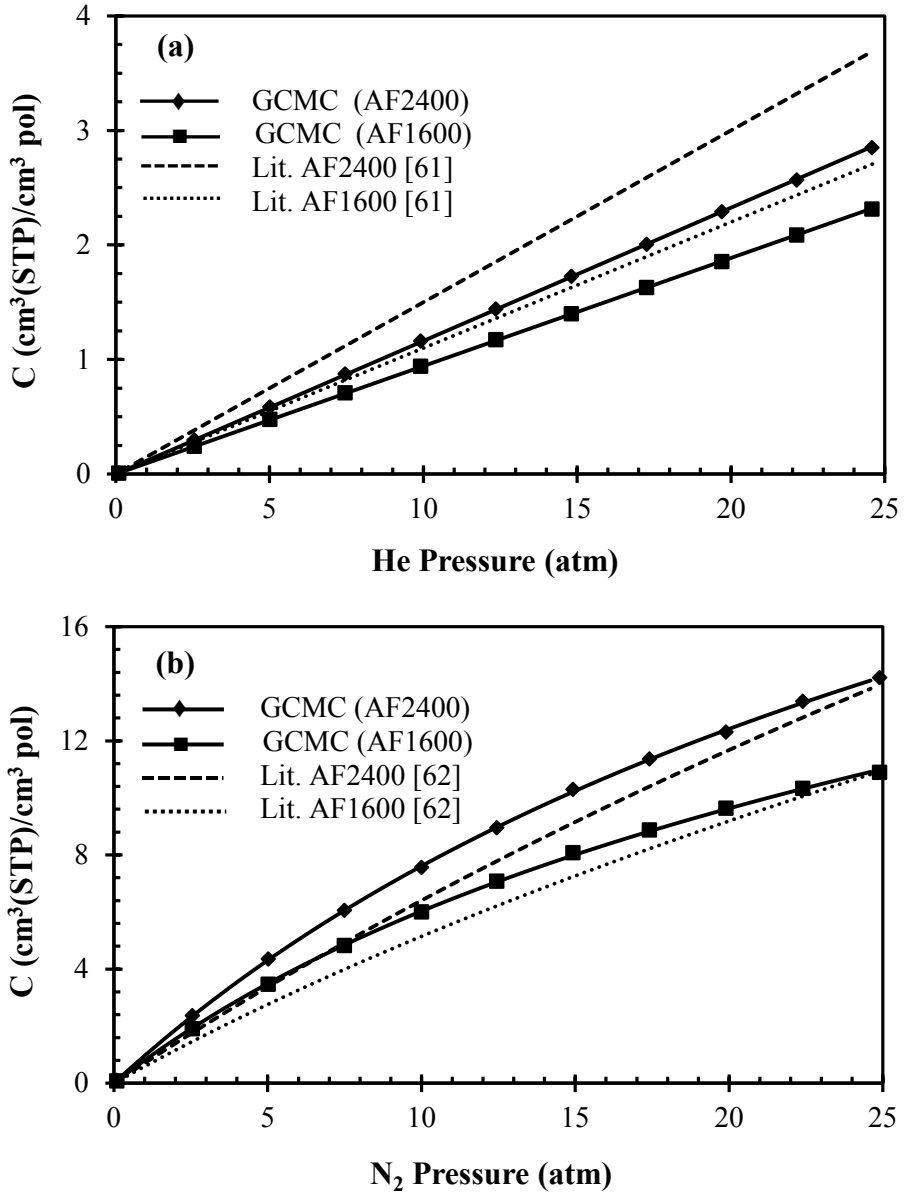

Figure 4.5: Comparison of simulated sorption isotherms of He (a) and N_2 (b) in AF2400 (♦) and AF1600 (■) at 30 °C with experimental literature data at 35 °C. The solid lines represent the non-linear least squares fit of the dual sorption model (Eq. (4.25)) to the data points obtained by GCMC simulations, and the dashed lines represent the corresponding literature isotherms for AF2400, and the dotted lines that of AF1600.

The data of Table 4.4 also shows that the GCMC simulations were rather successful at reproducing the experimental sorption behaviour of He and N_2. Furthermore, the generally lower solubility predicted by the GCMC sorption isotherms of He and N_2 in AF1600 compared to AF2400 (Fig. 4.5) also follows the experimentally observed trend as exemplified by the significantly lower N_2 Langmuir capacity parameter, C_H', of AF1600 compared to AF2400 (Table 4.4). This decrease in the sorption capacity is caused by the lower FFV of AF1600 compared to AF2400 [62], which was confirmed by the results of the geometric analysis (Sec. 4.3.2), shown in Table 4.3. Therefore, not only was it shown that the equilibrated packing models accurately reproduced the FFV of the polymers, they could also be used to obtain physically accurate results in terms of the predicted transport parameters as further illustrated in Table 4.5 and Table 4.6, where the transport properties are known to be closely related to the FFV [50, 59, 62, 63].

Table 4.4: Comparison of the dual sorption model parameters of He and N_2 as determined from GCMC simulations at 30 °C with experimental literature data at 35 °C.

Polymer	**Dual Sorption Parameter**	**He**		**N_2**	
		GCMC Sim.	**Exp.** [61]	**GCMC Sim.**	**Exp.** [62]
AF2400	k_D (cm^3(STP)/cm^3.atm)	0.116	~ 0.15	0.063	0.15
	C_H' (cm^3(STP)/cm^3)	N/A	N/A	27.79	37.6
	b (atm^{-1})	N/A	N/A	0.034	0.015
AF1600	k_D (cm^3(STP)/cm^3.atm)	0.094	~ 0.11	0.1	0.2
	C_H' (cm^3(STP)/cm^3)	N/A	N/A	15.82	14.8
	b (atm^{-1})	N/A	N/A	0.047	0.027

The infinite dilution solubilities (S_0) of N_2 in AF2400 (Table 4.5) and AF1600 (Table 4.6) was calculated from the dual sorption model parameters reported in Table 4.4 via Eq. (4.6). However, the k_D-values of He reported in Table 4.4 are equal to the infinite dilution solubilities (S_0) as explained above, and therefore are also reported in Table 4.5 and Table 4.6. In comparison with the previously reported simulation data of Hofmann *et al.* [14], it is clear that the solubility results for N_2 in both AF2400 (Table 4.5) and AF1600 (Table 4.6) obtained in this simulation study compared more favourably with the experimentally determined

solubilities. As such, the average S_0-value of N_2 for AF2400 calculated from the simulation results was larger than the average experimental literature value only by a factor of 1.3, and the S_0-value of N_2 for AF1600 was larger than the average experimental literature value by a factor of 1.4. The S_0-values of He was, however, slightly smaller than the literature values, as demonstrated by the graphical results of Fig. 4.5 (a). Further comparison of the diffusivities of He and N_2 calculated from the MD results of Fig. 4.4 (a) and (b) also suggest favourable correlation with the available experimental literature data.

Table 4.5: Comparison of the diffusivity, D, and solubility, S_0, calculated respectively from MD and GCMC simulations, and the resulting predicted permeability of AF2400 towards He and N_2 at 30 °C with the available literature data.

Source of Data	Reference	Diffusivity, D (10^{-6} cm^2/s)		Solubility, S_0 ($cm^3(STP)/cm^3.atm$)		Permeability (Barrer*)	
		He	**N_2**	**He**	**N_2**	**He**	**N_2**
Sim.	This Ch.	164 ± 2.3	4.71 ± 0.7	0.116 ± 0.006	0.995 ± 0.038	2503	617
Sim.	[14]	-	-	-	1.42 - 1.52	-	-
Exp.	Ch. 3	-	-	-	-	2501	479
Exp.	[61]	-	-	~ 0.15	~ 0.70	-	-
Exp.	[58]	-	5.36[a]	-	0.68	-	480
Exp.	[60]	>72.8[b]	5.91	<1.34[b]	0.902	2910	584

* 1 Barrer = 10^{-10} $cm^3(STP).cm/(cm^2.cmHg.s)$. [a] Calculated from the reported permeability and solubility values. [b] The diffusion coefficient value was reportedly underestimated, and the solubility value was reportedly overestimated.

In accordance with the lower FFV value of AF1600 compared to that of AF2400, it is clear that not only the solubilities (S_0) but also the diffusion coefficients of He and N_2 in AF1600 (Table 4.6) were predicted to be smaller compared to that obtained in the higher free volume AF2400 (Table 4.5). This trend is also observed with the experimental literature data, and again, indicates that the equilibrated packing models were of sufficient quality to reasonably describe the difference in the transport properties of He and N_2 with regard to AF2400 and AF1600. Therefore, to further gauge the performance of the MD and GCMC simulation methods, the predicted permeabilities, calculated through the well-known relationship $P = D.S$, was also compared to the experimentally determined permeabilities as reported in Chapter 3 as well as to literature data. From the data presented in Table 4.5 and Table 4.6, it is

clear that an excellent correlation was obtained between the predicted and experimentally measured permeability of AF2400 towards He, while a good correlation was obtained for N_2.

Table 4.6: Comparison of the diffusivity, D, and solubility, S_0, calculated respectively from MD and GCMC simulations, and the resulting predicted permeability of AF1600 towards He and N_2 at 30 °C with the available literature data.

Source of Data	Reference	Diffusivity, D (10^{-6} cm^2/s)		Solubility, S_0 (cm^3(STP)/cm^3.atm)		Permeability (Barrer*)	
		He	N_2	He	N_2	He	N_2
Sim.	This Ch.	125 ± 25	2.97 ± 0.61	0.094 ± 0.001	0.837 ± 0.09	1546	327
Sim.	[14]	-	-	-	1.32 - 1.42	-	-
Exp.	Ch. 3	-	-	-	-	1207	94
Exp.	[61]	-	-	~ 0.11	~ 0.6	-	-
Exp.	[62]	-	1.29[a]	-	0.60	-	~ 102
Exp.	[60]	>40.2[b]	1.16	<0.395[b]	0.567	861	75.6

* 1 Barrer = 10^{-10} cm^3(STP).cm/(cm^2.cmHg.s). [a] Calculated from the reported permeability and solubility values. [b] The diffusion coefficient value was reportedly underestimated, and the solubility value was reportedly overestimated.

In the case of AF1600, a slightly reduced accuracy was observed between the predicted and experimentally measured permeability values (Table 4.6), which in the case of N_2 can be attributed to a significant overestimation in the predicted diffusion and solubility coefficients. Compared to the predicted transport parameters of N_2 in AF2400, the better correlation in the predicted permeability with the experimentally measured values in this case can be attributed to a slight underestimation in the predicted diffusion coefficient, which was partially negated by the overestimation in the S_0-value.

The level of accuracy of the predicted transport parameters as compared to experimental data presented in Table 4.5 and Table 4.6 is typical of MD and GCMC simulation results in general [20-23, 29]. Nevertheless, the use of the equilibrated packing models of AF2400 and AF1600 together with MD and GCMC simulations was effective in elucidating the basic mechanism of He/N_2 permeability selectivity of these polymers, as shown in Table 4.7. Accordingly, satisfactory He/N_2 diffusion selectivity is predicted for both polymers, where that of AF1600 is clearly better than that of AF2400, in accordance with its lower FFV as

mentioned in the previous chapter. The higher diffusion selectivity of AF1600 compared to AF2400 is also verified by the estimations of Jansen *et al.* [60] as shown in Table 4.7. As N_2 is the larger, more condensable penetrant with respect to He, the GCMC simulation results also correctly predicted an appreciable N_2/He solubility selectivity, which was also slightly higher for the lower FFV AF1600 compared to AF2400. By combining the diffusion and solubility selectivity, it is clear (Table 4.7) that a permeability selectivity that correlated very well with the experimental data was obtained for AF2400. However, due to the overestimation in both the diffusivity and solubility of N_2 for AF1600 (Table 4.6), a reduced accuracy in the He/N_2 permeability selectivity was obtained.

Table 4.7: Comparison between the predicted diffusion and solubility selectivity of AF2400 and AF1600 towards He and N_2 at 30 °C, and corresponding experimentally determined selectivities.

Polymer	Source of Data	Reference	Selectivity		
			D_{He}/D_{N_2}	S_{N_2}/S_{He}	P_{He}/P_{N_2}
AF2400	Sim.	This Study	34.8	8.6	4.1
	Exp.	Ch. 3	-	-	5.2
	Exp.	[60]	>12.3[a]	>0.7[a]	5.0
AF1600	Sim.	This Study	42.1	8.9	4.7
	Exp.	Ch. 3	-	-	12.9
	Exp.	[60]	>34.7[a]	>1.4[a]	11.4

[a] The diffusion coefficient value was reportedly underestimated, and the solubility value was reportedly overestimated.

Based on the evidence presented, it can therefore be concluded that the equilibrated packing models of AF2400 and AF1600 gave a reasonable theoretical representation of the two high free volume polymers. Furthermore, since the predicted S_0-values of N_2 correlated better with the experimental data than that reported by Hofmann *et al.* [14] who concluded that their relaxed packing models gave an accurate representation of the FFV distribution, the same conclusion can be made here for the packing models used in this study. Also, it is shown that the packing models could effectively account for the higher diffusion selectivity of AF1600 compared to AF2400.

4.4.2 NF_3 and CF_4 Diffusivity Simulation Results

Since the equilibrated packing models of AF2400 and AF1600 could be effectively used to explain the observed diffusivity and solubility selectivity w.r.t. He and N_2, it was attempted to also elucidate the mechanism of NF_3/CF_4 permeability selectivity that was observed experimentally (Chapter 3). The MD simulation results (Fig. 4.6 (a) and (b)) indicates that a generally higher diffusivity was predicted for NF_3 compared to CF_4 for both AF2400 and AF1600, as can be deduced from the slopes of the MSD curves. The diffusive behaviour of the NF_3 and CF_4 probe molecules at least approached Fickian diffusion behaviour during the extensive MD production runs (Fig. 4.6) as shown in Fig. D.3 and Fig. D.4 (Appendix D). As such, the MD simulation of CF_4 in AF2400 exhibited the largest deviation from Fickain diffusion, as represented by a slope of m = 0.83 for the corresponding log(MSD) vs. log(t) plot (Fig. D.4 in Appendix D). This behaviour was due to the lower diffusivities of NF_3 and CF_4, as is clear from comparison of Fig. 4.4 with Fig. 4.6.

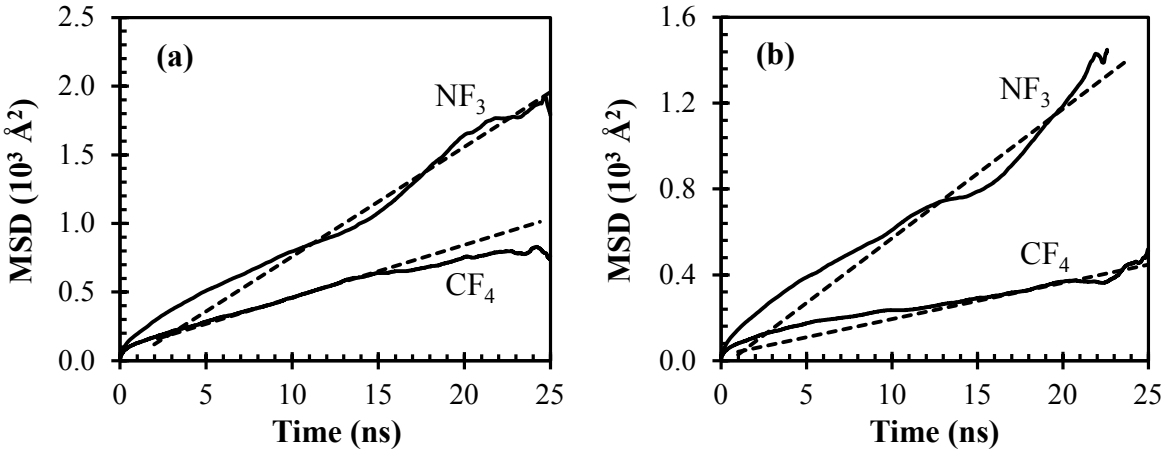

Figure 4.6: Mean square displacement (MSD) plots of NF_3 and CF_4 for AF2400 (a) and AF1600 (b) resulting from atomistic molecular dynamics (MD) simulations. Each of the curves represents the average MSD, calculated from at least two independent packing models of each polymer. The dashed lines are linear least square fits to the portions of the MSD curves that represent Fickian, or at least near-Fickian behavior.

Also evident from the graphical results presented in Fig. 4.6 (a) and (b) is that the slopes of the MSD curves showed larger deviation from each other with AF1600. As indicated by the calculated diffusion coefficients, summarised in Table 4.8, the MD simulations therefore predicted a higher NF_3/CF_4 diffusion selectivity for AF1600 compared to AF2400.

Although no experimental data for the transport coefficients was available for NF_3, the predicted CF_4 diffusion coefficients for AF2400 and AF1600 correlated reasonably with the available experimental data. As is apparent from the numerical results (Table 4.8), the calculated diffusion coefficients of CF_4 were just below 10^{-6} cm^2/s, while that of NF_3 was just above 10^{-6} cm^2/s and represents the lower limit of that which can be achieved through MD simulations. For this reason, the long simulation times (Fig. 4.6) were necessary to obtain a reasonable approximation of Fickian diffusion behaviour. Longer simulation times could possibly enhance the accuracy of the current selectivity predictions, although it is expected that the improvement in accuracy would not validate the increase in computation time. To enhance the computational efficiency, one could implement algorithms to allow one to use larger time steps than 1 fs in the MD simulations (Sec. 4.3.3). Alternatively one can use a Monte Carlo method to extend the trajectories of the penetrant molecules by using the original MD simulation results [18, 19]. None of these algorithms were available to us, and therefore the MD simulation time of 25 ns that were used was the only measure that could be used to obtain meaningful diffusion coefficient predictions. As a result, the movement of the NF_3 and CF_4 molecules during the MD simulations at least approached Fickian diffusion behaviour.

Table 4.8: Predicted infinite dilution diffusion coefficients of NF_3 and CF_4 in AF2400 and AF1600 together with the predicted diffusion selectivity at 30 °C. The available literature diffusivity data of CF_4 for the two polymers are also shown.

Gas	Source of Data	Reference	Diffusion Coefficient, D (10^{-7} cm^2/s)		Selectivity (D_{NF_3}/D_{CF_4})	
			AF2400	AF1600	AF2400	AF1600
NF_3	Sim.	This Ch.	13.3	10.0	2.1	3.5
	Sim.	This Ch.	6.38	2.82		
CF_4	Exp.	[58]	~ 2.0	-	-	-
	Exp.	[62]	~ 2.0	~ 1.6	-	-

Nevertheless, the predicted diffusion coefficient values as given in Table 4.8 predict that the perfluoropolymers possess a significant degree of diffusion selectivity towards NF_3 over CF_4. The notion in the previous chapter that the observed permeability selectivity of the perfluoropolymers towards NF_3 is probably due to significant diffusion selectivity therefore seems to be justified. As also noted in Chapter 3, the increase in permeability selectivity with decreasing FFV of the perfluoropolymers can also justifiably be ascribed to an increase in the

NF_3/CF_4 diffusion selectivity with decreasing FFV as is evident from comparison of the predicted D_{NF_3}/D_{CF_4} for AF2400 and AF1600 (Table 4.8). This follows the experimentally confirmed predicted trend for He and N_2 that was obtained through the MD simulation results shown in Table 4.7. Furthermore, the predicted NF_3 and CF_4 diffusion coefficients (Table 4.8) appears to be slightly overestimated, based on the fact that the $D_{calc}(CF_4) = 3.2D_{exp}(CF_4)$ for AF2400. Thus, it is probable that the predicted diffusion selectivity is slightly underestimated.

Nonetheless, the higher diffusivity of NF_3 over CF_4 that is predicted can be qualitatively explained based on the fact that NF_3 is a smaller molecule with a smaller molecular mass than CF_4. It can therefore be anticipated that NF_3 should have a slightly higher diffusivity in glassy polymer matrices. In this regard, an analogy to a microporous membrane that affords the separation of two gases that differs in size and molecular weight based on the principle of Knudsen diffusion can be made. For such a microporous membrane, the ideal Knudsen selectivity w.r.t. NF_3 and CF_4, $\alpha(NF_3/CF_4)_{ideal}$, can be predicted by the relation [64]:

$$\alpha\left(NF_3/CF_4\right)_{ideal} = \sqrt{M_{CF_4}/M_{NF_3}} \tag{4.27}$$

where M_i is the molecular weight of component i. It follows from Eq. (4.27) that $\alpha(NF_3/CF_4)_{ideal} = 1.11$, which is considerably lower than the diffusion selectivity predicted for Teflon AF2400 and Teflon AF1600 from the MD simulation results (Table 4.8). Thus, the relatively high diffusion selectivity that is predicted by the MD results, although supportive of the experimentally observed permeability selectivity (Chapter 3), might be further explained by considering the geometries of NF_3 and CF_4. As such, NF_3 has a pyramidal geometry, in contrast to the tetrahedral geometry of CF_4 [65]. Consequently, the tetrahedral arrangement of the atoms in CF_4 may hinder its passage in glassy polymer matrices from one free volume element to another due to steric hindrances. Simultaneously, passages formed between adjacent free volume elements due to the elastic movement of the polymer chains may be geometrically more accessible to the pyramidal NF_3 molecules. It is therefore postulated that this effect may contribute to the significant diffusion selectivity predicted by the MD simulation results, which is further enhanced by a decreasing FFV of the polymer matrix that translates into a reduced degree of interconnection between the free volume elements. Regardless, experimental measurement of the NF_3 and CF_4 diffusion coefficients would give

conclusive evidence of whether factors other than the rather small difference in the molecular weights of the two molecules are responsible for significant diffusion selectivity.

4.4.3 NF_3 and CF_4 Solubility Predictions

Although the MD simulations confirmed that the high free volume perfluoropolymers of AF2400 and AF1600 possesses a significant degree of NF_3/CF_4 diffusion selectivity as was postulated in Chapter 3, it remained to be determined whether favourable NF_3/CF_4 solubility selectivity was also probable. The N_2/He solubility predictions generally gave an accurate physical account of the experimental sorption behaviour of these gases in AF2400 and AF1600 as discussed in Sec. 4.4.1, and therefore indicated that the relaxed packing models used in this study was of adequate quality to explain the physical transport behaviour of gases in the two polymers. However, the comparison between the GCMC simulated sorption isotherms of CF_4 in AF2400 and AF1600 at 35 °C (Fig. 4.7) and the experimentally determined isotherms (constructed through the use of the dual sorption model parameters of Alentiev *et al.* [62]) indicates that a significant degree of deviation was prevalent. Specifically, the GCMC predicted sorption isotherms of CF_4 in AF2400 and AF1600 deviated significantly from the experimentally determined isotherms at low to moderate pressures. Consequently, the GCMC simulations predicted that AF2400 and AF1600 would already be mostly saturated with CF_4 at external pressures of ~ 10 bar, while the experimentally determined isotherms show that the CF_4 concentration increases more gradually with external pressure, which translated into a larger maximum sorption capacity. Also, because of the large slope of the sorption isotherm curves of CF_4 in the low pressure limit, the solubility coefficients at infinite dilution (S_0) according to Eq. (4.25) correlated poorly with the experimental literature data. More specifically, the S_0-value of CF_4 predicted for AF2400 was 3 times higher than the literature value, and that predicted for AF1600 was 4.7 times higher than the literature value.

It is however apparent from Fig. 4.7 (a) and (b), that the GCMC simulations predicted a generally higher NF_3 solubility in AF2400 and AF1600, but due to the large curvature of the CF_4 sorption isotherms at low pressure, and therefore large slopes as explained above, the S_0-values for CF_4 was slightly larger than those of NF_3. However, by calculating the slope of the sorption isotherm curves in the low pressure range as the slope of the straight line formed between the first two data points, a NF_3/CF_4 solubility selectivity of 1.1 is predicted for

AF2400 and 1.2 for AF1600. These estimations correlate better with the generally higher solubility that is predicted for NF_3 over CF_4 in both AF2400 and AF1600 by the GCMC simulation results (Fig. 4.7 (a) and (b)).

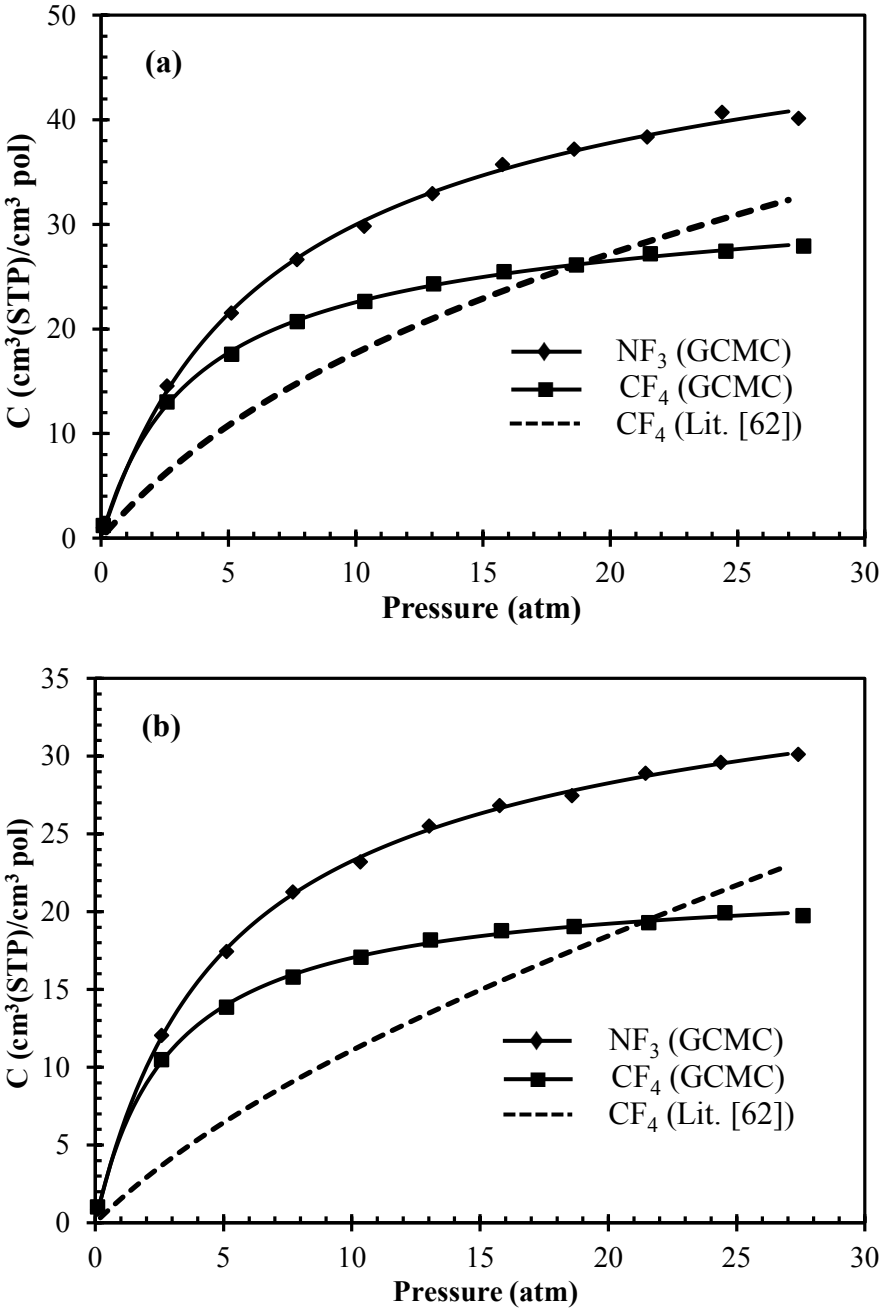

Figure 4.7: Comparison of simulated sorption isotherms of NF_3 (♦) and CF_4 (■) in AF2400 (a) and AF1600 (b) at 30 °C with experimental literature data of CF_4 at 35 °C (dashed lines). The solid lines represent the non-linear least squares fit of the dual sorption model (Eq. (4.25)) to the data points obtained by GCMC simulations.

Also, the GCMC simulation results indicate that a lower overall solubility of NF_3 and CF_4 in AF1600 compared to that in AF2400 was predicted, which is in accordance with the experimental data of CF_4 and the lower FFV of AF1600. The estimated NF_3/CF_4 solubility selectivity of 1.1 for AF2400 and 1.2 for AF1600 is also, as noted in the previous chapter, supported by literature evidence that indicates that NF_3 is more favourably adsorbed onto porous adsorbents [1-3] compared to CF_4, and is more soluble than CF_4 in perfluorocarbon and halogenated fluids [4]. As also shown in Chapter 2, NF_3 is more strongly adsorbed onto porous polymer packing materials used in analytical GC columns, causing it to frequently elute after CF_4 [5, 6].

However, because of the large discrepancy observed in the GCMC-predicted sorption behaviour of CF_4, further analysis of the dual sorption model parameters obtained by fitting Eq. (4.25) to the numerical results (which was done to obtain the curves presented in Fig. 4.7) will not be performed here. Also, because no experimental sorption isotherm data was available for NF_3, it is unknown to what extent the predicted NF_3 sorption isotherms deviate from what will be obtained in reality. Instead, a few explanations for the observed discrepancy in the predicted CF_4 sorption isotherm behaviour are given. In this regard, the following factors may have contributed to the high solubility of CF_4 in AF2400 and AF1600 that was predicted at low pressures [66, 67]:

1) *General incompatibility of the COMPASS forcefield to adequately describe the gas-polymer interactions:* Although the results are not shown, the use of different forcefields was also tested, but generally the COMPASS forcefield yielded the most physically accurate results. In this regards, it is anticipated that the COMPASS forcefield overestimated the gas-polymer interactions, which led to the rapid uptake of penetrant molecules at low pressures that resulted in saturation being obtained prematurely. To improve the forcefield performance, a unique forcefield may be constructed by evaluating the specific polymer-gas interactions using for example ab initio DFT methods [68], and using a fitting procedure to construct more accurate forcefield parameters.
2) *Inadequate representation of the FFV distributions:* An inadequate free volume distribution, i.e. containing many small "pores" rather than a random collection of large and small "pores", would also lead to higher than normal interaction energies at low pressures. However, the good correlation observed between the simulated and experimentally determined N_2 sorption behaviour, and the good correlations obtained

between the predicted and experimental diffusivities of He and N_2 suggests that the relaxed packing models gave a reasonably accurate representation of the FFV distribution.

3) *The GCMC method follows a static "hole-filling" procedure that may create artefacts:* The FFV distribution of the polymer matrix can "react" to a certain degree during the uptake of gas molecules and can therefore change as a function of penetrant concentration. In contrast, the GCMC method does not take this aspect into account, as the polymer framework is kept rigid and could also contribute to saturation begin reached prematurely.

Since the GCMC method failed to yield a conclusive description of the sorption behaviour of NF_3 and CF_4 in AF2400 and AF1600, the NELF model was therefore used as described in Sec. 4.2 in an attempt to further evaluate the solubility selectivity of AF2400 and AF1600 towards NF_3 and CF_4. As De Angelis *et al.* [35] already calculated the Sanchez-Lacombe characteristic model parameters for AF2400 and AF1600, their values were used for the prediction of the sorption isotherms of NF_3 and CF_4. However, although they also provided the characteristic model parameters for CF_4 [35], a different vapour-liquid equilibrium data set was used here [65] to determine the characteristic parameters of both NF_3 and CF_4 through a curve fitting procedure in which Eq. (4.6) was used. Thus, the characteristic parameters of AF2400, AF1600, NF_3 and CF_4 that was used in this study are summarised in Table 4.9.

Table 4.9: Sanchez-Lacombe equation of state characteristic parameters used in this study.

Polymer/ Gas	ρ^* (g/cm^3)	p^* (bar)	T^* (K)	Reference
AF2400	2.13	2500	624	[35]
AF1600	2.16	2800	575	[35]
NF_3	1.79	4241.4	199.8	[65][a]
CF_4	1.87	229.4	2820.8	[65][a]

[a] Source of vapour-liquid equilibrium data used to determine the characteristic parameters.

Using the newly obtained characteristic parameters of CF_4 (Table 4.9), with a constant polymer density of ρ_2^0 = 1.77 g/cm^3 for AF2400 and ρ_2^0 = 1.84 g/cm^3 for AF1600 [35], the sorption isotherm predictions shown in Fig. 4.8 (a) and (b) were obtained. The degree of

correlation between the predicted and experimental sorption isotherms of Alentiev *et al.* [62] coincided with that obtained by De Angelis *et al.* [35].

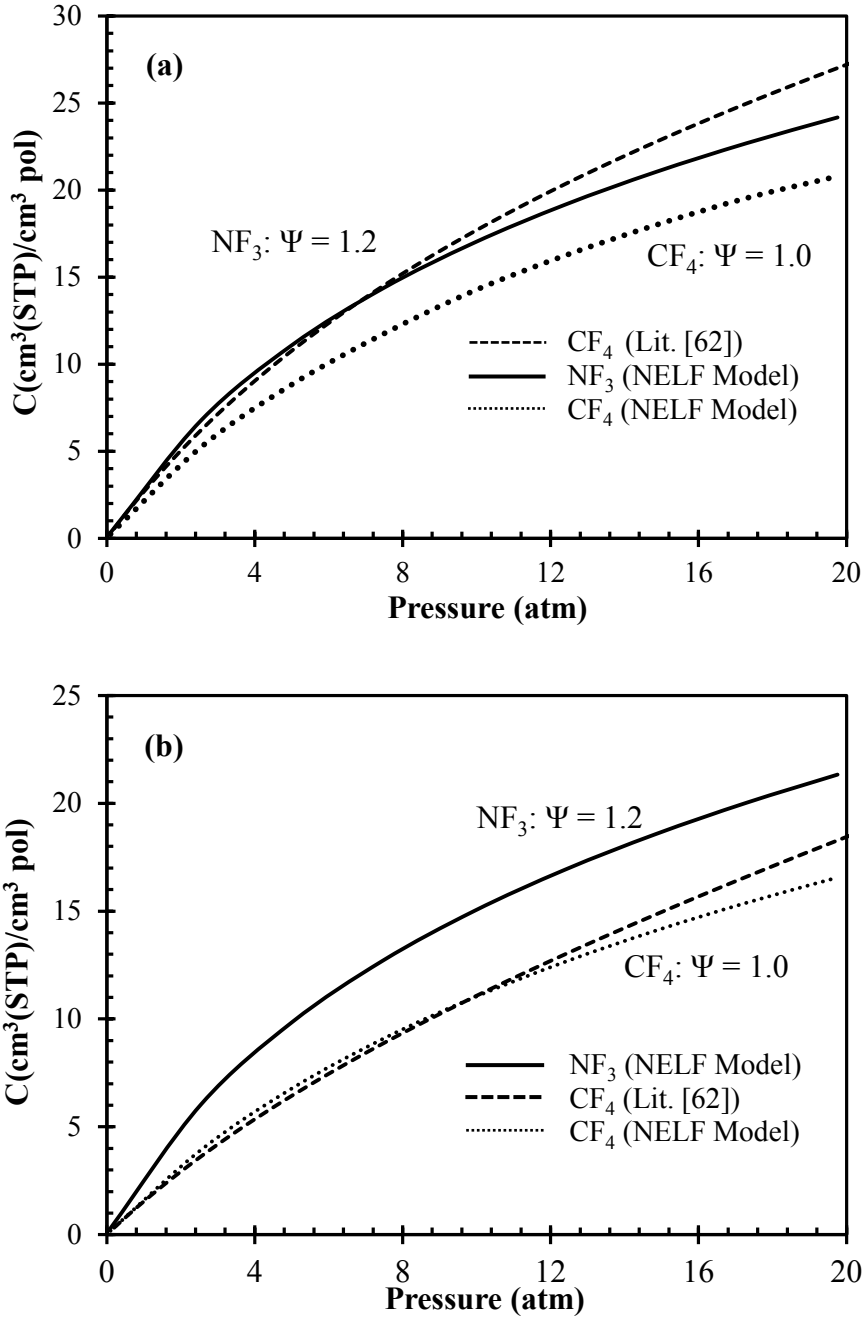

Figure 4.8: NELF Model predictions of NF_3 (solid lines) and CF_4 (dotted lines) sorption isotherms at 35 °C in AF2400 (a) and AF1600 (b), compared to the CF_4 sorption isotherms (dashed lines) taken from literature [62]. The adjustable interaction parameter was set to a value of $\Psi = 1.2$ for NF_3 for both AF2400 and AF1600 as explained in the text.

Thus, it is clear (Fig. 4.8 (a) and (b)) that the NELF model was much more successful at predicting the sorption behaviour of CF_4 in AF1600 compared to AF2400. However, compared to the GCMC simulation results (Fig. 4.7 (a) and (b)), the NELF model yielded much better correlations with the experimental data in both cases. Following the general trend of higher NF_3 solubility predicted by the GCMC simulations (Fig. 4.7 (a) and (b)), and the experimentally observed higher activity of NF_3 in solid and liquid adsorbents as noted above, a slight degree of NF_3/CF_4 solubility selectivity was expected with AF2400 and AF1600 to compliment the predicted diffusion selectivity (Table 4.8). However, the classic NELF model ($\Psi = 1.0$) predicted that NF_3 would have a lower solubility in AF2400 and AF1600 compared to CF_4 (results not shown). Therefore, in accordance with the higher adsorbent-phase activity of NF_3 compared to CF_4 that is frequently observed as noted above, the interaction parameter was set to a value of $\Psi = 1.2$ for NF_3 for the sorption isotherm predictions as shown in Fig. 4.8 (a) and (b). By using $\Psi = 1.2$, it is therefore postulated that the relative interaction energy between NF_3 and the polymer matrices is 20% larger than that of CF_4, which seems justified according to the abovementioned experimentally observed behaviour.

Adjustment of the interaction parameter is not uncommon. For example, De Angelis *et al.* have shown that adjustment of Ψ was necessary to correctly describe the sorption behaviour of hydrocarbon-fluorocarbon gas-polymer, and fluorocarbon-hydrocarbon gas-polymer systems [35, 36]. In this regard, Merkel *et al.* [61, 69] have reported that fluorocarbon penetrants display systematically higher solubility in fluorocarbon-based polymer matrices than their hydrocarbon analogues, while hydrocarbons have systematically higher solubility in hydrocarbon-based polymers compared to their fluorocarbon analogues. Consequently, examination of the NELF-model correlation results presented by De Angelis *et al.* confirm the theory presented by Merkel *et al.* [61, 69] that hydrocarbon-hydrocarbon interactions were favoured over hydrocarbon-fluorocarbon interactions and vice versa. This is because De Angelis *et al.* consistently needed to adjust Ψ to values smaller than unity to prevent overestimation of the concentrations of CH_4, C_2H_6, C_3H_8, and n-C_4H_{10} in AF2400 and AF1600 as a function of pressure, while the sorption isotherms of CF_4 and C_2F_6 was correctly described by $\Psi = 1$ [35]. Conversely, it was necessary to adjust Ψ to values of ca. 0.86 to prevent overestimation of the concentrations of CF_4 and C_2F_6 as a function of pressure in PDMS, while a smaller adjustment of $\Psi \approx 0.95$ was necessary to correctly describe the sorption isotherms of CH_4 and C_2H_6 in PDMS [36]. Thus, it was necessary to adjust Ψ to account for the weaker chemical interactions between fluorocarbon gases and hydrocarbon

polymers, and hydrocarbon gases and fluorocarbon polymers. Similarly, Ψ was adjusted in this study to 1.2 for NF_3 to account for its experimentally observed stronger chemical interaction with polymeric and inorganic adsorbents to explain the experimentally illustrated NF_3/CF_4 permeability selectivity of AF2400, AF1600 and Hyflon AD60 (Chapter 3). As also noted in Sec. 4.1, there is literature evidence that document the unique chemical interactions of NF_3 with different chemical species.

Therefore, it is conceivable that NF_3 can chemically interact with polymer matrices to a larger extent compared to CF_4 that may be described in this case by adjusting the NELF model interaction parameter, Ψ, to a value of 1.2 for NF_3. As a result, the NELF model predictions, with Ψ = 1.2 for NF_3, shown in Fig. 4.8 (a) and (b) indicate that a slight degree of NF_3/CF_4 solubility selectivity can be expected, and more noticeably so for AF1600 compared to AF2400. Specifically, the infinite dilution solubility coefficients calculated via a dual sorption model fit (Eq. (4.25)) to each data set and subsequent application of Eq. (4.26), showed that the predicted solubility selectivity for AF2400 was S_{NF_3}/S_{CF_4} = 1.4, and for AF1600 was S_{NF_3}/S_{CF_4} = 1.7 (Table 4.10).

Table 4.10: Predicted infinite dilution solubilities (NELF model) and the resulting solubility selectivity of NF_3 and CF_4 in AF2400 and AF1600 at 35 °C. Also shown is the predicted diffusion selectivity obtained from MD simulations (Table 4.8), and the predicted permeability selectivity, $\alpha(NF_3/CF_4)$ as compared to the experimentally determined ideal permeability selectivity.

Polymer	S_0 (cm^3(STP)/cm^3.atm)		Predicted Selectivity			Experimental $\alpha(NF_3/CF_4)$[b]
	NF_3	CF_4	S_{NF_3}/S_{CF_4}	D_{NF_3}/D_{CF_4}	$\alpha(NF_3/CF_4)$[a]	
AF2400	3.4	2.4	1.4	2.1	3.0	4.5
AF1600	3.0	1.8	1.7	3.5	5.9	6.0

[a] Calculated using Eq. (4.28). [b] Ideal permeability selectivity (Chapter 3).

The infinite dilution solubility predicted with the NELF model for CF_4 (Table 4.10) compared favourably with the experimental data of Alentiev *et al.* [62] who obtained $S_0(CF_4)$ = 2.9 for AF2400 and $S_0(CF_4)$ = 1.6 for AF1600 (both in units of cm^3(STP)/cm^3.atm). As a result of the lower sorption capacity of the lower FFV AF1600, an improved solubility selectivity is predicted, which is also paralleled by an increased diffusion selectivity compared to the

higher FFV AF2400. These observations confirm the hypotheses given in the previous chapter, i.e. that the observed increase in the NF_3/CF_4 permeability selectivity with decreasing FFV was due to an increasing diffusion selectivity as well as an increasing solubility selectivity. Using the predicted diffusion and solubility selectivity values, the NF_3/CF_4 permeability selectivity of AF2400 and AF1600 can thus be calculated by [64]:

$$\alpha(NF_3/CF_4) = \left(\frac{D_{NF_3}}{D_{CF_4}}\right)\left(\frac{S_{NF_3}}{S_{CF_4}}\right) \tag{4.28}$$

Accordingly, the predicted permeability selectivity (Table 4.10) compared excellently with the experimentally determined values (Chapter 3), especially in the case of AF1600. Based on these observations, Hyflon AD60, which showed the highest permeability selectivity (Chapter 3), would therefore exhibit the most significant diffusion and solubility selectivity towards NF_3, as it also possesses the lowest FFV. Although the diffusion selectivity is predicted to be the dominant factor responsible for the observed permeability selectivity (Chapter 3), it is clear that favourable solubility selectivity w.r.t. NF_3 would complement the diffusion selectivity, which increases relatively significantly with decreasing FFV. Based on the good correlation obtained between the predicted and experimental permeability selectivities, the diffusion and solubility selectivity predictions presented here most probably offer a good representation of what can be experimentally expected.

In fact, from the correlation between the logarithm of the infinite dilution solubilities (S_0) and penetrant critical temperature squared (T_c^2) (Fig. 4.9), which is frequently used to correlate penetrant condensability with solubility [58, 61, 62, 69], it is apparent that NF_3 and CF_4 obeys the general trend of increasing solubility as penetrant critical temperature increases (Fig. 4.9 (b)). Comparison of Fig. 4.9 (a) and (b) also shows that the solubility of the fluorinated gases (Fig. 4.9 (b)) increases more rapidly with increasing critical temperature than that of the permanent gases (N_2 and O_2), the hydrocarbon gases and CO_2 (Fig. 4.9 (a)). This also illustrates the general observation that fluorinated penetrants are significantly more soluble in fluorinated polymers such as AF2400 and AF1600 compared to their hydrocarbon analogues [58, 61, 62, 69]. The correlation of $\log(S_0)$ vs. T_c^2 therefore illustrates that penetrant solubility generally increases with increasing condensability, but that chemical affinity also plays an important role.

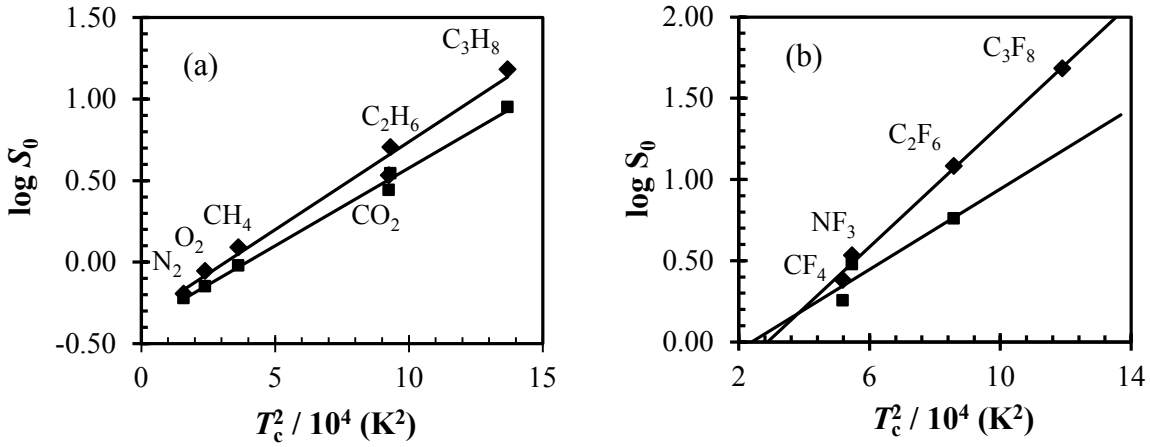

Figure 4.9: Correlation of infinite dilution solubility coefficients at 35 °C in Teflon AF2400 (♦) and Teflon AF1600 (■) with penetrant critical temperature for non-fluorinated gases and hydrocarbon gases (a), and fluorinated gases (b). The infinite dilution solubility coefficient data of Alentiev *et al*. [62] together with the NELF model results for NF3 and CF4 (Table 4.10) was used for the construction of the graphs.

Therefore, although the critical temperatures of NF_3 and CF_4 do not differ significantly (Table 1.1), the adjustment of the NELF interaction parameter to a value of $\Psi = 1.2$, i.e. assuming more favourable chemical interaction of NF_3 with the fluorinated polymer matrices, yielded calculated NF_3 and CF_4 solubilities that agrees reasonably well with this corresponding states correlation. A small deviation in the calculated S_{NF_3} to a higher S_0-value than that predicted by the trend was observed for both AF2400 and AF1600, while a small deviation in the calculated S_{CF_4} to a lower S_0-value than that predicted by the trend was also observed for both AF2400 and AF1600. However, as shown in Fig. 4.9 (a), such deviations from the T_c^2-correlation are possible, as is the case with the measured values of CO_2 for both AF2400 and AF1600.

Furthermore, a similar correlation between the diffusivities and penetrant critical volume (Fig. 4.10) as also presented by Alentiev *et al.* [62] illustrates that the simulated diffusivities of NF_3 and CF_4 (Table 4.8) also follows the general trend of decreasing diffusivity with increasing penetrant size, of which V_c is an indication. Although some deviation of the simulated diffusivities of NF_3 and CF_4 from the corresponding states correlation in terms of V_c are also apparent (Fig. 4.10), similar deviations are noticeable for the measured values of CF_4 and C_2H_6. Nonetheless, the diffusivities of NF_3 and CF_4 predicted by the MD simulations are therefore physically sound in that NF_3, the smaller molecule compared to CF_4 (Table 1.1), has

a higher diffusivity compared to CF_4 that also correlates with the smaller critical volume of NF_3 compared to that of CF_4 (Fig. 4.10). Although NF_3 has a slightly lower boiling point than CF_4, the correlation between the logarithm of the infinite dilution solubility coefficients and the critical temperature squared (Fig. 4.9 (b)) therefore also gave qualitative confirmation of the correctness of the NELF model predictions with regard to NF_3/CF_4 solubility selectivity (Table 4.10).

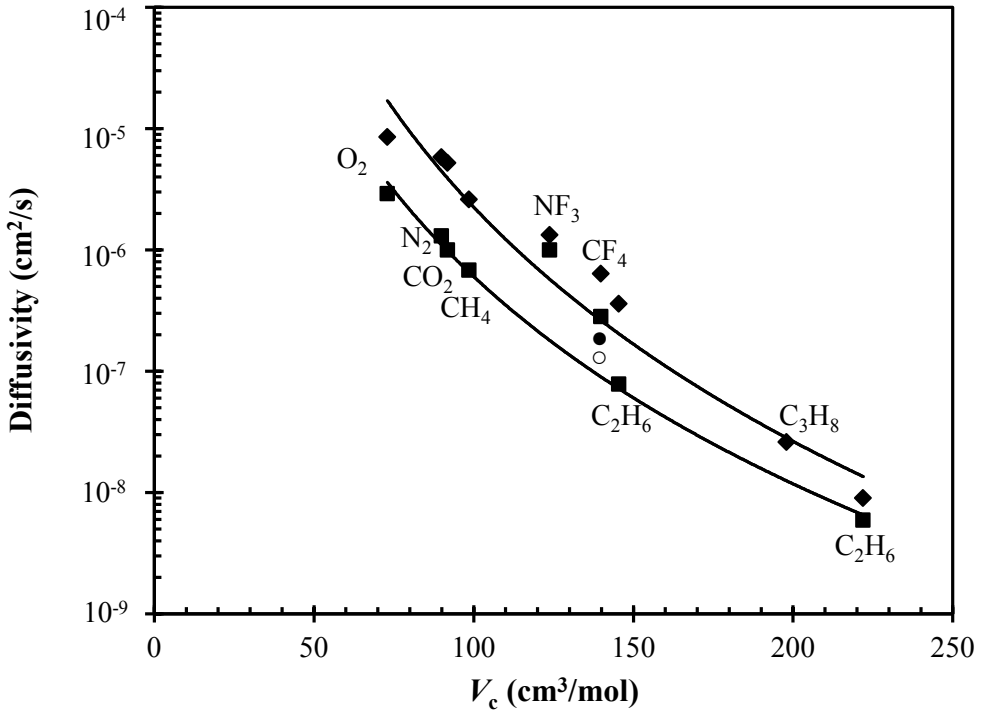

Figure 4.10: Correlation of infinite dilution diffusion coefficients with penetrant critical volumes (V_c) in Teflon AF2400 (♦) [58] and Teflon AF1600 (■) [62]. The diffusivities of all gases at 35 °C are shown, except for NF_3 and CF_4, which represent the simulated diffusivities at 30 °C as given in Table 4.8. The measured values of CF_4 at 35 °C for Teflon AF2400 (●) [58] and Teflon AF1600 (○) [62] are also included in the figure from which it is apparent that CF_4 deviates somewhat from the general trend.

Although the exact solubility and diffusivity values of NF_3 and CF_4 can still be elucidated by further experimental studies, it is apparent that the observed NF_3/CF_4 permeability selectivity (Chapter 3) is justifiably explained in terms of favourable solubility and diffusion selectivity with respect to NF_3. In this regard, NF_3 and CF_4 are analogous to the case of N_2 and O_2, since O_2 (the smaller molecule compared to N_2) has a higher diffusivity in AF2400 and AF1600 compared to N_2 as also apparent from Fig. 4.10. However, O_2 also has a higher T_c^2-value

compared to N_2 which also correlates with higher infinite dilution solubility values in AF2400 and AF1600 (Fig. 4.9 (a)). The combination of favourable O_2/N_2 diffusion and solubility selectivity also leads to favourable permeability selectivity, as is the case with NF_3 and CF_4.

The use of MD simulations coupled with the NELF model therefore provides an efficient method of evaluating the diffusion and sorption characteristics of polymers towards gaseous penetrants. In comparison to the NELF model, the use of GCMC, although very useful, still suffers from limitations such as forcefields that fail to accurately describe penetrant-polymer interactions while being very computationally intensive. Nonetheless, optimisation of forcefield parameters might be useful to efficiently screen a wide range of polymers for optimum NF_3/CF_4 solubility selectivity by efficiently accounting for the specific chemical interactions that seem to be prevalent between NF_3 and the perfluoropolymer matrices. Nonetheless, investigation of the transport characteristics of the different polymers towards NF_3 and CF_4 through experimental methods would ultimately be necessary to conclusively validate the mechanism of separation.

4.5 Conclusions

After obtaining fully equilibrated atomistic packing models of AF2400 and AF1600, it was shown through geometric analysis that the FFV predicted by the models compared well with literature results. By evaluating the diffusivity and solubility of He and N_2 through MD and GCMC simulations respectively, it was shown that reasonably accurate results compared to experimental data were obtained, thereby offering a second validation for the relaxed packing models of AF2400 and AF1600. As such, the He/N_2 diffusion selectivity was predicted to follow the experimental trend such that AF1600, which has a lower FFV than AF2400, was predicted to be the most selective w.r.t He/N_2 diffusion. Conversely, the GCMC results correctly predicted favourable N_2/He solubility selectivity for both polymers, and it was shown that the calculated sorption isotherms of He and N_2 correlated well with the experimental data.

Having validated the equilibrated packing models of AF2400 and AF1600, it was also shown that favourable diffusion selectivity was predicted for NF_3 over CF_4, that was also higher for AF1600, and it was concluded that NF_3/CF_4 diffusion selectivity is the major driving force behind the experimentally observed permeability selectivity. In addition, the diffusion

selectivity was also shown to improve with decreasing FFV, as can be anticipated and which was also the case with He and N_2. Unfortunately, the sorption isotherms of CF_4 calculated through GCMC simulations was significantly overestimated at low to moderate pressures compared to the available literature data, but predicted that NF_3 was generally more soluble in AF2400 and AF1600. This discrepancy was mainly attributed to inadequate forcefield parameters that failed to accurately describe the gas-polymer interactions, and it was concluded that forcefield development is necessary to accurately predict the solubility of non-classical fluids such as NF_3 and CF_4 in polymer and/or inorganic matrices.

In an attempt to gain a better representation of the solubility selectivity of AF2400 and AF1600 towards NF_3 and CF_4, the NELF model was implemented which gave significantly more accurate sorption isotherm predictions w.r.t. CF_4. By adjusting the NELF model interaction parameter Ψ to a value of 1.2 for NF_3, favourable NF_3/CF_4 solubility selectivity was predicted, which complemented the diffusion selectivity calculated from the MD simulation results such that NF_3/CF_4 permeability selectivity values were calculated that corresponded very well with the experimentally determined permeability selectivities. These results therefore gave supporting evidence for the hypothesis given in Chapter 3, namely that the favourable NF_3 permeability selectivity was caused not only by NF_3/CF_4 diffusion selectivity, but also favourable solubility selectivity w.r.t. NF_3. Also, both the diffusion and solubility selectivity showed an inverse functional dependence on the FFV, also explaining the improvement in the experimental NF_3/CF_4 permeability selectivity with decreasing FFV as reported previously.

Having obtained a good correlation between the predicted and experimental permeability selectivities by combining the MD simulation results and NELF model calculations with Ψ = 1.2, indicates that NF_3 most probably undergoes non-classical chemical interactions with the polymer matrices so that it dissolved more readily, although it has a lower normal boiling point compared to CF_4. As a higher activity is frequently observed for NF_3 compared to CF_4 in porous organic and inorganic adsorbents, the use of Ψ = 1.2 seems justified, and the solubility and solubility selectivity predictions presented here are anticipated to be reasonably accurate. This was qualitatively confirmed, since the calculated infinite solubility and diffusivity values of NF_3 and CF_4 obeyed corresponding state correlations in terms of $\log(S_0)$ vs. T_c^2 and D vs. V_c. However, it is advisable that the transport characteristics of NF_3 and CF_4 in polymeric membranes are studied experimentally to conclusively validate the mechanism

of separation and to clarify further routes of study to improve the performance and applicability of membrane separation for the purification of NF_3 from CF_4.

4.6 References

1. Y.-C. Park, W.-S. Jeong, K.-C. Hyun, J.-W. Lee, I.-H. Kwon, Process for refining nitrogen trifluoride gas using alkali earth metal exchanged and impregnated zeolite, U.S. Pat. 7,637,986 B2 (2009).
2. S.M. Igumnov, V.P. Kharitonov, N.V. Kharitonova, Method of purifying gaseous nitrogen trifluoride, U.S. Pat. 7,022,160 B2 (2006).
3. T. Suenaga, T. Fujii, Y. Kobayashi, Method of refining nitrogen trifluoride gas, U.S. Pat. 5,069,887 (1991).
4. D.A. Mukhortov, I.A. Blinov, E.S. Kurapova, P.S. Kambur, Solubility of nitrogen trifluoried and tetrafluoromethane in perfluorinated and highly halogenated fluids, Russ. J. Appl. Chem. 83 (2010) 31 – 35.
5. J.P. de Coning, J.M. Swinley, Optimisation of a gas chromatographic method for trace gaseous impurities in nitrogen trifluoride by column sequence reversal, J. Chromatogr. A 1180 (2008) 151 – 158.
6. C.-F.O. Yang, S.-H. Kam, C.-H. Lui, J. Tzou, J.-L. Wang, Assessment of removal efficiency of perfluorocompounds (PFCs) in a semiconductor fabrication plant by gas chromatography, Chemosphere 76 (2009) 1273 – 1277.
7. R. Miotto, A.C. Ferraz, G.P. Srivastava, Dissociative adsorption of NF_3 on Si(001)-(2×1), Surf. Sci. 454 – 456 (2000) 152 – 156.
8. I.I. Rzeźnicka, J. Lee, J.T. Yates Jr., Dynamics of NF_3 in a condensed film on Au(111) as studied by electron-stimulated desorption, Surf. Sci. 600 (2006) 4492 – 4500.
9. K.H. Junker, J.M. White, Adsorption of NF_3 on Pt(111): interactions with electrons and photons, Surf. Sci. 382 (1997) 67 – 78.
10. F. Grandinetti, V. Vinciguerra, Complexes of lithium cation with nitrogen trifluoride: a computational investigation on the structure and stability of Li^+–(NF_3) isomers, J. Mol. Struct.: THEOCHEM 574 (2001) 185 – 193.
11. K. Pei, J. Liang, H. Li, Gas-phase chemistry of nitrogen trifluoride NF_3: structure and stability of its M^+–NF_3 (M = H, Li, Na, K) complexes, J. Mol. Struct. 690 (2004) 159 – 163.

12. P. Antoniotti, S. Borocci, F. Grandinetti, Nitrogen trifluoride as bifunctional Lewis base: Implications for the adsorption of NF_3 on solid surfaces, Eur. J. Inorg. Chem. (2004) 1125 – 1130.
13. F. Blanco, I. Alkorta, I. Rozas, M. Solimannejad, J. Elguero, A theoretical study of the interactions of NF_3 with neutral ambidentate electron donor and acceptor molecules, Phys. Chem. Chem. Phys. 13 (2011) 674 – 683.
14. D. Hofmann, M. Entrialgo-Castano, A. Lerbret, M. Heuchel, Y.P. Yampolskii, Molecular modeling investigation of free volume distributions in stiff chain polymers with conventional and ultrahigh free volume: Comparison between molecular modeling and positron lifetime studies, Macromolecules 36 (2003) 8528 – 8538.
15. D. Hofmann, M. Heuchel, Yu. Yampolskii, V. Khotimskii, V. Shantarovich, Free volume distributions in ultrahigh and low free volume polymers: Comparison between molecular modelling and positron lifetime studies, Macromolecules 35 (2002) 2129 – 2140.
16. X.-Y. Wang, K.M. Lee, Y. Lu, M.T. Stone, I.C. Sanchez, B.D. Freeman, Cavity size distributions in high free volume glassy polymers by molecular simulation, Polymer 45 (2004) 3907 – 3912.
17. J.C. Jansen, M. Macchione, E. Tocci, L. De Lorenzo, Y.P. Yampolskii, O. Sanfirova, V.P. Shantarovich, M. Heuchel, D. Hofmann, E. Drioli, Comparative study of different probing techniques for the analysis of the free volume distribution in amorphous glassy perfluoropolymers, Macromolecules 42 (2009) 7589 – 7604.
18. S. Neyertz, D. Brown, S. Pandiyan, N.F.A. van der Vegt, Carbon dioxide diffusion and plasticization in fluorinated polyimides, Macromolecules 43 (2010) 7813 – 7827.
19. S. Neyertz, D. Brown, A trajectory-extending kinetic Monte Carlo (TEKMC) method for estimating penetrant diffusion coefficients in molecular dynamics simulations of glassy polymers, Macromolecules 43 (2010) 9210 – 9214.
20. F. Mozaffari, H. Eslami, J. Moghadasi, Molecular dynamics simulation of diffusion and permeation of gases in polystyrene, Polymer 51 (2010) 300 – 307.
21. M. Heuchel, D. Fritsch, P.M. Budd, N.B. McKeown, D. Hofmann, Atomistic packing model and free volume distribution of a polymer with intrinsic microporosity (PIM-1), J. Membr. Sci. 318 (2008) 84 – 99.
22. E. Tocci, A. Gugliuzza, L. De Lorenzo, M. Macchione, G. De Luca, E. Drioli, Transport properties of a co-poly(amide-12-b-ethylene oxide) membrane: A

comparative study between experimental and molecular modelling results, J. Membr. Sci. 323 (2008) 316 – 327.

23. X.-Y. Wang, A.J. Hill, B.D. Freeman, I.C. Sanchez, Structural, sorption and transport characteristics of an ultrapermeable polymer, J. Membr. Sci. 314 (2008) 15 – 23.
24. D. Hofmann, L. Fritz, J. Ulbrich, C. Schepers, M. Boëhning, Detailed atomistic molecular modeling of small molecule diffusion and solution processes in polymeric membrane materials. Macromol. Theory Simul. 9 (2000) 293 – 327.
25. A.A. Gusev, F. Müller-Plathe, W.F. van Gunsteren, U.W. Suter, Dynamics of Small molecules in bulk polymers, Adv. Polym. Sci. 116 (1994) 207 – 247.
26. L. Chen, Q. Hui, C. Wang, X. Jiang, Molecular simulation on the transport properties of poly[1-trimethylsilyl-1-propyne] for organic-vapor/permanent-gas separation, Fluid Phase Equilibr. 310 (2011) 142 – 149.
27. O. Hölck, M. Böhning, M. Heuchel, M.R. Siegert, D. Hofmann, Gas sorption isotherms in swelling glassy polymers-Detailed atomistic simulations, J. Membr. Sci. 428 (2013) 523 – 532
28. O. Hölck, M.R. Siegert, M. Heuchel, M. Böhning, CO_2 Sorption induced dilation in polysulfone: Comparative analysis of experimental and molecular modeling results, Macromolecules 39 (2006) 9590 – 9604.
29. K.-S. Chang, C.-C. Tung, K.-S. Wang, K.-L. Tung, Free volume analysis and gas transport mechanisms of aromatic polyimide membranes: A molecular simulation study, J. Phys. Chem. B. 113 (2009) 9821 – 9830.
30. I. Sanchez, R.H. Lacombe, An elementary theory of classic fluids. Pure fluids, J. Phys. Chem. 80 (1976) 2352 – 2362.
31. I. Sanchez, R.H. Lacombe, Statistical thermodynamics of polymer solutions, Macromolecules 11 (1978) 1145 – 1156.
32. F. Doghieri, G.C. Sarti, Nonequilibrium lattice fluids: A predictive model for the solubility in glassy polymers, Macromolecules 29 (1996) 7885 – 7896.
33. F. Doghieri, G.C. Sarti, Predicting the low pressure solubility of gases and vapors in glassy polymers by the NELF model. J. Membr. Sci. 147 (1998) 73 – 86.
34. G.C. Sarti, F. Doghieri, Predictions of the solubility of gases in glassy polymers based on the NELF model, Chem. Eng. Sci. 53 (1998) 3435 – 3447.
35. M.G. De Angelis, T.C. Merkel, V.I. Bondar, B.D. Freeman, F. Doghieri, G.C. Sarti, Gas sorption and dilation in poly(2,2-bistrifluoromethyl-4,5-difluoro-1,3-dioxole-*co*-

tetrafluoroethylene): Comparison of experimental data with predictions of the Nonequilibrium Lattice Fluid Model, Macromolecules 35 (2002) 1276 – 1288.

36. M.G. De Angelis, T.C. Merkel, V.I. Bondar, B.D. Freeman, F. Doghieri, G.C. Sarti, Hydrocarbon and fluorocarbon solubility and dilation in poly(dimethylsiloxane): Comparison of experimental data with predictions of the Sanchez-Lacombe equation of state, J. Polym. Sci. Pol. Phys. 37 (1999) 3011 – 3026.
37. M.G. Baschetti, F. Doghieri, G.C. Sarti, Solubility in glassy polymers: Correlations through the nonequilibrium lattice fluid model, Ind. Eng. Chem. Res. 40 (2001) 3027 – 3037.
38. Accelrys Software Inc., Materials Studio Modeling Environment, *Release 6.0*, Accelrys Software Inc., San Diego, 2011.
39. H. Sun, D. Rigby, Polysiloxanes: Ab initio force field and structural, conformational and thermophysical properties, Spectrochim. Acta 53 (1997) 1301 – 1323.
40. D. Rigby, H. Sun, B.E. Eichinger, Computer simulations of poly(ethylene oxide): Force field, PVT diagram and cyclization behaviour, Polym. Int. 44 (1997) 311 – 330.
41. M.P. Tosi, Cohesion of ionic solids in the born model, Solid State Physics 16 (1964) 1 – 120.
42. H.C. Andersen, Molecular dynamics simulations at constant pressure and/or temperature, J. Chem. Phys. 72 (1980) 2384 – 2393.
43. H.J.C. Berendsen, J.P.M. Postma, .F. van Gunsteren, A. DiNola, J.R. Haak, Molecular dynamics with coupling to an external bath, J. Chem. Phys. 81 (1984) 3684 – 3690.
44. M. Macchione, J.C. Jansen, G. de Luca, E. Tocci, M. Longeri, E. Drioli, Experimental analysis and simulation of the gas transport in dense Hyflon® AD60X membranes: Influence of residual solvent, Polymer 48 (2007) 2619 – 2635.
45. D.N. Theodorou, U.W. Suter, Detailed molecular structure of a vinyl polymer glass. Macromolecules 18 (1985) 1467 – 1478.
46. D.N. Theodorou, U.W. Suter, Atomistic modeling of mechanical properties of polymeric glasses. Macromolecules 19 (1986) 139 – 154.
47. G. Dlubek, J. Pionteck, K. Rätzke, J. Kruse, F. Faupel, Temperature Dependence of the Free Volume in Amorphous Teflon AF1600 and AF2400: A Pressure-Volume-Temperature and Positron Lifetime Study, Macromolecules 41 (2008) 6125 – 6133.
48. I. Pinnau, L.G. Toy, Gas and vapor transport properties of amorphous perfluorinated copolymer membranes based on 2,2-bistrifluoromethyl-4,5-difluoro-l,3-dioxole/tetrafluoroethylene, J. Membr. Sci. 109 (1996) 125 – 133.

49. A.Y. Alentiev, Y.P. Yampolskii, V.P. Shantarovich, S.M. Nemser, N.A. Platé, High transport parameters and free volume of perfluorodioxole copolymers, J. Membr. Sci. 126 (1997) 123 – 132.
50. J.Y. Park, D.R. Paul, Correlation and prediction of gas permeability in glassy polymer membrane materials via a modified free volume based group contribution method, J. Membr. Sci. 125 (1997) 23 – 39.
51. A. Bondi, van der Waals Volumes and Radii, J. Phys. Chem. 68 (1964) 441 – 451.
52. M. Meunier, Diffusion coefficients of small gas molecules in amorphous *cis*-1,4-polybutadiene estimated by molecular dynamics simulations, J. Chem. Phys. 123 (2005) 134906-1 – 134906-7.
53. F. Müller-Plathe, S.C. Rogers, W.F. van Gunsteren, Computational evidence of anomalous diffusion of small molecules in amorphous polymers. Chem. Phys. Lett. 199 (1992) 237 – 243.
54. N. Metropolis, A.W. Rosenbluth, M.N. Rosenbluth, A.H. Teller, E. Teller, Equation of state calculations by fast computing machines, J. Chem. Phys. 21 (1953) 1087 – 1092.
55. D. Peng, D.B. Robinson, A new two-constant equation of state, Ind. Eng. Chem. Fundam. 15 (1976) 59 – 64.
56. A.L. Myers, P.A. Monson, Adsorption in porous materials at high pressure: Theory and experiment. Langmuir 18 (2002) 10261 – 10273.
57. O. Talu, A.L. Myers, Molecular simulation of adsorption: Gibbs dividing surface and comparison with experiment, AIChE J. 47 (2001) 1160 – 1168.
58. T. C. Merkel, V. Bondar, K. Nagai, B. D. Freeman, Y.P. Yampolskii, Gas sorption, diffusion, and permeation in poly(2,2-bis(trifluoromethyl)-4,5-difluoro-1,3-dioxole-*co*-tetrafluoroethylene), Macromolecules 32 (1999) 8427 – 8440.
59. V.P. Shantarovich, I.B. Kevdina, Y.P. Yampolskii, A.Y. Alentiev, Positron annihilation lifetime study of high and low free volume glassy polymers: Effects of free volume sizes on the permeability and permselectivity, Macromolecules 33 (2000) 7453 – 7466.
60. J.C. Jansen, K. Friess, E. Drioli, Organic vapour transport in glassy perfluoropolymer membranes: A simple semi-quantitative approach to analyze clustering phenomena by time lag measurements, J. Membr. Sci. 367 (2011) 141 – 151.
61. T.C. Merkel, V. Bondar, K. Nagai, B.D. Freeman, Hydrocarbon and perfluorocarbon gas sorption in poly(dimethylsiloxane), poly(1-trimethylsilyl-1-propyne), and

copolymers of tetrafluoroethylene and 2,2-bis(trifluoromethyl)-4,5-difluoro-1,3-dioxole, Macromolecules 32 (1999) 370 – 374.

62. A.Y. Alentiev, V. P. Shantarovich, T. C. Merkel, V. I. Bondar, B. D. Freeman, Y.P. Yampolskii, Gas and vapor sorption, permeation, and diffusion in glassy amorphous Teflon AF1600, Macromolecules 35 (2002) 9513 – 9522.
63. A.W. Thornton, K.M. Nairn, A.J. Hill, J.M. Hill, New relation between diffusion and free volume: I. Predicting gas diffusion, J. Membr. Sci. 338 (2009) 29 – 37.
64. R.W. Baker, Membrane technology and applications, John Wiley & Sons, Chichester, 2nd ed., 2004.
65. W. Braker, A.L. Mossman, Matheson gas data book, Matheson, 6th ed., 1980.
66. C. Menke, Post-sales-support scientist, Accelrys, GmbH, Personal communication.
67. M. Fischer, Department of Chemistry, University College London, London, Personal communication.
68. M. Fischer, J.R.B. Gomes, M. Fröba, M. Jorge, Modeling adsorption in metal-organic frameworks with open metal sites: Propane/propylene separations, Langmuir 28 (2012) 8537 – 8549.
69. T.C. Merkel, V.I. Bondar, K. Nagai, B.D. Freeman, I. Pinnau, Gas sorption, diffusion and permeation in poly(dimethylsiloxane), J. Polym. Sci. Pol. Phys. 38 (2000) 415 – 434.

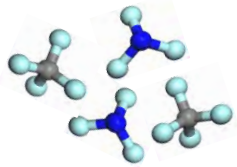

Chapter 5

Evaluation

5.1 Introduction

In this thesis the use of polymer membranes for the separation of nitrogen trifluoride (NF_3) and carbon tetrafluoride (CF_4) was investigated, which has remained unexplored to date. It is therefore of interest to determine whether membrane based gas separation of NF_3 and CF_4 might be a feasible alternative to the currently used processes of adsorption and distillation [1-4]. Therefore, as noted in Sec. 1.3, the aim was to evaluate the use of solution-cast membranes of Teflon AF2400, Teflon AF1600, and Hyflon AD60 for the membrane based gas separation of NF_3 and CF_4, where the main objectives were:

i. To provide experimental evidence of the permeability selectivity offered by these perfluoropolymer membranes towards NF_3 and CF_4,
ii. To provide a theoretical explanation for the observed permeability selectivity w.r.t. the solubility and diffusivity of the two gases in these perfluoropolymers, and
iii. To determine, at least semi-quantitatively, whether membrane gas separation using high free volume, glassy perfluoropolymers can, in principle, be used for the purification of NF_3 to meet the purity specifications w.r.t. CF_4.

Consequently, it will be illustrated in this chapter that the abovementioned objectives were successfully attained. However, to be able to study the polymer membrane based gas separation of NF_3 and CF_4, an experimental setup was used for which it was necessary to develop a convenient quantitative analysis system. Accordingly, it was shown that by implementing the newly developed gas chromatographic (GC) analysis system, the pure and mixed gas permeation of NF_3 and CF_4 could be studied using the custom built experimental setup. Consequently, solution-cast, high free volume glassy perfluoropolymers of Teflon AF 2400, Teflon AF1600 and Hyflon AD60 were studied that yielded appreciable NF_3/CF_4 pure and mixed gas selectivites ($\alpha(NF_3/CF_4)$) where it was found that the separation improved with decreasing fractional free volume (FFV) of the polymers. Although a relatively low NF_3 permeability of ca. 1.9 Barrer was obtained with Hyflon AD60, these membranes displayed

the highest NF_3/CF_4 pure and mixed gas selectivity ($\alpha(NF_3/CF_4) \approx 12$) of the three different perfluoropolymers that were studied.

Using atomistic Molecular Dynamics (MD) simulations it was shown that diffusion selectivity towards NF_3 was favoured by a lower FFV, as was indicated by the analysis of the experimental results. The results of the Grand Canonical Monte Carlo (GCMC) simulations and statistical thermodynamics calculations through the non-equilibrium lattice fluid (NELF) model also indicated that it is plausible that favourable solubility selectivity towards NF_3 supported the favourable NF_3/CF_4 diffusion selectivity. This combination of diffusion and solubility selectivity w.r.t. NF_3 therefore offered an explanation for the experimentally observed permeability selectivity. To further evaluate the success of the research and the applicability of polymer membrane gas separation for the purification of NF_3 from CF_4, each element of this thesis will be briefly discussed in the following sections. Subsequently, a semi-quantitative analysis of the efficiency of NF_3 purification using perfluoropolymer membranes of Hyflon AD60 and Teflon AD60 is presented to aid in the critical evaluation of the applicability of the separation technology investigated in this thesis.

5.2 Quantitative Gas Chromatographic Analysis Method

It was shown in Chapter 2 that the divinylbenzene-styrene co-polymer porous packing material Super Q could be efficiently implemented to offer a robust quantitative analytical method for the quantification of low and high concentrations of NF_3 and CF_4. Compared to the industrial analysis method designed by de Coning and Swinley [5], the use of a divinylbenzene-styrene co-polymer stationary phase, without coating the stationary phase with a fluorocarbon liquid, yielded sufficient resolution for the quantification of NF_3 and CF_4 in mixtures containing ppm amounts of both analytes, in which the concentrations differed by at least a factor of 10. In addition, the simplified GC method provided resolution and quantification of NF_3 and CF_4 mixtures within 8 min when the TCD channel was used for quantification of high concentrations, and within 4 min when the PDHID channel was used for the quantification of ppm-level concentrations. In addition, it was shown that absolute NF_3 and CF_4 amounts of between 10 – 500 nmol could be quantified on the TCD channel, while absolute amounts of between 0.01 – 2 nmol could be quantified on the PDHID channel. As a result, NF_3 and CF_4 concentrations of 1 mol% and upward on the TCD channel, and typically

between 40 – 4000 vppm on the PDHID channel could be conveniently quantified by using appropriate sample loop volumes.

The newly developed GC method could thus be used to measure the NF_3/CF_4 pure or mixed gas permeabilities of the lower-flux Teflon AF1600 and Hyflon AD60 membranes by using a He-sweep gas at the permeate side of the membranes. In addition to the versatility of the method in being able to quantify mixtures of NF_3 and CF_4 at both low and high concentrations, it was shown that adequate repeatability was also obtained, confirming the reliability of the method. Furthermore, the physical setup of the novel developed dual-channel GC method also allows the use of the stationary phases and column sequence reversal configuration of de Coning and Swinley [5] to enable quantification of even lower CF_4 concentrations in mixtures containing a predominant amount of NF_3. Consequently, it would also be possible to measure the permeability and efficiency of membranes being fed with an NF_3 feed with a low CF_4 concentration, when pilot scale studies are undertaken to further investigate the efficiency of membrane separation (or any other separation method) for the purification of NF_3 from CF_4.

5.3 Polymer Membrane Separation using Teflon AF and Hyflon AD60

The high free volume glassy perfluoropolymer membranes of Teflon AF2400, Teflon AF1600 and Hyflon AD60 were used to study the membrane based separation of NF_3 and CF_4 (Chapter 3). These materials were chosen based on the favourable permeability-selectivity trade-offs displayed by these polymers [6], and because it was postulated during the onset of this study that appreciably high permeabilities of the selectively permeable component will be required, while attaining optimum selectivity, to have a competitive alternative means of separating NF_3 and CF_4. Isotropic dense films of these polymers were manufactured by the solution casting method where it was shown, in accordance with literature [7, 8], that the films needed to be annealed at sufficiently high temperatures to obtain solvent-free non-swollen membranes. Thermal analysis of the annealed films was used to confirm the non-swollen character of the membranes. From the results it became apparent that the He and N_2 permeabilities and He/N_2 ideal selectivities corresponded well with the available literature data.

The pure gas permeabilities of NF_3 and CF_4 indicated that all the membranes used were selective towards NF_3. While all the glassy perfluoropolymers had a high FFV (32 % for Teflon AF2400, 28 % for Teflon AF1600, and 23 % for Hyflon AD60) compared to conventional low-permeability polymers, the NF_3 permeability displayed a sharp decrease with decreasing FFV, decreasing in the order Teflon AF2400 > Teflon AF1600 > Hyflon AD60. The decrease in NF_3 permeability with decreasing FFV of the perfluoropolymers was, however, accompanied by a more pronounced decrease in the CF_4 permeability and therefore an appreciable increase in the NF_3/CF_4 permeability selectivity. The NF_3 and CF_4 permeability and selectivity results of the Teflon AF2400, Teflon AF1600 and Hyflon AD60 membranes can be further summarised as follows:

- No significant increase in the pure gas permeability coefficients of NF_3 and CF_4 were observed with increasing trans-membrane pressure, Δp, suggesting that the non-swollen perfluoropolymers were inert towards penetrant induced swelling and plasticisation.
- Analysis of the activation energies of permeation, E_p, suggested that the activation energy of diffusion, E_D, was at a minimum for NF_3 and CF_4 with Teflon AF2400, which had the highest FFV. The observed increase in the E_p-values of both NF_3 and CF_4 with the decreasing FFV of Teflon AF1600 and Hyflon AD60 was therefore attributed to an increase in the E_D-values. Because the E_p-values of CF_4 were consistently higher for all the membranes used, it was concluded that the diffusivity of CF_4 was more strongly influenced by a change in the temperature compared to that of NF_3. Based on this analysis, the observed increase in the NF_3/CF_4 permeability selectivity with decreasing FFV was therefore attributed to an increase in the NF_3/CF_4 diffusion selectivity (D_{NF_3}/D_{CF_4}). This is in accordance with conventional wisdom, which dictates that the diffusion selectivity of glassy polymers increases with decreasing FFV, as also exemplified by the increasing He/N_2 permeability selectivity of the membranes in the order Teflon AF2400 < Teflon AF1600 < Hyflon AD60.
- The permeability and selectivity of the Hyflon AD60 membranes that was partially swollen with residual casting solvent showed a markedly reduced NF_3/CF_4 permeability selectivity and higher permeability values compared to the non-swollen Hyflon AD60 membranes. It was also shown that the CF_4 permeability of a swollen membrane increased significantly with increasing Δp, and based on the analysis by Merkel *et al.* [9] it was concluded that this was caused by an increased mobility of CF_4

due to the plasticisation of the polymer matrix by the residual casting solvent. It was therefore concluded that the increased mobility of both NF_3 and CF_4, which was more pronounced for CF_4, led to a reduced diffusion selectivity. However, based on the results obtained by Macchione *et al.* [8], it was postulated that the swollen Hyflon AD60 matrix also yielded reduced NF_3/CF_4 solubility selectivity (S_{NF_3}/S_{CF_4}) compared to the non-swollen membranes, and that favourable NF_3/CF_4 solubility selectivity supported the favourable NF_3/CF_4 diffusion selectivity to yield the observed permeability selectivities.

- The mixed gas NF_3 and CF_4 permeabilities and permeability selectivity, $\alpha(NF_3/CF_4)$, compared well with the pure gas permeabilities and selectivities except for Teflon AF2400, which displayed a mixed gas selectivity that was significantly lower than the pure gas, ideal selectivity. Although it is possible that the high free volume of Teflon AF2400 was less effective at discriminating between NF_3 and CF_4 with a mixed gas feed, this discrepancy might also have been due to experimental error. Nevertheless, the high correlation obtained between the pure and mixed gas selectivity and permeability values indicates that an appreciable degree of penetrant induced plasticisation w.r.t. NF_3 or CF_4 did not occur, as confirmed by practically constant pure gas permeabilities of NF_3 and CF_4 across the trans-membrane pressure range that was tested.
- The most selective membrane, Hyflon AD60, displayed a mixed gas selectivity, $\alpha(NF_3/CF_4)$, of ca. 12 which decreased slightly with decreasing CF_4 feed concentration. It was shown that this effect was caused by a small but noticeable increase in the permeability of NF_3 and CF_4 with decreasing CF_4 concentration (increasing NF_3 concentration). This indicates that NF_3 did have a slight but noticeable swelling effect on the polymer matrix. However, it also supports the notion that NF_3 is more selectively adsorbed by the perfluoropolymer matrices as corroborated by experimental evidence that shows NF_3 to be more readily adsorbed by organic and inorganic adsorbents [1-3, 10].

To summarise, it was therefore shown in this study that high NF_3/CF_4 selectivity could be obtained by using a perfluoropolymer membrane in the form of Hyflon AD60 that had a relatively high FFV of 23 %, albeit with a low NF_3 permeability of ca. 1.9 Barrer. It is apparent that higher NF_3/CF_4 permeability selectivities could be obtained using glassy

polymer membranes with even lower FFVs, although this will likely result in a further decrease in the NF_3 permeability.

5.4 Modeling of NF_3 and CF_4 Diffusivity and Solubility in Teflon AF

In Chapter 4 the gas transport of NF_3 and CF_4 in Teflon AF2400 and Teflon AF1600 was studied using atomistic molecular modeling and statistical thermodynamics simulations to determine the influence of diffusion and solubility selectivity on the experimentally observed permeability selectivities. Extensively equilibrated atomistic packing models of Teflon AF2400 and Teflon AF1600 were shown to adequately predict the FFV and density of both polymers, and were also used to calculate the sorption isotherms and diffusivities of He and N_2 in the two polymers as a second validation test. The results of the MD and GCMC simulations showed good correlation between the calculated and experimental transport data, where a better He/N_2 diffusion selectivity, and N_2/He solubility selectivity was correctly predicted for the lower FFV Teflon AF1600.

The simulation results obtained w.r.t. the diffusivity and solubility of NF_3 and CF_4 in Teflon AF2400 and Teflon AF1600 using the validated packing models can be summarised as follows:

- The MD simulation results confirmed the hypothesis made in Chapter 3 that the NF_3/CF_4 diffusion selectivity (D_{NF_3}/D_{CF_4}) was the major driving force behind the observed permeability selectivity of the glassy perfluoropolymer membranes. The calculated CF_4 diffusivities were, however, overestimated in comparison with experimental literature data.
- The calculated diffusion selectivity, (D_{NF_3}/D_{CF_4}), of Teflon AF1600 was 67 % higher than that predicted for Teflon AF2400, while the FFV of Teflon AF1600 is only 4 % lower compared to that of Teflon AF2400. The notion of Chapter 3 that diffusion selectivity increased with decreasing FFV of the glassy perfluoropolymer membranes that were studied experimentally, was therefore confirmed.
- The predicted diffusion selectivity is significant in light of the relatively small difference in the molecular weights of NF_3 and CF_4. For example, using a microporous membrane that affords the separation of two gases that differ in size and molecular weight based on the principle of Knudsen diffusion [11], the ideal Knudsen

selectivity w.r.t. NF_3 and CF_4, $\alpha(NF_3/CF_4)_{ideal}$, predicted by Eq. (4.27) equates to 1.11. This value is considerably lower than the diffusion selectivity predicted for Teflon AF2400 and Teflon AF1600 from the MD simulation results. Thus, it was proposed that the considerably higher diffusion selectivity, D_{NF_3}/D_{CF_4}, predicted for the dense perfluoropolymers could be due to the difference in the molecular geometry of NF_3 and CF_4, as NF_3 has a pyramidal geometry and CF_4 has a tetrahedral geometry. It was therefore postulated that the passages formed between adjacent free volume elements in the polymer matrices as a result of elastic thermal motions of the polymer chains might be geometrically more accessible to the pyramidal NF_3 molecules, which could give rise to differences in the diffusion coefficients. If this hypothesis is assumed to be true, the diffusion selectivity, D_{NF_3}/D_{CF_4}, would therefore be enhanced by a lower FFV, also explaining the high NF_3/CF_4 permeability selectivity observed for the Hyflon AD60 membranes (Chapter 3).

- The GCMC sorption isotherm results indicated that the concentration of CF_4 in Teflon AF2400 and Teflon AF1600 was significantly overestimated at low to moderate pressures in comparison with the experimental literature data. As the sorption isotherms of He and N_2 was reasonably accurately reproduced by the GCMC simulations with the same atomistic packing models, it was concluded that this discrepancy was probably not caused by inaccurate free volume distributions. Rather, it is suspected that the forcefield used inadequately estimated the fluid-solid interactions, which could not be improved upon by using other forcefields. It is also unknown how the free volume distribution varies during uptake of sorbent molecules, which cannot be taken into account with the GCMC simulation method, which may be another contributing factor to the observed deviation between the calculated and experimentally determined sorption isotherms. Nonetheless, the GCMC simulations predicted that NF_3 has a generally higher solubility in Teflon AF2400 than in Teflon AF1600.
- Due to the observed discrepancies as mentioned above, the suitability of the NELF model to predict the sorption isotherms of NF_3 and CF_4 in Teflon AF2400 and Teflon AF1600 was investigated. After citing the documented, unique chemical reactivity of NF_3 towards a range of different chemical species, and considering the higher activity of NF_3 that is frequently observed in porous inorganic and polymeric adsorbents, and halogenated fluids, the NELF model interaction parameter, Ψ, was set to a value of 1.2

for NF_3, while using $\Psi = 1.0$ for CF_4. In accordance with the NELF model calculation results of De Angelis *et al.* [12], the CF_4 sorption isotherms in Teflon AF2400 and Teflon AF1600 were adequately reproduced. Consequently, an appreciable NF_3/CF_4 solubility selectivity (S_{NF_3}/S_{CF_4}) was predicted for both Teflon AF2400 and Teflon AF1600, while being slightly higher for the lower FFV Teflon AF1600 variant as hypothesised in Chapter 3.

- The predicted NF_3/CF_4 permeability selectivity, $\alpha(NF_3/CF_4)_{calc}$, calculated according to Eq. (4.28) using the diffusion selectivity values calculated from the MD results and the solubility selectivity results calculated using the NELF model, compared well with the experimentally determined ideal selectivities. Thus, the simulation results were successful in providing a theoretical description of the experimentally observed permeability selectivities.
- The permeability selectivity predicted using Eq. (4.28) also followed the experimental trend w.r.t. to the FFV of Teflon AF2400 and Teflon AF1600 and gave supporting evidence that the favourable diffusion and solubility selectivity towards NF_3 was responsible for the experimentally obtained permeability selectivity.
- Based on the modelled permeability selectivities of Teflon AF2400 and Teflon AF1600, it is therefore apparent that NF_3 most likely undergoes unique chemical interactions with the polymer matrices, as literature evidence suggests it does, thus having a higher solubility compared to CF_4 in the polymer membranes. While this deduction needs experimental confirmation, it might serve useful when tailoring polymeric membranes to selectively increase the NF_3 permeability.

5.5 Semi-quantitative Process Evaluation

In this section, the efficiency and applicability of NF_3 and CF_4 separation using perfluoropolymer membranes of Teflon AF and Hyflon AD60 will be critically evaluated by discussing two different proposed configurations from a process design perspective. For this purpose, the theoretical design considerations as presented by Baker [11], modified for the special case of NF_3 and CF_4 separation, were used. In the following section, these design considerations will be discussed, which is subsequently applied to two proposed configurations, from which final conclusions will be drawn.

5.5.1 Theoretical Design Considerations

Since NF_3 preferentially permeates through the glassy perfluoropolymer membranes, it will be possible to obtain a permeate stream that is depleted of CF_4 to meet the purity specification of 20 ppm CF_4 or less in a single processing stage, considering the mixed gas selectivity ($\alpha(NF_3/CF_4) \approx 12$) obtained with Hyflon AD60 (Chapter 3). However, the resulting retentate stream from a single membrane module (Fig. 5.1) will be depleted in NF_3 and enriched in CF_4, and cannot be recycled to the feed side of the membrane as this will systematically increase the CF_4 concentration in the feed stream.

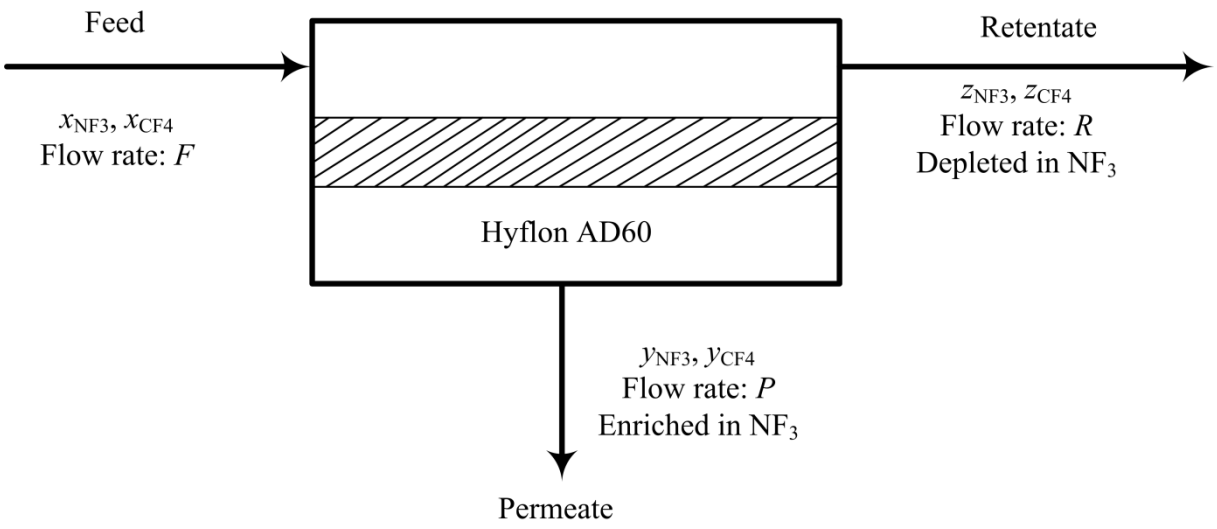

Figure 5.1: Schematic representation of a single-stage membrane gas separation process for separation of NF_3 and CF_4 using Hyflon AD60.

In addition, as NF_3 and CF_4 cannot be readily separated by distillation and condensation, the waste fraction (retentate stream) is not easily recoverable. Therefore, the stage-cut, θ, defined as the ratio of the permeate flow rate to the feed flow rate (Eq. (5.1)) [11] should be maximised to ensure that a minimal amount of NF_3 is lost as waste.

$$\theta = \frac{\text{Permeate Flow Rate}}{\text{Feed Flow Rate}} \tag{5.1}$$

In addition to the stage-cut the membrane selectivity, α, and the pressure ratio also influence the overall performance of a membrane gas separation process, in which the pressure ratio, φ, is defined as:

$$\varphi = \frac{p_f}{p_p} \tag{5.2}$$

where p_f is the feed pressure, and p_p is the retentate pressure. For the example shown in Fig. (5.1) where the feed mixture consists of NF_3 and CF_4 with volume fractions x_{NF3} and x_{CF4}, fed at a feed pressure of p_f, a flux of NF_3 across the membrane can only be achieved if the partial pressure of NF_3 on the feed side is larger than that on the permeate side of the membrane:

$$x_{NF_3} p_f > y_{NF_3} p_p \tag{5.3}$$

where y_{NF3} is the enriched concentration of NF_3 in the permeate stream. Thus, the maximum amount of enrichment that can be achieved cannot exceed the pressure ratio, irrespective of the membrane selectivity, α:

$$\frac{y_{NF_3}}{x_{NF_3}} \leq \frac{p_f}{p_p} \tag{5.4}$$

A relationship between the pressure ratio and the membrane selectivity may be derived from the expression of the fluxes of both components according to Fick's law:

$$J_i = \frac{P_i \left(p_{i,f} - p_{i,p} \right)}{\delta} \tag{5.5}$$

where J_i is the flux of component i (NF_3 or CF_4) in $cm^3(STP)/(cm^2.s)$, P_i is the permeability of component i in $cm^3(STP).cm/(cm^2.cmHg.s)$, $p_{i,f}$ and $p_{i,p}$ are the partial pressures of component i in the feed and permeate stream in cmHg respectively, and δ is the membrane thickness in cm. The total gas pressure on the feed and permeate sides are then given by the sum of the partial pressures:

$$p_f = p_{NF_3,f} + p_{CF_4,f} \tag{5.6}$$

$$p_p = p_{NF_3,p} + p_{CF_4,p} \tag{5.7}$$

Since the volume fractions of the components on the feed and permeate side are related to the partial pressures according to:

$$x_i = \frac{p_{i,f}}{p_f} \tag{5.8}$$

$$y_i = \frac{p_{i,p}}{p_p} \tag{5.9}$$

it then follows from mass balance considerations that:

$$\frac{J_{NF_3}}{J_{CF_4}} = \frac{y_{NF_3}}{y_{CF_4}} = \frac{y_{NF_3}}{1-y_{NF_3}} = \frac{1-y_{CF_4}}{y_{CF_4}} \tag{5.10}$$

By combining equations (5.6) – (5.10), Baker [11] showed that the following expression is obtained that gives the concentration of component *i* (in this case NF_3) on the permeate side of the membrane (y_{NF3}) as a function of the feed concentration (x_{NF3}), the pressure ratio (φ), and the membrane selectivity(α):

$$y_{NF_3} = \frac{\varphi}{2}\left[x_{NF_3} + \frac{1}{\varphi} + \frac{1}{\alpha - 1} - \sqrt{\left(x_{NF_3} + \frac{1}{\varphi} + \frac{1}{\alpha - 1} \right)^2 - \frac{4\alpha x_{NF_3}}{(\alpha - 1)\varphi}} \right] \tag{5.11}$$

Baker [11] has also shown that Eq. (5.11) can be simplified to represent two limiting cases where:

i. The membrane selectivity is significantly larger than the pressure ratio and the so-called pressure ratio limited region is entered where the membrane performance is limited by the pressure ratio and is independent of the membrane selectivity;
ii. The membrane selectivity is significantly smaller than the pressure ratio and the so-called selectivity limited region is entered where the membrane performance is limited by the membrane selectivity and is independent of the pressure ratio.

However, when the value of the membrane selectivity is comparable to the pressure ratio, the performance of the membrane is described by Eq. (5.11). Furthermore, from elementary mass balance considerations the following expression holds w.r.t. NF_3:

$$x_{NF_3}\dot{V}_f = y_{NF_3}\dot{V}_p + z_{NF_3}\dot{V}_r \tag{5.12}$$

where $\dot{V}_f$, $\dot{V}_p$ and $\dot{V}_r$ are the total volumetric flow rates of the respective feed, permeate and retentate streams in appropriate units, and z_{NF_3} is the volume fraction of NF_3 in the retentate (residue) stream. Using Eq. (5.12), the concentration of NF_3 in the retentate stream can be calculated, from which the CF_4 concentration follows from simple mass balance conditions.

5.5.2 Proposed Configurations for Enrichment of NF_3 by Membrane Separation

As noted above, a membrane module using Hyflon AD60 as the separating medium will need to be operated at a maximum stage-cut (θ) to obtain optimum recovery of the enriched NF_3. This cannot normally be achieved as there is also a trade-off between the stage-cut and the maximum enrichment that can be achieved [11] as will be discussed later in this section. In addition, since Hyflon AD60 displayed a relatively low mixed-gas NF_3 permeability (1.9 Barrer) a high stage-cut of for example 99% would require an inordinately large membrane area. It is therefore proposed that at least two membrane modules should be used, in which Hyflon AD60, with an experimentally obtained mixed-gas selectivity of ca. 12 (Chapter 3), is used to obtain the necessary purity, while Teflon AF1600, which possesses a higher NF_3 permeability and an experimentally obtained mixed-gas selectivity of ca. 6 (Chapter 3), is used to minimize the amount of NF_3 that is lost as waste. Based on this, two configurations are proposed as illustrated in Fig. 5.2 and Fig. 5.3.

Configuration 1: Two-step Membrane Separation Process

For both the proposed configurations (Fig. 5.2 and Fig. 5.3) a total feed flow rate of 1000 L(STP)/h was used as basis for the theoretical calculations, and a CF_4 feed concentration of 250 vppm, as is typical of LESA-grade NF_3, was assumed. In all cases, a uniform membrane thickness of 5 μm was assumed, and a conservative pressure ratio, φ, of 10 was chosen as it is also desirable to minimize the operating costs w.r.t. the energy consumption of the compressors that form part of each membrane unit operation. A pressure ratio of φ = 10

implies that the feed pressure is 10-fold higher than the pressure of the permeate stream (for example p_f = 10 bar and p_p = 1 bar).

In the proposed two-step membrane separation process of Configuration 1 (Fig. 5.2), the use of Hyflon AD60 would yield a permeate stream that is sufficiently enriched with NF_3 (containing only 23 vppm CF_4) in a single processing stage according to Eq. (5.11). Considering the operating conditions summarised in Table 5.1, the first membrane module would still need to operate at a high stage-cut of 83.2 %, and it should be noted that Eq. (5.11) does not account for the influence of the stage-cut on membrane performance. The theoretically calculated CF_4 permeate concentration of 23 vppm therefore represents the maximum NF_3 enrichment that can be achieved with a Hyflon AD60 membrane with a selectivity of α = 12, and a pressure ratio of 10.

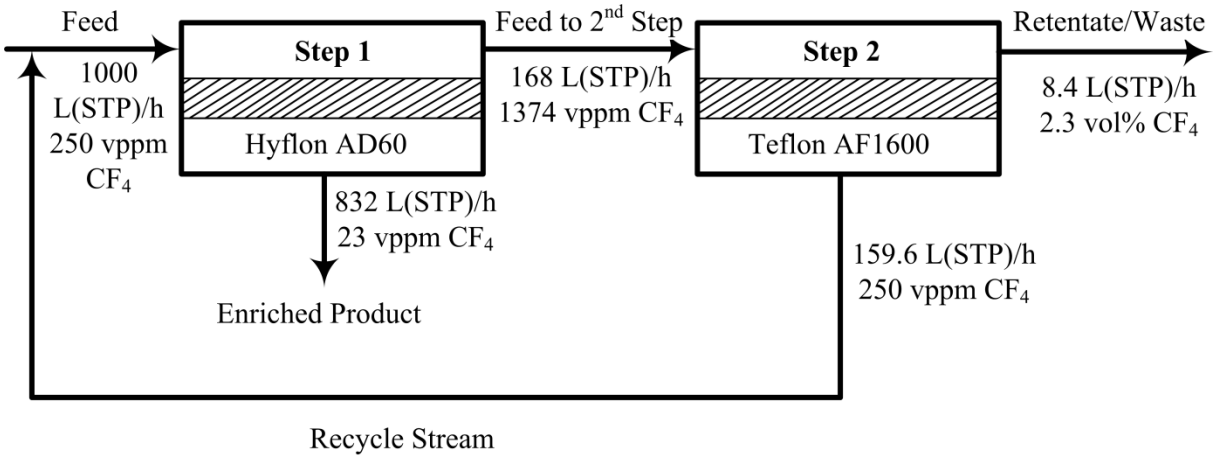

Figure 5.2: Proposed two-step process for the enrichment of NF_3 using a Hyflon AD60 membrane module with a second Teflon AF1600 membrane module for recovery of NF_3 from the retentate stream of the first step. Operating parameters are summarized in Table 5.1.

By using Eq. (5.11) it is therefore assumed that the stage-cut, φ, does not influence the amount of enrichment, or in other words, the enrichment calculated through Eq. (5.11) is the maximum that can be achieved at zero stage-cut. In reality, however, the concentration of the selectively permeable component (in this case NF_3) in the permeate stream diminishes as the stage-cut is increased, although the retentate stream becomes increasingly depleted of the more selectively permeable component [11]. In comparison, for the perfluoroethane (C_2F_6) recovery process of Wijmans *et al.* [13], in which C_2F_6 is recovered from an N_2 diluent stream

using Hyflon AD60 or ethyl cellulose membranes, the membrane modules also had to be operated at high stage-cuts (90% and higher) to essentially strip the feed stream of N_2. Consequently, they showed that the Hyflon AD60 membrane selectivity diminishes significantly at a stage-cut of 80 % and higher. Because of the low CF_4 feed concentration (250 vppm), the effect might be slightly less pronounced in the present case, where the results of Chapter 3 indicated that the mixed gas selectivity increased slightly with increasing CF_4 concentration (Fig. 3.9). Nevertheless, the effect of stage-cut on membrane performance will need to be determined empirically, and the results of the theoretical calculations (Eq. (5.11)) presented here therefore only give an indication as to the maximum attainable NF_3 enrichment under ideal conditions.

Table 5.1: Summary of the ideal operating parameters for the enrichment and recovery of NF_3 contaminated with 250 vppm CF_4 using two different membrane separation configurations involving Hyflon AD60 and Teflon AF1600.

Parameter	**Configuration**			
	Two-Step		**Two-Stage**	
	1st Step	**2nd Step**	**1st Stage**	**2nd Stage**
$\alpha(NF_3/CF_4)$	12	6	6	12
Pressure ratio (φ)	10	10	10	10
% Stage-cut (θ)	83.2	95	99	83.2
Membrane Area (m^2)*	94.6	1.1	6.5	93.6
CF_4 Permeate Concentration (vppm)	23	250	45	4
CF_4 Retentate Concentration (vol%)	0.14	2.3	2.1	0.025
Total % loss of NF_3	0.8		0.98	

* Calculated on the basis of a feed flow rate to the first membrane step/stage of 1000 L(STP)/h.

By treating the CF_4-enriched retentate stream (Fig. 5.2) with a second membrane module using a higher-flux Teflon AF1600 membrane, a small waste stream can theoretically be produced that is sufficiently depleted of NF_3 so that the total loss of NF_3 equals only 0.8%. Since the NF_3 concentration in the retentate stream of each process step was calculated using Eq. (5.12), the stage-cut of the Hyflon AD60 membrane module was adjusted so that the feed to the Teflon AF1600 module could be converted to a permeate stream containing 250 vppm CF_4 at a stage-cut of 95 %, which can be recycled to the feed to the first membrane step without any adverse effects. Again, the real CF_4 concentration in the recycle stream will also

be influenced by the stage-cut, and the results presented in Fig, 5.2 and Table 5.1 only represent an ideal scenario. With the proposed stage-cuts shown in Table 5.1, a Hyflon AD60 membrane area of 94.6 m^2 will be required on the basis of a feed stream of 1000 L(STP)/h, while a Teflon AF1600 area of 1.1 m^2 will be required. The effect of the low NF_3 permeability (ca. 1.9 Barrer) offered by Hyflon AD60 on the required membrane area is therefore apparent, and is one potential disadvantage in spite of the perfluoropolymer membrane officering a substantial selectivity of $\alpha(NF_3/CF_4) = 12$.

Configuration 2: Two-stage Membrane Separation Process

To obtain a higher NF_3 purity, the use of a Teflon AF1600 membrane module to provide partial NF_3 enrichment, which is then further processed in a second membrane stage with a Hyflon AD60 membrane might be useful as illustrated in Fig. 5.3. For this two-stage configuration, a stage-cut of 99% is required yielding a small enough retentate stream so that the total % loss w.r.t. NF_3 is only 0.98%. Under ideal conditions, i.e. if the the stage-cut does not influence the permeate composition, the permeate stream from the Teflon AF1600 membrane module contains 45 vppm, which is then further processed in a second membrane stage using the more selective Hyflon AD60 membrane. According to the calculations, this configuration would produce a highly enriched NF_3 product stream containing only 4 vppm CF_4, albeit under assumed ideal conditions. By adjusting the stage-cut of the Hyflon AD60 module to 83.2 % (as a simplification it is assumed that the stage-cute does not influence the permeate stream composition), the CF_4 concentration of the retentate stream calculated by Eq. (5.12) equals 250 vppm and can then be conveniently recycled to the feed of the first stage for reprocessing.

For this design a relatively small Teflon AF1600 membrane area of 6.5 m^2 would be required, which however is still larger than the membrane area required for the two-step configuration as a consequence of the higher stage-cut (99%) and the larger feed flow rate compared to that of the Teflon AF1600 module of the two-step design of Fig. 5.2. Similar to the 1st step of Configuration 1, the 2nd stage of Configuration 2 would require a significantly larger Hyflon AD60 membrane area to be able to remove the significant amount of NF_3 from the permeate stream of the first stage. Furthermore, it should be kept in mind that in this two-stage design configuration, an additional compressor would be required to recompress the feed stream to the second membrane stage to maintain the desired pressure ratio of $\varphi = 10$. For the two-step

process, a single compressor, however requiring a greater capacity, would be needed as the two membrane modules are operated in series.

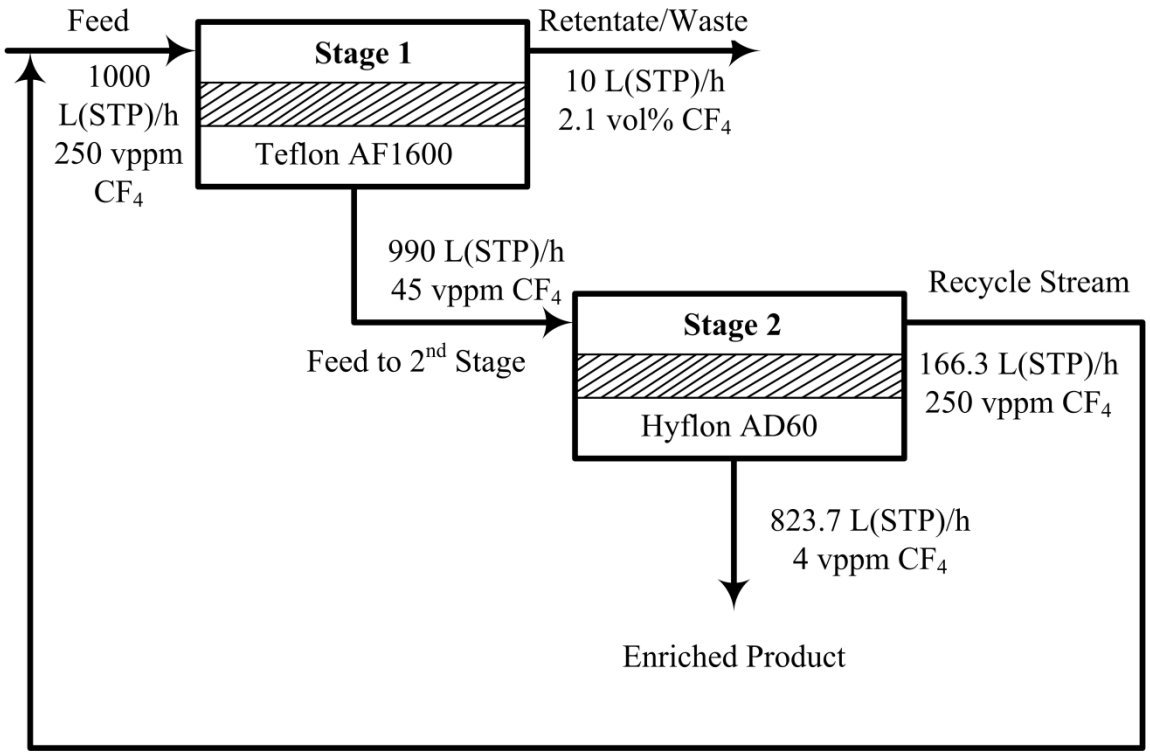

Figure 5.3: Proposed two-stage process for the enrichment of NF_3 using a Teflon AF1600 membrane module with a second Hyflon AD60 membrane module for recovery and enrichment of NF_3. Operating parameters are summarized in Table 5.1.

5.5.3 Qualitative Technological Evaluation

Considering the two proposed configurations for enrichment of NF_3 (Fig. 5.2, Fig. 5.3, and Table 5.1), the following conclusions may be drawn:

- Under ideal conditions, sufficient enrichment of NF_3 is achievable;
- Using Teflon AF1600 in conjunction with Hyflon AD60 in either a two-step or two-stage design, it is also possible, under ideal conditions, to limit the amount of NF_3 that is lost to waste;
- It could be worthwhile to attempt to recover the NF_3 from the NF_3-depleted waste streams through adsorption processes, where a relatively small adsorbent volume would be required since the volumetric flow rate of the waste streams are quite small;

- Although ideal conditions were assumed for the theoretical calculations (stage-cut does not influence the composition of the individual permeate streams), the membrane separation will be energy efficient, especially when compared to distillation processes;
- The theoretical calculations showed that a selectivity of $\alpha(NF_3/CF_4) > 10$ is sufficient to obtain adequate NF_3 enrichment, therefore
- An increase in the NF_3 membrane permeability, while maintaining a selectivity of $\alpha(NF_3/CF_4) > 10$ would be beneficial in achieving efficient NF_3 enrichment through membrane separation.

In addition to the conclusion listed above, it should also be kept in mind that:

- The influence of the stage-cut on the separation efficiency will have to be determined empirically before a more complete assessment of the applicability of the technology can be made;
- It is frequently observed that large-scale membrane modules are less selective compared to their laboratory-scale counterparts because of micro-defects [13]. Such defects would however be detrimental since the membrane selectivity is crucial to obtain the desired enrichment;
- A relatively high Hyflon AD60 membrane area will be required, because of the low NF_3 permeability offered by this perfluoropolymer membrane.

One possible solution to the relatively large Hyflon AD60 membrane area that would be required on the basis of a feed stream of 1000 L(STP)/h, is to use a hollow fibre membrane module with each of the porous fibres coated with Hyflon AD60 as has already been demonstrated by Jansen *et al.* [14]. This will permit a high Hyflon AD60 membrane surface area in a module with a relatively small foot-print, and can also be conveniently applied to any other selective polymer that might be identified in the future. Since the hollow fibres would have to be coated with a polymer solution using a dip-coating procedure [14], the resulting composite membranes would have to be annealed at high temperatures as shown in Chapter 3. This implies that the membrane support would have to be able to withstand the annealing temperatures to ensure that defect free composite hollow fibre gas separation membranes can be achieved in this way. Irrespective of the module design however, further studies directed towards improving the NF_3 permeability while maintaining a selectivity of $\alpha(NF_3/CF_4) > 10$ will ultimately determine the applicability of membrane gas separation to the

purification of NF_3 from CF_4 as discussed further in the following section. This is however a central theme within the field of polymer membrane gas separation technology, and unfortunately the implementation of this energy efficient technology is often hindered by the trade-off between the permeability and selectivity.

5.6 Conclusions and Recommendations

It was demonstrated that the purification of NF_3 from CF_4 as contaminant is, in principle, possible using a sufficiently selective polymer membrane, where it was shown that NF_3 selectively permeated through the perfluoropolymer membranes manufactured during this study. The selectivity observed towards NF_3 was further investigated using molecular simulation and statistical thermodynamics techniques. These results indicated that NF_3 has a higher diffusivity and solubility in the glassy perfluoropolymer membranes than CF_4. Since the favourable S_{NF_3}/S_{CF_4} solubility selectivity predictions were supported by empirical evidence that frequently shows NF_3 to be more selectively adsorbed by a range of adsorbents, it is anticipated that the solubility selectivity predictions gave a fair representation of what could be expected experimentally. Coupled with the favourable D_{NF_3}/D_{CF_4} diffusion selectivity that was predicted to increase with decreasing FFV, in accordance with the usual trend observed for glassy polymers, it would therefore be advisable to study the transport properties of NF_3 and CF_4 in different polymers using experimental techniques to identify a means of further optimising the NF_3 permeability and NF_3/CF_4 selectivity. Nonetheless, with regard to the mathematical description of the experimentally determined permeability selectivity in terms of the calculated solubility and diffusion selectivities, the first two objectives of this thesis (Sec. 1.3 and Sec. 5.1) were therefore successfully achieved.

Although it is desirable from a process design perspective to selectively remove CF_4 (the contaminant) from the NF_3 matrix during purification, the theoretical solubility and diffusivity predictions, and the experimentally determined permeability results suggested that this will not be possible through a membrane separation process. Nonetheless, by considering the two membrane separation configurations proposed in the previous section, it is however apparent that appreciable enrichment of NF_3 is possible, such that NF_3 containing CF_4 with a concentration of only 23 ppm or lower can be obtained under ideal conditions. Thus, the third objective of this thesis (Sec. 1.3 and Sec. 5.1) was also successfully assessed. In addition, the theoretical design calculation results presented in the previous section suggest that an

improvement of the NF_3 permeability by at least an order of magnitude, while maintaining a selectivity of $\alpha(NF_3/CF_4) > 10$ could lead to the development of a feasible alternative NF_3 purification technology.

Although the aim and the objectives of this thesis were therefore addressed, a few recommendations may be made for further studies regarding membrane gas separation of NF_3 and CF_4. As NF_3 was predicted to be selectively more soluble in glassy perfluoropolymer membranes than CF_4, this aspect should receive further attention to selectively increase the NF_3/CF_4 solubility selectivity (S_{NF_3}/S_{CF_4}), while maintaining sufficient diffusion selectivity (D_{NF_3}/D_{CF_4}), which would result in an increased NF_3 permeability. Since significant evidence exists that hints at the existence of unique chemical interactions between NF_3 and a range of different chemical species, it is advisable to investigate the incorporation of such NF_3-phyllic species in diffusion-selective glassy polymers to maximize both the NF_3 permeability and NF_3/CF_4 permeability selectivity. In this regard, the use of mixed matrix membranes (MMMs) that consist of diffusion-selective glassy polymers with appropriate filler materials could also be further investigated. Although NF_3-phylic adsorbents may be of potential use as filler materials in this regard, the use of organo-metallic transition-metal complexes in which the metallic center is sufficiently electrophilic to form weakly-bonded NF_3-complexes, which was shown to occur with ambidentate electron donor/acceptor systems such as HF and HCN [15], should also be considered. Such organo-metallic complexes can be easily incorporated into polymer matrices, whereby the frequent challenges associated with solid filler particles would be avoided.

When studying the sorption selectivity of different polymer and adsorbent materials to improve the NF_3/CF_4 solubility selectivity as noted above, molecular simulation tools such as Grand Canonical Monte Carlo (GCMC) simulations would be useful. However, as shown in Chapter 4, it will be necessary to improve the forcefield parameters to reliably screen different materials for optimum NF_3/CF_4 sorption selectivity. As such, more accurate forcefield parameters can be found by combining ab initio Density-Functional Theory (DFT) calculation results with experimentally determined data. This can be undertaken as an isolated study, and mainly for this reason was considered to be beyond the scope of this thesis. Nevertheless, an improvement of the forcefield parameters would not only be beneficial to studying NF_3 and CF_4 sorption behaviour, but could also contribute to a more accurate description of fluorine-

containing systems in general, which is less rigorously parameterised in comparison with classical hydrocarbon systems. Irrespective of the method used to study the sorption characteristics of different materials towards NF_3 and CF_4, i.e. experimentally or theoretically using molecular modeling tools, the knowledge gained from such studies could also contribute to a better understanding of adsorptive separation methods currently being used for the purification of NF_3 from CF_4. As a result, the efficiency of adsorption methods might also be improved using novel, more selective materials that display a specific chemical affinity towards NF_3.

It remains to be confirmed whether membrane gas separation can be efficiently used for the enrichment of NF_3, which will greatly depend on whether the current permeability-selectivity trade-off of $\alpha(NF_3/CF_4) = 12$ at $P = 1.9$ Barrer for Hyflon AD60 can be improved. Nonetheless, it would be advisable to at least consider whether the use of polymer membranes could be useful as part of other separation and purification processes, where the amount of enrichment or the recovery of NF_3 from membrane modules are less crucial. One area where membranes might be applicable in this regard is, for example, in recovering NF_3 from CF_4-enriched waste streams originating from adsorption or distillation processes. Such waste streams would typically have a relatively low volumetric flow rate, and would therefore require a much smaller membrane area to achieve a given processing target.

5.7 References

1. Y.-C. Park, W.-S. Jeong, K.-C. Hyun, J.-W. Lee, I.-H. Kwon, Process for refining nitrogen trifluoride gas using alkali earth metal exchanged and impregnated zeolite, U.S. Pat. 7,637,986 B2 (2009).
2. S.M. Igumnov, V.P. Kharitonov, N.V. Kharitonova, Method of purifying gaseous nitrogen trifluoride, U.S. Pat. 7,022,160 B2 (2006).
3. T. Suenaga, T. Fujii, Y. Kobayashi, Method of refining nitrogen trifluoride gas, U.S. Pat. 5,069,887 (1991).
4. R.N. Miller, C.-P.C. Kao, B.A. Mahler, Process for purifying perfluorinated products, U.S. Pat. 6,458,249 B2 (2002).
5. J.P. de Coning, J.M. Swinley, Optimisation of a gas chromatographic method for trace gaseous impurities in nitrogen trifluoride by column sequence reversal, J. Chromatogr. A 1180 (2008) 151 – 158.

6. L.M. Robeson, The upper bound revisited, J. Membr. Sci. 320 (2008) 390 – 400.
7. J.C. Jansen, M. Macchione, E. Drioli, On the unusual solvent retention and the effect on the gas transport in perfluorinated Hyflon AD® membranes, J. Membr. Sci. 287 (2007) 132 – 137.
8. M. Macchione, J.C. Jansen, G. de Luca, E. Tocci, M. Longeri, E. Drioli, Experimental analysis and simulation of the gas transport in dense Hyflon® AD60X membranes: Influence of residual solvent, Polymer 48 (2007) 2619 – 2635.
9. T. C. Merkel, V. Bondar, K. Nagai, B. D. Freeman, Y.P. Yampolskii, Gas sorption, diffusion, and permeation in poly(2,2-bis(trifluoromethyl)-4,5-difluoro-1,3-dioxole-*co*-tetrafluoroethylene), Macromolecules 32 (1999) 8427 – 8440.
10. D.A. Mukhortov, I.A. Blinov, E.S. Kurapova, P.S. Kambur, Solubility of nitrogen trifluoried and tetrafluoromethane in perfluorinated and highly halogenated fluids, Russ. J. Appl. Chem. 83 (2010) 31 – 35.
11. R.W. Baker, Membrane technology and applications, John Wiley & Sons, Chichester, 2nd ed., 2004.
12. M.G. De Angelis, T.C. Merkel, V.I. Bondar, B.D. Freeman, F. Doghieri, G.C. Sarti, Gas sorption and dilation in poly(2,2-bistrifluoromethyl-4,5-difluoro-1,3-dioxole-*co*-tetrafluoroethylene): Comparison of experimental data with predictions of the Nonequilibrium Lattice Fluid Model, Macromolecules 35 (2002) 1276 – 1288.
13. J.G. Wijmans, Z. He, T.T. Su, R.W. Baker, I. Pinnau, Recovery of perfluoroethane from chemical vapor deposition operations in the semiconductor industry. Separ. Purif. Technol. 35 (2004) 203 – 213.
14. J.C. Jansen, F. Taselli, E. Tocci, E. Drioli, High-flux composite perfluorinated gas separation membranes of Hyflon® AD on a hollow fibre ultrafiltration membrane support, Desalination, 192 (2006) 207 – 213.
15. F. Blanco, I. Alkorta, I. Rozas, M. Solimannejad, J. Elguero, A theoretical study of the interactions of NF_3 with neutral ambidentate electron donor and acceptor molecules, Phys. Chem. Chem. Phys. 13 (2011) 674 – 683.

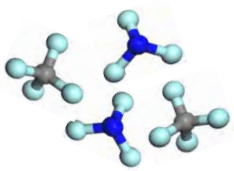

Appendix A

Operating Procedure for the Correct Operation of the NF_3/CF_4 Experimental Membrane Separation Setup

A.1 Introduction

Because of the risks involved in working with NF_3 [1], the experimental setup shown in Fig. A.1 has been designed with a fail-safe interlock system to control potential temperature and pressure hazards, in the event of undesirably high temperature and pressure being reached inside the membrane cell. Also, an NF_3 monitor was used as additional interlock to reduce the risk of accidental exposure to NF_3. However, to reduce potential hazards relating to high flow velocities and sudden pressure increases in NF_3 flow lines [1], it is paramount that the correct operating procedure be followed. Also contained within this operating procedure is the method to be followed when resetting the interlock system, if activated. In the following sections, the relevant piping and instrumentation diagrams, and wiring diagram for the interlock system is given, and the appropriate operating procedures are described in Sec. A.3 to Sec. A.8. In addition, maintenance considerations and safety procedures are given in Sec. A.9 and Sec. A.10.

A.2 Piping and Instrumentation Diagrams

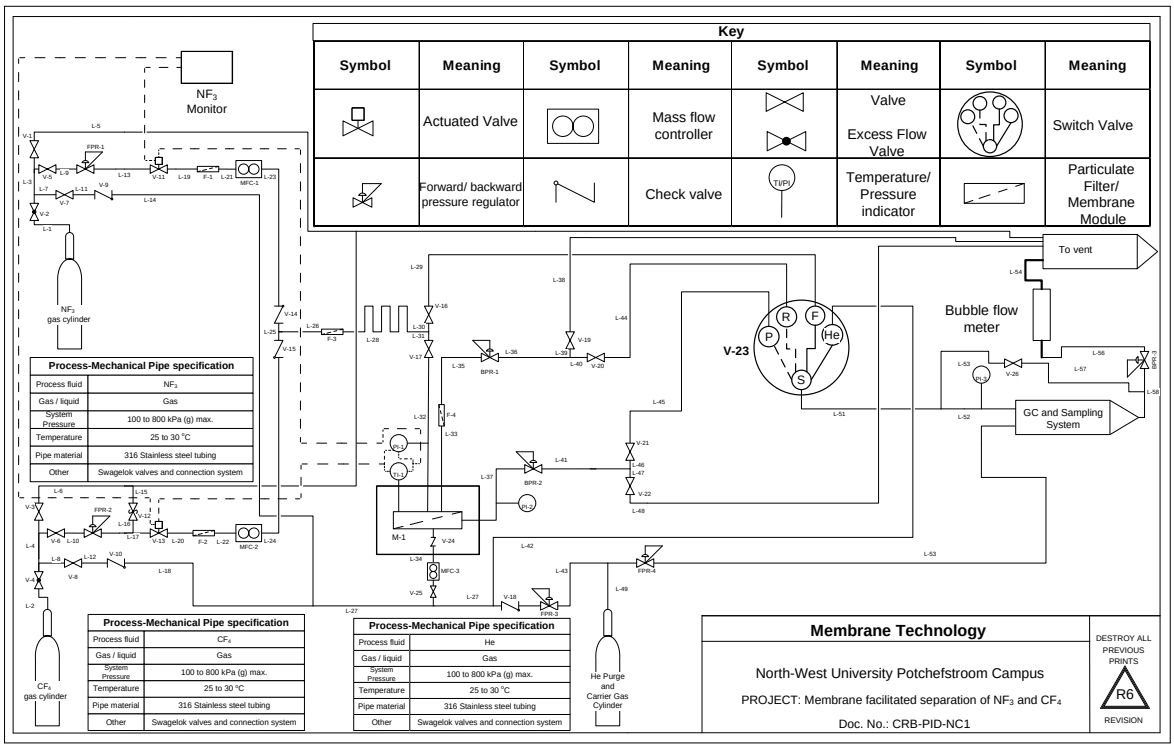

Figure A.1: Piping and instrumentation diagram of the experimental setup used to study membrane facilitated separation of NF_3 and CF_4.

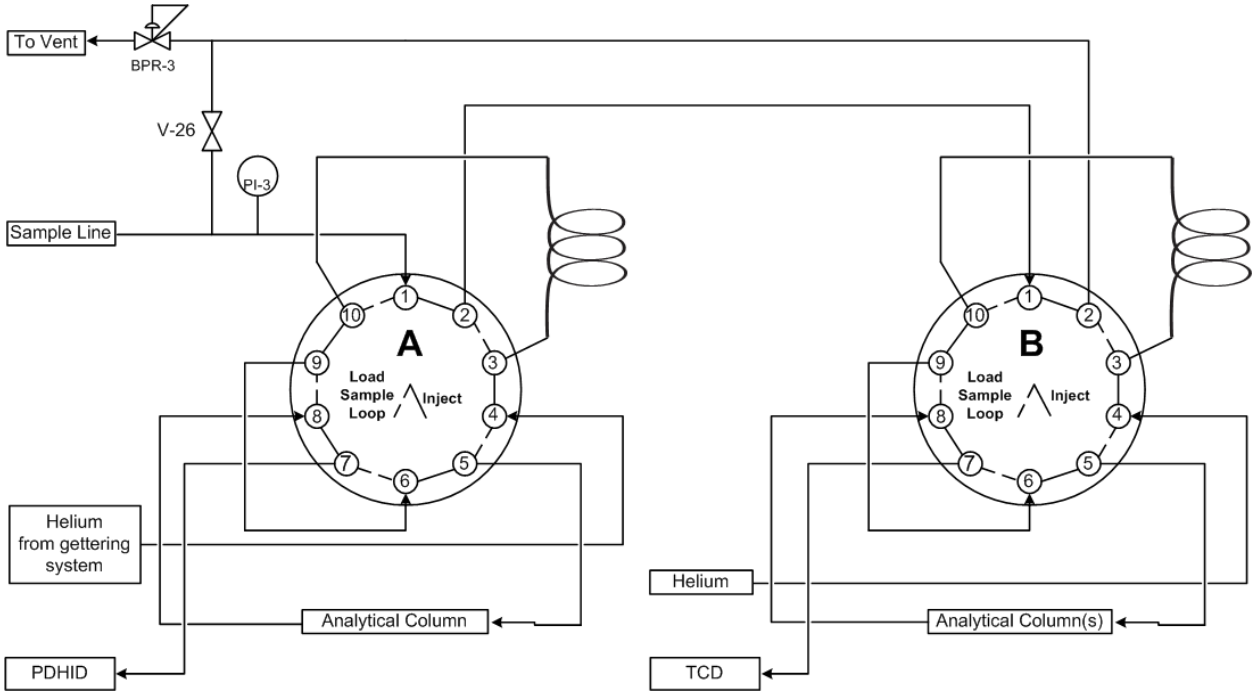

Figure A.2: GC Setup used for quantitative NF_3 and CF_4 analysis.

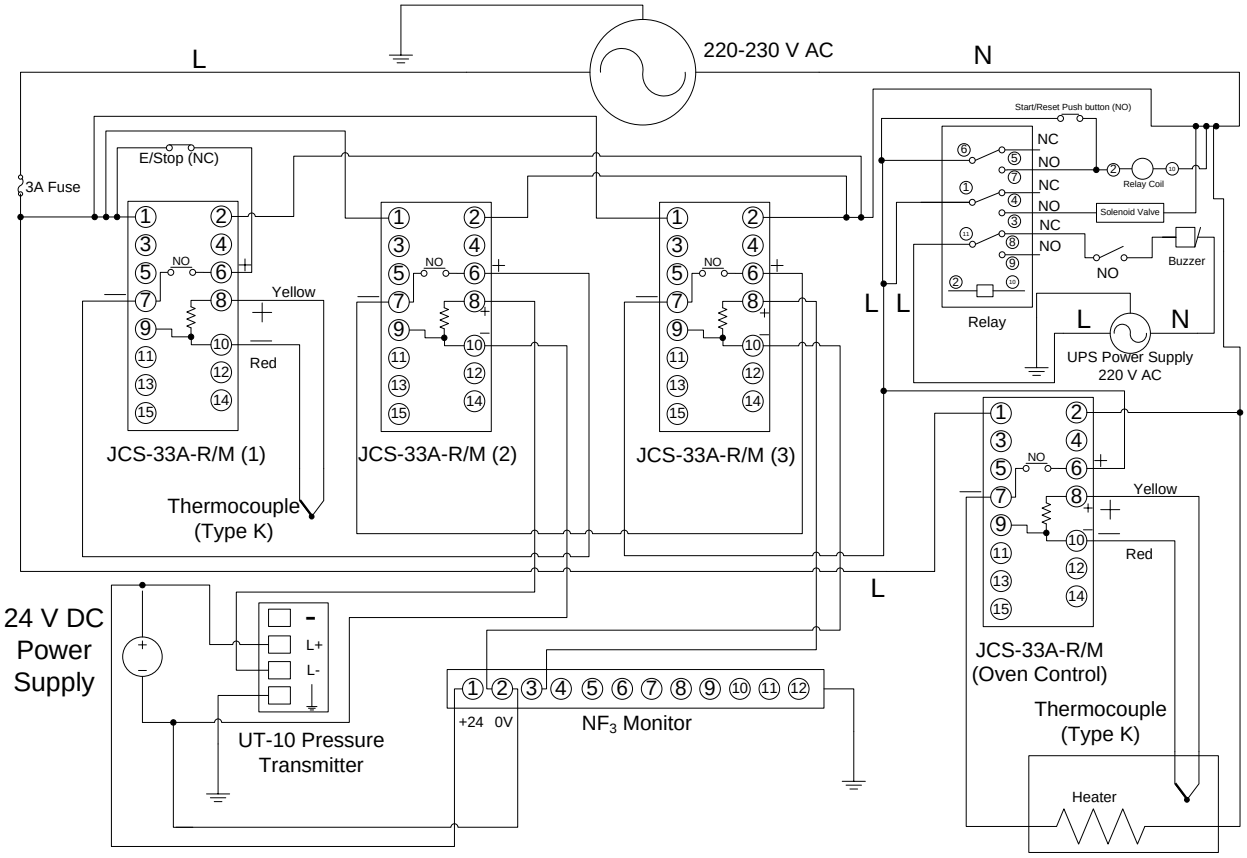

Figure A.3: Wiring diagram of the controller box used to control the different interlocks.

A.3 Start-up Diagnostics

Before the system is run for the first time, or after changes has been made to the system, the following diagnostic tests should be performed, with reference to Fig. A.1 and Fig. A.3.

1) The system must be pressure-tested using He to determine whether all fittings are leak-tight. This may be performed by pressurizing sections of the setup and monitoring pressure as a function of time. Leaks can be detected using soap water.
2) When exchanging a membrane for another, the membrane cell should especially be checked for leaks, by pressure testing using He.
3) It should be confirmed that the mains power supply to the interlock system is switched on, and that the different controllers on the interlock system is functioning.
4) It should be confirmed that the interlock system functions correctly, and in tandem with the solenoid valve and actuated valves V-11 and V-13. The emergency stop switch on the controller box can be used for this. In addition, interlock conditions can be simulated using He as process fluid and inducing temperature-high and pressure-

high conditions that should lead to automatic shutoff of the NF_3 and CF_4 feed lines via valves V-11 and V-13.

5) The NF3 monitor may be tested in a controlled manner by loading some tubing with NF3 using the appropriate procedures described in the following sections and then venting the NF3 until the NF3 pressure inside the tubing has dropped below a measurable value. Residual NF3 gas can then be released near the NF3 monitor by loosening tube fittings, which should engage the interlock to close valves V-11 and V-13. This test must be performed inside a fume cupboard, and adequate protective equipment must be worn. Another way of testing the monitor is to vent NF3 to the fume cupboard and connect tubing to the inlet of the monitor and hold the other end of the connecting tubing in the vicinity of the vent line inside the fume cupboard, while adjusting the pump of the NF3 monitor the appropriate setting.

A.4 Preparation of the GC System

Before system startup, the GC system should be prepared as follows to ensure accurate and reliable functioning, especially after the system was not operational for a period of time. Refer to Fig. A.1 and Fig. A.2.

1) The carrier gas supply to the GC is opened and set to the correct pressure on FPR-6. The gettering system is not switched on at this time.
2) The synthetic air supply to the GC is opened and set to the correct pressure using the corresponding FPR (not shown).
3) The GC is switched on.
4) If necessary, the carrier gas lines are purged, with the gettering system switched off, for at least 30 min with a reasonable flow rate to allow enough time for the GC plumbing system to be flushed.
5) After purging and flushing is complete, the gettering system can be turned on, and the carrier gas supply kept open, with the 10-port switch valves set to the load position.

For continuous experimental work, the gas saver mode may be turned on, and the carrier gas supply left open, with the 10-port switch valves left in the load position.

A.5 Startup Procedure

Before starting an experimental run, the following startup procedure should be followed. Refer to Fig. A.1 and Fig. A.2.

1) The startup diagnostics should be performed as described in Sec. A.3.
2) The GC system is prepared as described in Sec. A.4.
3) The venting system is switched on. Check that it is functioning properly, and that the backup power system is connected. Also ensure that the bubble flow meter is placed inside the fume cupboard, and/or the outlet is placed inside the fume cupboard.
4) FPR-1 and FPR-2 is closed, if not closed already.
5) The He-flush supply is opened via FPR-3, and set to a pressure of 1.5 bar (gauge).
6) Valve V-23 is either set to the He-inlet position or to the feed-line position, while BPR-3 and valve V-26 is opened completely.
7) The 10-port switch valves on the GC is set to the load position, as described in Sec. A.4.
8) It is important to note that care should be taken not to exceed the range of pressure transducer PI-3. This can easily occur with a high volumetric flow rate, while valve V-26 is closed, or when V-23 is set to the He-position and with FPR-3 set to large enough pressure (also keep in mind that the local outlet gauge of FPR-3 gives a gauge-pressure reading). Thus, when V-23 is set to the He-position, FPR-3 must be set to an appropriate pressure, and V-26 should also be opened. The GC sampling valves can then be flushed with He by throttling the flow using V-26. This applies to all other subsequent sections, in which mention is given to the GC sampling system.

A.5.1 Flushing of NF_3 and CF_4 Supply Lines

Flushing of the supply lines are performed to clear out air from the supply lines after changing of cylinders or after an experimental run to clear out NF_3 and/or CF_4 from the supply lines. The procedures to be followed are detailed below.

A.5.1.1 Flushing of the NF_3 supply line

With reference to Fig. A.1:

1) The He flush supply is opened and set to a pressure of at least 2 bar (gauge) using FPR-3. The outlet pressure set on FPR-3 should be less than the NF_3 cylinder pressure.

2) Valve V-1 is closed, if not closed already, and FPR-1 is closed, if not closed already.
3) Valves V-5 and V-7 are opened, if closed. The pressure on the inlet gauge of FPR-1 should rise according to the pressure set on FPR-3.
4) If a new cylinder is connected, it should be done at this point, with He (at a low pressure) flushing air out of line L-1 while the cylinder is being connected. After the cylinder has been firmly connected using the appropriate fitting, the lines can be cycle-purged a couple of times to ensure that no air is present inside the lines. Thereafter, it should be checked whether the fitting are leak tight by increasing the He pressure and checking for leaks using soap water.
5) After the cylinder has been connected, or if step 4 was skipped because a cylinder was already connected, and the pressure has stabilized on the inlet gauge of FPR-1, valve V-7 is closed, after being opened first.
6) Valve V-1 is opened slowly to bleed the supply line and closed again. To ensure that reverse flow into line L-4 through valve V-3 cannot occur, valve V-3 should be closed beforehand, whenever valve V-1 is opened to bleed the NF_3 supply line.
7) Steps 3 - 6 are performed two or three times to ensure that air or NF_3 have been purged from the supply lines.
8) After steps 3 – 6 has been performed two or three times, valve V-7 is opened and then closed again.

To ensure that L-5 does not present a low-flow or no-flow hazard due to clogging of the line, a helium blow-down test can be performed simultaneously during bleeding of the supply line as described in step 6.

A.5.1.2 Flushing of the NF_3 supply line

1) Valve V-3 is closed, if not closed already, and FPR-2 is closed, if not closed already.
2) The He flush supply is opened and set to a pressure of at least 2 bar (gauge) using FPR-3. The outlet pressure set on FPR-3 should be less than the CF_4 cylinder pressure.
3) Valves V-6 and V-8 are opened, if closed. The pressure on the inlet gauge of FPR-2 should rise according to the pressure set on FPR-3.
4) If a new cylinder is connected, it should be done at this point, with He (at a low pressure) flushing air out of line L-2 while the cylinder is being connected. After the cylinder has been firmly connected using the appropriate fitting, it should be checked

whether the fitting is leak tight by increasing the He pressure and checking for leaks using soap water.

5) After the cylinder has been connected, and the pressure has stabilized on the inlet gauge of FPR-2, valve V-8 is closed.
6) If a new cylinder is not connected, steps 3 - 5 can be skipped. However, valve and V-8 should still be closed, after being opened first, if not closed already and valve V-6 should be opened, if not opened already.
7) The supply line is bled off by opening of valve V-3 and closing it again. To ensure that reverse flow into line L-3 through valve V-1 cannot occur, valve V-1 should be closed beforehand, whenever valve V-3 is opened to bleed the CF_4 supply line.
8) Steps 3 - 7 are performed two or three times, with the exception of step 4, which should have been completed during the first run.
9) To ensure that L-5 and L-6 do not present a low-flow or no-flow hazard due to clogging of the lines, a helium blow-down test can be performed simultaneously during bleeding of the supply line as described in step 7.

A.5.2 Initiation of the Interlock System

Before any experimental work can be done on the system, the interlock system must be initiated to open valves V-11 and V-13. With reference to Fig. A.1 and Fig. A.3, the procedure to be followed is:

1) The mains power supply to the controller box is switched on.
2) The emergency stop switch is switched to the “on” position, if switched “off”.
3) The buzzer switch is switched to the “off” position, if switched “on”.
4) The air feed to the solenoid (pneumatic) valve is opened and set to the appropriate pressure. Ensure that the air pressure is sufficient to guarantee correct operation of the solenoid valve.
5) Ensure that a temperature reading is given on controller 1, and that it is below the upper threshold value set on the controller.
6) Ensure that a pressure reading is given on controller 2, and that it is below the upper threshold value set on the controller. Also ensure that the UT-10 pressure transmitter (PI-1) is functioning.

7) Ensure that an NF_3-concentration reading is given on controller 3, and that it is below the upper threshold value set on the controller. Also ensure that the NF_3 monitor is functioning.
8) Ensure that a temperature reading is given on the standalone controller that controls the convection oven (heater), and that the oven and standalone controller is functioning.
9) Press and hold the push button to engage the relay, and thus the solenoid valve, to open the pneumatically actuated valves V-11 and V-13.
10) Switch the buzzer switch to the "on" position.

A.5.3 Opening of the NF_3 and CF_4 Feeds

After the supply lines for NF_3 and CF_4 have been flushed, NF_3 and/or CF_4 can be fed to the membrane cell or sampled directly for analysis via the on-line GC.

A.5.3.1 Opening of the NF_3 feed

With reference to Fig. A.1 and Fig. A.2:

1) The interlock system is readied, following the procedure described in Sec. A.5.2.
2) The procedure described in Sec. A.5.1.1 is followed.
3) The NF_3 cylinder valve is opened slowly, and only slightly while observing the pressure increase as measured using the inlet gauge on FPR-1, and closed again immediately. Note that it should always be ensured that valve V-1 is closed before opening the NF_3 cylinder valve, otherwise a high-flow hazard can occur in L-1, L-3 and L-5 if valve V-2 does not operate correctly or not as effectively as hoped.
4) Valve V-1 is opened slowly to bleed the supply line and closed again. To ensure that reverse flow into line L-4 through valve V-3 cannot occur, valve V-3 should be closed beforehand, whenever valve V-1 is opened to bleed the NF_3 supply line.
5) Steps 3 - 4 are performed two or three times to ensure that pure NF_3 is fed to the system.
6) The mass flow controller MFC-1 is readied to allow flow of NF_3 through the feed line.
7) The destination of the NF_3 flow, or combined NF_3 and CF_4 flow is preselected by opening or closing either valve V-16 or V-17.

8) If GC analysis is to be performed, the feed stream is selected using valve V-23 with valve V-16 open and V-17 closed.
9) FPR-1 is opened slowly and carefully and set to the desired pressure.
10) BPR-3 and V-26 is opened completely.
11) The 10-port switch valves on the GC is set to the load position, if not already in that position.
12) The Bubble flow metering system is readied accordingly.
13) The desired pressure is then set on BPR-3 using PI-3. A measurable flow should be detected through the bubble flow meters.
14) Dynamic sampling for GC analysis is performed to ensure correct mixing of the NF_3 and CF_4 feed streams. This is facilitated using BPR-3 and V-26. It should be noted that dynamic sampling must always be performed in this way, and this therefore applies to any GC analysis step mentioned in the following sections. Dynamic sampling at a desired pressure is done by fully opening BPR-3 and V-26 so that the GC sampling system is mostly bypassed. The desired sampling pressure is set with BPR-3, and the flow is throttled through the sampling loops using V-26 (resulting in an appreciable rise in pressure as measured using PI-3), until steady state is achieved. V-26 is then opened fully again, and is closed slowly so that the pressure in the sample loops as measured using PI-3 rises only about 0.5 kPa – thus ensuring flow through the sample loops together with a minimal pressure drop across the sampling system.
15) Always ensure that when the procedure described in the above steps is followed that valve V-7 is closed and remains closed while the supply line is pressurized with NF_3. This is to prevent reverse flow through line L-14 contamination of this and the other connecting lines with NF_3.

A.5.3.2 Opening of the CF_4 feed

1) After the NF_3 feed has been opened, the mass flow controller MFC-2 is readied to allow flow of CF_4 through the feed line.
2) The procedure described in Sec. A.5.1.2 is followed.
3) The CF_4 cylinder valve is opened briefly and closed again immediately. Note that it should always be ensured that valve V-3 is closed before opening the CF_4 cylinder valve, otherwise a high-flow hazard can occur in L-2, L-4 and L-6 if valve V-4 does not operate correctly or not as effectively as hoped.

4) Valve V-3 is opened to bleed the supply line and closed again. To ensure that reverse flow into line L-3 through valve V-1 cannot occur, valve V-1 should be closed beforehand, whenever valve V-3 is opened to bleed the CF_4 supply line.
5) Steps 3 – 4 are performed two or three times.
6) The destination of the CF_4 flow, or combined NF_3 and CF_4 flow is preselected by opening or closing either valve V-16 or V-17.
7) If GC analysis is to be performed, the feed stream is selected using valve V-23, with Valve V-16 open and valve V-17 closed.
8) FPR-2 is opened and set to the desired pressure.
9) BPR-3 and V-26 is opened completely.
10) The 10-port switch valves on the GC is set to the load position, if not already in that position.
11) The Bubble flow metering system is readied accordingly.
12) The desired pressure is then set on BPR-3 using PI-3.
13) The sample stream is analyzed via the GC to ensure correct mixing of the NF_3 and CF_4 feed streams. Refer to step 14, Sec. A.5.3.1 for the correct procedure.
14) Always ensure that when the procedure described in the above steps is followed that valve V-8 is closed and remains closed while the supply line is pressurized with CF_4. This is to prevent reverse flow through line L-18 and contamination of this and the other connecting lines with CF_4.

A.6 Membrane System Operation

After the combined NF_3 and CF_4 feed streams have been analyzed via GC, the feed can be channeled to the membrane cell, and the effluents analyzed, and the flow rate measured to determine membrane characteristics.

A.6.1 Starting a new experiment

With the configuration unchanged from that resulting from following the procedure described in Sec. A.5.3, the procedure to be followed when evaluating membrane performance is given below, with reference to Fig. A.1 and Fig. A.2.

1) Ensure that the 10-port switch valves on the GC is set to the load position.
2) Open BPR-1, BPR-2, BPR-3 and V-26 completely, if not already open.

3) Preselect the destination of the two effluent streams by opening valves V-19 and V-22, and closing valves V-20 and V-21.
4) With valve V-16 still open, slowly open valve V-17.
5) With valve V-17 open, slowly close valve V-16.
6) Keep valve V-23 in the position used to sample the feed stream (Sec. A.5.3) and allow enough time for the pressure in the accompanying lines to be relieved through the vent. This may be monitored using the bubble flow meter.
7) Set the desired pressure of the feed and retentate stream via FPR-1, FPR-2, and BPR-1 using PI-1.
8) Set the desired pressure of the permeate stream via BPR-2, FPR-3 and MFC-3 using PI-2.
9) After the pressure in the sample stream has been relieved (step 6), switch valve V-23 to select the He flush line and allow some time for the sampling line to be flushed (while the analytical column(s) are simultaneously flushed by the carrier gas).
10) After completion of step 9, preselect the next sample stream by switching valve V-23 to the correct position (either permeate or retentate stream).
11) Slowly open either valve V-20 or V-21 (depending on the sample stream that is preselected via valve V-23), while valves V-19 and V-22 are still open.
12) Depending on which valve was opened in step 11, slowly close the corresponding valve, i.e. either valve V-19 or V-22.
13) Set the desired pressure of the sampling line using BPR-3 and PI-3 for GC analysis.
14) When enough time has been allowed to flush the sample loop with the sample stream, slowly close either valve V-20 or V-21 (depending on the sample stream that is preselected via valve V-23), after opening the corresponding valve V-19 or V-22 .
15) The desired sample loop pressure must then be set using BPR-3 and V-26 for analysis of a dynamic gas sample. Afterwards, V-26 should be opened again to relieve any upstream pressure that could have arose during sampling.
16) If helium must be used as sweep gas on the permeate side, the helium pressure and flow is to be set using FPR-3 and MFC-3, where V-25 is used to control the feed to MFC-3. The pressure and flow of the helium sweep gas on the permeate side should always be lower than that of the feed and retentate lines. Thus, the permeate pressure, measured using PI-2, should always be lower than the feed and retentate pressure, measured using PI-1. Also, either V-21 (and the permeate stream selected on V-23) or V-22 should always be open to prevent systematic pressure build-up in the permeate

and helium sweep lines. In addition, the helium flow, as controlled using MFC-3 must be such that a high-flow hazard does not present itself.

17) To prevent reverse flow through L-34 due to malfunctioning of V-24, it should always be ensured that V-25 is either closed when the feed (L-32) and retentate (L-33) lines are active, or if V-25 must be open, that the pressure set on FPR-3, as measured using its local outlet gauge is higher than that on FPR-1 and FPR-2.

A.6.2 Switching to a different stream for GC analysis

After following the procedures detailed in Sec. A.5.3 and Sec. A.6.1, it will be necessary at some point to select another stream for GC analysis and flow measurement, or to switch between streams using valve V-23 during an experimental run. The following procedure must be followed when switching between streams, where switching from analyzing the retentate stream to analyzing the permeate stream is used as example, with reference to Fig. A.1 and Fig. A.2. Starting from this point (analyzing the retentate stream), valves V-19 and V-21 are closed, where valves V-20 and V-22 are open, and the retentate stream is selected on valve V-23. To switch to the permeate stream on valve V-23:

1) Ensure that the 10-port switch valves on the GC is set to the load position.
2) Open valve V-19 slowly while keeping valve V-20 open.
3) Close valve V-20 slowly, while keeping valve V-19 open.
4) Keep valve V-23 in the position used to sample the retentate stream and allow enough time for the pressure in the accompanying lines to be relieved through the vent. This may be monitored using the bubble flow meter.
5) After the pressure in the sample stream has been relieved, switch valve V-23 to select the He flush line and allow some time for the sampling line to be flushed (while the analytical column(s) are simultaneously flushed by the carrier gas).
6) After completion of step 5, preselect the permeate stream using valve V-23.
7) Open BPR-3 and V-26 completely and ready the bubble flow meter accordingly.
8) Slowly open valve V-21, while keeping valve V-22 open.
9) Slowly close valve V-22.
10) Set the desired pressure on BPR-3 and V-26 using PI-3 for GC analysis.
11) After enough time has been allowed for flow to reach steady state, valve V-22 is opened and valve V-21 is closed, and the desired sample loop pressure is set using BPR-3 and V-26.

A.7 Shutdown Procedure

A.7.1 Shutoff of the NF_3 and CF_4 Feeds

After completion of an experimental run, the following procedure should be used to close the NF_3 and CF_4 feeds, with reference to Fig. A.1, Fig. A.2 and Fig. A.3.

1) Any stream that was analyzed via GC should be vented by setting the 10-port switch valves to the load position.
2) Additionally, all streams should be vented by slowly opening valves V-19 or V-22, while keeping valves V-20 or V-21 open (depending on which valves were open and which were closed).
3) The NF_3 cylinder valve is closed slowly, and the CF_4 cylinder valve is closed.
4) All back-pressure regulators BPR-1, BPR-2 and BPR-3 should be opened slowly, and completely.
5) Valve V-23 is switched to select the feed stream.
6) Valve V-16 is opened slowly, while keeping valve V-17 open.
7) After the pressure in the system, as monitored using the local gauges on the regulators, as well as PI-1, PI-2 and PI-3, has been relieved, the system can be flushed using He as described in Sec. A.7.2.
8) The interlock system is only shut down after the system has been flushed with He (Sec. A.7.2).
9) The 10-port valves on the GC is left in the load position and the GC set to gas saver mode, while keeping the carrier gas supply open.

A.7.2 Flushing Procedure

After each experiment, the system is flushed using He to remove the corrosive NF_3 from the setup, thereby improving the lifespan of the equipment and preventing accidental release of NF_3 to the ambient environment by unauthorized persons or any other means. The procedure to be followed is given below, with reference to Fig. A.1 and Fig. A.2:

1) The system is shut down as described in Sec. A.7.1, without shutting down the interlock system.
2) Ensure that the system pressure has relaxed to below 1 bar before the system is flushed.

3) While keeping FPR-1, FPR-2, and the mass flow controllers, MFC-1, and MFC-2, MFC-3, and valves V-11 and V-13 open, and valves V-7 and V-8 closed, FPR-3 can be opened, if not still open, and set to an outlet pressure of at 1.5 bar (gauge).
4) All valves, except valves V-7 and V-8 can be opened slowly, if not already open.
5) Valves V-7 and V-8 is then opened slowly at first, after which they may be opened normally.
6) The outlet pressures on FPR-1 and FPR-2 can then be set to the desired setting in accordance with the outlet pressure of FPR-3.
7) While flushing the system, valve V-23 is switched to the different positions and left in a specific position for at least 5 min.
8) The system should also be bled-off intermittently one or two times by closing the mass flow controllers MFC-1, MFC-2 and MFC-3 and allowing enough time for the pressure in the system to equalize. After the pressure has equalized, the mass flow controllers are opened again.
9) After sufficient flushing, valves V-16, V-20 and V-21 are closed.
10) FPR-3 is closed while keeping all valves open, except those closed in step 9.
11) Valve V-23 is then switched to the different ports, while FPR-3 is closed, to alleviate the pressure from each port.
12) After the pressure from each port has been relaxed, valve V-23 is switched to the He-flush port and left in that position.
13) After the He pressure in the rest of the system has been relieved, valves V-7 and V-8 are closed.
14) Valves V-19 and V-22 are closed.
15) FPR-1 and FPR-2 are closed.
16) All other valves are closed.
17) The mass flow controllers are closed (and can be left switched on as this ensures that the electronics and thermal compartments stays stable).
18) The interlock system is shut down by switching off the mains power supply.
19) The NF_3 and CF_4 supply lines can then be flused by following the procedures described in Sec. A.5.1.1 and Sec. A.5.1.2 respectively.

A.8 Manual Restart of the Interlock System

In the event of automatic shutoff of the NF_3 and/or CF_4 supplies via valves V-11 and V-13 due to engagement of one of the interlocks, or a power failure, the following procedure should

be used to resume the flow of NF_3 and/or CF_4, with reference to Fig. A.1, Fig. A.2 and Fig. A.3.

1) If the interlock system was activated due to a power failure, the system can be restarted simply by pressing the Start/Reset button. As a safety precaution, the forward pressure regulators FPR-1 and FPR-2 should be closed first before pressing the Start/Reset button where after it can be opened again and set to the desired pressure.

In the event of a serious error such as high temperature, high pressure or release of NF_3 to the surrounding atmosphere, the following procedure should be followed:

1) Close the NF_3 and/or CF_4 cylinder valves slowly.
2) Open the He flush supply using FPR-3 and set the pressure to 1.5 bar (gauge).
3) Turn off the buzzer with the buzzer switch.
4) Inspect each controller visually to determine which interlock was engaged.
5) Slowly open valves V-19 and/or V-22.
6) Slowly open BPR-1 and BPR-2 completely so as not to constrict the flow of gas from the membrane cell in any way.
7) Set the 10-port switch valves on the GC to the load position, if not in that position already, and openV-26 and BPR-3 completely.
8) Set valve V-23 to select the feed stream.
9) Slowly open valve V-16, while keeping valve V-17 open.
10) Slowly open valve V-1 to vent the NF_3 supply line (first ensure that the cylinder valve is closed as described in step 1). Close valve V-1 again.
11) Open valve V-3 to vent the CF_4 supply line (first ensure that the cylinder valve is closed as described in step 1). Close valve V-3 again.
12) Open valves V-7 and V-8 so that the inlet pressure on the local gauges of FPR-1 and FPR-2 rises.
13) If the normal interlock conditions have been returned, restart the interlock system according to the procedure given in Sec. A.5.2.
14) Allow the system to be thoroughly flushed with He by following the procedure in Sec. A.7.2.
15) If the problem that caused the automatic shutdown has successfully been controlled by the procedure outlined in the steps given above, and the system thoroughly inspected, the system can be restarted by following the procedure given in Sec. A.5.3. Before the system is restarted however, it should be ensured that the problem that caused the shutdown has been eradicated.

16) After successfully restarting the system, normal operation can be resumed by following the procedures given in Sec. A.6 and Sec. A.7.

A.9 Maintenance Considerations

The following aspects should be kept in mind with respect to maintaining the experimental setup in a safe and accurate working condition.

1) The setup should be pressure tested and leak-tested at least bi-annually to ensure that all valves, regulators, MFCs and fittings are leak tight. This excludes the membrane cell, which should be leak-tested after each membrane changeover.
2) Quarterly inspection of the particulate filters should be undertaken to ensure that blockage does not become a problem. If necessary, filters must be replaced.
3) Quarterly inspection of the interlocks should be undertaken according to the method outlined in steps 4 and 5 of Sec. A.3 to ensure that these safety features are functioning.
4) Quarterly inspection of the pressure relief valve V-12 should be undertaken by simulating the pressure at which the valve should open using He to test whether the valve is still functioning correctly.
5) Quarterly inspection of check valves should be performed to ensure system integrity.
6) Bi-annually inspection of the venting system should be undertaken to ensure that adequate ventilation is maintained.
7) If replacement of the bolts used on the membrane cell is required, it must be ensured that the bolts are made from high tensile strength steel.

A.10 Safety Procedures

In case of accidental release of either NF_3 or CF_4 the following guidelines should be followed when the area is entered to shut off the supplies. In case of one of the interlocks being engaged, the procedure described in Sec. A.8 should be followed, together with these guidelines, depending on the situation.

1) In the event of accidental release of NF_3 (which will be detected by the NF_3 monitor), or CF_4 (which is not exceptionally harmful in low concentrations, whereas a considerable release of the gas will be immediately detected), a full facemask respirator must be worn when attempting to shut off of the NF_3 and CF_4 supplies.

2) Appropriate gloves and a lab coat must also be worn when shutting off the NF_3 and CF_4 supplies in the event of accidental release.
3) The procedure described in Sec. A.7.1 should be followed when closing the NF_3 and CF_4 supplies.
4) If accidental release occurred, the venting system should be left operational, the GC and other equipment should be switched off and the laboratory should be locked (after the abovementioned steps have been completed). The laboratory should then be kept locked while the venting system is operational for at least an hour to extract the released gases before entering the laboratory again. The NF_3 monitor can be used to determine whether NF_3 has been extracted (in the case of NF_3 release). In the case of CF_4 release, more time should be allowed for extraction, after which the laboratory should only be entered to switch off any equipment still running. Thereafter more time should be allowed for extraction via the ventilation system.
5) If the problem has been contained, and if the release did not occur due to damage to, or failure of equipment, tubing or cylinder valves, normal operation of the system may be undertaken by following the procedures described in the previous sections.
6) If any person inhaled significant amounts of NF_3 or CF_4, and if the person is suffering any sort of respiratory discomfort, medical attention should be sought immediately. The physician should also be informed that the person could be suffering from anoxia (if CF_4 was inhaled) or methemoglobinemia (if NF_3 was inhaled).
7) The NF_3 and CF_4 Material Safety Data Sheets can also be consulted for further information.

A.11 References

1. J.-P. Barbier, G. Bissolotti, K. Cleaver, J.-C. Goffinet, B. Hussler, P. Wolf, 2009, Code of practice nitrogen trifluoride, IGC Doc. 92/10/E. European Industrial Gases Association, EIGA. Available: http://www.eiga.org/fileadmin/docs_pubs/Doc_92_10_E.pdf. Date of access: 05 November 2011.

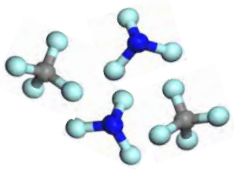

Appendix B

Supplementary Graphical and Tabular Data for Chapter 2

B.1 Introduction

This appendix contain representative calibration curves that were obtained with the TCD and PDHID detectors using the GC method, parameters and sampling system as described in Chapter 2. Although some calibration curve equations and correlation coefficients are reported in Chapter 2, the figures presented below provide visual verification thereof. Raw data used to calculate the concentrations of NF_3 and CF_4 in the prepared calibration mixture as mentioned in Chapter 2 (Table 2.3) are also reported in Tables B.1 and B.2.

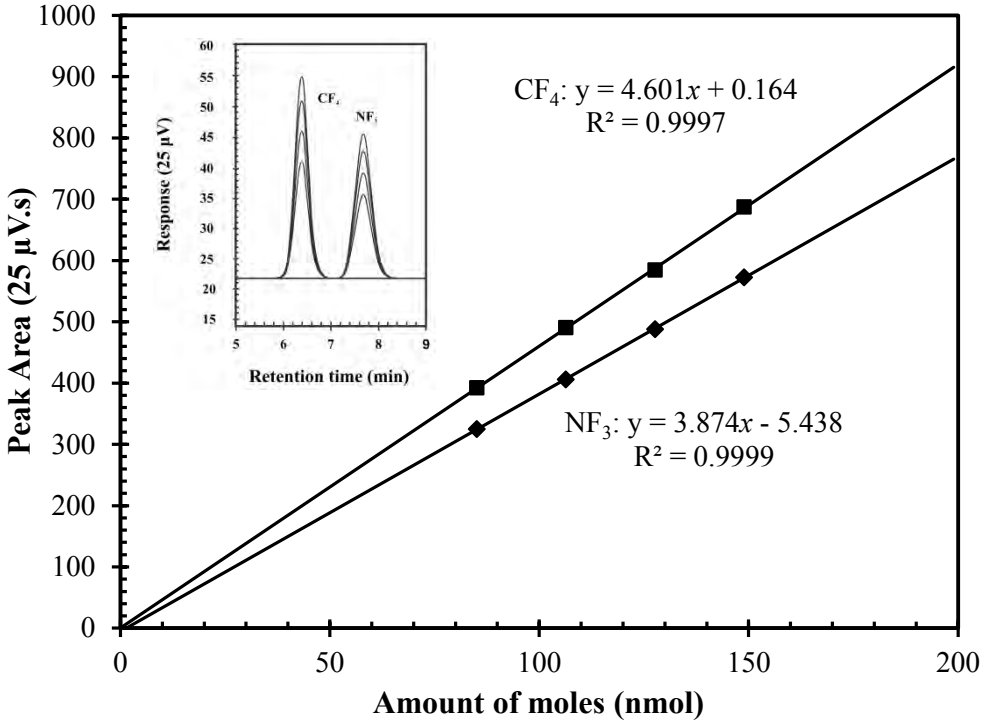

Figure B.1: Representative calibration curves obtained on the TCD channel of the current GC setup (Fig. 2.2). Regression was performed on the average of each data point resulting from three consecutive sets of calibrations for ■ – CF_4, and ♦ - NF_3. Note that for calibration, the sample loop and helium carrier at the GC inlet was kept constant at 80°C as mentioned in Sec. 2.2.4.

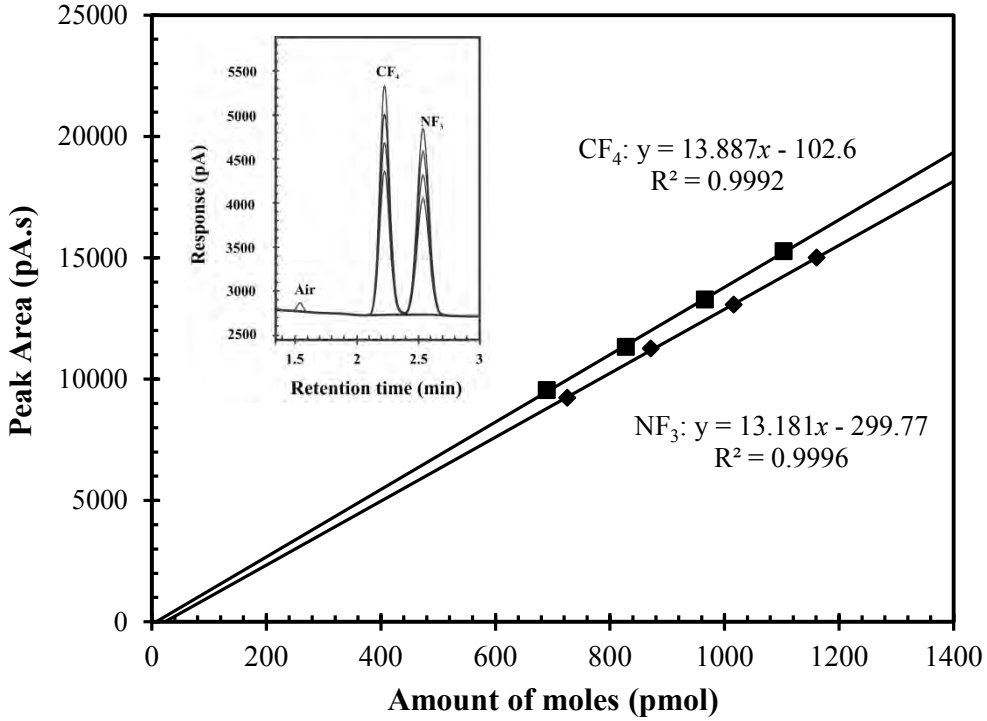

Figure B.2: Representative calibration curves obtained on the PDHID channel of the current GC setup (Fig. 2.2), with a 2 m, 3.2 mm O.D. stainless steel column packed with Super Q (100/120 mesh) . Regression was performed on the average of each data point resulting from three consecutive sets of calibrations for ■ – CF_4, and ♦ - NF_3. The conditions and the method used for calibration are discussed in Sec. 2.2.4.

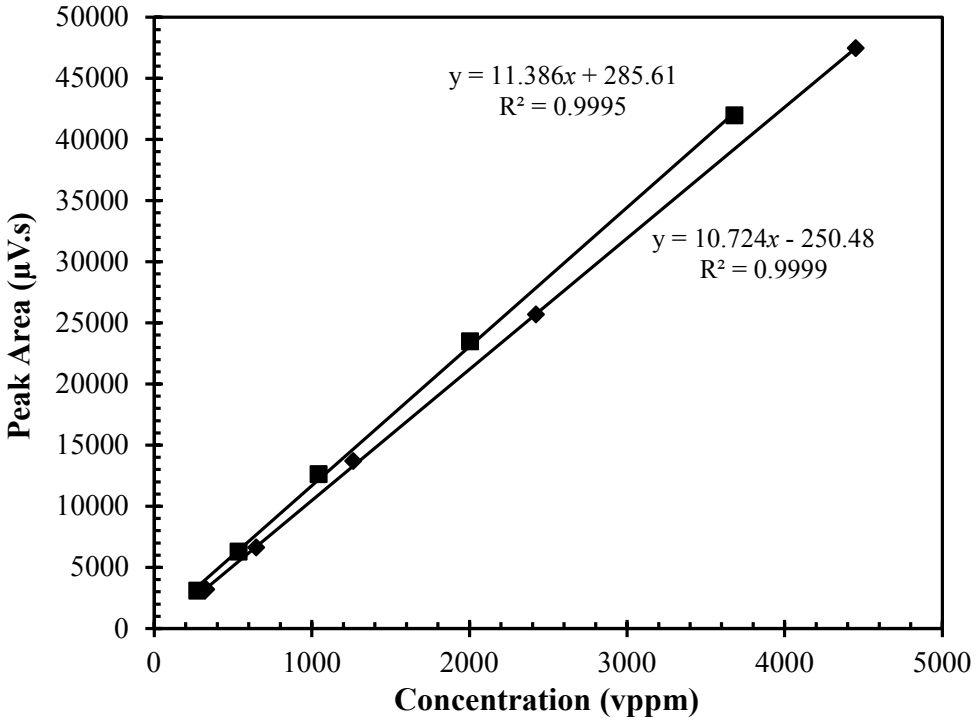

Figure B.3: Representative calibration curves obtained on the PDHID channel of the current GC setup (Fig. 2.2) for CF_4(■) and NF_3(♦), that was used for measuring the concentrations of NF_3 and CF_4 in the permeate stream originating from the membrane module as shown in Fig. 2.5 that was equipped with a polymer membrane with relatively low permeability. Representative chromatograms for the concentration measurements are shown in Fig. 2.6 (a).

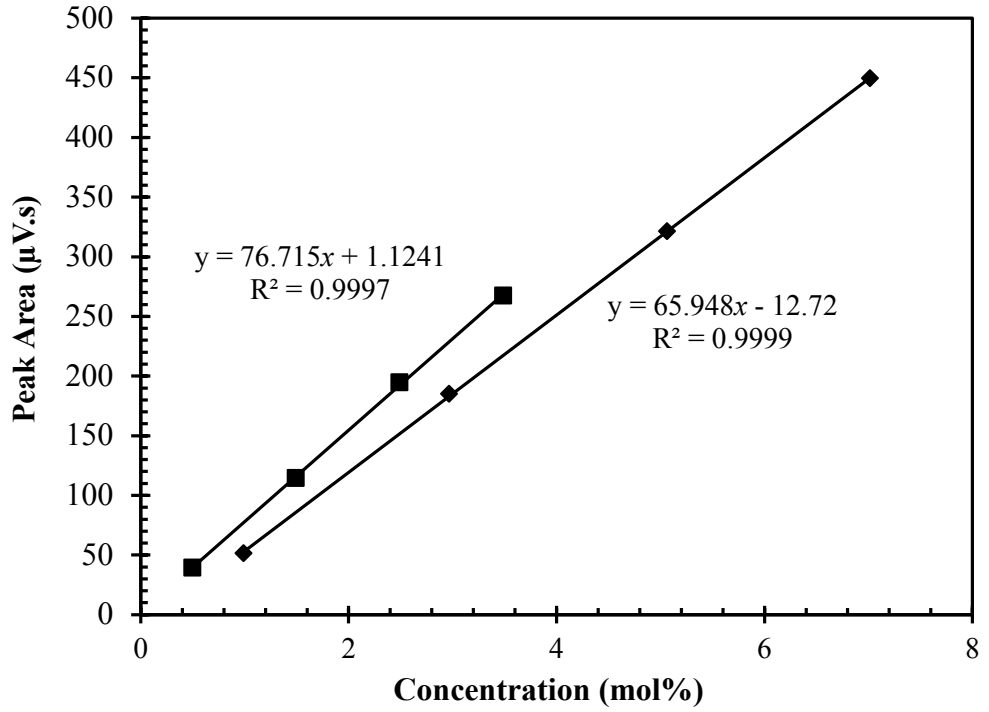

Figure B.4: Representative calibration curves obtained on the PDHID channel of the current GC setup (Fig. 2.2) for CF_4(■) and NF_3(♦), that was used for measuring the concentrations of NF_3 and CF_4 in the permeate stream originating from the membrane module as shown in Fig. 2.5 that was equipped with a polymer membrane with a relatively high permeability. Representative chromatograms for the concentration measurements are shown in Fig. 2.6 (b).

Table B.1: Data from the first run that was used to determine the average NF_3 and CF_4 concentrations of the prepared calibration-mixture with the TCD channel (Table 2.3).

Absolute Sampling Pressure (kPa)	**Number of moles (nmol)**		**Concentration (vppm) ***	
	NF_3	**CF_4**	**NF_3**	**CF_4**
160.0	106.2	99.7	339.3	318.4
170.1	115.5	109.1	347.1	328.0
179.8	121.5	115.7	345.5	329.0
190.0	129.6	123.0	348.7	331.0
200.1	133.4	127.2	340.8	325.0

* Concentrations in vppm calculated from the number of moles detected and the theoretical total number of moles, calculated from the sample loop volume, temperature and pressure.

Table B.2: Data from the second run that was used to determine the average NF_3 and CF_4 concentrations of the prepared calibration-mixture with the TCD channel (Table 2.3).

Absolute Sampling Pressure (kPa)	Number of moles (nmol)		Concentration (vppm) *	
	NF_3	CF_4	NF_3	CF_4
160.1	105.3	100.4	336.2	320.7
170.3	114.1	108.6	342.4	325.9
180.0	121.2	114.9	344.2	326.4
190.0	128.4	122.7	345.5	330.2
200.1	134.3	127.4	343.1	325.4

* Concentrations in vppm calculated from the number of moles detected and the theoretical total number of moles, calculated from the sample loop volume, temperature and pressure.

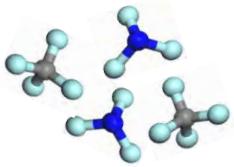

Appendix C

Supplementary Graphical Data for Chapter 3

C.1 Introduction

Representative TGA curves of various annealed and swollen membrane film samples are shown in this Appendix. Together with the DSC results as presented in Chapter 3, it is evident that the annealed perfluoropolymer films, prepared via the solution casting method described in Chapter 3, were not swollen by residual solvent to an appreciable extent. However, the solution cast films that were not annealed at a temperature close to or above their respective glass transition temperatures (T_g) showed considerable weight loss as indicated by the TGA results shown below. As explained in Sec. 3.3.1, this correlated with reduced glass transition temperatures, confirming that the residual solvent caused significant swelling of the fluoropolymer matrices.

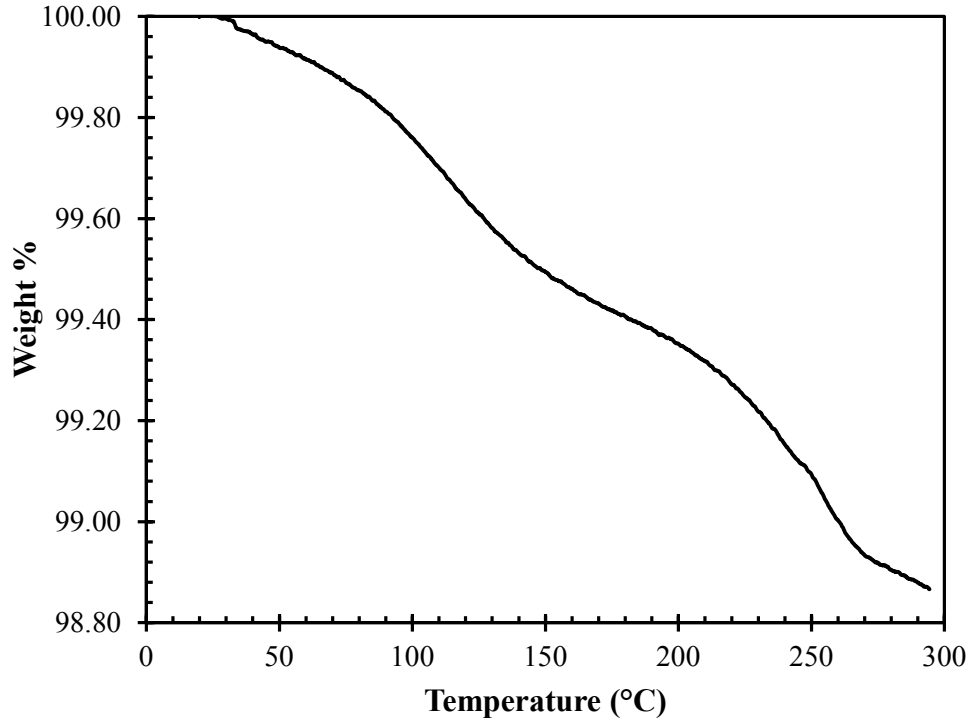

Figure C.1: A Representative TGA curve of an annealed Teflon AF2400 film sample showing very little weight loss during in-situ heating up to approximately 300 °C.

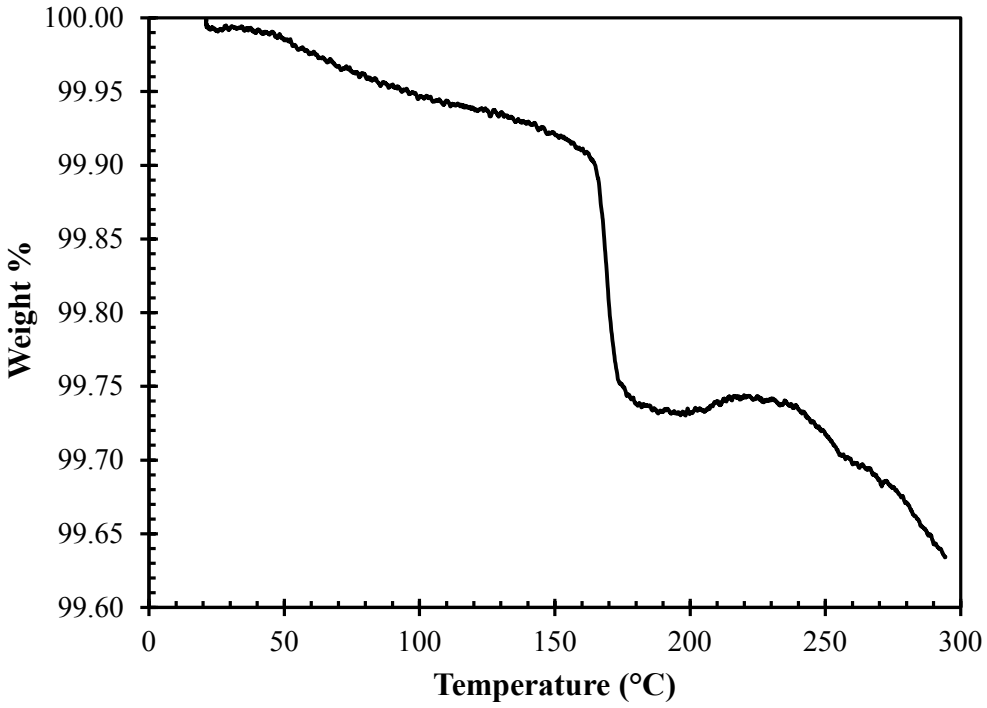

Figure C.2: A Representative TGA curve of an annealed Teflon AF1600 film sample showing very little weight loss during in-situ heating up to approximately 300 °C.

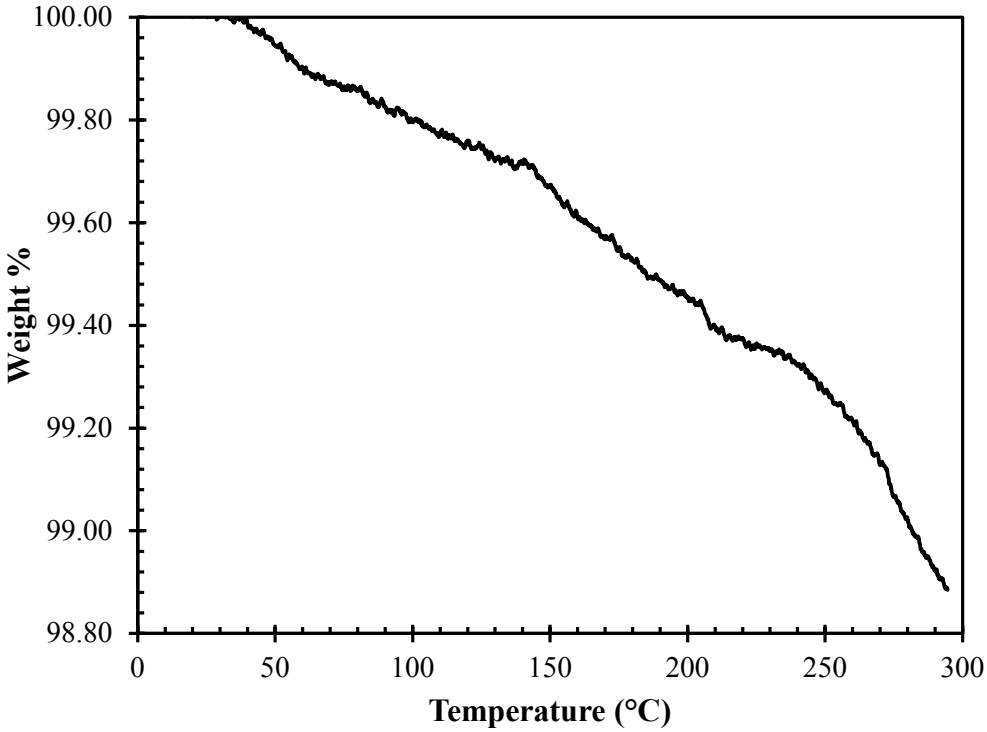

Figure C.3: A Representative TGA curve of an annealed Hyflon AD60 film sample showing very little weight loss during in-situ heating up to approximately 300 °C.

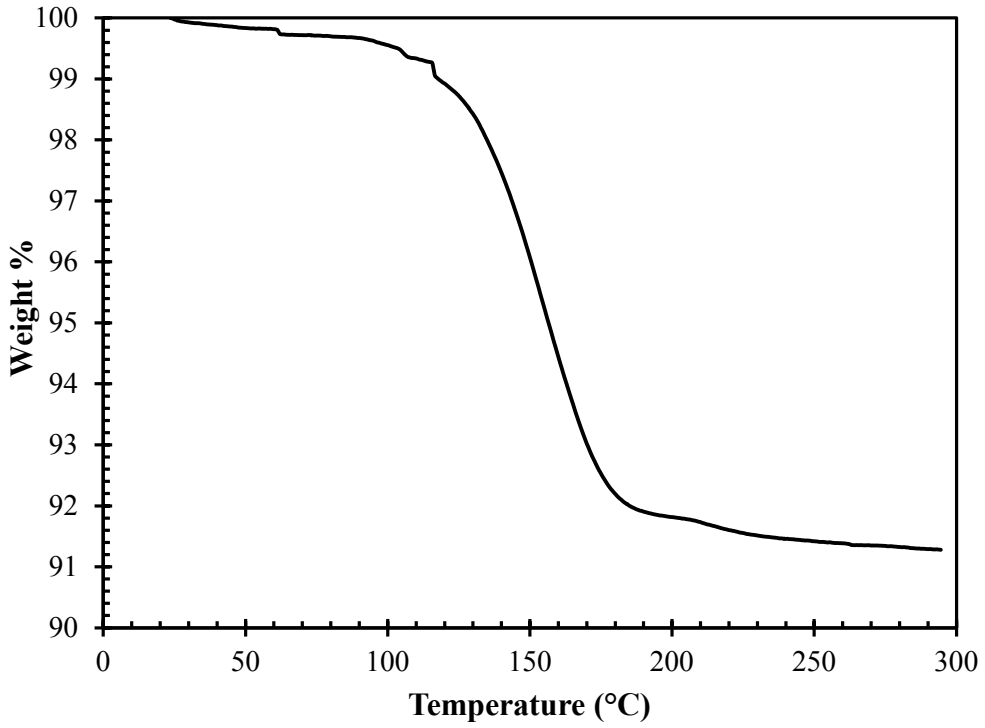

Figure C.4: A Representative TGA curve of a film sample of a partially swollen Hyflon AD60 membrane that was heated to 95 °C while secured inside the permeation cell (Sec. 3.2.2) which shows significant weight loss (approximately 8 %) during in-situ heating up to approximately 300 °C.

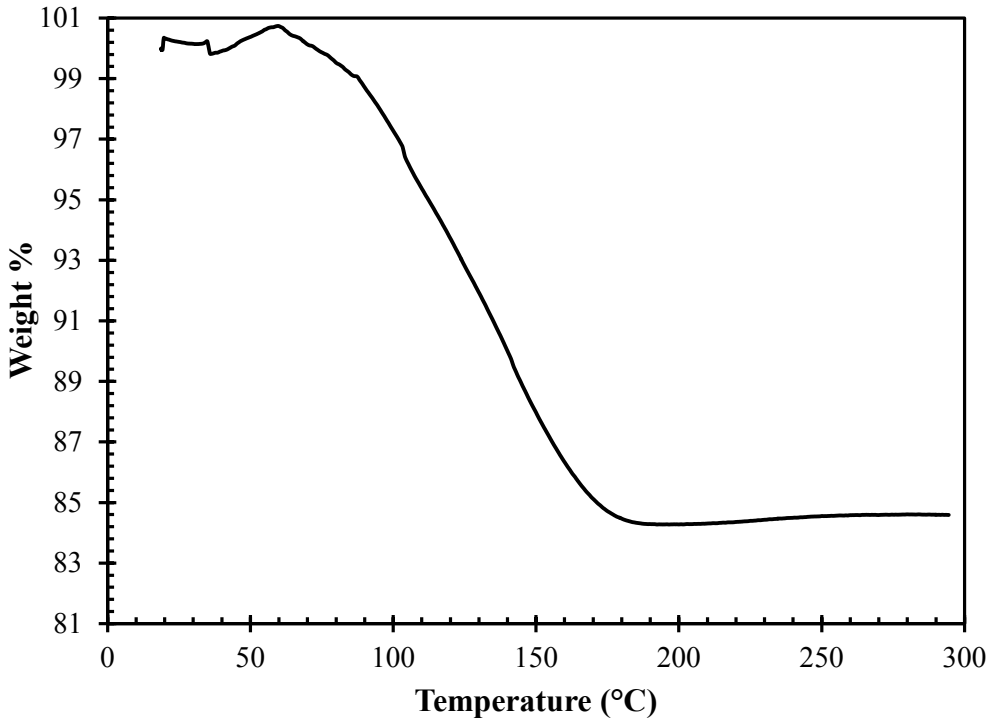

Figure C.5: A Representative TGA curve of a film sample of a swollen Hyflon AD60 membrane that was heated to only 50 °C after the solution casting procedure (Sec. 3.2.2) which shows considerable weight loss (approximately 16 %) during in-situ heating up to approximately 300 °C.

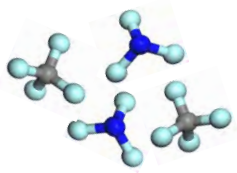

Appendix D

Supplementary Graphical Data for Chapter 4

D.1 Introduction

This appendix contain log(MSD) vs. log(t) graphs for the MD simulation runs of He, N_2, NF_3 and CF_4 that was used to determine whether the Fickian diffusion regime was obtained, or at least approached during the MD simulations. Linear least square fits were applied to the portions of the graphs that yielded a slope that was as close as possible to unity (m = 1), i.e. where Fickian diffusion was reached or at least approached. As a result, the diffusion coefficients for He, N_2, NF_3 and CF_4 were calculated from the slopes of the corresponding MSD graphs over the same simulation-time range (Fig. 4.4 and Fig. 4.6).

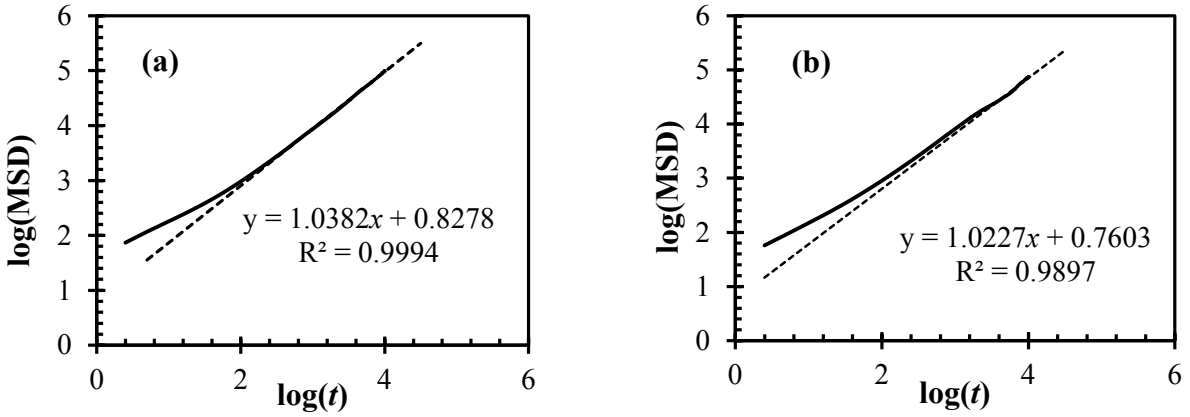

Figure D.1: log(MSD) vs. log(t) plots of He for AF2400 (a) and AF1600 (b) resulting from atomistic molecular dynamics (MD) simulations. Each of the curves represents the average, calculated from at least two independent packing models of each polymer. The dashed lines are linear least square fits to the portions of the curves that represent Fickian behavior.

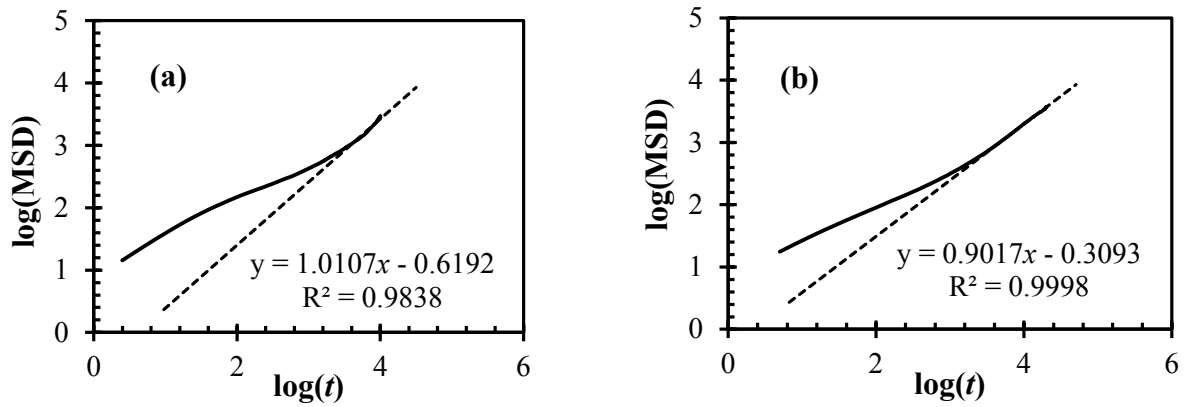

Figure D.2: log(MSD) vs. log(*t*) plots of N_2 for AF2400 (a) and AF1600 (b) resulting from atomistic molecular dynamics (MD) simulations. Each of the curves represents the average, calculated from at least two independent packing models of each polymer. The dashed lines are linear least square fits to the portions of the curves that represent Fickian, or at least near-Fickian behavior.

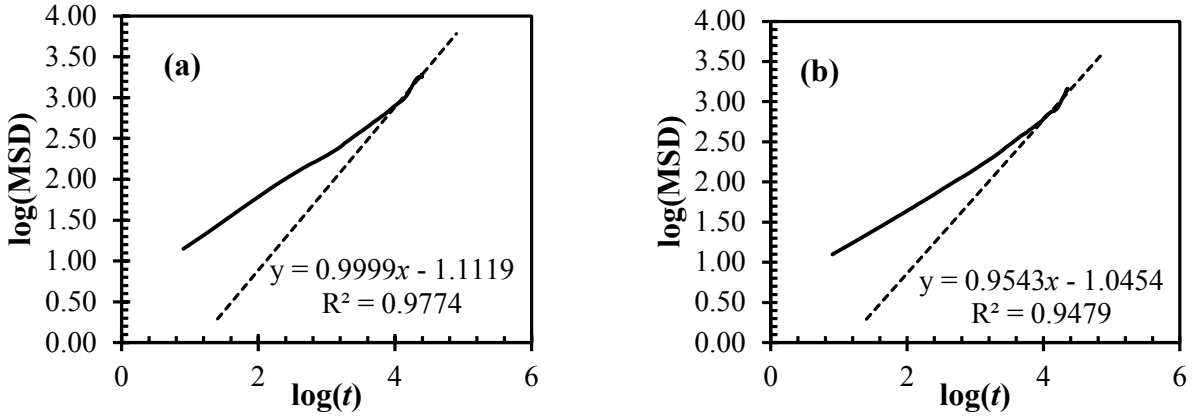

Figure D.3: log(MSD) vs. log(*t*) plots of NF_3 for AF2400 (a) and AF1600 (b) resulting from atomistic molecular dynamics (MD) simulations. Each of the curves represents the average, calculated from at least two independent packing models of each polymer. The dashed lines are linear least square fits to the portions of the curves that represent Fickian, or at least near-Fickian behavior.

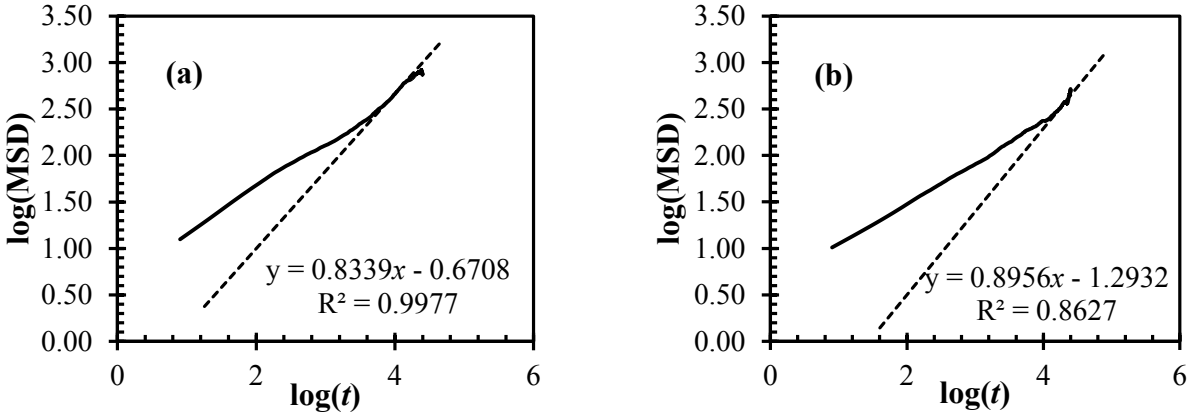

Figure D.4: log(MSD) vs. log(*t*) plots of CF_4 for AF2400 (a) and AF1600 (b) resulting from atomistic molecular dynamics (MD) simulations. Each of the curves represents the average, calculated from at least two independent packing models of each polymer. The dashed lines are linear least square fits to the portions of the curves that represent near-Fickian behavior.

Membrane facilitated separation of NF_3 and CF_4

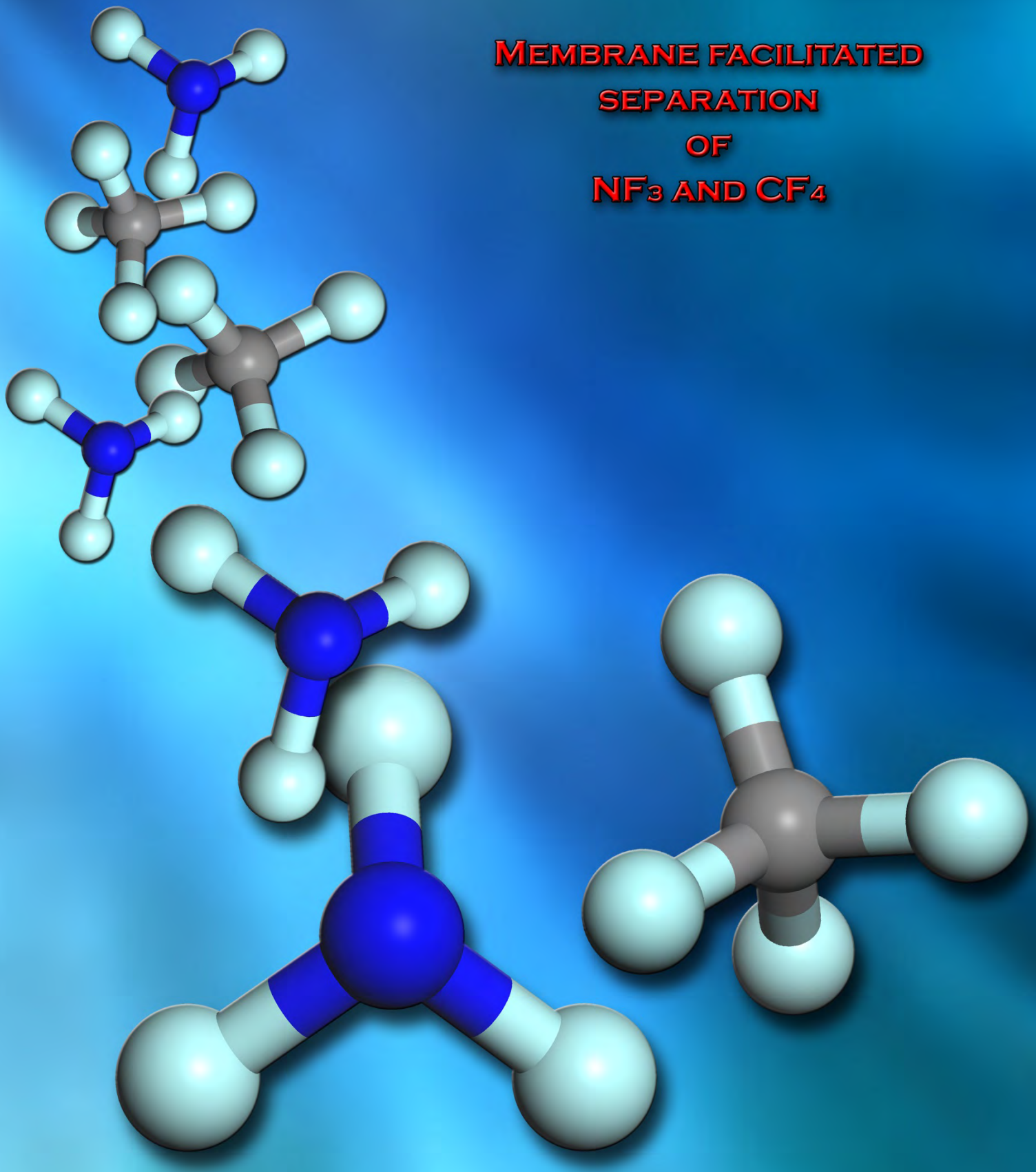

D.J. Branken

September 2013